Modal Analysis Based on the Random Decrement Technique

application to civil engineering structures

Asmussen, J. C.

Publication date:
1997

Document Version
Publisher's PDF, also known as Version of record

MODAL ANALYSIS BASED ON THE RANDOM DECREMENT TECHNIQUE

-

APPLICATION TO CIVIL ENGINEERING STRUCTURES

by

John Christian Asmussen

Department of Building Technology and Structural Engineering
University of Aalborg
Sohngaardholmsvej 57
9000 Aalborg
Denmark
www.civil.auc.dk/i6

Preface

The present thesis *Modal Analysis Based on the Random Decrement Technique - Application to Civil Engineering Structures* has been made as part of my Ph.D.-study programme carried out in the period September 1994 - August 1997 at the Department of Building Technology and Structural Engineering, Aalborg University, Denmark. The Ph.D. work is part of the frame programme *Dynamics of Structures* sponsored by the Danish Technical Research Council.

The proof-reading was made by Kirsten Aakjær, Senior Secretary at my department. Her careful work is grately appreciated.

I would like to thank Professor G.C. Manos from the Department of Civil Engineering, Aristotle University, Thessaloniki, Greece, for making my visit at his department in the period 1/6 1995 - 1/9 1995 possible and enjoyable. Furthermore, special thanks to the staff at his department for solving a lot of logistic problems.

Several persons from the staff at the laboraty have performed excellent work in connection with my experimental tests and preparation of the Bridge Measurement System used for ambient testing of bridges. Thanks to Henning Andersen, engineering assistent, Carl Carstens, electrician, and Jørgen Hasselgren, engineering assistent. The valuable advice from Peter Mossing, Senior Engineer, from the Danish Building Research Institute in connection with the Bridge Measurement System design is grately appreciated.

Thanks to Palle Andersen, Ph.D., for discussions and help during the Ph.D.-study. Especially his simulation tools based on ARMAV-models have increased the quality of most of the simulation studies performed in this thesis.

Thanks also to my advisers Associate Professor Rune Brincker, Department of Building Technology and Structural Enginering, Aalborg University, and Professor Sam Ibrahim, Department of Mechanical Engineering, Old Dominion University, Virginia, USA for sharing their ideas and experience in Identification and Random Decrement.

Finally the support from my wife Pernille has been invaluable. She has never complained, although she had to spent many weekends and holidays on her own. And she never asked the evident question. *How can you spend so much time on estimating constants in linear differential equations?*

John Christian Asmussen

Aalborg, 5 August, 1997

Nomenclature

Abbreviations

ARMAV	=	Vector auto regressive moving average.
ASD	=	Average Spectral Density.
DOF	=	Degrees of freedom.
FFT	=	Fast Fourier transform.
FRF/FRM	=	Frequency response function/matrix.
IRF/IRM	=	Impulse response function/matrix.
ITD	=	Ibrahim time domain.
ln	=	Natural logaritm.
MAC	=	Modal assurance criterion.
MPF	=	Modal participation factor.
PTD	=	Polyreference time domain.
RD	=	Random decrement.
rms	=	Root mean square.
SIC	=	Shape invariance criterion.
VRD	=	Vector random decrement.

Roman

$\mathbf{a}$, $\tilde{\mathbf{a}}$	=	Triggering level vector.
$\mathbf{A}$	=	State matrix.
$\tilde{\mathbf{A}}$	=	State matrix.
$\mathbf{b}$, $\tilde{\mathbf{b}}$	=	Triggering level vector.
$\mathbf{B}$	=	State matrix.
$\tilde{\mathbf{B}}$	=	State matrix.
$\mathbf{C}$	=	Damping matrix. Symmetric and positive definite.
COV[]	=	Covariance operator.
$\mathbf{D}$	=	Observation matrix.
D_{xx}	=	Auto Random Decrement function.
D_{xy}	=	Cross Random Decrement function.
$\mathbf{D}_{\mathbf{x}x_i}$	=	Random Decrement functions in vector form.
D_{x_i}	=	Vector Random Decrement function.
$\mathbf{D}_{\mathbf{x}}$	=	Vector Random Decrement functions in vector form.
$E[\cdot]$	=	Mean value operator.
$\mathcal{E}$	=	Error function.
$\mathbf{f}$	=	Force vector.
$\mathbf{F}$	=	State force vector.
$\mathbf{h}$	=	Impulse response matrix/function.
$\mathbf{H}$	=	Frequency response matrix/function.
i, j	=	Integers or $\sqrt{-1}$.

$\mathbf{I}$	=	Identity matrix.
k	=	Constant.
$\mathbf{K}$	=	Stiffness matrix. Symmetric and positive definite.
m, $\mathbf{m}$	=	Integer Modal masses, Modal mass matrix.
$\mathbf{M}$	=	Mass matrix. Diagonal and positive definite.
n	=	Integer. E.g. DOFs or vector/matrix size.
N	=	Integer, e.g. number of time points, triggering points.
p	=	Density function (multivariate).
P	=	Distribution function (multivariate).
$\mathcal{P}$	=	Probability.
$\mathbf{q}_0$	=	Modal initial vector condition.
$\mathbf{q}(t)$	=	Modal response vector.
$\mathbf{R_{XX}}$	=	Auto correlation matrix/function.
$\mathbf{R_{XY}}$	=	Cross correlation matrix/function.
$\mathbf{R}', \mathbf{R}''$	=	One and two time time derivative of R.
t, τ	=	Time variables.
$S_{XX}(\omega)$	=	Auto spectral density.
$S_{YX}(\omega)$	=	Cross spectral density.
T^E	=	Local extremum triggering condition.
T^{G_T}	=	Theoretical general triggering condition.
T^{G_A}	=	Applied general triggering condition.
T^L	=	Level crossing triggering condition.
T^P	=	Positive point triggering condition.
T^Z	=	Zero crossing triggering condition.
T^v	=	Vector triggering condition.
$U(t)$	=	Noise process.
$u(t)$	=	Realization of noise process.
$\mathbf{V}$	=	Covariance matrix/function.
$\mathbf{x}$	=	Displacement response vector.
$\dot{\mathbf{x}}$	=	Velocity response vector.
$\ddot{\mathbf{x}}$	=	Acceleration response vector.
$\mathbf{x}_0$	=	Initial displacement condition.
$\dot{\mathbf{x}}_0$	=	Initial velocity condition.
$\mathbf{X}, \mathbf{Y}$	=	Stochastic vector process.
$\dot{\mathbf{X}}, \dot{\mathbf{Y}}$	=	Time derivative of $\mathbf{X}, \mathbf{Y}$.
$\ddot{\mathbf{X}}, \ddot{\mathbf{Y}}$	=	Double time derivative of $\mathbf{X}, \mathbf{Y}$.
$\mathbf{x}, \mathbf{y}$	=	Realizations of stochastic vector process, $\mathbf{X}, \mathbf{Y}$.
$\dot{\mathbf{x}}, \dot{\mathbf{y}}$	=	Realizations of stochastic vector process, $\dot{\mathbf{X}}, \dot{\mathbf{Y}}$.
$\ddot{\mathbf{x}}, \ddot{\mathbf{y}}$	=	Realizations of stochastic vector process, $\ddot{\mathbf{X}}, \ddot{\mathbf{Y}}$.
$\mathbf{z}$	=	State vector.
$\dot{\mathbf{z}}$	=	Time derivative of state vector.
$\mathbf{z}_0$	=	Initial state condition.
Z_{XY}	=	Fourier transform of D_{XY}.

$\Box^T$	=	Matrix transposed.
$\Box^{-1}$	=	Matrix inverse.
$\Box^*$	=	Matrix complex conjugate.
$\hat{\Box}$	=	Estimate of $\Box$

Greek

ΔT	=	Sampling interval.
Δt	=	Time shift.
$\mathbf{\Delta t}$	=	Time shifts in vector form.
γ	=	Discrete-time eigenvalue.
γ_{xy}^2	=	Coherence function.
λ	=	Continuous-time eigenvalue.
μ	=	Mean value - vector/scalar.
ω	=	Cyclic eigenfrequency.
ω_d	=	Damped cyclic eigenfrequency.
$\mathbf{\Phi}_i$, $\mathbf{\Phi}$	=	Mode shape vector/matrix.
$\mathbf{\Psi}_i$, $\mathbf{\Psi}$	=	Eigenvector/matrix or modal matrix.
σ	=	Standard deviation.
τ	=	Time variable.
ζ	=	Modal damping ratio.
$\mathbf{\Lambda}$	=	Diagonal matrix with eigenvalues, λ.
$\mathbf{\Gamma}$	=	Diagonal matrix with discrete eigenvalues.

Contents

Chapter 1

Introduction

The purpose of this chapter is to give an appropriate approach to the topic of this thesis: Modal analysis based on the Random Decrement technique. It is the intention that the chapter should give a short background and motivation for the work presented in this thesis. A clear delimitation of this work will also be presented. This chapter should give an overview of the contents of this thesis.

Section 1.1 describes the basic procedures in vibration testing and some of the traditional applications. In this section some main choices, which delimits this work to deal with the Random Decrement technique are presented. Section 1.2 contains a review of the Random Decrement technique. This is a natural starting point in order to identify the advantages/disadvantages of the technique and to detect any missing knowledge to the technique. Section 1.3 delimits the work presented in this thesis in detail and brings up questions, which will be investigated throughout the thesis. Section 1.4 summarizes the contents of each chapter in order to make a selective reading possible. Finally a reader's guide finishes this introduction in section 1.5.

1.1 Background and Motivation

There are several purposes for performing vibration testing of a structure. This could e.g. be comparison of the measured response of a structure and the theoretically predicted response, updating of a theoretical model of the structure, inspection of a structure based on its dynamic characteristics, force identification etc., see e.g. Ewins [1], or the purpose could simply be to estimate the vibration levels of a structure in its natural environment.

Common for most of the arguments for carrying out a vibration test of a structure is that identification of the dynamic characteristics of the structure is either the main purpose or necessary halfway results. This thesis only deals with such part of a vibration test, which includes identification of the dynamic characteristics of the structure. Further applications of these dynamic characteristics are not considered.

Vibration tests differs from each other by the forces bringing the structure into vibration. Many different types of forces exist: Step excitation, impact excitation, harmonic excitation, random or white noise excitation, ambient excitation etc., see e.g. Ewins. [1]. This thesis only considers vibrations of structures subjected to loads, which can be modelled by

white noise. The loads might be created artificial using e.g. a frequency analyser together with a shaker attached to the structure or they might be ambient. Ambient loads are the natural loads of a structure such as e.g. wind, waves, traffic etc. It is not unusual that these forces are modelled using white noise. A mathematical description of the models of the loads is given in chapter 2.

If the aim of a vibration test of a structure is to identify the dynamic characteristics of the structure, the following three processes should all be carried out with high accuracy in order to make the test succesful. These are, see e.g. Ewins [1].

- The mathematical modelling of the structural vibrations.
- Measurements of the vibrations.
- Data analysis of the measurements.

These three processes are in practice coherent, so that a separation followed up by an individual solution and performance is not possible. This is illustrated by fig. 1.1, where it is indicated that results of the data analysis could lead to a change of the mathematical model or a change in the experimental setup.

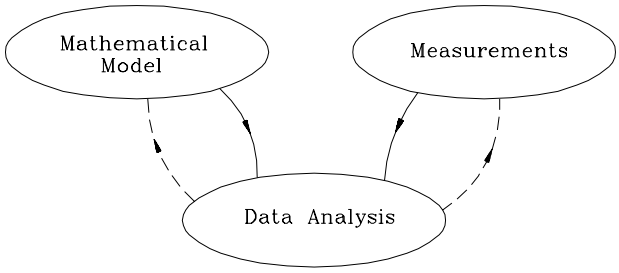

Figure 1.1: *Illustration of the processes in vibration testing. The data analysis may result in a reformulation of the mathematical model or a change in the experimental setup.*

This thesis mainly deals with the data analysis procedure in vibration testing. This is the process where the measurements of the vibrations of a structure are used to calibrate or identify the parameters of the mathematical model of the structure. The parameters of the mathematical model describe the dynamic characteristics of the structure.

Collecting the measurements of the vibrating structure is the fundamental basis for a succesful test. If the measurements are not collected carefully, it is impossible to obtain satisfactorily accurate dynamic characteristics of the structure, no matter of the mathematical modelling and data analysis. Although this thesis also will include experimental work the process of measuring the vibrations of a structure is not described or reported in detail. This is beyond the scope of this work.

Structures are continuous or distributed systems. The mass, damping and stiffness properties are distributed throughout the spatial definition of the structure. In this thesis

the mathematical model used to describe the vibrations of a structure is a discrete model: The linear lumped mass parameter model. The damping forces, which model all energy dissipation from the structure, are assumed to be proportional to the velocity of the lumped masses, and the stiffness forces are assumed to be proportional to the displacements of the lumped masses. The principle is illustrated in fig. 1.2.

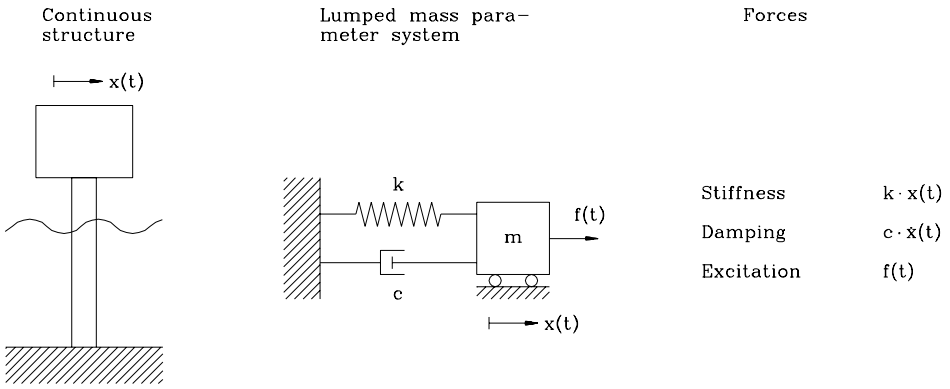

Figure 1.2: *Example of a continuous structure modelled by a lumped mass parameter system. The displacements at the top of the monopile offshore platform are modelled by a lumped mass parameter system. The loads on the structure, wind and waves, are modelled by $f(t)$, the damping forces are modelled by $c \cdot \dot{x}(t)$ and the stiffness forces are modelled by $k \cdot x(t)$. $x(t)$ is the displacement and $\dot{x}(t)$ is the velocity of the top of the platform.*

In principle any material point of the continuous structure has a mass, damping and stiffness property attached. So a structure should intuitively have infinitely many of such dynamic degrees of freedom. Since the structure is assumed to be linear, the properties of the dynamic degrees of freedom, which are local properties, can be converted to the dynamic characteristics called modal parameters, which are global parameters of the structure. The modal parameters consist of eigenfrequencies, damping ratios and mode shape vectors. Sometimes the term structural mode or just mode is used. A structural mode is described by an eigenfrequency, damping ratio and a mode shape vector, which belongs together. An eigenfrequency can be interpreted as a frequency where the structure will have a high response level to a harmonic force with that frequency. The eigenfrequencies of a structure are therefore sometimes also denoted resonant frequencies. A damping ratio gives information about how fast the vibrations of the structure at the corresponding eigenfrequency dissipate. The mode shape vectors describe the relative displacements of the material points of the structure at the corresponding eigenfrequency. These properties make the modal parameters global parameters.

Theoretically structures have infinitely many modes and thereby inifinitely many modal parameters. In vibration testing the number of modes, that can be identified, are limited by the force. The forces work in a limited frequency area, so only structural modes with an eigenfrequency within that frequency area are brought into vibration and can therefore be identified. This also means that the lumped mass parameter model of the structure can also be limited. It does not have to contain an infinite number of degrees of freedom. These are the arguments for using the linear lumped mass parameter model with a finite number of masses and thereby finite number of degrees of freedom. This is the mathematical

model used to describe the vibrations of the structures considered in the present thesis.

The above assumptions of the mathematical modelling of the structure might seem very restrictive. But it is a very general mathematical model and has been used to model various structures from large civil engineering structures such as high-rise buildings, bridges, offshore platforms to small mechanical systems. It is important that the mathematical model assumes that the dynamic characteristics of the structures are time-invariant during the measurement period. This is also widely assumed.

1.1.1 Data Analysis

The data analysis process is denoted identification or modal analysis, since the aim is to identify the modal parameters of the linear lumped mass parameter system. The main topic of this thesis is how these modal parameters can be identified from the measurements. Since the late 1960s where the Fast Fourier Transformation (FFT) algorithm became well-known, see Cooley & Tukey [2], the main part of the data analysis of the measured vibrations and forces has been based on this algorithm.

Consider two stochastic processes $X(t)$ and $Y(t)$. They could e.g. describe the measured response and force of a structure. The Fourier transforms of the processes are defined as

$$X(\omega) = \frac{1}{2\pi}\int_{-\infty}^{\infty} X(t)e^{-i\omega t}dt \qquad Y(\omega) = \frac{1}{2\pi}\int_{-\infty}^{\infty} Y(t)e^{-i\omega t}dt \tag{1.1}$$

The data analysis is based on the cross and auto spectral density functions. Several different methods are developed to extract the modal parameters of the structure from the spectral densities. They are formulated in both the frequency and the time domain. So the spectral densities constitute a connection between the measured vibrations and the parameters of the mathematical model. The cross spectral density function is defined from, see e.g. Bendat & Piersol [3], Schmidt [4]

$$S_{XY}(\omega) = \lim_{T\to\infty}\frac{1}{T}E[X^*(\omega,T)Y(\omega,T)] \tag{1.2}$$

where $E[\cdot]$ denotes the mean value operator, superscript * denotes complex conjugate and $X(\omega,T)$, $Y(\omega,T)$ are defined from eq. (1.1) by replacing the integration limits $\pm\infty$ with $\pm T$. The auto spectral densities are special cases of the cross spectral density and is defined by replacing X with Y or the opposite. The FFT algorithm is a fast and reliable method for estimating $X(\omega,T)$ and $Y(\omega,T)$ used in eq. (1.2). The above approach (and similar approaches) has by far been the most frequently used data analysis procedure, since the introduction of the FFT algorithm. In practice the above cross spectral density function can never be calculated. The reason is that infinite long measurements are in practice impossible to obtain. Therefore the estimate of the cross spectral density function is

$$\hat{S}_{XY}(\omega,T) = \frac{1}{T}E[X^*(\omega,T)Y(\omega,T)] \tag{1.3}$$

The mean value operation is calculated from the finite FFTs of pairs of realizations $x(t)$ and $y(t)$ of the processes $X(t)$ and $Y(t)$. As indicated in eq. (1.3) the estimated spectral

density becomes a function of the finite time record length, T. The practical limit of realizations with finite time period can be modelled mathematically by multiplying the realization with a *virtual* infinite time period by a window function. The simplest possible window function is the boxcar or rectangular window.

$$W(t,T) = \left\{ \begin{array}{ll} 1 & |t| < T/2 \\ 0 & |t| > T/2 \end{array} \right\} \tag{1.4}$$

So the finite FFTs used in the estimate of the spectral densities are calculated from records of infinite time length multiplied by a window function, to end up with a time record of finite time length. This result is one of the major disadvantages of data analysis based on the FFT algorithm. In practice the necessary introduction of a window function results in a bias problem, usually denoted leakage, since the FFT is calculated from the measurements multiplied by the window function. This bias error results in a too high estimation of the energy dissipation of the different modes of a system. The window functions leak energy from one frequency to another. The bias problem can be reduced by choosing another and more complicated window function than the rectangular window in eq. (1.4), but in general never removed.

Another disadvantage is that a finite frequency resolution of at least $\Delta w = \frac{2\pi}{T}$ is obtained, see e.g. Bendat & Piersol [3]. Furthermore, in practice the mean value operation cannot be calculated exactly since only a finite number of realizations exist. Sometimes only a single realization of the processes exists, but assuming that the processes are ergodic the above procedure can still be followed.

It should be made clear that despite these problems data analysis based on Fourier transformation is a fast and reliable method. One of the reasons is that persons with experience in modal analysis and vibration testing can immediately extract valuable information from a plot of the data transformed into the frequency domain, such as spectral densities compared to a time domain plot of the data. An area which illustrates the popularity of data analysis based on Fourier transformations is ambient testing of bridges. Ambient testing means testing of a structure, which vibrates due to natural loads such as wind, traffic, waves etc. In a review of ambient testing of bridges, see Farrar et al. [6], a bibliography of about 100 papers is listed. At least 95% of all this work is based on the FFT algorithm.

1.1.2 The Random Decrement Technique

Although data analysis based on the FFT algorithm has many advantages, the disadvantages motivated the development of alternative approaches. One of these alternative approaches, the Random Decrement (RD) technique, was introduced by H.A. Cole at NASA during the late 1960s and early 1970s, see e.g. Cole [7] - [10]. The topic of this thesis is the RD technique. The RD technique is a simple and easily implemented method for analysis of vibrations of structures loaded by stochastic forces, but the technique has never been used in a wide sense. Figure 1.3 shows the number of papers, reports, articles, thesis etc. which have been published each year, from the introduction of the technique in 1968 to 1997.

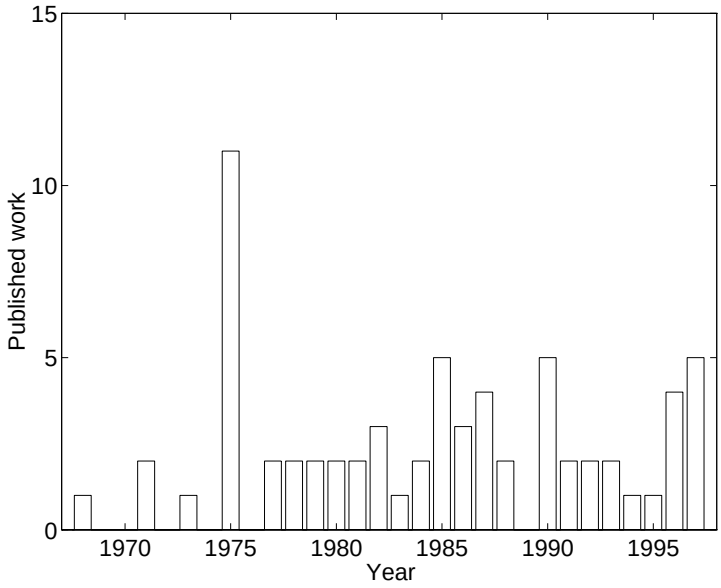

Figure 1.3: *The literature published each year (conference papers, reports, articles Ph.D.-thesis etc.) concerning the RD technique.*

The numbers in the figure are based on the bibliography at the end of this chapter. Only a handful of people have published several papers concerning either theoretical work or application work. One of the reasons for the lack of interest in this technique is perhaps that for many years the theoretical background did not include a statistical description in the same sense as the methods based on Fourier transformations. During the late 1980s the mathematical background of the RD technique was extended to include nearly a full statistical description.

This motivates the work reported in the present thesis, where the topic is modal analysis based on the the RD technique. The results of applying the RD technique will several times be compared with analysis based on the FFT algorithm. The RD technique could be compared with other time domain algorithms, but the FFT algorithm is chosen, since it is the most well-known and well-documented method. This will give a solid basis for comparison.

1.2 Review of the Random Decrement Technique

The natural starting point of this work is to make a review of the development and the progress of the RD technique made up to the 1990s. Thereby a proper introduction to the technique will be given. Theoretical work and applications of the technique published in this period are reviewed. Since some of the results obtained in the 1990s are described in detail later in this thesis, only selected papers from this period are reviewed. It is the intention that the bibliography of this chapter presents a reference list to the published literature dealing with the RD technique. Any paper, thesis, report, etc. dealing with the RD technique, which are not included in the bibliography is unknown to the author.

Throughout the literature several names such as Random Dec, Randomdec, RD etc. have

been used. In this thesis, the Random Decrement technique will be abbreviated the RD technique.

1.2.1 Development of the Random Decrement Technique

The RD technique was developed by H.A. Cole at NASA during the late 60s and early 70s. Cole was working with analysis of the dynamic response of space structures subjected to ambient loads. His main tasks were identification of the dynamic characteristics and in-service damage detection of space structures from the measured response. The first papers on the RD technique were published in the period 1968-1973, see Cole [7], [8], [9] and [10]. Cole was looking for "*a simple and direct method for translating the time history into a form meaningful to the observer*", Cole [7]. The damping ratios estimated from the half power bandwidth of the spectral densities, estimated using the FFT algorithm, of the random time series were found to have a large variance. Furthermore, no approach to detect non-linearities from the spectral densities of the response to the unmeasurable ambient loads was known. Instead, Cole used the sample estimates of the auto correlation functions of the time series for identification and damage detection. Damping ratios and eigenfrequencies of the structure were extracted from the envelope of the auto correlation function. Damage detection was suggested to be based on changes in the auto correlation functions. But problems arised, since the auto correlation function was found to change with variations in the ambient loads. These problems with both auto correlation functions and spectral densities motivated the development of the RD technique. Basically, Cole introduced the RD technique as a method to transform a random time series into a free decay of the structure in question. Free decays only contains information of the structure and not the random loads. At first the modal parameters (especially the damping ratios) were extracted from the decay (or decrement). This is probably the explanation for the name given to this technique.

To explain the concept of the RD technique and to argument for the validity of the technique, Cole used the following explanation. The random response of a structure at the time $t_0 + t$ is composed of three parts: 1) The step response from the initial *displacements* at the time t_0. 2) The impulse response from the initial *velocity* at the time t_0. 3) A random part which is due to the load applied to the structure in the period, t_0 to $t_0 + t$.

What happens if a time segment is picked out every time the random response, $x(t)$, has an initial displacement, say $x(t) = a$, and these time segments are averaged?

This question indicates the first concept of the RD technique and was answered by: As the number of averages increase the random part due to the random load will eventually average out and be negligible. Furthermore, the sign of the initial velocity is expected to vary randomly with time so the resulting initial velocity will be zero. The only part left is the free decay response from the initial displacement, a. The principle is illustrated in figure 1.4.

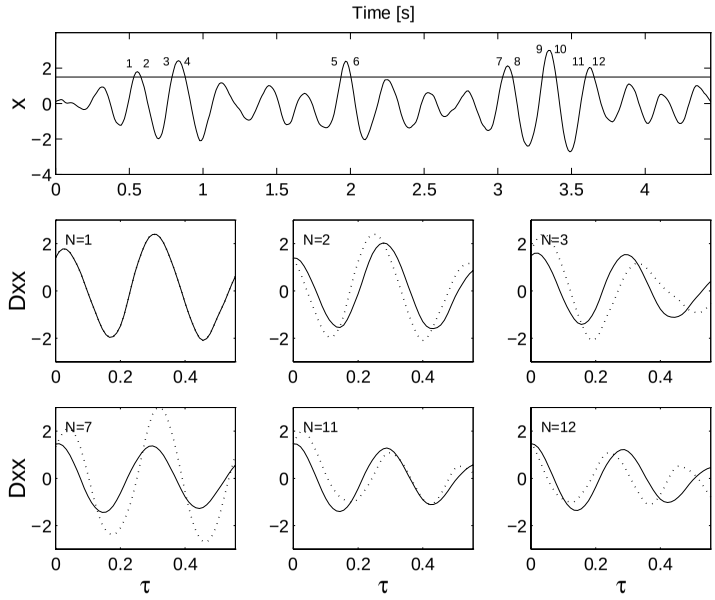

Figure 1.4: *Concept of the RD technique. Random time series, x, (top figure) with triggering points and averaging process (sub figures) with both the resulting RD function (full line) and the current time segment (dashed line).*

In figure 1.4 the initial displacement is chosen to be $a = 1.5 \cdot \sigma_x$. It is commonly accepted to denote the initial displacement, a, as the triggering level and the time points, t_0, where $x = a$, as triggering points. Furthermore, the triggering level a is usually given as a multiplum of the standard deviation, σ_x, of the time series. The process of estimating RD functions illustrated in figure 1.4 can be formulated as a sum of time segments picked out from the response on condition that the time segments have the value a at the start.

$$\hat{D}_{XX}(\tau) \;=\; \frac{1}{N}\sum_{i=1}^{N} x(t_i+\tau)|x(t_i) = a \tag{1.5}$$

where $\hat{D}_{XX}$ is the estimated RD function, τ is the time variable in $\hat{D}_{XX}$ as illustrated in fig. 1.4, and N is the total number of triggering points. The simplicity of the estimation process is obvious, since only detection of triggering points and averaging of the corresponding time segments are performed.

In applications of the RD technique the measurements, x_j, are discrete (time series). This means that a problem arises since the probability of having the value $x(t_i) = a$ in the time series is zero, unless a is chosen carefully. The problem is solved by implementing the triggering condition as a level crossing problem. Therefore the name adopted to the condition illustrated in fig. 1.4 and eq. (1.5) is the level crossing triggering condition.

The introduction of this technique was followed up by a simulation study by Chang [11]. Chang investigated the significance of the length of the RD function, τ, and the number of ensemble averages (triggering points). Based on simulations of the response of 1 and 2 DOF systems loaded by white noise, he recommended about 2000 ensemble averages in order to extract accurate damping ratios (and eigenfrequencies) from the RD functions.

The length of the RD functions was suggested to be in the range of 50% and 125% of the beat period of the two eigenfrequencies.

Chang investigated the level crossing triggering condition and the zero crossing with a positive slope triggering condition. This triggering condition was introduced by Cole, see Cole [10]. A time segment is picked out and used in the averaging process if the time series crosses zero with a positive slope at the start of the time segment. The resulting RD function was believed to be equal to the impulse response function of the structure, since the initial displacement is zero. Houbolt, see Houbolt [12], improved this triggering condition by also picking out time segments if the time series crosses zero with a negative slope. The sign of these time segments is changed before they are averaged with time segments picked out by positive slopes. This approach can be adopted to any triggering condition, see Brincker et al. [57].

1.2.2 Theoretical Aspects of the Random Decrement Technique

Although the RD technique has been applied in connection with a broad band of structures, only a few papers have considered theoretical aspects of the RD technique. This also includes the solution of implementation problems, bias problems etc.

In 1977 Ibrahim introduced the concept of auto and cross RD function, see Ibrahim [22], [23]. Up to this point the RD technique had only been applied to single channel measurements, which resulted in estimation of eigenfrequencies and damping ratios, but with no possibility to extract mode shape information. The concept of the auto and cross RD functions is based on multi-channel measurements. Consider two measurements $x(t)$ and $y(t)$. The auto, D_{XX}, and cross, D_{YX}, RD functions are estimated using the level crossing triggering condition as:

$$\hat{D}_{XX}(\tau) = \frac{1}{N}\sum_{i=1}^{N} x(t_i+\tau)|x(t_i)=a \tag{1.6}$$

$$\hat{D}_{YX}(\tau) = \frac{1}{N}\sum_{i=1}^{N} y(t_i+\tau)|x(t_i)=a \tag{1.7}$$

The first sub-script refers to the measurement, where the time segments are picked out and averaged, whereas the second subscript refers to the measurements, where the triggering points are detected. Alternatively, zero upcrossings or downcrossings could be used as the triggering condition. The approach made it possible to estimate mode shapes corresponding to the measurement points by combining a method for determination of modal parameters from free decays or impulse response functions, such as e.g. the Ibrahim Time Domain method, see Ibrahim [22], [23]. This was an important improvement of the RD technique.

In Reed [26] it is suggested that the RD estimation process is also applied backwards to the time series. The RD functions should be the same. This corresponds to using both positive and negative time lags, τ, in the time segments. This new approach raised a problem, since it is difficult to describe a negative time lag in terms of free decays. This problem was partly solved by Vandiver et al. [32] in 1982.

Vandiver et al. published a paper where it was proven that an auto RD function, estimated using the level crossing triggering condition, is proportional to the auto correlation function of a stationary process, if it has a zero mean Gaussian distribution. The paper is important, since the proportionality between auto RD functions and auto correlation functions made the RD technique directly comparable with the spectral density functions estimated using FFT. This is due to the Wiener-Khintchine relations, which describe the correlation functions as the inverse Fourier transform of the spectral density functions. A description in terms of correlation functions has the advantage that negative time lags can be interpreted without any problems.

Brincker et al. [54] and [60] extended the link between RD functions and correlation functions. By introducing a theoretical general triggering condition it was proven that auto and cross RD functions are proportional to the auto and cross correlation functions, respectively. This interpretation of RD functions will be introduced, discussed and further generalized in later chapters, so a detailed description of the results is omitted at this stage. It should be noted that in Bedewi [45], Bedewi & Yang [52] and [56] there also are some theoretical consideration about the link between RD functions and free decays and/or correlation functions.

The papers reviewed above are the most important papers concerning the theoretical aspects of the RD technique. A couple of papers concerning the implementation of this technique have also been published, see e.g. Chang [11], Caldwell [25], Kiraly [33], Nasir & Sunder [34], Brincker et al. [53], [54], [57], [58]. These problems and their solution will also be discussed in this thesis.

Finally its worth mentioning that a recent paper by Desforges et al. [64] concludes that the RD technique is an accurate way of estimating spectral densities and modal parameters. They compared the RD technique with several other methods for estimating correlation functions/spectral density functions.

1.2.3 Application of the Random Decrement Technique

After the introduction and development the RD technique was mainly used in the estimation of damping ratios and eigenfrequencies in flutter testing. This is illustrated by the references [12] - [19]. In these papers the RD technique is applied to experimentally obtained data and damping ratios and eigenfrequencies are extracted from the RD functions using a least squares approach. The assumption is that the auto RD functions is equivalent to free decays.

The two main applications of the RD technique are damage detection (on-line) and estimation of modal parameters. The work with these topics resulted in the development of the RD technique. In damage detection applications the RD functions are used as a basis for detecting incipient cracks and flaws. The basic idea is that an incipient failure will change the stiffness and the damping characteristics of a structure. Since the RD functions of a random time series are interpreted as a free decay, these functions will change with incipient failure. The triggering level a, see eq. (1.5), is kept constant which means that the RD functions are independent of the level of the input. Several authors, Cole [10], Yang [24], conclude that any non-linearity will change the auto correlation function with

a change in the input level, wheras the RD functions remain unchanged.

Damage detection based on RD functions has been applied to several structures, such as aerospace structures, Cole [10], laboratory beams, Yang & Caldwell [21], piping systems, Yang & Caldwell [24], offshore platform models, Yang et al. [29], Yang et al. [36] and simulation of MDOF systems, Ibrahim [43], etc. One of the main problems in damage detection is to decide whether or not an identified change in structural characteristics such as eigenfrequencies and damping ratios is due to a decrease in stiffness (cracks). A different mass loading or changes in the environmental conditions would also result in a change of modal parameters. Furthermore, the identified modal parameters should not be interpreted as deterministic parameters but as stochastic variables, since there will always be uncertainty connected to the identification process. An identified change in e.g. an eigenfrequency could only be an *adverse* realization of the stochastic variable.

In Yang et al. [29] this uncertainty is taken into account. During the reference or virgin state of the structures a reference RD function is estimated by averaging a number of RD functions. A standard deviation to the reference RD function is estimated at the same time. Figure 1.5 shows a typical reference RD function and the 95 % confidence intervals.

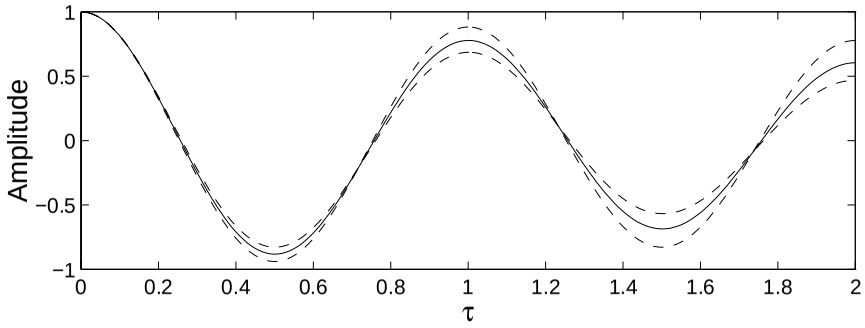

Figure 1.5: *Reference RD function and 95 % confidence intervals.*

Next time an inspection is performed by measuring the random response of the structure a new RD function is estimated. If this RD function at a certain time, e.g. $\tau = 1.5$ seconds, is within the 95 % confidence bounds, no damage is detected. Otherwise the decision is that a damage is detected. This approach was also used in Kummer et al. [30] and Yang et al. [36]. One major problem in this technique is how to choose the value of the confidence bound to have a proper balance between detecting a non-existing crack and disregard an existing crack. Although this approach takes the statistical nature of the problem into consideration, it is not independent of changes of the load on the structure.

The second main application of the RD technique is identification of structures. The technique has mainly been applied to measurements of offshore structures and aeroplanes subjected to ambient loads, see Yang et al. [31] and Ibrahim [27]. But the technique has also been applied to identification of railway vehicle kinematic behaviour, see Siviter & Pollard [41], and soil testing, see Al-Sannad et al. [44]. One of the advantages in identification by RD is the simplicity of the approach. Basically RD functions are estimated as a simple averaging process of time segments. This should make the technique especially

favourable in connection with large structures such as bridges, where the experiments includes a large number of measurements.

Finally the RD technique has also been used to identify non-linear structures, see e.g. Ibrahim et al [49], Caldwell [25] and Haddara [59]. The fundamental idea is to identify several RD functions at different initial conditions or triggering levels, a. From the RD functions parameters (e.g. modal parameters) can be extracted as a function of the triggering level. The non-linearity can then be detected from changes in the modal parameters with the triggering level, a.

1.3 Scope of Work

The delimitations made in the previus sections are

- The vibrations of the structure can be described by a linear lumped mass parameter model.
- The loads on the structure are stationary and can be modelled using random white noise.
- The measurements are assumed to be carried out as carefully as possible.
- The data analysis is based on the RD technique.
- The aim of the vibration test is only to estimate the modal parameters.

From these delimitations the scope of this thesis can be defined as

The objective of the present Ph.D.-thesis is a description, implementation and further development of the theory behind the RD technique as well as a comparison of the performance of the RD technique with the FFT algorithm.

From this definition it follows that a natural starting point is to describe the linear lumped mass parameter system mathematically in terms of modal parameters. Furthermore, the modelling of the load should be described in order to be able to describe the response of the system to the loads. This will make it possible to derive the correlation functions of the systems, which are important in order to interpret the RD functions.

The next natural task is to define the RD functions mathematically and establish the relations to the correlation functions of the measurements. This step will include the description of the present known relations, which will lead to detection of the strength and the weakness of these relations. From this point the technique can be futher developed.

Another task is implementation and application of the technique. The technique should be implemented in a general way and the technique should be applied in the data analyis of complicated and large structures. The reason is that, since it is already known that the technique is fast due to the simple averaging process, this advantage is best exploited in the analysis of structures with a large quantity of data. By analysing complicated structures the RD technique is tested properly.

1.4 Thesis Outline

The following presents an overview of the contents of this thesis and allows a selective reading.

Linear vibration theory and linear stochastic vibration theory are briefly described in chapter 2. The linear lumped mass parameter model is defined, the modal parameters are defined and the load modelling is described. The main purpose is to show that under certain circumstances the free decays of the model and the correlation functions of the stochastic response of the model have equal mathematical description. This allows modal parameters to be extracted from correlation functions using methods, which originally were developed to extract modal parameters from free decays. These methods have been used for decades and their performance is thereby well tested. The chapter summarizes in practice how modal parameters are extracted from free decays or correlation.

In chapter 3 the RD technique is introduced. RD functions are defined mathematically and it is shown how RD functions are estimated. The RD functions are linked to correlation functions under the assumptions that the stochastic processes are stationary and zero mean Gaussian distributed by introducing the applied general triggering condition. Different formulations of the technique are explained. It is suggested how the quality of an estimated RD function can be assessed. The chapter is finished with a simulation study of the quality and estimation time of the RD technique versus 2 other well-known methods. The chapter is supported by appendix A, where the theory of the RD technique is derived in detail. The procedure and theory described does not assume that the loads are measured.

Based on experience with the RD technique some weaknesses were discovered. This leads to the introduction in chapter 4 of the Vector Random Decrement (VRD) technique, which can be interpreted as a generalization of the RD technique. The VRD technique can be used with advantage on data with several measurements collected simultaneously. The theory of this new technique is described in detail and several examples are given. Corresponding to the RD technique, the VRD technique does not assume that the loads are measured. The results of the VRD technique is compared with results from traditional formulations of the RD technique.

In chapter 5 a new approach for predicting the variance of RD functions is suggested. The performance of the approach is compared with the performance of a simple method for predicting the variance of RD functions based on the assumption of uncorrelated time segments. The simple method is derived in appendix A and chapter 3.

Chapter 6 discusses bias and implementation problems. The chapter is of special interest for persons, which are going to implement the RD technique. The implementations made as part of this Ph.D.-work are described.

Chapter 7 introduces the RD technique in combination with the FFT algorithm for estimation of the frequency response function from measured response and force. The previous chapters mainly concern the application of the RD technique in situations with unmeasured forces, such as e.g. ambient testing. This application of the RD technique has the advantage that leakage errors are suppressed. This can never be done if pure FFT is used.

The approach is illustrated on both simulated and experimentally obtained data.

Different experimental studys are described in chapter 8. The ambient vibration testing of the Queensborough bridge and the Vestvej bridge. Furthermore, a vibration study of a laboratory bridge mode is reported. These studies document the applicability of the RD technique. In the analysis of the Vestvej bridge the software developed to analyse data from ambient excited bridges is illustrated.

The thesis is finished in chapter 9 with a conclusion of the present work and a pespectivation towards future tasks. Chapter 10 contains a summary in Danish.

1.5 Reader's Guide

Each chapter in this thesis is finished with a bibliography where the references are listed in the order they are quoted. The exception is this chapter where the references are listed in chronological order in the bibliography. The references are quoted as NAME [1], NAME1 & NAME2 [1] or NAME et al. [1] dependent on one, two or three and more authors. Tables, figures and equations are referred to as table NUMBER, fig. NUMBER and eq. (NUMBER). NUMBER could be e.g. 4.7 referring to the seventh table, figure or equation in chapter 4.

The investigations in this thesis will be based on both simulated data and experimentally obtained data. In the situations were the data have been simulated, this has always been performed using Auto Regressive Moving Average Vector-models. The interested reader is referred to Andersen [5] for a description of this technique and the software used. This method has been chosen, since it preserves the covariance function in the simulated discrete-time response from the continuous-time response.

Bibliography

[1] Ewins, D.J. *Modal Testing: Theory and Practice.* Research Studies Press, Ltd., Staunton, Somerset, England, 1984 (reprinted 1995). ISBN 0 86380 017 3.

[2] Cooley, J.W. & Tukey, J.W. *An Algorithm for the Machine Calculation of Complex Fourier Series.* Mathematics of Computation, Vol. 19, pp. 297-301, April 1965.

[3] Bendat, J.S. & Piersol, A.G. *Random Data - Analysis and Measurement Procedures.* John Wiley & Sons, 1986. ISBN 0-471-04000-2.

[4] Schmidt, H. *Resolution Bias Errors in Spectral Density, Frequency Response and Coherence Function Measurements. I-V.* Journal of Sound and Vibration, 101(3), pp. 347-427, 1985.

[5] Andersen, P. *Identification of Civil Engineering Structures using Vector ARMA Models.* Ph.D.-thesis Aalborg University 1997.

[6] Farrar, C.R., Baker, W.E., Bell, T.M., Cone, K.M., Darling, T.W., Duffey, T.A., Eklund, A. & Migliori, A. *Dynamic Characterization and Damage Detection in the*

I-40 Bridge Over the Rio Grande. Los Alamos National Laboratories. LA-12767-MS. UC-906, June 1994.

1968

[7] Cole, H.A. *On-The-Line Analysis of Random Vibrations.* AIAA Paper No. 68-288. 1968.

1971

[8] Cole, H.A. *Method and Apparatus for Measuring the Damping Characteristics of a Structure.* United States Patent No. 3, 620,069, Nov. 16. 1971.

[9] Cole, H.A. *Failure Detection of a Space Shuttle Wing by Random Decrement.* NASA TMX-62,041, May 1971.

1973

[10] Cole, H.A. *On-Line Failure Detection and Damping Measurements of Aerospace Structures By Random Decrement Signature.* NASA CR-2205, 1973.

1975

[11] Chang, C.S. *Study of Dynamic Characteristics of Aeroelastic Systems Utilizing Randomdec Signatures.* NASA-CR-132563, Feb. 1975.

[12] Houbolt, J.C. *On Identifying Frequencies and Damping in Subcritical Flutter Testing.* Proc. NASA Symposium on Flutter Testing Techniques, Edwards, California, Oct. 9-10, 1975. NASA SP-415, pp. 1-41.

[13] Bennet, R.M. & Desmarais, R.N. *Curve Fitting of Aeroelastic Transient Response Data with Exponential Functions.* Proc. NASA Symposium on Flutter Testing Techniques, Edwards, California, Oct. 9-10, 1975. NASA SP-415, pp. 43-57.

[14] Hammond, C.E. & Dogget, R.V. *Determination of Subcritical Damping by Moving Block/Randomdec Applications.* Proc. NASA Symposium on Flutter Testing Techniques, Edwards, California, Oct. 9-10, 1975. NASA SP-415, pp. 59-76.

[15] Huttsell, L.J. & Noll, T.E. *Wind Tunnel Investigation of Supersonic Wing-Tail Flutter.* Proc. NASA Symposium on Flutter Testing Techniques, Edwards, California, Oct. 9-10, 1975. NASA SP-415, pp. 193-211.

[16] Lenz, R.W. & McKeever, B. *Time Series Analysis in Flight Flutter Testing at the Air Force Flight Test Center: Concepts and Results.* Proc. NASA Symposium on Flutter Testing Techniques, Edwards, California, Oct. 9-10, 1975. NASA SP-415, pp. 287-317.

[17] Perangelo, H.J. & Milordi, F.W. *Flight Flutter Testing Technology at Grumman.* Proc. NASA Symposium on Flutter Testing Techniques, Edwards, California, Oct. 9-10, 1975. NASA SP-415, pp. 319-375.

[18] Abla, M.A. *The Application of Recent Techniques in Flight Flutter Testing.* Proc. NASA Symposium on Flutter Testing Techniques, Edwards, California, Oct. 9-10, 1975. NASA SP-415, pp. 395-411.

[19] Brignac, W.J., Ness, H.B., Johnson, M.K. & Smith, L.M. *YF-16 Flight Flutter Test Procedures.* Proc. NASA Symposium on Flutter Testing Techniques, Edwards, California, Oct. 9-10, 1975. NASA SP-415, pp. 433-457.

[20] Reed, R.E. & Cole, H.A. *Applicability of Randomdec Technique to Flight Simulator for Advanced Aircraft.* NASA CR-137609, 1975.

[21] Yang, J.C.S. & Caldwell, D.W. *The Measurement of Damping and the Detection of Damages in Structures by the Random Decrement Technique.* 46th Shock and Vibration Symposium and Bulleting, San Diego, California, Nov. 1975.

1977

[22] Ibrahim, S.R. *Random Decrement Technique for Modal Identification of Structures.* Journal of Spacecraft and Rockets, Vol. 14, No. 11., Nov. 1977, pp. 696-700.

[23] Ibrahim, S.R. *The Use of Random Decrement Technique for Identification of Structural Modes of Vibration.* AIAA paper, Vol. 77, 1977, pp. 1-9.

1978

[24] Yang, J.C.S. & Caldwell, D.W. *A Method for Detecting Structural Deterioration in Piping Systems.* ASME Probabilistic Analysis and Design of Nuclear Power Plant Structures Manual PVB-PB-030, 1978, pp. 97-117.

[25] Caldwell, D.W. *The Measurement of Damping and the Detection of Damage in Linear and Nonlinear Systems by the Random Decrement Technique.* Ph.D.-Thesis, University of Maryland, 1978.

1979

[26] Reed, R.E. *Analytical Aspects of Randomdec Analysis.* AIAA/ASME/AHS 20th Structures, Structural Dynamics and Materials Conf. St. Louis, Mo. April 1979, pp. 404-409.

[27] Ibrahim, S.R. *Application of Random Time Domain Analysis to Dynamic Flight Measurements.* The Shock and Vibration Bulletin, Bulletin 49, Part 2 of 3, Sept. 1979, pp. 165-170.

1980

[28] Ibrahim, S.R. *Limitations on Random Input Forces in Randomdec Computation for Modal Identification.* The Shock and Vibration Bulletin. Bulletin 50 (Part 3 of 4), Dynamic Analysis, Design Techniques. Sept. 1980, pp. 99-112.

[29] Yang, J.C.S., Dagalakis, N. & Hirt, M. *Application of the Random Decrement Technique in the Detection of an Induced Crack on an Offshore Platform Model.* Computer Methods for Offshore Structures. Winter Annual Meeting of ASME, Nov 165-21, 1980, pp. 55-67.

1981

[30] Kummer, E., Yang, J.C.S. & Dagalakis, N. *Detection of Fatigue Cracks in Structural Members.* Proc. 2nd ASCE/EMD Specialty Conference on Dynamic Response of Structures. Atlanta, Georgia, Jan. 1981, pp. 445-460.

[31] Yang, J.C.S., Aggour, M.S., Dagalakis, N. & Miller, F. *Damping of an Offshore Platform Model by Random Dec Method.* Proc. 2nd ASCE/EMD Specialty Conference on Dynamic Response of Structures. Atlanta, Georgia, Jan. 1981, pp. 819-832.

1982

[32] Vandiver, J.K., Dunwoody, A.B., Campbell, R.B. & Cook, M.F. *A Mathematical Basis for the Random Decrement Vibration Signature Analysis Technique.* Journal of Mechanical Design, Vol. 104, April 1982, pp. 307-313.

[33] Kiraly, L.J. *A High Speed Implementation of the Random Decrement Algorithm.* NASA Technical Memorandum 82853, NASA-TA-82853. (Prepared for the 1982 Aerospace/Test Measurement Symposium, Las Vegas, Nevada, May 2-6 1982.)

[34] Nasir, J. & Sunder, S.S. *An Evaluation of the Random Decrement Technique of Vibration Signature Analysis for Monitoring Offshore Platforms.* Massachussets Institute of Technology, Department of Civil Engineering, Research Report R82-52. Sept. 1982.

1983

[35] Huan,S.-L., McInnis, B.C. & Denman, E.D. *Analysis of the Random Decrement Method.* Int. J. Systems Sci., 1983, Vol. 14, No. 4, 417-423.

1984

[36] Yang, J.C.S., Chen, J. & Dagalakis, N.G. *Damage Detection in Offshore Structures by the Random Decrement Technique.* ASME, Journal of Energy Resources Technology, March 1984, Vol. 106, pp. 38-42.

[37] Ibrahim, S.R. *Time-Domain Quasilinear Identification of Nonlinear Dynamic Systems.* AIAA Journal, Vol. 6, No. 6, June, 1984, pp. 817-823.

1985

[38] Tsai, T. Yang, J.C.S. & Chen, R.Z. *Detection of Damages in Structures by the Cross Random Decrement Technique.* Proc. 3rd International Modal Analysis Conference, Jan. 28-31, Orlando, Florida, 1985, pp. 691-700.

[39] Yang, J.C.S. Tsai, T., Tsai, W.H. & Chen, Z. *Detection and Identification of Structural Damage from Dynamic Response Measurements.* Proc. 4th Internatianal Offshore Mechanics and Arctic Engineering Symposium, Dallas, Texas, 1985, pp. 496-504.

[40] Yang, J.C.S., Tsai, T., Pavlin, V., Chen, J. & Tsai, W.H. *Structural Damage Detection by the System Identification Technique.* The Shock and Vibration Bulletin, Bulletin 55, Part 3 of 5, June 1985, pp. 57-66.

[41] Siviter, R. & Pollard, M.G. *Measurement of Railway Vehicle Kinematic Behaviour using the Random Decrement Technique.* Vehicle Systems Dynamics, Vol. 14. No. 1-3 June 1985, pp. 136-140.

[42] Yang, J.C.S., Marks, C.H., Jiang, J., Chen, D., Elahi, A. & Tsai, W.-H. *Determination of Fluid Damping using Random Excitation.* ASME Journal of Energy Resources Technology, Vol. 107, June 1985, pp. 220-225.

1986

[43] Ibrahim, S.R. *Incipient Failure Detection from Random-Decrement Time Functions.* The International Journal of Analytical and Experimental Modal Analysis. Vol. 1, No. 2, April 1986, pp. 1-9.

[44] Al-Sannad, H.A., Aggour, M.S. & Amer, M.I. *Use of Random Loading in Soil Testing.* Indian Geotechnical Journal, Vol. 16, No. 2, April 1986, pp. 126-135

[45] Bedewi, N.E. *The Mathematical Foundation of the Auto and Cross Random Decrement Technique and the Development of a System Identification Technique for Detection of Structural Deterioration.* Ph.D.-Dissertation, University of Maryland, 1986.

1987

[46] Bedewi, N.E., Kung, D.-N., Qi, G.-Z. & Yang, J.C.S. *Use of the Random Decrement Technique for Detecting Flaws and Monitoring the Initiation and Propagation of Fatigue Cracks in High-Performance Materials.* Proc. Nondestructive Testing of High-Performance Ceramics, Boston, MA, August 25-27, 1987, pp. 424-441.

[47] Bedewi, N.E. & Yang, J.C.S. *A System Identification Technique Based on the Random Decrement Signatures. Part 1: Theory and Simulation.* Proc. 58th Shock and Vibration Symposium, Huntsville, Alabama, October 13-15, 1987, Vol.1 pp. 257-273.

[48] Bedewi, N.E. & Yang, J.C.S. *A System Identification Technique Based on the Random Decrement Signatures. Part 2: Experimental Results.* Proc. 58th Shock and Vibration Symposium, Huntsville, Alabama, October 13-15, 1987, Vol.1 pp. 275-287.

[49] Ibrahim, S.R., Wentx, K.R, & Lee, J. *Damping Identification from Non-Linear Random Responses using a Multi-Triggering Random Decrement Technique.* Mechanical Systems and Signal Processing (1987) 1(4), pp 389-397.

1988

[50] Kung, D.-N., Qi, G.-Z., Yang, J.C.S. & Bedewi, N. *Fatique Life Characterization of Composite Structures using the Random Decrement Modal Analysis Technique.* Proc. 6th International Modal Analysis Conference, Kissimee, Florida, Feb. 1-4, 1988, pp. 350-356.

[51] Bernard, P. *Identification de Grandes Structures: Une Remarque sur la Méethode du Décrement Aléatoire.* Journal of Theoretical and Applied Mechanics. Vol. 7, No. 3, 1988, pp. 269-280. (In French).

1990

[52] Bedewi, N.E. & Yang, J.C.S. *The Random Decrement Technique: A More Efficient Estimator of the Correlation Function.* Proc. 1990 ASME International Conference and Exposition, Boston, MA, USAm Aug. 5-9, pp. 195-201.

[53] Brincker, R., Jensen, J.L. & Krenk, S. *Spectral Estimation by the Random Dec Technique.* Proc. 9th International Conference on Experimental Mechanics, Lyngby, Copenhagen, Aug. 20-24, 1990.

[54] Brincker, Krenk, S. & R., Jensen, J.L. *Estimation of Correlation Functions by the Random Dec Technique.* Proc. Skandinavisk Forum for Stokastisk Mekanik, Lund, Sweden, Aug. 30-31, 1990.

[55] Yang, J.C.S., Qi, G.Z. & Kan, C.D. *Mathematical Base of Random Decrement Technique.* Proc. 8th International Modal Analysis Conference, Kissimee, Florida, USA, 1990, pp. 28-34.

[56] Bedewi, N.E. & Yang, J.C.S. *The Relationship Between the Random Decrement Signature and the Free Decay Response of Multidegree-Of-Freedom Systems.* Proc. 1990 ASME International Comp. In Engineering Conference and Exposition. Boston, MA, USA, Aug 5-9 1990 pp. 77-86.

1991

[57] Brincker, R., Kirkegaard, P.H. & Rytter, A. *Identification of System Parameters by the Random Decrement Technique.* Proc. 16th International Seminar on Modal Analysis, Florence, Italy, Sept. 9-12, 1991.

[58] Brincker, R., Krenk, S. & Jensen, J.L. *Estimation of Correlation Functions by the Random Decrement Technique.* Proc. 9th International Modal Analysis Conference and Exhibit, Firenze, Italy, April 14-18, 1991.

1992

[59] Haddara, M.R. *On the Random Decrement for Nonlinear Rolling Motion.* 1992 OMAE, Vol. 2, Safety and Reliability, ASME 1992, pp. 321-324.

[60] Brincker, R., Krenk, S., Kirkegaard, P.H. & Rytter, A. *Identification of Dynamical Properties from Correlation Function Estimates.* Bygningsstatiske Meddelelser, Vol. 63, No. 1, 1992, pp. 1-38.

1993

[61] Bodruzzaman, M., Li, X., Wang, C. & Devgan, S. *Identifying Modes of Vibratory System Excited by Narrow Band Random Excitations.* 1993 Souteastcon '93.

[62] Tamura, Y., Sasaki, A. & Tsukagoshi, H. *Evaluation of Damping Ratios of Randomly Excited Buildings Using the Random Decrement Technique.* Journal of Structural and Construction Engineering, AIJ, No. 454, Dec. 1993. (In Japanese)

1994

[63] Brincker, R., Demosthenous, M. & Manos, G.C. *Estimation of the Coefficient of Restitution of Rocking Systems by the Random Decrement Technique.* Proc. 12th International Modal Analysis Conference, Honolulu, Hawaii, Jan 31 - Feb 3 1994.

1995

[64] Desforges, M.J., Cooper, J.E. & Wright, J.R. *Spectral and Modal Parameter Estimation From Output-Only Measurements.* Journal of Mechanical Systems and Signal Processing, Vol 9, No. 2, March 1995, pp. 169-186.

1996

[65] Asmussen, J.C. & Brincker, R. *Estimation of Frequency Response Functions by Random Decrement.* Proc. 14th International Modal Analysis Conference, Dearborn, Michigan, USA, February 1996, Vol I, pp. 246-252.

[66] Ibrahim, S.R., Asmussen, J.C. & Brincker, R. *Modal Parameter Identification from Responses of General Unkonwn Random Inputs.* Proc. 14th International Modal Analysis Conference, Dearborn, Michigan, USA, February 1996, Vol I, pp. 446-452.

[67] Asmussen, J.C., Ibrahim, S.R. & Brincker, R. *Random Decrement and Regression Analysis of Traffic Responses of Bridges.* Proc. 14th International Modal Analysis Conference, Dearborn, Michigan, USA, February 1996, Vol I, pp. 453-458.

[68] Asmussen, J.C. & Brincker, R. *Estimation of Correlation Functions by Random Decrement.* Proc. ISMA21 - Noise and Vibration Engineering, Leuven, Belgium, September 18-20 1996, Vol II, pp. 1215-1224.

1997

[69] Chalko, T.J. & Haritos, N. *Scaling Eigenvectors obtained from Ambient Excitation Modal Testing.* Proc. 15th International Modal Analysis Conference, Orlando, Florida, USA, February 3-6 1997, Vol. I, pp. 13-19.

[70] Fasana, A., Garibaldi, L., Giorcelli, E., Ruzzene, M. & Sabia, D. *Analysis of a Motorway Bridge Under Random Traffic Excitation.* Proc. 15th International Modal Analysis Conference, Orlando, Florida, USA, February 3-6 1997, Vol. I, pp. 293-300.

[71] Brincker, R. & Asmussen, J.C. *Random Decrement Based FRF Estimation.* Proc. 15th International Modal Analysis Conference, Orlando, Florida, USA, February 3-6 1997, Vol. II, pp. 1571-1576.

[72] Ibrahim, S.R., Asmussen, J.C. & Brincker, R. *Theory of Vector Triggering Random Decrement.* Proc. 15th International Modal Analysis Conference, Orlando, Florida, USA, February 3-6 1997, Vol. I, pp. 502-509.

[73] Asmussen, J.C., Ibrahim, S.R. & Brincker, R. *Application of Vector Triggering Random Decrement.* Proc. 15th International Modal Analysis Conference, Orlando, Florida, USA, February 3-6 1997, Vol. II pp. 1165-1171.

Chapter 2

Theoretical Background for Linear Structures

The purpose of this chapter is to establish the tools, which are used to extract the modal parameters from the RD functions. The following is assumed.

- The structures are time-invariant during the measurement period.
- The loads are stationary and Gaussian distributed.
- The vibrations of the structure can be modelled by a linear lumped mass parameter system.

The response of a structure to non-zero initial conditions, denoted free decays, is discussed in detail. These free decays will be derived and the different approaches to extract the modal parameters from free decays are described. Especially the practical application of these methods is considered. The argument of introducing these principles, is that on certain assumptions the RD functions are proportional to the correlation functions of the measurements. On the same assumptions the correlation functions of the response of the lumped mass parameter system to Gaussian white noise loading have exactly the same relations as the response of the model to non-zero initial conditions only. This means that the approaches developed to extract modal parameters from free decays can be used to extract modal parameters from the RD functions. This is an advantage, since methods for extracting modal parameters from free decays are well developed. The procedure does not assume that the loads are measured. The theory presented in this chapter can be seen in parts in most books on linear vibration theory and linear stochastic vibration theory, see e.g. references [1] - [7]. So during this chapter references are as a rule omitted.

Section 2.1 establishes the mathematical model of the vibrations of a linear lumped mass parameter system. The modal parameters are defined. The equations for free vibrations and forced vibrations of the structure are given. Free vibrations (or decays) correspond to the response of the structure to some non-zero initial conditions only. The forced vibrations are calculated in both time and frequency domain based on knowledge of the loads and the modal parameters.

Section 2.2 concerns identification of the parameters in the linear lumped mass parameter system from measured free decays of a structure. Two different techniques are imple-

mented and used: The Ibrahim Time Domain (ITD) technique and the Polyreference Time Domain (PTD) technique. A detailed mathematical derivation is not given, instead the implementation and the practical applications of the techniques are discussed.

Section 2.3 introduces the concepts of correlation, covariance and spectral densities. These considerations are important, since correlation functions are the link between the mathematical model and the RD functions. It is assumed that the lumped parameter system is loaded by filtered Gaussian white noise. Section 2.3.2 defines this load modelling. In section 2.3.3 it is shown that the characteristics of the filter and the system are preserved in the response of the system and remain uniquely identifiable from the correlation functions. It is shown that the correlation functions have exactly the same relations as free decays.

2.1 Lumped Mass Parameter System

This section introduces the linear lumped mass parameter systems. The main results of this section are the definition of the modal parameters, relations for calculating the forced response of the system and relations for calculating the response to non-zero initial conditions.

A lumped mass parameter system is characterized by a number of discrete masses. The number of masses is also denoted the number of dynamic Degrees Of Freedom (DOF). Each mass has stiffness and damping properties attached. An example of a 2 DOF system is shown in fig. 2.1.

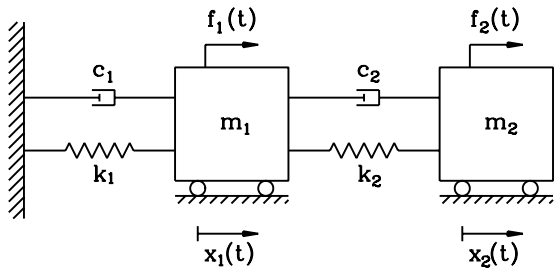

Figure 2.1: *Example of 2 DOF system.*

The system is assumed to behave linearly. The energy dissipation from the system is proportional to the velocity of the masses, and the stiffness of the structure is proportional to the displacements of the masses. The structure is thereby characterized by having viscous damping and elastic stiffness. For a general n DOF system the equations of motion become

$$\begin{aligned} &\mathbf{M}\ddot{\mathbf{x}}(t) + \mathbf{C}\dot{\mathbf{x}}(t) + \mathbf{K}\mathbf{x}(t) = \mathbf{f}(t) \\ &\mathbf{x}(0) = \mathbf{x}_0, \quad \dot{\mathbf{x}}(0) = \dot{\mathbf{x}}_0 \end{aligned} \tag{2.1}$$

This expresses a force equilibrium between external and internal forces. All matrices have the dimension $n \times n$ and the response vectors and force vector have the dimension $n \times 1$, where n is the number of DOFs. $\mathbf{M}$ is a diagonal and positive definite mass matrix. The stiffness matrix, $\mathbf{K}$, is symmetric and positive definite. The dissipation of energy

is modelled by the symmetric and positive semi-definite damping matrix $\mathbf{C}$. Although several other damping models exist, see e.g. Nashif et al. [2], the linear viscous damping model is the only one considered in this thesis. This is a widely used assumption in the modal analysis community. As indicated in eq. (2.1) the system is assumed time-invariant, since $\mathbf{M}$, $\mathbf{C}$ and $\mathbf{K}$ do not depend on time. The acceleration, velocity and displacement response are denoted $\ddot{\mathbf{x}}$, $\dot{\mathbf{x}}$ and $\mathbf{x}$, respectively.

2.1.1 Modal Decomposition of Free Decays

In order to find a solution to eq. (2.1) a state space formulation is applied

$$\begin{aligned} \mathbf{A}\dot{\mathbf{z}}(t) \; + \; \mathbf{B}\mathbf{z}(t) \; &= \; \mathbf{F}(t) \\ \mathbf{z}(0) \; &= \; \mathbf{z}_0 \\ \mathbf{x}(t) \; &= \; \mathbf{D}\mathbf{z}(t) \end{aligned} \tag{2.2}$$

where the state matrices, $\mathbf{A}$ and $\mathbf{B}$, force vector, $\mathbf{F}$, and state vector, $\mathbf{z}$ are given by

$$\mathbf{A} \; = \; \begin{bmatrix} \mathbf{C} & \mathbf{M} \\ \mathbf{M} & \mathbf{0} \end{bmatrix} \quad , \qquad \mathbf{B} = \begin{bmatrix} \mathbf{K} & \mathbf{0} \\ \mathbf{0} & -\mathbf{M} \end{bmatrix} \quad , \qquad \mathbf{D} = [\mathbf{I} \; \mathbf{0}] \tag{2.3}$$

$$\mathbf{z}(t) \; = \; \begin{bmatrix} \mathbf{x}(t) \\ \dot{\mathbf{x}}(t) \end{bmatrix} \quad , \quad \mathbf{z}_0 \; = \; \begin{bmatrix} \mathbf{x}_0 \\ \dot{\mathbf{x}}_0 \end{bmatrix} \quad , \quad \mathbf{F}(t) \; = \; \begin{bmatrix} \mathbf{f}(t) \\ \mathbf{0} \end{bmatrix} \tag{2.4}$$

The last relation in eq. (2.2) is denoted the observation matrix, since it picks out the response $\mathbf{x}(t)$ which corresponds to the measurements or observations. The matrix $\mathbf{D}$ consists of an $n \times n$ identity matrix and an $n \times n$ zero matrix. The state matrices $\mathbf{A}$ and $\mathbf{B}$ are symmetric, but not positive definite. The solution to the homogeneous part of eq. (2.2) is assumed to be of the form

$$\mathbf{z}(t) \; = \; e^{\lambda t}\mathbf{\Psi} \tag{2.5}$$

which inserted into eq. (2.2) yields the standard eigenvalue problem of dimension $2n \times 2n$

$$(\lambda\mathbf{A} + \mathbf{B})\mathbf{\Psi} \; = \; \mathbf{0} \tag{2.6}$$

The solution of the eigenvalue problem gives $2n$ eigenvalues, λ_i, and $2n$ corresponding eigenvectors, $\mathbf{\Psi}_i$, i=1,2,...,$2n$. It is assumed that all eigenvalues are distinct, which means that there are no repeatedly eigenvalues. Most structures are characterized by being critically underdamped. This means that the eigenvalues and the eigenvectors will be complex. The structures are assumed to be dissipative, so the real part of the eigenvalues must be negative. The eigenvalues and the eigenvectors, which can only be calculated except for a constant scaling factor, appear as complex conjugated pairs. The complex eigenvalue, λ_i, is physically interpreted by considering the complex numbers arising from the solution of the homogeneous part of eq. (2.1) for a critically underdamped SDOF system.

$$\begin{aligned} \lambda_i \quad &= \; -\zeta_i\omega_i \; - \; \omega_i\sqrt{1-\zeta_i^2}j \\ \lambda_{i+1} \; &= \; -\zeta_i\omega_i \; + \; \omega_i\sqrt{1-\zeta_i^2}j \end{aligned} \tag{2.7}$$

where $j = \sqrt{-1}$, ω_i is the undamped cyclic eigenfrequency and ζ_i is the modal damping ratio associated with the ith mode. The system is critically underdamped if $\zeta_i < 1$.

The eigenvectors have the following form due to eq. (2.5)

$$\mathbf{\Psi}_i \;=\; \begin{bmatrix} \mathbf{\Phi}_i \\ \lambda_i \mathbf{\Phi}_i \end{bmatrix} \qquad \mathbf{\Phi}_i \;=\; \mathbf{D}\mathbf{\Psi}_i \tag{2.8}$$

The vector $\mathbf{\Phi}$ is denoted the mode shape vector. Equations (2.7) and (2.8) defines the modal parameters of the lumped mass parameter system. Estimation of these parameters is the main task in modal analysis. The displacements, $\mathbf{x}(t)$, are taken as the upper half of the state vector, $\mathbf{z}(t)$, computed as the sum of all solutions to the homogeneous equation given by eq. (2.5), where the parameters are given by the solutions to the eigenvalue in eq. (2.6).

$$\mathbf{z}(t) \;=\; \mathbf{\Psi} e^{\mathbf{\Lambda} t} \mathbf{q}_0 \tag{2.9}$$

The following matrices have been introduced

$$\mathbf{\Psi} = [\mathbf{\Psi}_1 \;\; \mathbf{\Psi}_2 \;..\; \mathbf{\Psi}_{2n}] \;\; e^{\mathbf{\Lambda} t} = diag([e^{\lambda_1 t} \;\; e^{\lambda_2 t} \;..\; e^{\lambda_{2n} t}]) \;\; \mathbf{q}_0 = [q_{1,0} \;\; q_{2,0} \;..\; q_{2n,0}]^T \tag{2.10}$$

where $\mathbf{q}_0$ contains the modal initial conditions and $\mathbf{\Psi}$ is denoted the modal matrix.

The following orthogonality relations of the state matrices $\mathbf{A}$ and $\mathbf{B}$ can be shown using the symmetry relations of the state matrices only. These relations are introduced in order to derive the response of the system

$$\mathbf{\Psi}^T \mathbf{A} \mathbf{\Psi} = \mathbf{m} \;, \qquad \mathbf{m} \;=\; diag([m_1 \;\; m_2 \;\; ... \;\; m_{2n}]) \tag{2.11}$$

$$\mathbf{\Psi}^T \mathbf{B} \mathbf{\Psi} = -\mathbf{\Lambda}\mathbf{m} \;, \quad -\mathbf{\Lambda}\mathbf{m} \;=\; diag(-[\lambda_1 m_1 \;\; \lambda_2 m_2 \;\; ... \;\; \lambda_{2n} m_{2n}]) \tag{2.12}$$

$$\mathbf{\Lambda} \;=\; diag([\lambda_1 \;\; \lambda_2 \;\; ... \;\; \lambda_{2n}]) \tag{2.13}$$

The constants m_i are denoted modal masses. The modal initial conditions, $\mathbf{q}_0$, can be calculated from eq. (2.9) by combining the initial conditions from eq. (2.2) and the orthogonality condition in eq. (2.11).

$$\mathbf{q}_0 \;=\; \mathbf{m}^{-1} \mathbf{\Psi}^T \mathbf{A} \mathbf{z}_0 \tag{2.14}$$

The displacements, velocity and acceleration response of the lumped mass parameter system to initial conditions become

$$\mathbf{x}(t) \;=\; \mathbf{\Phi} e^{\mathbf{\Lambda} t} \mathbf{q}_0 \tag{2.15}$$

$$\dot{\mathbf{x}}(t) \;=\; \mathbf{\Phi} e^{\mathbf{\Lambda} t} \mathbf{\Lambda} \mathbf{q}_0 \tag{2.16}$$

$$\ddot{\mathbf{x}}(t) \;=\; \mathbf{\Phi} e^{\mathbf{\Lambda} t} \mathbf{\Lambda}^2 \mathbf{q}_0 \tag{2.17}$$

As seen, the difference between the free decay displacement response, velocity response and acceleration response is only a complex scaling factor in form of the eigenvalue matrix, $\mathbf{\Lambda}$. This scaling factor changes the amplitude and the phase of the exponentially damped sinusoidal free decay response. The relations are important, since the modal parameters can be extracted from all free decay responses in eqs. (2.15) - (2.17) using the same algorithm, which will be illustrated in section 2.2.

2.1.2 Forced Vibration

The forced vibration of a linear lumped parameter system is calculated using a reformulation of the state response by inserting the modal matrix

$$\mathbf{z}(t) \;=\; \mathbf{\Psi q}(t) \tag{2.18}$$

where $\mathbf{q}(t)$ is defined equivalently to $\mathbf{q}_0$ in eq. (2.10)

$$\mathbf{q}(t) \;=\; [q_1(t)\; q_2(t)\; ...\; q_{2n}(t)]^T \tag{2.19}$$

Inserting the above relation in eq. (2.2), multiplying on the right hand side by $\mathbf{\Psi}^T$ and using the orthogonality relations in eqs. (2.11) - (2.12) yields

$$\dot{\mathbf{q}}(t) \;-\; \mathbf{\Lambda q}(t) \;=\; \mathbf{m}^{-1}\mathbf{\Psi}^T\mathbf{F}(t) \tag{2.20}$$

The solution to these decoupled differential equations is given by the convolution integral and the initial condition

$$\mathbf{q}(t) \;=\; \int_{-\infty}^{t} e^{\mathbf{\Lambda}(t-\tau)}\mathbf{m}^{-1}\mathbf{\Psi}^T\mathbf{F}(\tau)d\tau \;+\; e^{\mathbf{\Lambda}t}\mathbf{q}_0 \tag{2.21}$$

Using eq. (2.18) the response of the system becomes

$$\mathbf{z}(t) \;=\; \int_{-\infty}^{t} \mathbf{h}(t-\tau)\mathbf{F}(\tau)d\tau \;+\; \mathbf{\Psi}e^{\mathbf{\Lambda}t}\mathbf{q}_0 \tag{2.22}$$

where the Impulse Response Matrix (IRM) has been defined as

$$\mathbf{h}(t) \;=\; \mathbf{\Psi}e^{\mathbf{\Lambda}t}\mathbf{m}^{-1}\mathbf{\Psi}^T\;, \quad t \geq 0 \qquad \mathbf{h}(t) \;=\; 0\;, \quad t < 0 \tag{2.23}$$

Equation (2.22) is transformed into the frequency domain using the Fourier transformation. It is assumed that the response due to the non-zero initial conditions can be neglected

$$\mathbf{z}(\omega) \;=\; \mathbf{H}(\omega)\mathbf{F}(\omega) \tag{2.24}$$

where

$$\mathbf{z}(\omega) \;=\; \frac{1}{2\pi}\int_{-\infty}^{\infty} \mathbf{z}(t)e^{-i\omega t}dt \tag{2.25}$$

$$\mathbf{F}(\omega) \;=\; \frac{1}{2\pi}\int_{-\infty}^{\infty} \mathbf{F}(t)e^{-i\omega t}dt \tag{2.26}$$

$$\mathbf{H}(\omega) \;=\; \int_{-\infty}^{\infty} \mathbf{h}(t)e^{-i\omega t}dt \;=\; \int_{0}^{\infty} \mathbf{h}(t)e^{-i\omega t}dt \tag{2.27}$$

$$\mathbf{H}(\omega) \;=\; \mathbf{\Psi}\mathbf{m}^{-1}(i\omega - \mathbf{\Lambda})^{-1}\mathbf{\Psi}^T \tag{2.28}$$

The matrix, $\mathbf{H}(\omega)$, is denoted the Frequency Response Matrix (FRM). The relation in eq. (2.24) is important, since it establishes a simple way of estimating the FRM of the system if the response and the load are measured and transformed into the frequency domain. As seen, the FRM contains exactly the same information in the form of modal parameters as the IRF. This relation is used as a basis for the RD technique applied to measured response and load. This issue is investigated in chapter 6. The modal parameters can be extracted from the FRM or the IRM. The IRM and FRM are constructed so that it is only necessary to know a row or a column in order to extract modal parameters.

The IRM and FRM transferring the load, $\mathbf{f}(t)$, into the response $\mathbf{x}(t)$ are given directly from the IRM and FRM in eqs. (2.23) and (2.28)

$$\mathbf{h}(t) \;=\; \mathbf{\Phi} e^{\mathbf{\Lambda} t} \mathbf{m}^{-1} \mathbf{\Phi}^T \;, \quad t \geq 0 \qquad \mathbf{h}(t) = 0 \;, \quad t < 0 \qquad \mathbf{h}(t) \;=\; \mathbf{h}^T(t) \tag{2.29}$$

$$\mathbf{H}(\omega) \;=\; \mathbf{\Phi}(i\omega - \mathbf{\Lambda})^{-1} \mathbf{m}^{-1} \mathbf{\Phi}^T \qquad \mathbf{H}(\omega) \;=\; \mathbf{H}^T(\omega) \tag{2.30}$$

Until now it has been assumed that the response of all masses in the lumped parameter system is measured or observed. Usually the number of modes is higher than the number of known responses. This can be modelled by changing the observation equation. If e.g. a system with $2n$ degrees of freedom is measured at m locations the observation equation becomes

$$\mathbf{x}(t) = \mathbf{D}\mathbf{z}(\mathbf{t}) \qquad \mathbf{D} \;=\; [\mathbf{I}\ \mathbf{0}\ \mathbf{0}] \tag{2.31}$$

where the identity matrix has the dimensions $m \times m$, the first zero matrix has the dimensions $n - m \times n - m$ and the second zero matrix has dimensions $n \times n$. The relation between the modal matrices $\mathbf{\Psi}$ and $\mathbf{\Phi}$ still holds

$$\mathbf{\Phi} \;=\; \mathbf{D}\mathbf{\Psi} \tag{2.32}$$

Equations (2.15) - (2.17), (2.23) and (2.27) all contain information about the modal parameters. This means that if any of these functions/matrices are known the modal parameters can be extracted. In the next section it is described how modal parameters can be extracted from free decays using eqs. (2.15) - (2.17) in practice. The motivation is that these methods can be used to extract modal parameters from the RD functions. This relation will be shown in section 2.3.

2.2 Identification of Modal Parameters From Free Decays

This section introduces the principles behind two different algorithms for extracting modal parameters from free decays. Several different algorithms have been developed. In Fladung et al. [8] the different algorithms are reviewed and compared. In this thesis two different algorithms, the Ibrahim Time Domain (ITD) technique, see e.g. Ibrahim [9] and the Polyreference Time Domain (PTD) technique, see e.g. Vold et al. [10], are implemented and applied. In the following, the algorithms are described in general terms and the practical use of these algorithms for identification of the modal parameters from free decays

is explained. It is not the intention to present a detailed mathematical derivation of the algorithms. The interested reader is referred to the original papers, where the algorithms have been introduced. The aim is to present the philosophy behind the implementation and the application of these algorithms.

Figure 2.2 shows a diagram for extraction of modal parameters from free decays using ITD or PTD.

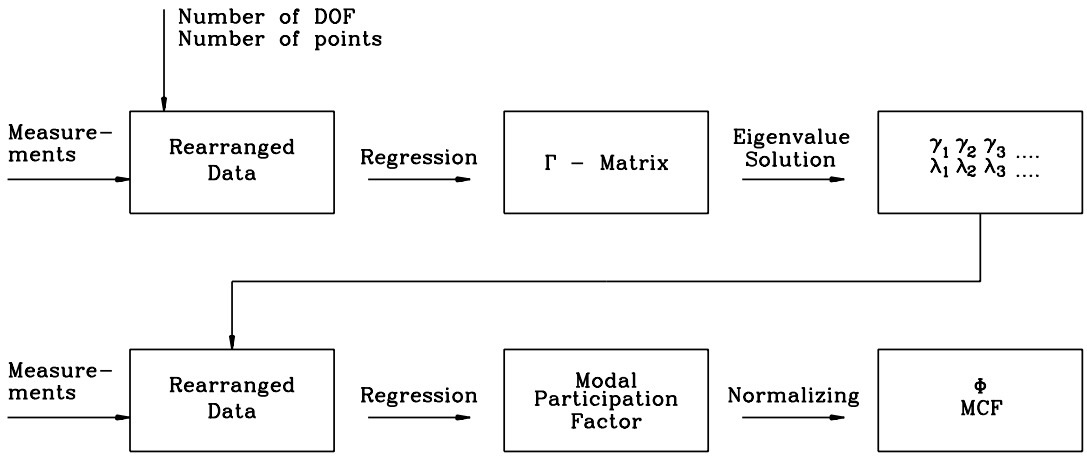

Figure 2.2: *Diagram for extracting modal parameters from free decay measurements.*

The first step is to rearrange the measurements to obtain an overdetermined system for estimation of the $\mathbf{\Gamma}$-matrix. The eigenvalues of the $\mathbf{\Gamma}$-matrix are directly related to the eigenvalues of the continuous-time system, see eq. (2.7). The $\mathbf{\Gamma}$-matrix is defined and the procedure is shown in sections 2.2.1 and 2.2.2. In section 2.2.3 it is discussed how the noise present in the free decay measurements is modelled and in section 2.2.4 the extraction of eigenfrequencies and damping ratios from the $\mathbf{\Gamma}$-matrix is shown. Section 2.2.5 describes how the mode shapes are estimated from the measurements by introduction of the Modal Participation Factors (MPF). Sections 2.2.6 and 2.2.7 describe the practical application and the methods used to separate noise modes from physical modes.

2.2.1 General Equations

The difference between the two algorithms is that the ITD technique has its starting point in eqs. (2.15) - (2.17) and the PTD technique has its starting point in eq. (2.23). However, for convenience the following description has its starting point in eqs. (2.15) - (2.17) but this choice has no influence on the principles. Common to both algorithms is that the measured free decays are assumed to be instantaneously sampled at equidistant time points. The interval between the sampling points is denoted the sampling period, ΔT. If the response of a structure is sampled simultaneously at n different channels in N time points, the measured response, $\mathbf{x}$, is assumed to be of the following form

$$\mathbf{x}(k\Delta T) = \mathbf{\Phi} e^{\mathbf{\Lambda}(k\Delta T)}\mathbf{q}_0 = \mathbf{\Phi}\mathbf{\Gamma}^k\mathbf{q}_0 \qquad k = 0, 1, 2, ..., N-1 \tag{2.33}$$

$$\dot{\mathbf{x}}(k\Delta T) = \mathbf{\Phi} e^{\mathbf{\Lambda}(k\Delta T)}\mathbf{\Lambda}\mathbf{q}_0 = \mathbf{\Phi}\mathbf{\Gamma}^k\mathbf{\Lambda}\mathbf{q}_0 \qquad k = 0, 1, 2, ..., N-1 \tag{2.34}$$

$$\ddot{\mathbf{x}}(k\Delta T) \;=\; \mathbf{\Phi} e^{\mathbf{\Lambda}(k\Delta T)}\mathbf{\Lambda}^2\mathbf{q}_0 \;=\; \mathbf{\Phi}\mathbf{\Gamma}^k\mathbf{\Lambda}^2\mathbf{q}_0 \qquad k = 0,1,2,...,N-1 \tag{2.35}$$

where the matrix $\mathbf{\Gamma}$ has been introduced

$$\mathbf{\Gamma} \;=\; e^{\mathbf{\Lambda}\Delta T} \;=\; diag([e^{\lambda_1\Delta T}\; e^{\lambda_2\Delta T}\; e^{\lambda_{2n}\Delta T}]) \tag{2.36}$$

In order to model a system where the number of modes, $2m$, differs from the number of known responses, n, the size of the modal matrix, $\mathbf{\Phi}$, is given by the size of the observation matrix $\mathbf{D}$ in the observation equation, see eqs. (2.2) and (2.32). However, eqs. (2.33) - (2.35) can be rewritten in order to obtain a relation for the responses at l time points later

$$\mathbf{x}((k+l)\Delta T) = \mathbf{\Phi}\mathbf{\Gamma}^l\mathbf{\Gamma}^k\mathbf{q}_0 \tag{2.37}$$

$$\dot{\mathbf{x}}((k+l)\Delta T) = \mathbf{\Phi}\mathbf{\Gamma}^l\mathbf{\Gamma}^k\mathbf{\Lambda}\mathbf{q}_0 \tag{2.38}$$

$$\ddot{\mathbf{x}}((k+l)\Delta T) = \mathbf{\Phi}\mathbf{\Gamma}^l\mathbf{\Gamma}^k\mathbf{\Lambda}^2\mathbf{q}_0 \tag{2.39}$$

In general the above relations form the basis of the ITD technique and the PTD technique. They illustrate that the present free decay response can be expressed as a function of past free decay response using the time difference, $l\Delta t$ and the $\mathbf{\Gamma}$-matrix, which contains information about the frequencies and damping ratios of the modes. This relation is valid no matter if the displacement, velocity or acceleration responses are measured. The difference in the form of the $\mathbf{\Gamma}$-matrix is simply interpreted as another set of initial conditions. This makes the algorithms versatile.

In the formulation of the ITD and PTD algorithm on the basis of eqs. (2.37) - (2.39) different demands on the ratio between the number of measurement points and the number of modes exist. This is a clear delimitation to these techniques, since the number of modes is dependent on the number of measurement points. In order to lift this restriction the concept of pseudo measurements was introduced, see Ibrahim [9].

2.2.2 Pseudo Measurements

The idea is to create pseudo measurements by time delaying a number of true measurements in order to increase the total number of measurements. Using this approach the number of modes, which it is possible to use in the model, becomes totally independent of the actual number of measurements.

Consider an mDOF system, where the free decay response has been measured at n_1 points and $n_1 + n_2 = m$. If e.g. the displacement response is measured eq. (2.33) becomes

$$\mathbf{x}(k\Delta T) \;=\; \mathbf{\Phi}\mathbf{\Gamma}^k\mathbf{q}_0 \qquad \begin{matrix}\mathbf{x} & \mathbf{\Phi} & \mathbf{\Gamma}^k & \mathbf{q}_0 \\ n_1\times 1 & n_1\times 2m & 2m\times 2m & 2m\times 1\end{matrix} \tag{2.40}$$

A second measurement vector denoted the pseudo measurements is constructed

$$\mathbf{x}_1((k+l)\Delta T) \;=\; \mathbf{\Phi_1}\mathbf{\Gamma}^l\mathbf{\Gamma}^k\mathbf{q}_0 \qquad \begin{matrix}\mathbf{x} & \mathbf{\Phi_1}\mathbf{\Gamma}^l & \mathbf{\Gamma}^k & \mathbf{q}_0 \\ n_2\times 1 & n_2\times 2m & 2m\times 2m & 2m\times 1\end{matrix} \tag{2.41}$$

The $\mathbf{x}_1$ vector is only the time delayed version of the first n_2 points of $\mathbf{x}$. Stacking these measurements yields an equation where the modal matrix has the same dimensions as the $\mathbf{\Gamma}$-matrix

$$\begin{bmatrix} \mathbf{x}(k\Delta T) \\ \mathbf{x}_1((k+l)\Delta T) \end{bmatrix} = \begin{bmatrix} \mathbf{\Phi} \\ \mathbf{\Phi}\mathbf{\Gamma}^l \end{bmatrix} \mathbf{\Gamma}^k \mathbf{q}_0 = \underset{2m \times 2m}{\tilde{\mathbf{\Phi}}} \quad \underset{2m \times 2m}{\mathbf{\Gamma}^k} \quad \underset{2m \times 1}{\mathbf{q}_0} \tag{2.42}$$

The example illustrates how the concept of pseudo measurements can be used to fulfil any demand of the algorithms to the ratio between the size of the measurement vector and the number of modes. It is possible to use any number of modes independently of the actual number of measurements.

2.2.3 Modelling of Noise

Since any free decay measurement contains noise, the theoretical expression for a free decay has to be reformulated to include the differences between the mathematical model and the measurements.

$$\hat{\mathbf{x}}(k\Delta T) = \mathbf{x}(k\Delta T) + \mathbf{e}(k\Delta T) = \mathbf{\Phi}\mathbf{\Gamma}^k\mathbf{q}_0 + \mathbf{e}(k\Delta T) \tag{2.43}$$

where the vector $\mathbf{e}(k\Delta T)$ is added in order to model the differences between the measurements and the theoretical predictions. So the process $\mathbf{e}(k\Delta T)$ consists of measurement noise, differences arising if the mathematical model is incorrect, etc. This means that the differences $\mathbf{e}(k\Delta T)$ should be modelled as a stochastic process. This is not the case for the ITD and PTD algorithms. The influence of $\mathbf{e}(t)$ is minimized by extending the dimensions of the problem by assuming that a part of the noise behaves exactly as the free decays of the structure. The principle is that the model in eq. (2.43) is extended by a number of noise modes

$$\begin{aligned} \hat{\mathbf{x}}(k\Delta T) &= \tilde{\mathbf{\Phi}}\tilde{\mathbf{\Gamma}}^k\hat{\mathbf{q}}_0 \\ &= [\mathbf{\Phi}\ \mathbf{\Phi}_n] \begin{bmatrix} \mathbf{\Gamma}^k & \mathbf{0} \\ \mathbf{0} & \mathbf{\Gamma}_n^k \end{bmatrix} \begin{bmatrix} \mathbf{q}_0 \\ \mathbf{q}_{0,n} \end{bmatrix} \\ &= \mathbf{\Phi}\mathbf{\Gamma}^k\mathbf{q}_0 + \mathbf{\Phi}_n\mathbf{\Gamma}_n^k\mathbf{q}_0^n \end{aligned} \tag{2.44}$$

Subscript n indicates that the modal parameters originates from noise modes. So the differences at any time step are assumed to be modelled as

$$\mathbf{e}(k\Delta T) = \mathbf{\Phi}_n\mathbf{\Gamma}_n^k\mathbf{q}_{0,n} \tag{2.45}$$

This modelling of noise results in estimation of both physical and computational noise modes. In practice noise modes which have negative damping ratios and/or do not appear as complex conjugated pairs are often observed. A method or procedure to separate the physical modes from the computational modes has to be applied. This issue is discussed in section 2.2.7. A major problem in the application of the ITD and PTD algorithms is to choose the number of noise modes.

2.2.4 Extraction Eigenfrequencies and Damping Ratios

Once the $\mathbf{\Gamma}$-matrix has been estimated the eigenvalues can be calculated. These eigenvalues are denoted the discrete-time eigenvalues, γ_i. The continuous-time eigenvalues are calculated from the discrete-time eigenvalues and the time difference between the measurements

$$\mathbf{\Gamma} \;=\; diag([e^{\lambda_1 \Delta T}\; e^{\lambda_2 \Delta T}\; e^{\lambda_{2n} \Delta T}]) \qquad \Rightarrow \qquad \lambda_i \;=\; \frac{\ln(\gamma_i)}{\Delta T} \tag{2.46}$$

The damping ratios and the eigenfrequencies are extracted from the continuous-time eigenvalues using eq. (2.7).

2.2.5 Modal Participation Factors

The mode shapes of the structure are calculated from eqs. (2.37) - (2.39) using regression. The approach is to reformulate the equations and use the already estimated eigenvalues. For example for the displacement response

$$\mathbf{x}((k+1)\Delta t) \;=\; \mathbf{\Phi \Gamma}^{k+l}\mathbf{q}_0 \;=\; \mathbf{\Phi}\tilde{\mathbf{q}}_0\tilde{\mathbf{\Gamma}}^{k+l} \tag{2.47}$$

where

$$\tilde{\mathbf{q}}_0 \;=\; diag([q_{1,0}\; q_{2,0}\; ...\; q_{2n,0}]) \qquad \tilde{\mathbf{\Gamma}} \;=\; [e^{\lambda_1 \Delta t}\; e^{\lambda_2 \Delta t}\; ...\; e^{\lambda_{2n} \Delta t}\; ...\;]^T \tag{2.48}$$

and it has been utilized that $\mathbf{\Gamma}$ is a diagonal matrix. Equation (2.47) constitutes a basis for the determination of the MPFs using regression, since both the measurements on the left-hand side and the eigenvalue vector, $\tilde{\mathbf{\Gamma}}$ on the right-hand side are known. The MPFs are defined as follows for the displacement, velocity and acceleration response, respectively

$$\text{MPF}_x \;=\; \mathbf{\Phi}\tilde{\mathbf{q}}_0 \tag{2.49}$$

$$\text{MPF}_{\dot{x}} \;=\; \mathbf{\Phi \Lambda}\tilde{\mathbf{q}}_0 \tag{2.50}$$

$$\text{MPF}_{\ddot{x}} \;=\; \mathbf{\Phi \Lambda}^2\tilde{\mathbf{q}}_0 \tag{2.51}$$

As seen, each mode has an MPF value at each measurement location. The mode shapes are extracted from the MPFs using column-wise normalization, since $\mathbf{\Lambda}$ and $\tilde{\mathbf{q}}_0$ are only a scaling of the mode shapes. The absolute value of the MPFs are not only a function of the mode shapes, but also of the modal initial conditions and the eigenvalues.

2.2.6 Practical Application

In the application of the algorithms for extraction of modal parameters from free decays several questions must always be answered: How many modes do the measurements contain? How many noise modes should be added in order to model the noise? How many points from the measured free decays should be used? In order to investigate the influence of the chosen number of modes and the number of points from the free decay measurements different combinations of the number of modes and the number of points are used in the modal parameter identification algorithms. The following flow chart illustrates the approach using different models.

- Loop 1 (i):
- Number of modes = function(i)
  - Loop 2 (j):
  - Number of points = function(j)
  - Calculate modal parameters (function(i),function(j))
  - End loop 2 (j)
- End Loop 1 (i).

Using a stabilization diagram, which is a plot of the estimated frequencies versus the identification number, the structural modes can be detected and a final appropriate identification number (number of points and number of modes) can be found. A structural mode should be represented in all identifications, so a trend will be visible at the structural modes.

If it is necessary to use many modes it is not always sufficient to use a stabilization diagram in order to detect structural modes. Therefore, different methods to separate noise modes from physical modes are applied.

2.2.7 Separation of Noise Modes and Physical Modes

Noise modes are distinguished from physical modes by a combined application of five different approaches

- Complex conjugated pairs.
- Damping ratios.
- Modal Participation Factors (MPFs).
- Modal Confidence Factors (MCFs).
- Modal Assurence Criteria (MAC).

The first four approaches are most frequently applied since they can separate noise modes from physical modes from a single model, whereas the MAC uses comparison of mode shapes of different models. In the following the different methods are described.

Complex conjugated pairs

As described previously, structural modes are usually critically underdamped so they appear as complex conjugated pairs. If any eigenvalue does not have a complex conjugate it is interpreted as a noise mode.

Damping ratios

Usually, structural modes have low damping. This information can be used to separate noise modes from structural modes. Modes with e.g. $\zeta > 0.05$ or $\zeta > 0.1$ can be characterized as noise modes.

Modal Participation Factors

The MPFs defined in eqs. (2.49) - (2.51) can also be used to separate noise modes from physical modes. If a mode has a low MPF at all measurement points, it indicates that the mode is a noise mode. Physical modes can have low MPFs if the mode shape has a low amplitude, but not at all measurement points. The MPFs should, however, be used carefully in connection with measurements having a low signal-to-noise ratio. In such a situation the noise modes might generally have as high MPFs as the structural modes.

Modal Confidence Factors

Perhaps the most efficient approach to distinguish between noise modes and physical modes is to use the MCFs. The philosophy behind this approach was presented in Ibrahim [11] and extended to the PTD technique by Vold et al. [12]. Assume that the eigenvalues have been estimated. In order to calculate the MCFs the measurements are time delayed and stacked

$$\begin{bmatrix} \mathbf{x}(k\Delta T) \\ \mathbf{x}((k+l)\Delta T) \end{bmatrix} = \begin{bmatrix} \mathbf{\Phi} \\ \mathbf{\Phi}\mathbf{\Gamma}^l \end{bmatrix} \mathbf{\Gamma}^k \mathbf{q}_0 = \begin{bmatrix} \mathbf{\Phi} \\ \mathbf{\Phi}^l \end{bmatrix} \mathbf{\Gamma}^k \mathbf{q}_0 \tag{2.52}$$

The eigenvalue matrix $\mathbf{\Gamma}$ is known so the mode shape matrix can be calculated using regression as described in section 2.2.5. The modal initial conditions only involve a column-wise scaling of the mode shapes. The MCF of the ith component of the jth mode shape is calculated as

$$\mathrm{MCF}_{i,j} = \frac{\hat{\mathbf{\Phi}}_{i,j} \cdot \mathbf{\Gamma}^l_{j,j}}{\hat{\mathbf{\Phi}}^l_{i,j}} \quad |\mathrm{MCF}_{i,j}| > 1 \ , \quad \mathrm{MCF}_{i,j} = \frac{1}{\mathrm{MCF}_{i,j}} \tag{2.53}$$

Theoretically all the MCFs should be unity. In practice the MCFs will approximately be unity for structural modes and lower for non-structural modes. If the magnitude of an MCF is higher than unity, the reciprocal value is used. In general the MCFs are complex numbers, so a phase and an magnitude, which should be zero and unity, respectively, are defined and used.

In a practical situation the following restrictions could be applied in order to characterize a mode as a structural mode.

- The eigenvalue of the mode should have a complex conjugate.
- The damping ratio should be below 10 %.
- The MCF magnitude should be above 90 %.
- The MCF phase should be below 10°.

Notice that the numbers are a result of the experience obtained by analysing the structures described in this thesis and can only be considered as guidelines. Especially the MCFs are capable of separating noise and structural modes. The decision of the criteria applied to the damping ratios should be obtained from experience with the present structure.

To separate the physical modes from the noise modes the approaches described above are applied first. Then a stabilization diagram is used. Such a diagram is a simple plot of the estimated frequencies versus the model number. A structural mode should not depend on the model chosen (the number of modes and the number of points used from the free decays). So a trend is visible at the frequency of a structural modes. Stabilization diagrams are usually a very efficient method in combinations with the other methods to extract the structural modes. Stabilization diagrams also give an indication of the optimal choice of model structure.

Modal Assurance Criteria

The last-mentioned approach used for selecting structural modes is the Modal Assurance Criteria (MAC). This is a correlation coefficient between two different mode shapes

$$\text{MAC} \;=\; \frac{|\boldsymbol{\Phi}_j^T \boldsymbol{\Phi}_i|^2}{|\boldsymbol{\Phi}_j|^2 |\boldsymbol{\Phi}_i|^2} \tag{2.54}$$

The idea is that the mode shape of a structural mode should not change significantly with a small change in the model structure. A noise mode may change with just a slight change in the model structure, so noise modes will have a low correlation. The MAC can also be used to compare two mode shapes estimated from two different approaches such as the RD technique or a technique based on the FFT algorithm. This option will be used later in this thesis.

2.3 Structures Loaded by Gaussian White-Noise

The purpose of this section is to describe the modelling of the loads on the linear lumped mass system. The concept of correlation functions is also defined. This makes it possible to derive the correlation functions of the response of the linear lumped mass parameter system subjected to the loads. It is shown that these correlation functions are constructed corresponding to the free decays of the system. This means that on the given assumptions of the load and the structure, the modal parameters can be extracted without any knowledge of the realization of the load. Only the response has to be measured.

2.3.1 Correlation Functions

Consider a stationary stochastic vector process $\mathbf{X}(t)$. The correlation functions of the vector process are defined as

$$\mathbf{R}_{\mathbf{XX}}(\tau) \;=\; E[\mathbf{X}(t+\tau)\mathbf{X}^T(t)] \tag{2.55}$$

It will be assumed that the vector process has zero mean value vector. This implies that there is no difference between the correlation functions and the covariance functions

$$\mathbf{V}_{\mathbf{XX}}(\tau) \;=\; \mathbf{R}_{\mathbf{XX}}(\tau) \;-\; E[\mathbf{X}(t)]E[\mathbf{X}(t)]^T \;=\; \mathbf{R}_{\mathbf{XX}}(\tau) \tag{2.56}$$

The term *correlation* function is preferred. For stationary processes the following symmetry relation is valid

$$\mathbf{R}_{\mathbf{XX}}(\tau) \;=\; \mathbf{R}_{\mathbf{XX}}^T(-\tau) \tag{2.57}$$

The correlation functions of the time derivatives of the process $\mathbf{X}(t)$ can be calculated from the correlation functions of $\mathbf{X}(t)$ using the following differential rules

$$\mathbf{R}_{\dot{\mathbf{X}}\dot{\mathbf{X}}}(\tau) = -\frac{d^2}{d\tau}(\mathbf{R}_{\mathbf{XX}}(\tau)) \qquad \mathbf{R}_{\ddot{\mathbf{X}}\ddot{\mathbf{X}}}(\tau) = \frac{d^4}{d\tau}(\mathbf{R}_{\mathbf{XX}}(\tau)) \tag{2.58}$$

The spectral densities are defined by the Wiener-Khintchine relations. These relations link the correlation functions and the power spectral densities using Fourier transformation. The spectral densities $\mathbf{S}_{\mathbf{XX}}(\tau)$ can be calculated from the correlation functions by

$$\mathbf{S}_{\mathbf{XX}}(\omega) = \frac{1}{2\pi}\int_{-\infty}^{\infty}\mathbf{R}_{\mathbf{XX}}(\tau)e^{-i\omega\tau}d\tau \tag{2.59}$$

$$\mathbf{R}_{\mathbf{XX}}(\tau) = \int_{-\infty}^{\infty}\mathbf{S}_{\mathbf{XX}}(\omega)e^{i\omega\tau}d\omega \tag{2.60}$$

The definition of spectral densities using eq. (2.59) and the definition via finite Fourier transforms presented in chapter 1 are equivalent, see e.g. Bendat & Piersol [3].

2.3.2 Load Modelling

The load which excites the lumped mass parameter system is assumed to be a stationary zero mean Gaussian distributed vector process, see eq. (A.1). In order to generalize the load process it is assumed that the load process can be described as a white noise vector process passed through a linear shaping filter. This is an extension of the traditional white noise assumption. The idea behind this approach and the theory are presented in Ibrahim et al. [13], where the filter is referred to as a pseudo-force filter. The principle is shown in figure 2.3.

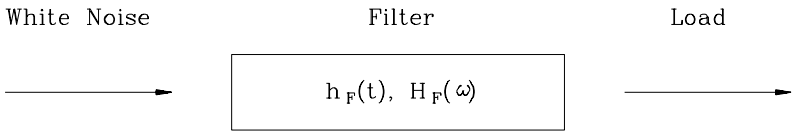

Figure 2.3: *Outline diagram for modelling of loads using a shaping filter. $h(t)$ and $H(\omega)$ are the IRM and FRM, respectively*

$\mathbf{W}$ is a Gaussian white noise process having the following statistical relations

$$E[\mathbf{W}(t)] = \mathbf{0} \tag{2.61}$$

$$E[\mathbf{W}(t+\tau)\mathbf{W}^T(t)] = \mathbf{R}_{\mathbf{WW}}\cdot\delta(\tau) \tag{2.62}$$

$$\mathbf{S}_{\mathbf{WW}}(\omega) = \frac{1}{2\pi}\mathbf{R}_{\mathbf{WW}} \tag{2.63}$$

The FRM and IRM of the shaping filter are assumed to be given by eqs. (2.64) - (2.65). Subscript F indicates that the matrices describe the filter characteristics

$$\mathbf{H}_F(\omega) = \mathbf{\Phi}_F(i\omega - \mathbf{\Lambda}_F)^{-1}\mathbf{m}_F^{-1}\mathbf{\Phi}_F^T \qquad \mathbf{H}_F(\omega) = \mathbf{H}_F^T(\omega) \tag{2.64}$$

$$\mathbf{h}_F(t) = \mathbf{\Phi}_F e^{\mathbf{\Lambda}_F(t)}\mathbf{m}_F^{-1}\mathbf{\Phi}_F^T \qquad \mathbf{h}_F(t) = \mathbf{h}_F^T(t) \tag{2.65}$$

where $\mathbf{m}_F$ is an $m \times m$ normalization corresponding to the modal masses in eq. (2.11), $\mathbf{\Phi}_F$ is an $n \times m$ matrix containing the modal vectors corresponding to eq. (2.8) and $\mathbf{\Lambda}_F$ is an $m \times m$ diagonal matrix containing the eigenvalues. The real part of all eigenvalues is negative. This ensures that the resulting force is stationary. The force exciting the structure is modelled by

$$\mathbf{f}(\omega) = \mathbf{H}_F(\omega)W(\omega) \tag{2.66}$$

$$\mathbf{f}(t) = \int_{-\infty}^{t} \mathbf{h}_F(t-\tau)W(\tau)d\tau \tag{2.67}$$

In order to illustrate the significance of a shaping filter the auto spectral densitity and auto correlation function of the white noise process and the resulting force obtained by filtering the Gaussian white noise process are given in fig. 2.4.

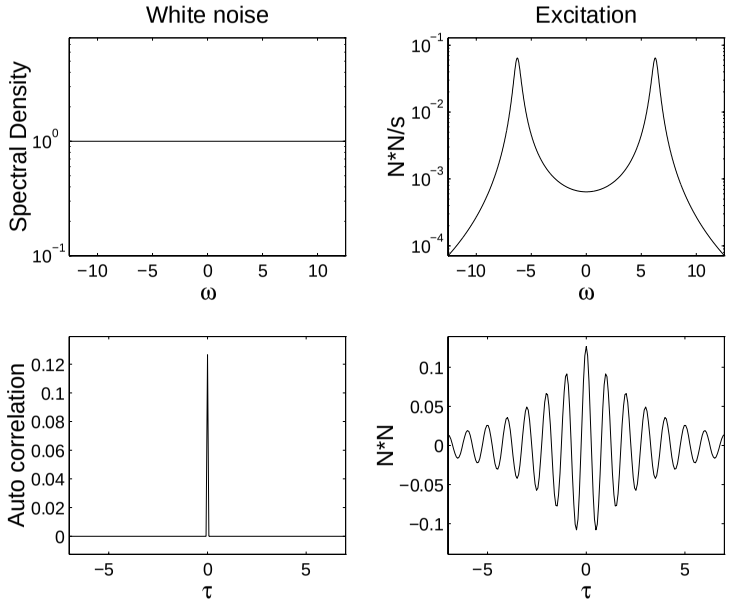

Figure 2.4: *The effect of modelling the excitation as a filtered white noise process, where the filter has an SDOF.*

Since $\mathbf{W}(t)$ is Gaussian distributed it also follows that the load applied to the structure, $\mathbf{f}(t)$, is Gaussian. The filter performs linear operations to the white noise process $\mathbf{W}(t)$, so the distribution of the force is still Gaussian. This is important, since it follows from an equivalent argument, that the response will also be Gaussian. The effect of applying a pseudo force filter is that the filter characteristics also are identified together with the characteristics of the structure.

The number of output channels from the filter should be equal to the number of modes of the structual system, n. In order to make the filter versatile it will be assumed that the filter can have more modes than output and input channels, $m > n$.

2.3.3 Correlation Functions of the Response

The response of a lumped parameter system with $2n$-DOF measured at n points to the load described in section 2.3.2 is calculated using eq. (2.24)

$$\mathbf{X}(\omega) \;=\; \mathbf{H}(\omega)\mathbf{f}(\omega) \;=\; \mathbf{H}(\omega)\mathbf{H}_F(\omega)\mathbf{W}(\omega) \;=\; \mathbf{H}_c(\omega)\mathbf{W}(\omega) \tag{2.68}$$

In order to calculate the response the FRM of the combined system, $\mathbf{H}_c(\omega)$, consisting of the structure and the shaping filter is defined as

$$\begin{aligned}
\mathbf{H}_c(\omega) &= \mathbf{H}(\omega)\mathbf{H}_F(\omega) \\
&= \mathbf{\Phi}\mathbf{m}^{-1}(i\omega - \mathbf{\Lambda})^{-1}\mathbf{\Phi}^T \cdot \mathbf{\Phi}^F\mathbf{m}^{F^{-1}}(i\omega - \mathbf{\Lambda}^F)^{-1}\mathbf{\Phi}^{F^T} \\
&= \sum_{j=1}^{2n} \frac{\mathbf{\Phi}_j\mathbf{\Phi}_j^T}{m_j(i\omega - \lambda_j)} \sum_{l=1}^{m} \frac{\mathbf{\Phi}_l^F\mathbf{\Phi}_l^{F^T}}{m_l^F(i\omega - \lambda_l^F)} \;=\; \sum_{j=1}^{2n} \frac{\mathbf{B}_j}{(i\omega - \lambda_j)} \sum_{l=1}^{m} \frac{\mathbf{B}_l^F}{(i\omega - \lambda_l^F)} \\
&= \sum_{j=1}^{2n}\sum_{l=1}^{m} \frac{\mathbf{B}_j\mathbf{B}_l^F}{(i\omega - \lambda_j)(\lambda_j - \lambda_l^F)} \;+\; \frac{\mathbf{B}_j\mathbf{B}_l^F}{(\lambda_l^F - \lambda_j)(i\omega - \lambda_l^F)} \\
&= \sum_{j=1}^{2n} \frac{\mathbf{B}_j\mathbf{a}_j}{(i\omega - \lambda_j)} \;+\; \sum_{l=1}^{m} \frac{\mathbf{b}_l\mathbf{B}_l^F}{(i\omega - \lambda_l^F)}
\end{aligned} \tag{2.69}$$

where the following vectors, $\mathbf{a}_j$ and $\mathbf{a}_l$, have been introduced

$$\mathbf{a}_j \;=\; \sum_{l=1}^{m} \frac{\mathbf{B}_l^F}{(\lambda_j - \lambda_l^F)} \tag{2.70}$$

$$\mathbf{b}_l \;=\; \sum_{j=1}^{2n} \frac{\mathbf{B}_j}{(\lambda_l^F - \lambda_j)} \tag{2.71}$$

The last term in eq. (2.69) shows that all eigenvalues of the shaping filter and the structural system are uniquely preserved. Furthermore, the mode shapes of the structural system can be reconstructed from the columns of the FRM, and the mode shapes of the filter can be reconstructed from the rows of the FRM. The above proof is first time given in Ibrahim et al. [13].

Using matrix notation the FRM and the IRM of the combined system become

$$\mathbf{H}_c(\omega) \;=\; \tilde{\mathbf{\Phi}}\tilde{\mathbf{m}}^{-1}(i\omega - \tilde{\mathbf{\Lambda}})^{-1}\tilde{\mathbf{b}}^T \;=\; \sum_{j=1}^{2n+m} \frac{\tilde{\mathbf{\Phi}}_j\tilde{\mathbf{b}}_j^T}{\tilde{m}_j(i\omega - \tilde{\lambda}_j)} \tag{2.72}$$

$$\mathbf{h}_c(t) \quad = \quad \tilde{\mathbf{\Phi}}\tilde{\mathbf{m}}^{-1}e^{\tilde{\mathbf{\Lambda}}t}\tilde{\mathbf{b}}^T \qquad = \quad \sum_{j=1}^{2n+m}\frac{\tilde{\mathbf{\Phi}}_j\tilde{\mathbf{b}}_j^T}{\tilde{m}_j}e^{\tilde{\lambda}_j t} \tag{2.73}$$

where the following matrices have been introduced

$$\begin{aligned}
\tilde{\mathbf{\Phi}} &= [\mathbf{\Phi}_1\ \mathbf{\Phi}_2 ... \mathbf{\Phi}_{2n}\ \mathbf{b}_1\mathbf{\Phi}_\mathbf{1}^\mathbf{F}\ \mathbf{b}_2\mathbf{\Phi}_\mathbf{2}^\mathbf{F} ... \mathbf{b}_m\mathbf{\Phi}_\mathbf{m}^\mathbf{F}] \\
\tilde{\mathbf{b}} &= [\mathbf{a}_1^T\mathbf{\Phi}_1\ \mathbf{a}_2^T\mathbf{\Phi}_2 ... \mathbf{a}_{2n}^T\mathbf{\Phi}_{2n}\ \mathbf{\Phi}_1^F\ \mathbf{\Phi}_2^F ... \mathbf{\Phi}_m^F]
\end{aligned} \tag{2.74}$$

$$\tilde{\mathbf{m}} = diag([m_1\ m_2\ ...\ m_{2n}\ m_1^F\ m_2^F\ ...\ m_m^F]) \tag{2.75}$$

$$\tilde{\lambda} = diag([\lambda_1\ \lambda_2\ ...\ \lambda_{2n}\ \lambda_1^F\ \lambda_2^F\ ...\ \lambda_m^F]) \tag{2.76}$$

$$e^{\tilde{\mathbf{\Lambda}}} \ = \ diag([e^{\lambda_1 t}\ e^{\lambda_2 t}\ ...\ e^{\lambda_{2n} t}\ e^{\lambda_1^F t}\ e^{\lambda_2^F t}\ ...\ e^{\lambda_m^F t}]) \tag{2.77}$$

The time response is given by

$$\mathbf{X}(t) = \int_{-\infty}^{t}\mathbf{h}_c(t-\tau)\mathbf{W}(\tau)d\tau \tag{2.78}$$

Since this is a linear operation on the Gaussian distributed white noise excitation it follows that the response is Gaussian distributed. The correlation functions of the structural system loaded by filtered Gaussian white noise can be calculated using the above results

$$\begin{aligned}
\mathbf{R_{XX}}(\tau) &= E[\mathbf{X}(t+\tau)\mathbf{X}^T(t)] \\
&= E[\int_{-\infty}^{t+\tau}\int_{-\infty}^{t}\mathbf{h}_c(t+\tau-\alpha_1)\mathbf{W}(\alpha_1)\mathbf{W}(\alpha_2)^T\mathbf{h}_c^T(t-\alpha_2)d\alpha_1 d\alpha_2] \\
&= \int_0^\infty \mathbf{h}_c(t+\tau)\mathbf{R_{WW}}(0)\mathbf{h}_c^T(t)dt \\
&= \sum_{i=1}^{2n+m}\sum_{j=1}^{2n+m}\frac{\tilde{\mathbf{\Phi}}_i\tilde{\mathbf{b}}_i^T}{\tilde{m}_i}\mathbf{R_{WW}}(0)\frac{\tilde{\mathbf{b}}_j\tilde{\mathbf{\Phi}}_j^T}{\tilde{m}_j}e^{\tilde{\lambda}_i\tau}\int_0^\infty e^{(\tilde{\lambda}_i+\tilde{\lambda}_j)t}dt \\
&= \sum_{i=1}^{2n+m}\frac{\tilde{\mathbf{\Phi}}_i\tilde{\mathbf{b}}_i^T}{\tilde{m}_i}e^{\tilde{\lambda}_i\tau}\mathbf{R_{WW}}(0)\sum_{j=1}^{2n+m}\frac{\tilde{\mathbf{b}}_j\tilde{\mathbf{\Phi}}_j^T}{\tilde{m}_j}\frac{-1}{\tilde{\lambda}_i+\tilde{\lambda}_j} \\
&= \tilde{\mathbf{\Phi}}e^{\tilde{\mathbf{\Lambda}}\tau}\tilde{\mathbf{m}}^{-1}\tilde{\mathbf{c}}
\end{aligned} \tag{2.79}$$

where the matrix $\tilde{\mathbf{c}}$ has been introduced

$$\tilde{\mathbf{c}} \ = \ [\mathbf{c}_1\ \mathbf{c}_2\ ...\ \mathbf{c}_{2n+m}]^T \quad \mathbf{c}_i \ = \ \tilde{\mathbf{b}}_i^T\mathbf{R_{WW}}(0)\sum_{i=1}^{2n+m}\frac{\tilde{\mathbf{b}}_j\tilde{\mathbf{\Phi}}_j}{\tilde{m}_j}\frac{-1}{\lambda_i+\lambda_j} \tag{2.80}$$

From the last statement of eq. (2.79) it is seen that any column in the correlation function matrix can be written as

$$\mathbf{R}^i_{\mathbf{XX}}(\tau) \;=\; \tilde{\mathbf{\Phi}} e^{\tilde{\mathbf{\Lambda}}\tau} \tilde{\mathbf{m}}^{-1} \tilde{\mathbf{c}}_i \tag{2.81}$$

where $\mathbf{R}^i_{\mathbf{XX}}$ is an abbreviation of the ith column in the correlation matrix and the scaling constant $\tilde{\mathbf{q}}_i$ is the ith column of the matrix $\tilde{\mathbf{c}}$. Equation (2.81) is of exactly the same form as eq. (2.15), which is the standard equation for a free decay due to some initial conditions. This means that the mode shape vector $\tilde{\mathbf{\Phi}}$ and the matrix $\mathbf{\Lambda}$ containing the eigenvalues can be extracted from the correlation functions using methods described in section 2.2. If the velocities or the accelerations of the system are measured instead of the displacements the correlation functions can be calculated using eq. (2.81) and the results of eq. (2.55).

$$R^i_{\dot{\mathbf{X}}\mathbf{X}}(\tau) \;=\; -\tilde{\mathbf{\Phi}} e^{\tilde{\mathbf{\Lambda}}\tau} \tilde{\mathbf{\Lambda}}^2 \mathbf{c}_i \tag{2.82}$$

$$R^i_{\ddot{\mathbf{X}}\ddot{\mathbf{X}}}(\tau) \;=\; \tilde{\mathbf{\Phi}} e^{\tilde{\mathbf{\Lambda}}\tau} \tilde{\mathbf{\Lambda}}^4 \mathbf{c}_i \tag{2.83}$$

Equations (2.81) - (2.83) correspond exactly to eqs. (2.15) - (2.17), so in the modal parameter extraction procedure there is no reason to distinguish between the correlation functions of the displacements, velocities or the accelerations of the structure.

2.4 Summary

The lumped mass parameter model has been introduced and the modal parameters of this model have been defined in section 2.1. The response of this system to initial conditions and to arbitrary loads has been derived. Thereby the impulse response matrix and the frequency response matrix have been defined. In section 2.2 the process of extracting modal parameters from free decays has been discussed. The basic principles of the two algorithms, the Ibrahim Time Domain and the Polyreference Time Domain, which have been implemented, are described. Furthermore, the practical applications of these techniques have been the main issue. In section 2.3 the response of the lumped mass parameter system subjected to white noise passed through a shaping filter is discussed. This modelling assures a versatile description of the loads and that the response is Gaussian distributed. The correlation functions of the response are defined and it is shown that these correlation functions can be described equivalently to free decays. This means that modal parameters can be extracted from the correlation functions of the lumped mass parameter system loaded by filtered white noise using methods developed in connection with free decays. Since RD functions are interpreted in terms of correlation functions, this allows extraction of the modal parameters from the RD functions using methods like the Ibrahim Time Domain or the Polyreference Time Domain. This approach is used throughout this thesis. The chosen modelling of the loads also ensures that it is not necessary to measure the loads of a structure in order to extract modal parameters.

Bibliography

[1] Caughey, T.K. & o'Kelley, M.E.J. *Classical Normal Modes in Damped Linear Systems.* ASME Journal of Applied Mechanics, Vol. 49 pp. pp. 867-870, 1965.

[2] Nashif, A.D., Jones, D.I.G., Henderson, J.P. *Vibration Damping.* 1985 John Wiley & Sons. ISBN 0-471-86772-1.

[3] Bendat, J. & Piersol, A. *Random Data - Analysis and Measurement Procedures.* John Wiley & Sons, Inc. ISBN 0-471-04000-2.

[4] Pandit, S.M. *Modal and Spectrum Analysis: Data Dependent Systems in State Space.* 1991 John Wiley & Sons USA, Inc. ISBN 0-471-63705-X.

[5] Ewins, D.J. *Modal Testing: Theory and Practice.* 1995 Research Studies Press Ltd, England. ISBN 0-86380-017-3.

[6] Inman, D.J. *Engineering Vibration.* 1996 Prentice-Hall USA, Inc. ISBN 0-13-518531-9.

[7] Wirsching, P.H., Paez, T.L. & Ortiz K. *Random Vibrations. Theory and Practice.* 1995 John Wiley & Sons, Inc. ISBN 0-471-58579-3.

[8] Fladung, W.J., D.L. Brown & R.J. Allemang. *Modal Parameter Estimation - A Unified Matrix Polynomial Approach.* Proc. 12th International Modal Analysis Conference, Honolulu, Hawaii, USA, 1994.

[9] Ibrahim, S.R. *An Upper Hessenberg Sparse Matrix Algorithm for Modal Identification on Minicomputers.* Journal of Sound and Vibration (1987) 113(1) pp. 47-57.

[10] Vold ,H., Kundrat, J., Rocklin, G.T. & Russel, R. *A Multi-Input Modal Estimation Algorithm for Minicomputers.* SAE Paper No. 820194, 1982.

[11] Ibrahim, S.R. *Modal Confidence Factor in Vibration Testing.* Journal of Spacecraft, Sept.-Oct. 1978 Vol. 15, No. 5, pp. 313-316.

[12] Vold, H. & Crowley, J. *A Modal Confidence Factor for the Polyreference Time Domain Technique.* Proc. 3rd International Modal Analysis Conference, 1985, pp. 305-310.

[13] Ibrahim, S.R., Brincker, R. & Asmussen, J.C. *Modal Parameter Identification From Responses of General Unknown Random Inputs.* Proc. 14th International Modal Analysis Conference, Dearborn, Michigan, USA, Feb. 12-15, 1996, Vol. I, pp. 446-452.

Chapter 3

The Random Decrement Technique

The purpose of this chapter is to introduce the RD technique, present the mathematical background and illustrate the applicability of this technique. It is not the intention that the mathematical background of the RD technique should be derived in detail. Only the final results are presented and discussed. The interested reader is referred to appendix A, where a detailed derivation and résumé of the mathematical background of the RD technique are given.

Section 3.1 defines the RD functions theoretically and illustrates how the RD functions are estimated. The RD functions are in general defined for stationary processes, but the estimation of RD functions demands that the processes are assumed to be ergodic. Thus the RD technique is restricted to deal with ergodic processes. Section 3.2 introduces the link between the RD functions defined on the applied general triggering condition and the correlation functions of stationary zero mean Gaussian distributed processes. The assumptions of stationary zero mean Gaussian distributed processes are sufficient in terms of describing the RD technique mathematically. It is not necessary to assume anything about the physical system describing the processes. In spite of this the processes will be interpreted as the response of a linear lumped mass parameter system loaded by Gaussian white noise or filtered Gaussian white noise as described in chapter 2.

Sections 3.3 - 3.6 describe the four most well known triggering conditions. The relation between the RD functions and the correlation functions is given and approximate formulas for the variance of the RD functions are presented. In order to illustrate the different triggering conditions two examples are described in each section. First a very simple example using a very short time series is described. The purpose is to illustrate the estimation process and the different triggering conditions. Secondly an example based on the response of a 2DOF system loaded by Gaussian white noise is described in each section.

Section 3.7 introduces the concept of quality assessment of RD functions. The shape invariance relation of the RD functions and the symmetry relations for the correlation functions of stationary processes are used as a basis for quality assesment. Section 3.8 illustrates how the triggering levels should be chosen for the different triggering conditions.

In section 3.9 the RD technique is compared with other approaches for estimation of correlation functions. The comparison is based on speed and accuracy of the different approaches. Several different triggering conditions are considered. The examples illustrates advantages and disadvantages of the RD technique.

3.1 Definition of Random Decrement Functions

The RD technique is a method which transforms the stochastic processes *X(t)* and *Y(t)* into RD functions. It is assumed that $X(t)$ and $Y(t)$ are stationary processes. The index t is interpreted as time. The auto RD functions are defined as the mean value of a stochastic process on condition, T, of the process itself

$$D_{XX}(\tau) = \mathrm{E}[X(t+\tau)|T_{X(t)}] \tag{3.1}$$

$$D_{YY}(\tau) = \mathrm{E}[Y(t+\tau)|T_{Y(t)}] \tag{3.2}$$

An RD function is referred to as e.g. $D_{YY}(\tau)$. The first subscript refers to the process from which the mean value is calculated and the second subscript refers to the process where the condition is fulfilled. The conditions $T_{X(t)}$ and $T_{Y(t)}$ are denoted triggering conditions. Equivalent to eqs. (3.1) and (3.2) the cross RD functions are defined as the mean value of a stochastic process on condition of another stochastic process

$$D_{XY}(\tau) = \mathrm{E}[X(t+\tau)|T_{Y(t)}] \tag{3.3}$$

$$D_{YX}(\tau) = \mathrm{E}[Y(t+\tau)|T_{X(t)}] \tag{3.4}$$

The definitions of the auto RD functions in eqs. (3.1) and (3.2) are immediately obtained by interchanging the triggering conditions in the definitions of the cross RD functions in eqs. (3.3) - (3.4).

Example:

Consider a 3×1-dimensional stochastic vector process. It could e.g. describe the response at three different points of a vibrating structure. The stochastic process is given by $\mathbf{X}(t) = [X_1(t)\ X_2(t)\ X_3(t)]^T$. From this stochastic process it is possible to define nine RD functions, three auto RD functions and six cross RD functions

$$\begin{bmatrix} D_{X_1X_1}(\tau) & D_{X_1X_2}(\tau) & D_{X_1X_3}(\tau) \\ D_{X_2X_1}(\tau) & D_{X_2X_2}(\tau) & D_{X_2X_3}(\tau) \\ D_{X_3X_1}(\tau) & D_{X_3X_2}(\tau) & D_{X_3X_3}(\tau) \end{bmatrix} = \tag{3.5}$$

$$\begin{bmatrix} \mathrm{E}[X_1(t+\tau)|T_{X_1(t)}] & \mathrm{E}[X_1(t+\tau)|T_{X_2(t)}] & \mathrm{E}[X_1(t+\tau)|T_{X_3(t)}] \\ \mathrm{E}[X_2(t+\tau)|T_{X_1(t)}] & \mathrm{E}[X_2(t+\tau)|T_{X_2(t)}] & \mathrm{E}[X_2(t+\tau)|T_{X_3(t)}] \\ \mathrm{E}[X_3(t+\tau)|T_{X_1(t)}] & \mathrm{E}[X_3(t+\tau)|T_{X_2(t)}] & \mathrm{E}[X_3(t+\tau)|T_{X_3(t)}] \end{bmatrix}$$

A column in eq. (3.5) is denoted a RD setup, whereas the process where the triggering condition is fulfilled is denoted the reference measurement or triggering measurement.

$\diamond$

In practical applications of the RD technique only a single realization of the stochastic process is available. Or in other words, usually only a single measurement at each chosen

location of a vibrating structure is collected. In order to estimate the conditional mean value correctly from a single observation it is necessary to assume that the stochastic process is not only stationary but also ergodic. In this case the auto RD functions can be estimated as the empirical conditional mean value from a single realization

$$\hat{D}_{XX}(\tau) = \frac{1}{N} \cdot \sum_{i=1}^{N} x(t_i + \tau) | T_{x(t_i)} \tag{3.6}$$

$$\hat{D}_{YY}(\tau) = \frac{1}{N} \cdot \sum_{i=1}^{N} y(t_i + \tau) | T_{y(t_i)} \tag{3.7}$$

where N is the number of points in the process which fulfils the triggering condition and $y(t)$ and $x(t)$ are realizations of $X(t)$ and $Y(t)$. Correspondingly, the cross RD functions are estimated as

$$\hat{D}_{XY}(\tau) = \frac{1}{N} \cdot \sum_{i=1}^{N} x(t_i + \tau) | T_{y(t_i)} \tag{3.8}$$

$$\hat{D}_{YX}(\tau) = \frac{1}{N} \cdot \sum_{i=1}^{N} y(t_i + \tau) | T_{x(t_i)} \tag{3.9}$$

The absolute decisife variable in estimation of RD functions is the number of triggering points, N. N has to be large enough to secure that eqs. (3.6) - (3.9) has converged sufficiently towards eqs. (3.1) - (3.4).

It is important that the estimates of the RD functions in eqs. (3.6) - (3.9) are unbiased, e.g.

$$\mathrm{E}[\hat{D}_{XY}(\tau)] = \frac{1}{N} \sum_{i=1}^{N} \mathrm{E}[x(t_i + \tau) | T_{y(t_i)}] = D_{XY}(\tau) \tag{3.10}$$

Until now no restriction or formulation of the triggering condition has been made. Obviously the formulation of the triggering conditions controls the actual number of triggering points. This means that the convergence of the estimates in eqs. (3.6) - (3.9) is controlled by the triggering condition and of course of the absolute length of the observations of the processes. In the next sections different formulations of the triggering conditions are described.

The definitions of the RD functions in eqs. (3.1) - (3.4) assume that the index of the processes $X(t)$ and $Y(t)$ is continuous time. Measurements of the response of a structure consist of simultaneously sampled values of the response at equidistant time points at the sampling interval ΔT. So the variables t_i and τ used in the estimation of RD function are discrete-time variables and functions of the sampling rate.

3.2 Applied General Triggering Condition

This section introduces the applied general triggering condition. The results are not derived, only presented. The interested reader is referred to appendix A for a detailed derivation. In a real estimation situation this triggering condition does not have any interest, but the results obtained using this condition are important. The link between the RD functions of any triggering condition of practical interest and the correlation functions of stationary zero mean Gaussian distributed processes can be derived directly from the results of this triggering condition. The applied general triggering condition, $T^{G_A}_{X(t)}$, of the stochastic process $X(t)$ is defined as

$$T^{G_A}_{X(t)} = \{a_1 \leq X(t) < a_2, b_1 \leq \dot{X}(t) < b_2\} \tag{3.11}$$

Superscript G_A refers to the *G*eneral *A*pplied triggering condition. Using this general triggering condition the RD functions becomes a weighted sum of the correlation function and the time derivative of the correlation functions

$$D_{XX}(\tau) = \frac{R_{XX}(\tau)}{\sigma^2_X} \cdot \tilde{a} - \frac{R'_{XX}(\tau)}{\sigma^2_{\dot{X}}} \cdot \tilde{b} \tag{3.12}$$

$$D_{YX}(\tau) = \frac{R_{YX}(\tau)}{\sigma^2_X} \cdot \tilde{a} - \frac{R'_{YX}(\tau)}{\sigma^2_{\dot{X}}} \cdot \tilde{b} \tag{3.13}$$

where the triggering levels $\tilde{a}$ and $\tilde{b}$ are functions of the triggering bounds and the density functions.

$$\tilde{a} = \frac{\int_{a_1}^{a_2} x p_X(x) dx}{\int_{a_1}^{a_2} p_X(x) dx} \qquad \tilde{b} = \frac{\int_{b_1}^{b_2} \dot{x} p_{\dot{X}}(\dot{x}) d\dot{x}}{\int_{b_1}^{b_2} p_{\dot{X}}(\dot{x}) d\dot{x}} \tag{3.14}$$

Equations (3.12) and (3.13) illustrate how versatile the RD technique is. By adjusting the triggering bounds a_1, a_2 and/or b_1, b_2 the contribution of the correlation functions and the time derivative of the correlation functions to the resulting RD functions can be changed. In the limit by choosing one of the triggering level sets, $[a_1\ a_2]$ or $[b_1\ b_2]$, to $[-\infty\ \infty]$ or $[0\ 0]$ the resulting RD functions becomes proportional to either the correlation functions or their time derivatives.

Another important aspect of the RD technique is the actual number of triggering points. The RD functions are estimated as the empirical mean from a single realization of the stochastic processes. This assumes that the processes are ergodic

$$\hat{D}_{XX}(\tau) = \frac{1}{N} \sum_{i=1}^{N} x(t_i + \tau) | \{a_1 \leq x(t_i) < a_2, b_1 \leq \dot{x}(t_i) < b_2\} \tag{3.15}$$

$$\hat{D}_{YX}(\tau) = \frac{1}{N} \sum_{i=1}^{N} y(t_i + \tau) | \{a_1 \leq x(t_i) < a_2, b_1 \leq \dot{x}(t_i) < b_2\} \tag{3.16}$$

The number of triggering points, N, can be adjusted by changing the triggering levels $[a_1\ a_2]$ and $[b_1\ b_2]$. This means that the convergence of the estimates in eqs. (3.15) and (3.16) is controlled by the triggering levels.

In applications of the RD technique only special formulations of the applied general triggering condition are used. The explanation is that usually only the correlation functions or the time derivative of the correlation function is needed. Furthermore, since the technique is applied to discrete measurements, noise will be introduced by calculating the time derivative of the measurements numerically. It is usually necessary to calculate the time derivative, since only realizations of the process itself are available. This will lead to erroneous triggering points corresponding to erroneous values of the time derivative of the measurement. This leads to the formulation of four triggering conditions described in sections 3.3 - 3.6. In order to demonstrate the applicability of the RD technique and the different triggering conditions two through examples are given in each section.

The first time RD functions are described mathematically by correlation functions is presented in Vandiver et al. [1]. They proved that for stationary zero mean Gaussian distributed processes the RD functions obtained using the level crossing triggering condition are proportional to the auto correlation function. They also derived an approximate formula for the variance of the RD functions. Brincker et al. [2] extended this concept by deriving a proportional relationship between the cross RD functions of a theoretical general triggering condition and the cross correlation functions and the time derivative of the cross correlation function. They also derived approximate formulas for the variance of the cross RD functions in terms of cross correlation functions. The results obtained using the applied general triggering condition are a generalization of the results obtained by Vandiver and Brincker. From this triggering condition the result of any particular triggering condition can be derived directly, see appendix A.

3.2.1 Example 1: Illustration of Triggering Conditions

The time series shown in fig. 3.1 will be analysed in sections 3.3 - 3.6. The continuous line shows the original process. The $*$ shows where the process has been sampled at equidistant time points.

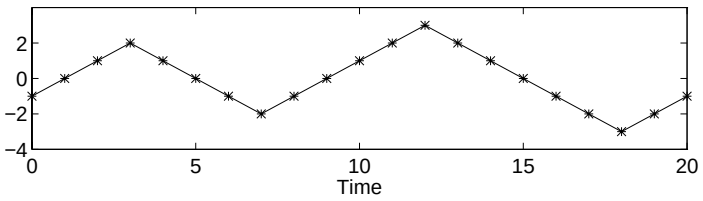

Figure 3.1: *Continuous process and the corresponding sampled discrete time series.*

The discrete time series will be analysed applying the different triggering conditions in order to illustrate the basic idea of the RD technique with a simple example.

3.2.2 Example 2: 2DOF System

The system, which will be analysed in sections 3.3 - 3.6 for illustration purposes, is a 2DOF-system loaded by uncorrelated Gaussian white noise processes at each mass. The

mass, damping and stiffness matrix are

$$\mathbf{M} = \begin{bmatrix} 1 & 0 \\ 0 & 1 \end{bmatrix}, \quad \mathbf{C} = 1.5 \cdot \begin{bmatrix} 0.9 & -1 \\ -1 & 1.8 \end{bmatrix}, \quad \mathbf{K} = \begin{bmatrix} 700 & -200 \\ -200 & 500 \end{bmatrix} \tag{3.17}$$

The units of the matrices are kg, Ns/m and N/m. All matrices are symmetric. The modal parameters of this system are listed in table 3.1:

	f [Hz]	ζ %	$\lvert\Phi\rvert^1$	$\lvert\Phi\rvert^2$	$\angle\Phi^1$	$\angle\Phi^2$
Mode 1	3.09	1.69	1.00	1.61	0	4.7
Mode 2	4.56	3.56	1.00	0.62	0	173.0

Table 3.1: *Modal parameters of the general example.*

The sampling rate is chosen as 120 Hz. The system is highly oversampled in order to obtain a better graphical illustration of the estimated and the theoretical RD functions. Figure 3.2 shows the simulated displacement response (10000 points) of each mass.

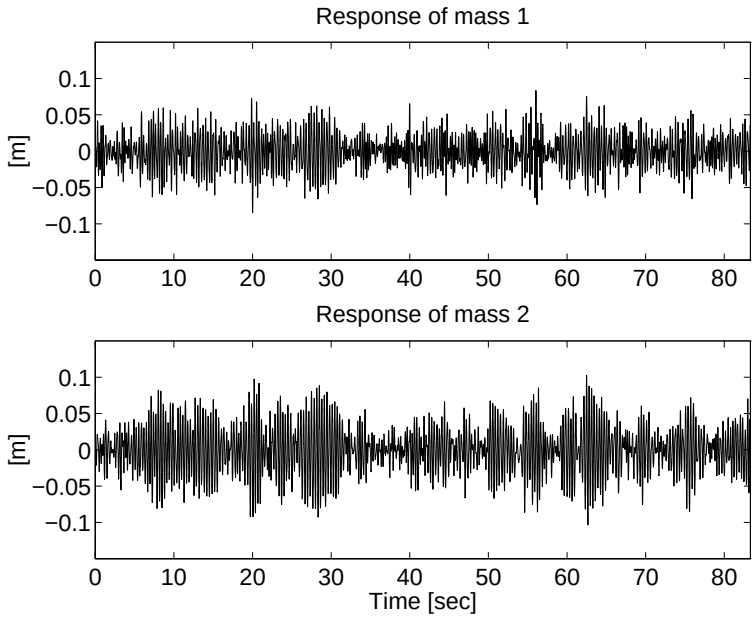

Figure 3.2: *Measurement 1 and measurement 2. The displacement response of mass 1 and mass 2, respectively.*

As described in the introduction the response is simulated using ARMAV-models. The approach is to simulate the Gaussian white noise loads, which together with the $\mathbf{M}$, $\mathbf{C}$, $\mathbf{K}$ matrices and the sampling rate are the inputs to the algorithm.

3.3 Level Crossing Triggering Condition

The level crossing triggering condition is the most popular triggering condition in applications of the RD technique. Cole used this condition, when he introduced the RD technique. Level crossing triggering, T^L, states that a triggering point is detected if the process is equal to the chosen triggering level, a.

$$T^L_{X(t)} = \{X(t) = a\} \tag{3.18}$$

The condition is reformulated to be of the same form as the applied general triggering condition, see eq. (3.11)

$$T^L_{X(t)} = \{a \leq X(t) < a + \Delta a, -\infty \leq \dot{X}(t) < \infty\} \tag{3.19}$$

From eq. (3.19) and the results of eqs. (3.12), (3.13) and (3.14) it follows that the RD functions are proportional to the correlation functions

$$D_{XX}(\tau) = \frac{R_{XX}(\tau)}{\sigma_X^2} \cdot a \tag{3.20}$$

$$D_{YX}(\tau) = \frac{R_{YX}(\tau)}{\sigma_X^2} \cdot a \tag{3.21}$$

The RD functions defined by the level triggering condition are calculated as the empirical mean. The processes are assumed to be ergodic

$$\hat{D}_{XX}(\tau) = \frac{1}{N}\sum_{i=1}^{N} x(t_i + \tau) | \{x(t_i) = a\} \tag{3.22}$$

$$\hat{D}_{YX}(\tau) = \frac{1}{N}\sum_{i=1}^{N} y(t_i + \tau) | \{x(t_i) = a\} \tag{3.23}$$

where $x(t)$ and $y(t)$ are realizations of $X(t)$ and $Y(t)$, respectively. If the time segments in the averaging process are assumed to be uncorrelated the variance of the estimated RD functions can be estimated as, see appendix A.

$$\mathrm{Var}[\hat{D}_{XX}(\tau)] \approx \frac{\sigma_X^2}{N}\left(1 - \left(\frac{R_{XX}(\tau)}{\sigma_X^2}\right)^2\right) \tag{3.24}$$

$$\mathrm{Var}[\hat{D}_{YX}(\tau)] \approx \frac{\sigma_Y^2}{N}\left(1 - \left(\frac{R_{YX}(\tau)}{\sigma_X \sigma_Y}\right)^2\right) \tag{3.25}$$

The results of eqs. (3.20) - (3.25) constitute the mathematical basis of the level crossing triggering condition. The estimate of the variance of the estimated RD functions should be used cautiously, since the assumption of uncorrelated time segments can be highly violated. Notice that the variance is independent of the chosen triggering level. It is interesting that the variance of the auto RD functions predicted by eq. (3.24) states that the variance is zero at time lag zero. The variance of the RD functions predicted by eq. (3.24) will converge towards $\frac{\sigma_X^2}{N}$ for $|\tau| \to \infty$, since $R_{XX}(\tau) \to 0$ for $|\tau| \to \infty$. The strength of the relations in eqs. (3.24) - (3.25) is that the variance only is a function of the number of triggering points and the correlation functions (which is known by a scaling of the RD functions). The estimate of the variance can be calculated without increasing the computational time significantly.

3.3.1 Example 1: Illustration of Triggering Conditions

The time series in fig. 3.3 is considered.

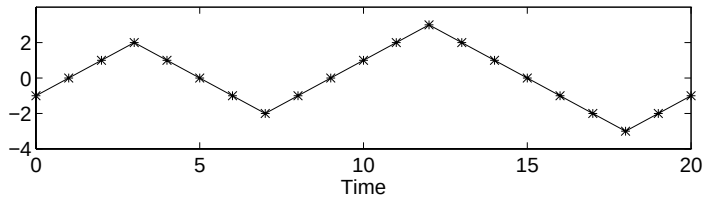

Figure 3.3: *Continuous process and the corresponding sampled discrete time series.*

The RD function is estimated using level crossing with the triggering level $T^L_{X(t)} = \{x(t) = a\}$. It is chosen to use 3 points in each RD function.

Figure 3.4 shows the time segments which have been picked out using the level crossing triggering condition and the resulting RD function and the resulting average of the time segments. The time axis of the time segments corresponds to the time axis in fig. 3.3.

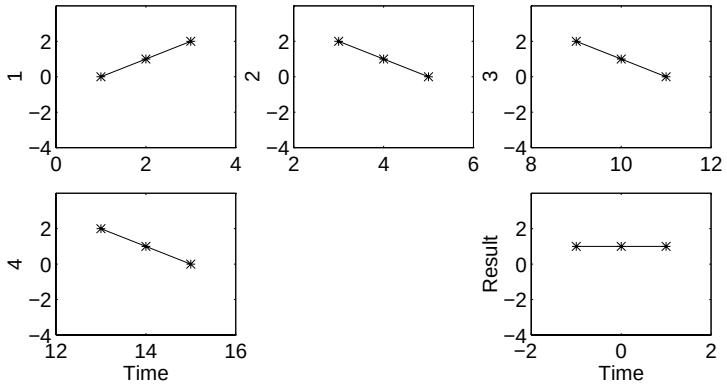

Figure 3.4: *The time segments and the resulting RD function estimated using level crossing triggering with* $a = 1$.

As illustrated, two upcrossings and two downcrossings are detected.

3.3.2 Example 2: 2DOF System

The purpose of this analysis is to illustrate the level crossing triggering condition. The system described in section 3.2.2 is considered. The triggering condition is chosen to

$$T^L_{X(t)} \;=\; \{X(t) = \sqrt{2}\sigma_X\} \tag{3.26}$$

The triggering levels are usually expressed as a multiplum of the standard deviation of the process. The RD functions of the response shown in fig. 3.2 are calculated. The triggering condition is first applied to the response of the first mass and then to the second mass. The estimated RD functions and the theoretical RD functions (see eqs. (3.20) and (3.21)) are shown in figs. 3.5 - 3.6.

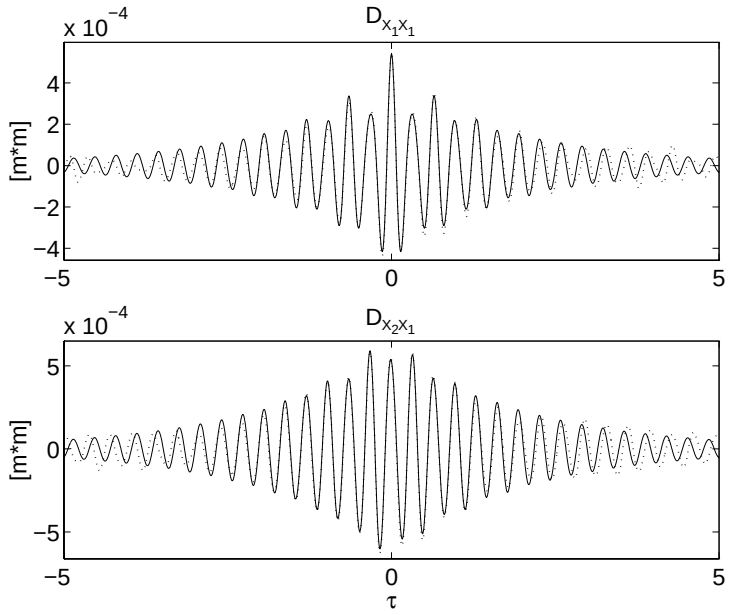

Figure 3.5: *Normalized RD functions estimated using level crossing triggering applied to the response of the first mass. [------]: Theoretical RD functions, [· · · · ·]: Estimated RD functions.*

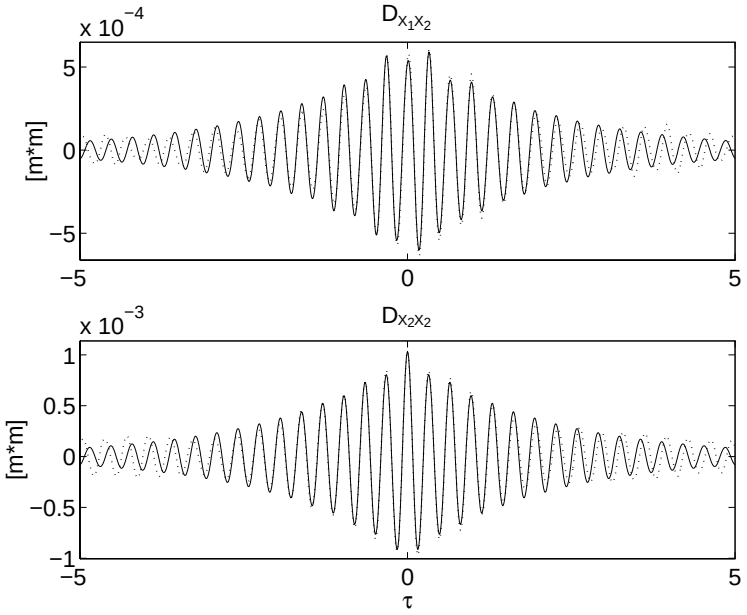

Figure 3.6: *Normalized RD functions estimated using level crossing triggering applied to the response of the second mass. [------]: Theoretical RD functions, [· · · · ·]: Estimated RD functions.*

The expected number of triggering points were 191 and 172 predicted by eq. (A.56) and the actual number of triggering points was 212 and 182. The figures illustrate how the accuracy of the RD functions decreases with increasing time lag, $|\tau|$. It is a standard observation that the estimate of the RD functions does not dissipate as fast as the theoretical RD functions.

3.4 Local Extremum Triggering Condition

The local extremum triggering condition, $T^E_{X(t)}$, is not a commonly used triggering condition compared to the level crossing triggering condition. Nevertheless, this triggering condition is attractive, since it requires that the contribution from the time derivative of the process is zero, instead of averaging out the contributions as does the level crossing triggering condition. A triggering point is detected if the time series has a local extremum

$$T^E_{X(t)} = \{a_1 \leq X(t) < a_2, \dot{X}(t) = 0\} \tag{3.27}$$

It is extremely important that the triggering condition states that both local maxima and local minima are triggering points. If only the local maxima are used as triggering points, the following equations are not valid. The condition is reformulated to be of the same form as the applied general triggering condition, see eq. (3.11)

$$T^E_{X(t)} = \{a_1 \leq X(t) < a, 0 \leq \dot{X}(t) < 0 + \Delta b\}\ , \quad \Delta b \to 0 \tag{3.28}$$

It follows from eqs. (3.12) - (3.14) that the RD functions are proportional to the correlation functions

$$D_{XX}(\tau) = \frac{R_{XX}(\tau)}{\sigma^2_X} \cdot \tilde{a} \tag{3.29}$$

$$D_{YX}(\tau) = \frac{R_{YX}(\tau)}{\sigma^2_X} \cdot \tilde{a} \tag{3.30}$$

where the triggering level $\tilde{a}$ is given by a_1, a_2 and the density function

$$\tilde{a} = \frac{\int_{a_1}^{a_2} x p_X(x) dx}{\int_{a_1}^{a_2} p_X(x) dx} \tag{3.31}$$

The bounds a_1 and a_2 should be chosen to have equal signs in order to extract maximum information from each time segment. If $a_1 < 0$ and $a_2 > 0$ with $a_2 > |a_1|$ the resulting RD function corresponds to the RD functions estimated using $[|a_1|\ a_2]$ as triggering levels. The contributions from $[a_1\ |a_1|]$ is zero, so the only difference is the computational time vasted. The RD functions defined by the local extremum triggering condition are estimated as the empirical mean. The processes are assumed to be ergodic

$$\hat{D}_{XX}(\tau) = \frac{1}{N} \sum_{i=1}^{N} x(t_i + \tau) | \{a_1 \leq x(t_i) < a_2, \dot{x}(t_i) = 0\} \tag{3.32}$$

$$\hat{D}_{YX}(\tau) = \frac{1}{N} \sum_{i=1}^{N} y(t_i + \tau) | \{a_1 \leq x(t_i) < a_2, \dot{x}(t_i) = 0\} \tag{3.33}$$

where $x(t)$ and $y(t)$ are realizations of $X(t)$ and $Y(t)$. The time segments are assumed to be uncorrelated. Thereby the variance of the estimated RD functions can be approximated by, see appendix A

$$\mathrm{Var}[\hat{D}_{XX}(\tau)] \approx \frac{\sigma^2_X}{N} \left(1 - \left(\frac{R_{XX}(\tau)}{\sigma^2_X} \right)^2 - \left(\frac{R'_{XX}(\tau)}{\sigma_X \sigma_{\dot{X}}} \right)^2 \right) + \frac{k^E}{N} \left(\frac{R_{XX}(\tau)}{\sigma^2_X} \right)^2 \tag{3.34}$$

$$\mathrm{Var}[\hat{D}_{YX}(\tau)] \approx \frac{\sigma_Y^2}{N}\left(1 - \left(\frac{R_{YX}(\tau)}{\sigma_Y\sigma_X}\right)^2 - \left(\frac{R'_{YX}(\tau)}{\sigma_Y\sigma_{\dot{X}}}\right)^2\right) + \frac{k^E}{N}\left(\frac{R_{YX}(\tau)}{\sigma_Y\sigma_X}\right)^2 \tag{3.35}$$

where k^E is given by the triggering levels and the density function

$$k^E = \frac{\int_{a_1}^{a_2} x^2 p_X(x)dx}{\int_{a_1}^{a_2} p_X(x)dx} - \left(\frac{\int_{a_1}^{a_2} x p_X(x)dx}{\int_{a_1}^{a_2} p_X(x)dx}\right)^2 \tag{3.36}$$

The results of eqs. (3.29), (3.30) and eqs. (3.34), (3.35) constitute the mathematical basis of the local extremum triggering condition. The assumption of uncorrelated time segments can be violated, so eqs. (3.34) and (3.35) should be used cautiously. In contrast to the level crossing triggering condition the variance of the auto RD functions predicted by eq. (3.34) is not zero at time lag zero.

$$\mathrm{Var}[\hat{D}_{XX}(0)] = \frac{k^E}{N} \neq 0 \tag{3.37}$$

The variance will converge towards $\frac{\sigma_X^2}{N}$, corresponding to the results for the level crossing triggering condition, since $R_{XX}(\tau), R'_{XX}(\tau) \rightarrow 0$ for $|\tau| \rightarrow \infty$. The variance predicted by eqs. (3.34) and (3.35) is not independent of the chosen triggering levels.

3.4.1 Example 1: Illustration of Triggering Conditions

The time series in fig. 3.7 is considered again.

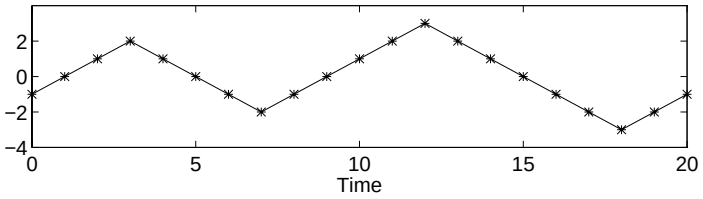

Figure 3.7: *Continuous process and the corresponding sampled discrete time series.*

The RD function is estimated using local extremum with the triggering levels $T^E_{X(t)} = \{0 \leq x(t) < \infty\}$. It is chosen to use 3 points in each RD functions. Figure 3.8 shows the time segments which have been picked out using the local extremum triggering condition and the resulting RD function. The time axis of the time segments corresponds to the time axis in fig. 3.7.

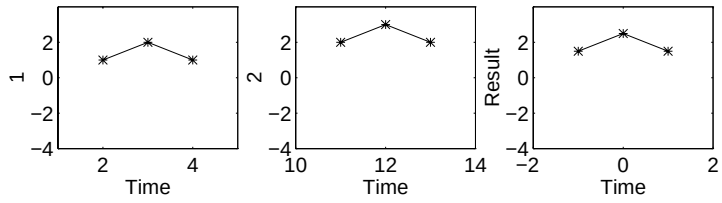

Figure 3.8: *The time segments and the resulting RD function estimated using local extremum triggering with* $[a_1\ a_2] = [0\ \infty]$.

As illustrated, two local maxima and no local minima are detected.

3.4.2 Example 2: 2DOF System

The results of the analysis of the 2DOF system illustrate the local extremum triggering condition. The triggering condition is chosen as

$$T^E_{X(t)} \ = \ \{\sigma_X \leq X(t) < \infty, \dot{X}(t) = 0\} \tag{3.38}$$

The estimated and the theoretical RD functions are shown in figs. (3.9) - (3.10).

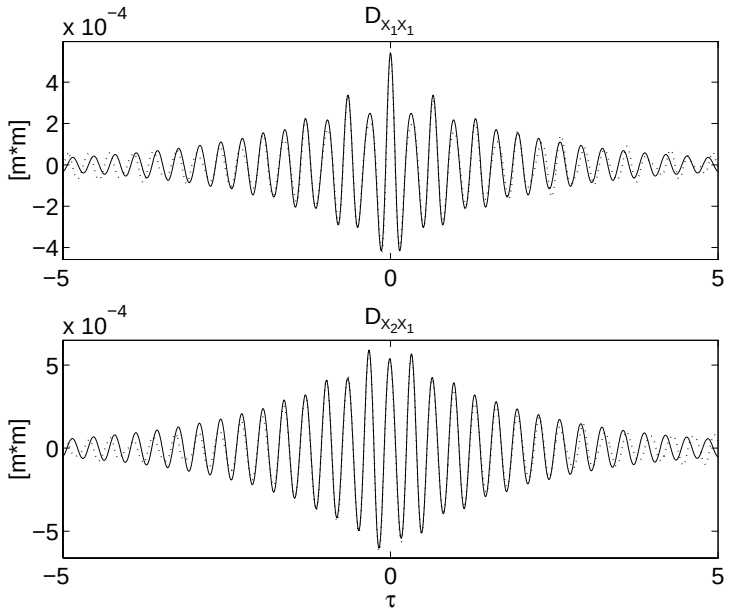

Figure 3.9: *Normalized RD functions estimated using local extremum triggering applied to the response of the first mass. [------]: Theoretical RD functions, [· · · · ·]: Estimated RD functions.*

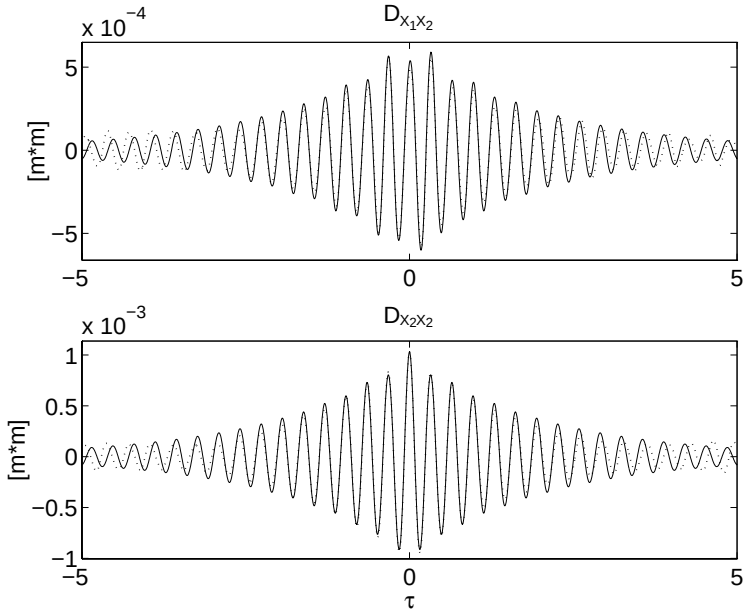

Figure 3.10: *Normalized RD functions estimated using local extremum triggering applied to the response of the second mass. [——]: Theoretical RD functions, [· · · · ·]: Estimated RD functions.*

The figures illustrate that the estimation errors of the RD functions increase with increasing distance from the triggering condition. Again it is seen that the errors result in an overestimation of the RD functions. The number of triggering points was 162 and 152 for the RD functions shown in figures 3.9 and 3.10, respectively. This is an important difference compared to the results of the level crossing triggering condition. Although the triggering conditions theoretically estimate the same functions, there is a significant difference, since the number of triggering points differs.

3.5 Positive Point Triggering Condition

The positive point triggering condition, $T^P_{X(t)}$, is perhaps the simplest of all triggering conditions, since a triggering point is detected simply if the time series has a value in between two bounds a_1 and a_2, which are usually chosen to have equal (positive) signs.

$$T^P_{X(t)} = \{a_1 \leq X(t) < a_2\} \tag{3.39}$$

Although the positive point triggering condition is simple the condition is versatile. If e.g. the triggering levels are chosen as $[0\ \infty]$ half of the points in the time series will be triggering points. On the other hand, if the triggering conditions are chosen as $[a\ a + \Delta a]$ and $\Delta a \to 0$ then the level crossing triggering condition is obtained. So the positive point triggering condition can be interpreted as a generalization of the level crossing triggering condition. The condition is reformulated to be of the same form as the applied general triggering condition.

$$T^P_{X(t)} = \{a_1 \leq X(t) < a_2, -\infty \leq \dot{X}(t) < \infty\} \tag{3.40}$$

These bounds are inserted in eqs. (3.12) - (3.14). The RD functions are proportional to the correlation functions

$$D_{XX}(\tau) = \frac{R_{XX}(\tau)}{\sigma_X^2} \cdot \tilde{a} \tag{3.41}$$

$$D_{YX}(\tau) = \frac{R_{YX}(\tau)}{\sigma_X^2} \cdot \tilde{a} \tag{3.42}$$

where the triggering level $\tilde{a}$ is given by the triggering levels a_1, a_2 and the density function.

$$\tilde{a} = \frac{\int_{a_1}^{a_2} x p_X(x) dx}{\int_{a_1}^{a_2} p_X(x) dx} \tag{3.43}$$

Equations (3.41) - (3.43) are exactly the same as eqs. (3.29) - (3.31) from the local extremum triggering condition. The difference between the two triggering conditions is that the local extremum triggering condition demands that the time derivative of the time series is zero, whereas the positive point triggering condition averages the contribution of the time derivative towards zero. This also means that the number of triggering points is significantly different. The RD functions are estimated as the empirical mean. The processes are assumed to be ergodic.

$$\hat{D}_{XX}(\tau) = \frac{1}{N} \sum_{i=1}^{N} x(t_i + \tau) | \{a_1 \leq x(t_i) < a_2\} \tag{3.44}$$

$$\hat{D}_{YX}(\tau) = \frac{1}{N} \sum_{i=1}^{N} y(t_i + \tau) | \{a_1 \leq x(t_i) < a_2\} \tag{3.45}$$

where $x(t)$ and $y(t)$ are realizations of $X(t)$ and $Y(t)$. If the time segments are uncorrelated the variance of the estimated RD functions are given by, see appendix A.

$$\mathrm{Var}[\hat{D}_{XX}(\tau)] \approx \frac{\sigma_X^2}{N} \left(1 - \left(\frac{R_{XX}(\tau)}{\sigma_X^2} \right)^2 \right) + \frac{k^P}{N} \left(\frac{R_{XX}(\tau)}{\sigma_X^2} \right)^2 \tag{3.46}$$

$$\mathrm{Var}[\hat{D}_{XX}(\tau)] \approx \frac{\sigma_Y^2}{N} \left(1 - \left(\frac{R_{YX}(\tau)}{\sigma_Y \sigma_X} \right)^2 \right) + \frac{k^P}{N} \left(\frac{R_{YX}(\tau)}{\sigma_Y \sigma_X} \right)^2 \tag{3.47}$$

where k^P is given by:

$$k^P = \frac{\int_{a_1}^{a_2} x^2 p_X(x) dx}{\int_{a_1}^{a_2} p_X(x) dx} - \left(\frac{\int_{a_1}^{a_2} x p_X(x) dx}{\int_{a_1}^{a_2} p_X(x) dx} \right)^2 \tag{3.48}$$

The variance predicted by eqs. (3.46) and (3.47) should be used with utmost care. In situations where broad triggering levels as $[a_1\ a_2] = [0\ \infty]$ have been applied, eqs. (3.46) and (3.47) are invalid, since they will highly underestimate the variance. Only in situations where $a_1 \approx a_2$ eqs. (3.46) and (3.47) will predict reasonable variances. This problem is one of the topics of chapter 5.

3.5.1 Example 1: Illustration of Triggering Conditions

The time series in fig. 3.11 is considered again.

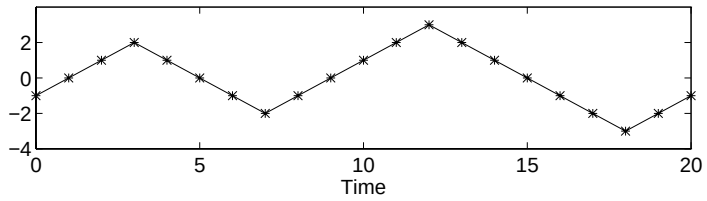

Figure 3.11: *Continuous process and the corresponding sampled discrete time series.*

The RD function is estimated using positive point with the triggering levels $T^P_{X(t)} = \{2 \leq x(t) = \infty\}$. It is chosen to use 3 points in each RD functions. Figure 3.12 shows the time segments which have been picked out using the positive point triggering condition and the resulting RD function. The time axis of the time segments corresponds to the time axis in fig. 3.11.

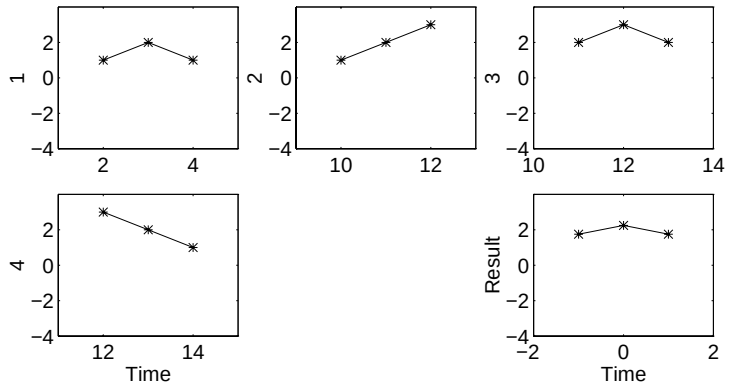

Figure 3.12: *The time segments and the resulting RD function estimated using positive point triggering with* $[a_1\ a_2] = [2\ \infty]$.

As illustrated, 4 positive points exist in the chosen interval. This small example indicates that the positive point triggering condition results in more triggering points than the other triggering conditions.

3.5.2 Example 2: 2DOF System

The response of the 2DOF system described in section 3.2.2 is analysed. The triggering condition is chosen as

$$T^P_{X(t)} \ = \ \{\sigma_X \leq X(t) < \infty\} \tag{3.49}$$

The estimated and the theoretical RD functions are shown in figures 3.13 - 3.14.

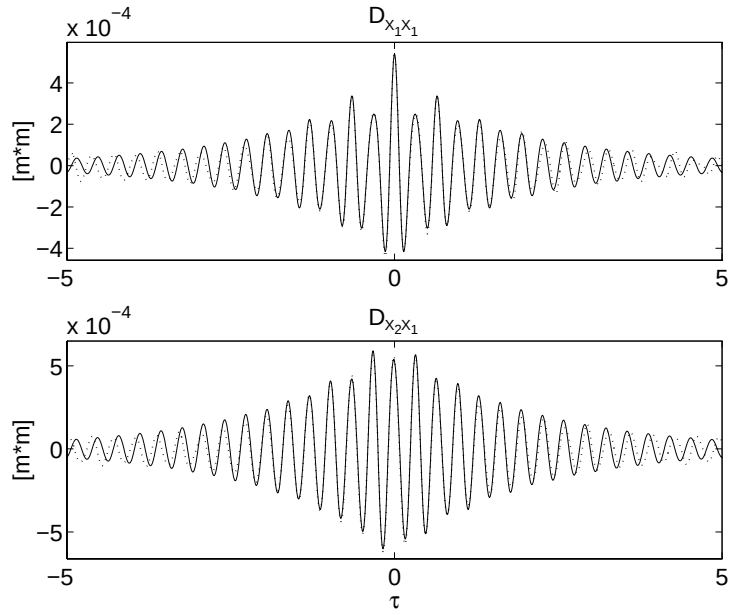

Figure 3.13: *Normalized RD functions estimated using positive point triggering applied to the response of the first mass. [------]: Theoretical RD functions, [· · · · ·]: Estimated RD functions.*

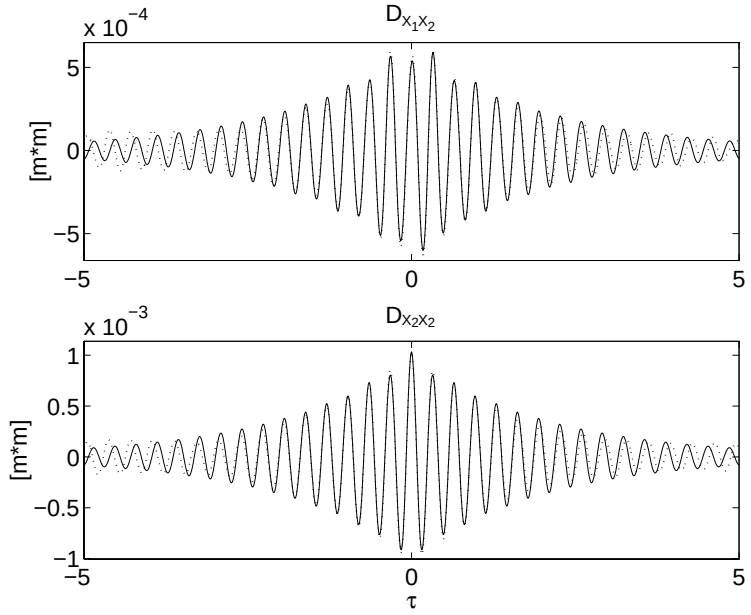

Figure 3.14: *Normalized RD functions estimated using positive point triggering applied to the response of the first mass. [------]: Theoretical RD functions, [· · · · ·]: Estimated RD functions.*

The number of triggering points is 1464 and 1464, and the expected number of triggering points are 1397 in both situations. Compared to the results obtained using level crossing and local extremum triggering, this condition illustrates the versatility of the RD technique. The number of triggering points can be adjusted by selecting the triggering condition and bounds carefully. Figures 3.13 and 3.14 again illustrate that the estimation

errors of the RD functions increase with the distance from time lag zero.

3.6 Zero Crossing Triggering Condition

The zero crossing with positive slope triggering condition, $T^Z_{X(t)}$, was the second triggering condition introduced. Originally the resulting RD functions obtained from this triggering condition were interpreted as impulse response functions. A triggering point is detected if the process crosses the zero line with positive slope

$$T^Z_{X(t)} = \{X(t) = 0, \dot{X}(t) > 0\} \tag{3.50}$$

The condition is reformulated to be of the same form as the applied general triggering condition

$$T^Z_{X(t)} = \{0 \leq X(t) < 0 + \Delta a, 0 \leq \dot{X}(t) < \infty\}\ , \quad \Delta a \to 0 \tag{3.51}$$

The bounds are inserted in eqs. (3.12) - (3.14) and the RD functions become proportional to the time derivative of the correlation functions

$$D_{XX}(\tau) = -\frac{R'_{XX}(\tau)}{\sigma^2_{\dot{X}}} \cdot \tilde{b} \tag{3.52}$$

$$D_{YX}(\tau) = -\frac{R'_{YX}(\tau)}{\sigma^2_{\dot{X}}} \cdot \tilde{b} \tag{3.53}$$

The triggering level $\tilde{b}$ is given by eq. (3.54), since all positive time derivatives are used.

$$\tilde{b} = \frac{\int_0^\infty \dot{x} p_{\dot{X}}(\dot{x})}{\int_0^\infty p_{\dot{X}}(\dot{x})} = \sqrt{\frac{2}{\pi}}\sigma_{\dot{X}} \tag{3.54}$$

The triggering levels are always chosen as $[b_1\ b_2] = [0\ \infty]$. The argument is that usually only a realization of $X(t)$ is available. If the triggering levels are refined numerical differentiation has to be applied, which will result in false triggering points. The RD functions are estimated as the empirical mean. This assumes that the processes are ergodic

$$\hat{D}_{XX}(\tau) = \frac{1}{N}\sum_{i=1}^{N} x(t_i + \tau) | \{x(t_i) = 0, \dot{x}(t_i) > 0\} \tag{3.55}$$

$$\hat{D}_{YX}(\tau) = \frac{1}{N}\sum_{i=1}^{N} y(t_i + \tau) | \{x(t_i) = 0, \dot{x}(t_i) > 0\} \tag{3.56}$$

where $x(t)$ and $y(t)$ are realizations of $X(t)$ and $Y(t)$. An estimate of the variance of the estimated RD functions is derived in appendix A. The assumption is that the time segments in the averaging process, see eqs. (3.55) - (3.56) are independent

$$\mathrm{Var}[\hat{D}_{XX}(\tau)] \approx \frac{\sigma^2_X}{N}\left(1 - \left(\frac{R_{XX}(\tau)}{\sigma^2_X}\right)^2 - \frac{2}{\pi}\left(\frac{R'_{XX}(\tau)}{\sigma_X \sigma_{\dot{X}}}\right)^2\right) \tag{3.57}$$

$$\mathrm{Var}[\hat{D}_{YX}(\tau)] \approx \frac{\sigma^2_Y}{N}\left(1 - \left(\frac{R_{YX}(\tau)}{\sigma_Y \sigma_X}\right)^2 - \frac{2}{\pi}\left(\frac{R'_{YX}(\tau)}{\sigma_Y \sigma_{\dot{X}}}\right)^2\right) \tag{3.58}$$

Since $R_{XX}(0) = \sigma^2_X$ and $R'_{XX}(0) = 0$ it follows that $Var(\hat{D}_{XX}(\tau)) = 0$ corresponding to the result for the level crossing triggering condition.

3.6.1 Example 1: Illustration of Triggering Conditions

The time series in fig. 3.15 is considered again.

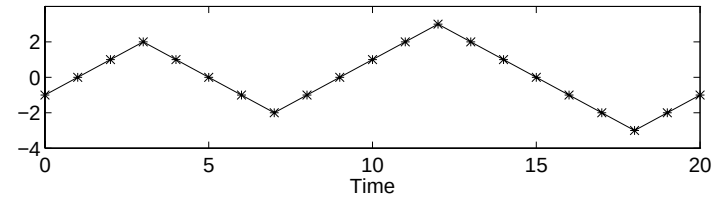

Figure 3.15: *Continuous process and the corresponding sampled discrete time series.*

The RD function is estimated using zero crossing with positive slope triggering. It is chosen to use 3 points in each RD functions. Figure 3.16 shows the time segments which have been picked out using the positive point triggering condition and the resulting RD function. The time axis of the time segments corresponds to the time axis in fig. 3.15.

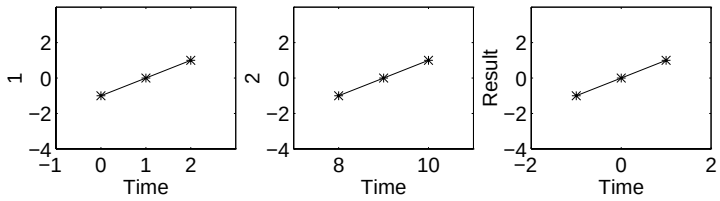

Figure 3.16: *The time segments and the resulting RD function estimated using zero crossing triggering with positive slope.*

As illustrated, 2 zero crossings with positive slope are detected.

3.6.2 Example 2: 2DOF System

The response of the 2DOF system described in section 3.2.2 is analysed. The estimated and theoretical RD functions are shown in figs. 3.17 and 3.18.

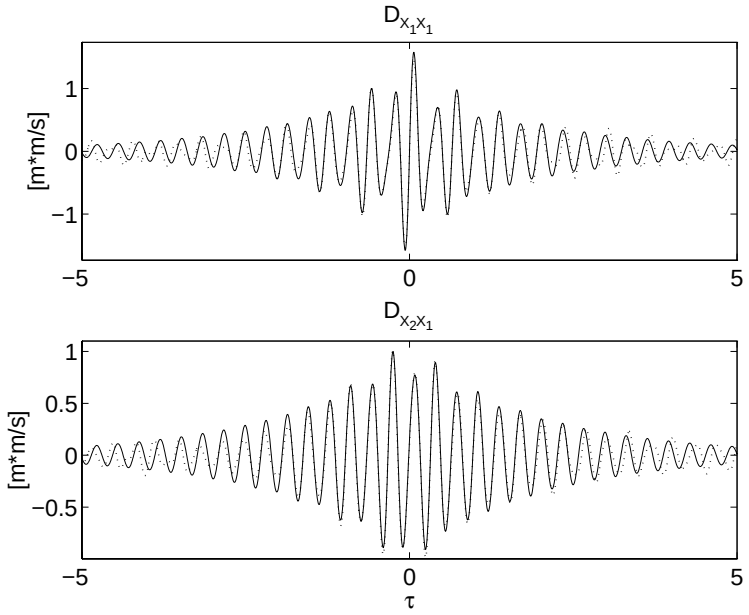

Figure 3.17: *Normalized RD functions estimated using zero crossing triggering applied to the response of the first mass. [------]: Theoretical RD functions, [· · · · ·]: Estimated RD functions.*

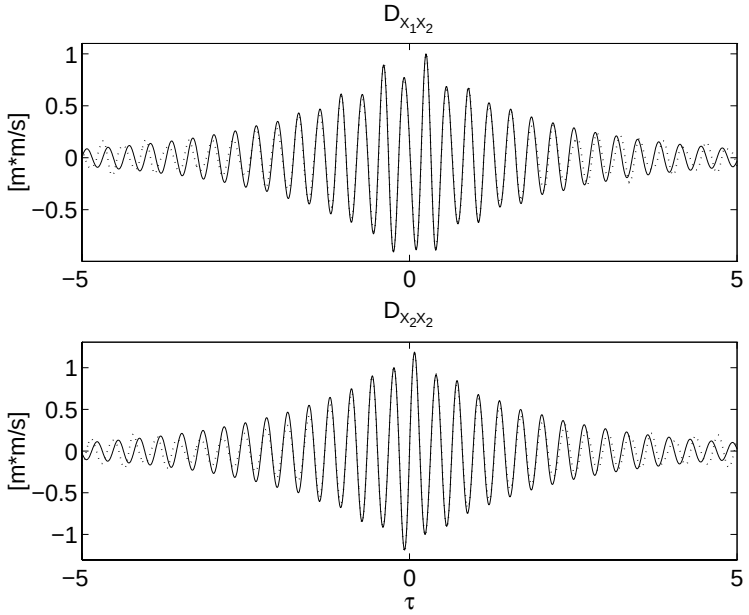

Figure 3.18: *Normalized RD functions estimated using zero crossing triggering applied to the response of the second mass. [------]: Theoretical RD functions, [· · · · ·]: Estimated RD functions.*

The auto RD functions illustrate why these functions are interpreted as impulse response functions. The number of triggering points was 263 and 236, respectively. The expected number of triggering points predicted by eq. (A.97) was 261 and 233, respectively.

3.7 Quality Assesment of RD Functions

In application of the RD technique it is an advantage to have some standard methods to assess the quality of the estimated RD functions. The advantage of standard methods is that valuable experience with this technique can be transferred between different data sets obtained from different physical systems. The purpose of quality assesment of RD functions is to answer the following questions.

- How well do the data approximate the assumption of stationarity and Gaussianity?
- Has the empirical mean value converged sufficiently towards the true mean value (or: Is the number of triggering points adequate)?
- How many points in the RD functions are estimated with sufficient accuracy?

These questions are correlated in some sense. They cannot be answered individually. Whether or not the data are realizations of a stationary process can often be judged with a pre-knowledge of the physical system and the loads. It is a common assumption that the physical system is time-invariant during the period where the measurements are collected. Then if the load is stationary the measurements will also be stationary. How well the data approximate a Gaussian distribution can be analysed by e.g. a normal probability plot or various tests. Usually the measurements are only approximately Gaussian distributed, but the RD technique is applied anyway under critical observation. Two different types of tests or investigations are suggested as standard methods for quality assesment of RD functions: Shape invariance test and symmetry test.

3.7.1 Shape Invariance Test

Testing the shape invariance of RD functions is based on several different estimations of a correlation function using different triggering levels for the same triggering condition

$$R^1_{YX}(\tau) = \frac{D_{YX}(\tau)}{a_1}\sigma_X^2 \ , \quad R^2_{YX}(\tau) = \frac{D_{YX}(\tau)}{a_2}\sigma_X^2 \ , \quad ... \tag{3.59}$$

where superscript $1, 2, ...$ refers to the different choice of triggering levels. If different estimates of a correlation function are calculated two different approaches exist to evaluate the shape invariance of the RD functions. First a plot of the different correlation functions is usually sufficient to validate the different estimates of the correlation functions. If a single estimate differ significantly from the rest, the corresponding triggering levels should not be used. If all estimates differs significantly the data should be analysed carefully with the RD technique. So the shape invariance test can also be used in a pre-analysis to select proper triggering levels for a full analysis.

If more than e.g. 5 or 6 different RD functions are estimated it might be difficult to asses the different triggering levels graphically. Instead it is suggested to calculate the correlation between the different RD functions. This corresponds to calculating the MAC values for different estimates of a mode shape in modal analysis, see eq. (2.54). Instead of using the MAC as an abbreviation it is chosen to denote the correlation coefficient as Shape Invariance Criteria (SIC).

The result of calculating the SIC values between all different estimates of the correlation functions is a matrix with unity in the diagonals. The off-diagonal elements all have values between 0 and 1. If the value is 1 the RD functions are fully correlated and if the value is 0 the RD functions are uncorrelated. The shape invariance test is illustrated in the following examples.

Example:

The system described in section 3.2.2 is considered again. In order to check the shape invariance of the RD functions only the response of mass 1 is considered. The positive point triggering condition with the triggering levels below is used.

$$[a_1\ a_2] = [0\ 0.5] \cdot \sigma_{X_1} \quad [a_1\ a_2] = [0.5\ 1.5] \cdot \sigma_{X_1} \quad [a_1\ a_2] = [1.5\ \infty] \cdot \sigma_{X_1} \tag{3.60}$$

The RD functions are estimated and normalized to be theoretically equal to the correlation functions. Figure 3.19 shows the normalized RD functions and the theoretical correlation function.

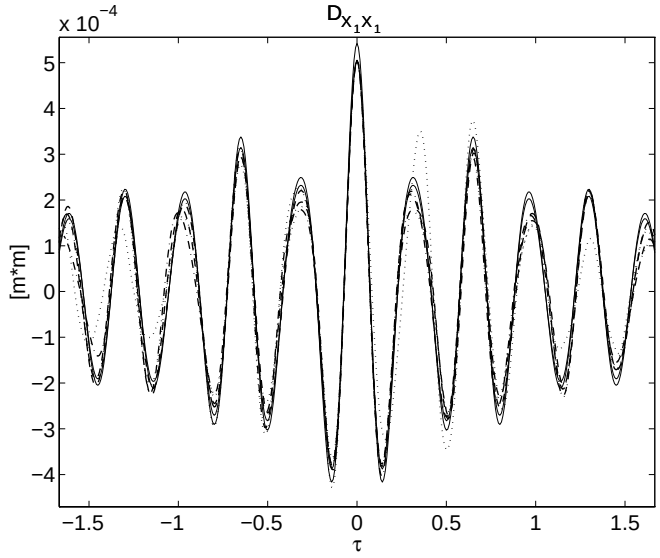

Figure 3.19: *Shape invariance of RD functions. [——]= Theoretical correlation function. [·····]=Estimated RD function with* $[a_1\ a_2] = [0\ 0.5] \cdot \sigma_{X_1}$. *[– · – · – · –]=Estimated RD function with* $[a_1\ a_2] = [0.5\ 1.5] \cdot \sigma_{X_1}$. *[- - - -]=Estimated RD function with* $[a_1\ a_2] = [1.5\ \infty] \cdot \sigma_{X_1}$.

Visually it seems as if the RD functions estimated using $[a_1\ a_2] = [0\ 0.5]\sigma_X$ are the most inaccurate function compared to the theoretical function. The SIC values are calculated between all estimates and the theoretical correlation function. The results are seen in table 3.2. The different functions are ordered so that the first three components correspond to the three RD functions and the fourth component is the theoretical correlation function.

$[a_1\ a_2]$	$[0\ 0.5]\sigma_X$	$[0.5\ 1.5]\sigma_X$	$[1.5\ \infty]\sigma_X$	Theo
$[0\ 0.5]\sigma_X$	1.00	0.88	0.88	0.89
$[0.5\ 1.5]\sigma_X$	0.88	1.00	0.97	0.97
$[1.5\ \infty]\sigma_X$	0.88	0.97	1.00	0.99
Theo	0.89	0.97	0.99	1.00

Table 3.2: *Shape Invariance criteria between three estimated RD functions and the theoretical correlation function.*

The number of triggering points for the different estimates of the RD functions were $N = [1712\ 2346\ 675]$. The shape invariance test shows that all three RD functions have a reasonable agreement both visually and using the SIC values. It is seen that the correlation between the RD functions and the theoretical correlation function is not a simple function of the number of triggering points. The estimates with the lowest number of triggering points have the highest correlation with the theoretical function. It is not unusual to observe that the accuracy of the RD functions increases with increasing triggering level, although the number of triggering points is decreasing.

◇

Example:

The system described in section 3.2.2 is considered again. The auto RD function of the response of the first mass is calculated using level crossing triggering condition. Two different triggering levels $a = \sqrt{2}\sigma_X$ and $a = -\sqrt{2}\sigma_X$ are used. The estimated correlation functions and the theoretical correlation functions are shown in fig. 3.20.

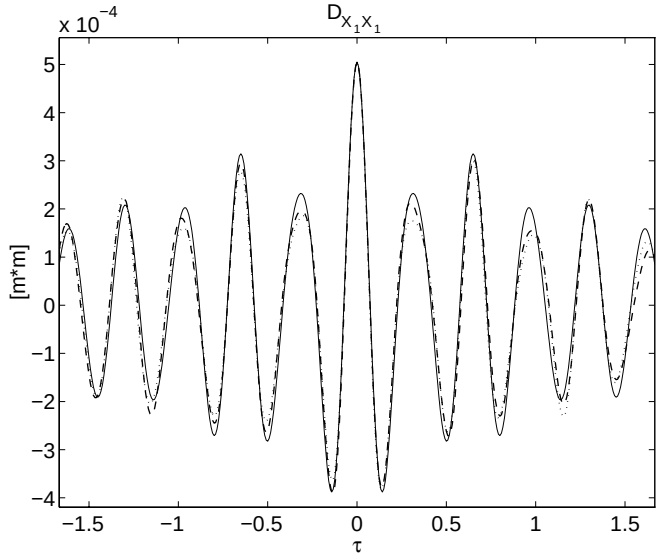

Figure 3.20: *Shape invariance of RD functions. [——]= Theoretical correlation function. [·····]=Estimated correlation function with* $a = 1.5\sigma_{X_1}$. *[- - - -]=Estimated correlation function with* $a = -1.5\sigma_{X_1}$.

The above figure illustrates that there is only a small difference between the two RD functions estimated using the same triggering level but with changed sign. If the average

of these two functions is used, maximum information is extracted from the measurements using the level crossing triggering condition.
◇

3.7.2 Symmetry Test

The second approach to quality assessment of the RD functions is based on the symmetry relations for correlation functions of stationary stochastic processes. This approach generally assumes that all possible RD functions are estimated, corresponding to estimating the full correlation matrix of the measurements at each time step. The approach can still be used if only a part of the correlation matrix is estimated, but this is considered to be a special case. The symmetry relation is.

$$R_{YX}(\tau) \;=\; R_{XY}(-\tau) \tag{3.61}$$

If the estimated RD functions are scaled to be equal to the correlation functions (normalized with the triggering levels) then an error function can be defined as.

$$\mathcal{E} \;=\; \frac{\hat{R}_{YX}(\tau) \;-\; \hat{R}_{XY}(-\tau)}{2} \tag{3.62}$$

A final estimate of the correlation functions can be calculated as the average value of the above RD functions.

$$\hat{R}_{YX}^{final}(\tau) \;=\; \frac{\hat{R}_{YX}(\tau) \;+\; \hat{R}_{XY}(-\tau)}{2} \tag{3.63}$$

If the above procedure is applied the number of RD functions is still the same, but there is only an estimate for the positive time lags and the corresponding error function. The quality of the RD functions can now be evaluated by plotting the final RD functions versus the error function. This procedure also can be used to choose the number of points used in the estimation of modal parameters.

Example:

The system described in section 3.2.2 is considered again. The RD functions of the responses are calculated using the positive point triggering condition. The triggering levels are chosen as $[0.5\sigma_X \;\infty]$. From the RD functions the error functions and the final RD functions are calculated. Figures 3.21 and 3.22 show the error functions and the final RD functions.

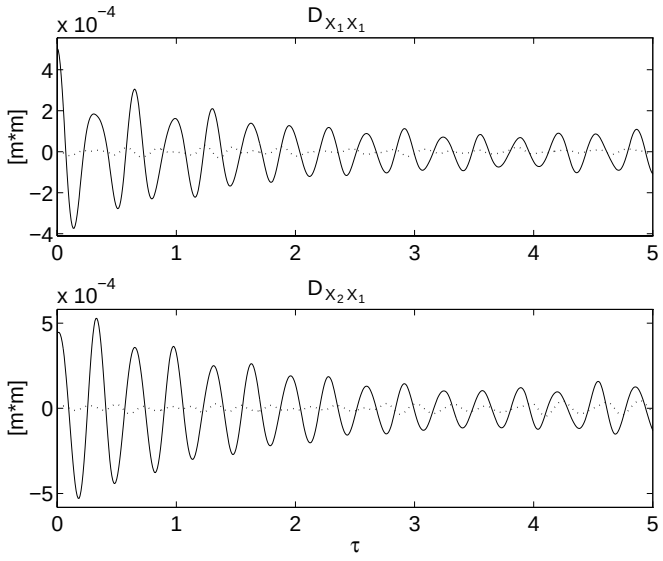

Figure 3.21: *Time averaged RD functions. [——]= Final RD function. [· · · · · ·]=Error function.*

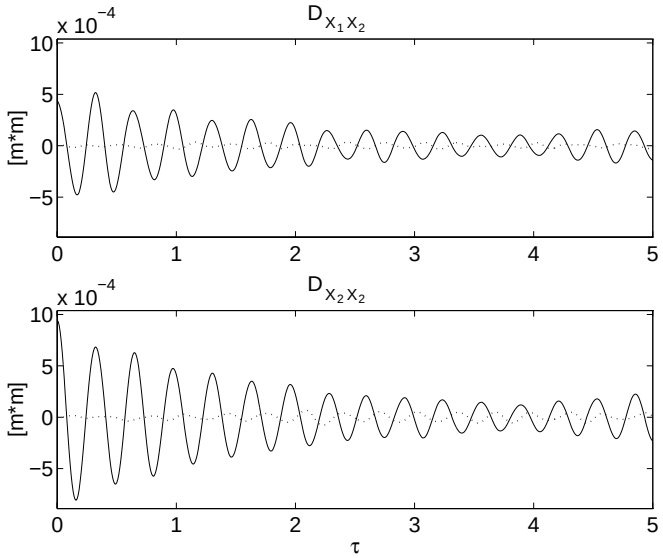

Figure 3.22: *Time averaged RD functions. [——]= Final RD function. [· · · · · ·]=Error function.*

The figures show that the error function is small compared to the RD function. The errors increase with increasing time lags. This is obvious since it is natural that the errors increase with increasing time lags from the triggering condition. The variances predicted by e.g. eq. (3.46) also state that the uncertainty of the RD functions increases with increasing time lags.

◇

If the number of measurements get too high, it becomes very tedious to evaluate the final RD functions and the error functions graphically. If e.g. 8 measurements are available 64

different RD and error functions have to be evaluated. This is not an adequate approach. Instead it is suggested that a proper measure for the quality of the RD functions is the fraction between the sum of the absolute value of the error function and the sum of the absolute value of the RD function

$$\mathcal{E}(k) \;=\; \sqrt{\left(\frac{\sum_{i=1}^{n} \mathcal{E}(\tau_i)^2}{\sum_{i=1}^{n} D_{YX}^{final}(\tau_i)^2} \right)} \tag{3.64}$$

where k is varying from 1 to the square of the number of measurements. This allows the quality of all the RD functions to be assessed in a single graph. Such a graph will illustrate if one of the measurements are unusable as triggering measurement.

3.8 Choice of Triggering Levels

One of the difficulties in applications of the RD technique is how to choose the triggering levels $[a_1 \; a_2]$ for a given triggering condition. From a user point of view it is important to know how to choose a proper triggering level and to know how sensitive the results are to the choice of triggering level. This section discusses how this choice can be made. The optimal choice of triggering level is defined as the choice which minimizes the variance of the RD functions normalized with the triggering level.

$$\min(\mathrm{Var}[\frac{\hat{D}_{XX}(\tau)}{\tilde{a}}]) \;\rightarrow\; [a_1 \; a_2] \tag{3.65}$$

For the level triggering condition eq. (3.65) has been solved using eqs. (3.24) and (A.56). The solution is a triggering level of $a \;=\; \sqrt{2}\sigma_X$. This result was derived by Hummelshøj et al. [11]. The assumptions are that the processes are stationary zero mean Gaussian distributed and that the time segments used in the averaging process are independent. The latter assumption is of course violated in some sense. However the above result is considered to be a good basis for selecting the triggering level for the level crossing triggering condition. The result has been supported by a simulation study in Brincker et al. [3]. The simulation study indicates that choices of the triggering level in between $\sigma_X - 2\sigma_X$ are appropriate. The simulation study takes the correlation between the segments into account. This supports the choice of $a \;=\; \sqrt{2}\sigma_X$.

For the local extremum triggering condition an equivalent study can be performed. The variance of the estimated RD functions using the local extremum triggering condition can be approximated by eq. (3.34).

$$\mathrm{Var}[\hat{D}_{XX}(\tau)] = \frac{\sigma_X^2}{N} \left(1 - \left(\frac{R_{XX}(\tau)}{\sigma_X^2} \right)^2 - \left(\frac{R'_{XX}(\tau)}{\sigma_X \sigma_{\dot{X}}} \right)^2 \right) + \frac{k^E}{N} \left(\frac{R_{XX}(\tau)}{\sigma_X^2} \right)^2 \tag{3.66}$$

The constant k^E is a function of the triggering levels.

$$k^E \;=\; \frac{\int_{a_1}^{a_2} x^2 p_X(x) dx}{\int_{a_1}^{a_2} p_X(x) dx} \;-\; \left(\frac{\int_{a_1}^{a_2} x p_X(x) dx}{\int_{a_1}^{a_2} p_X(x) dx} \right)^2 \tag{3.67}$$

In order to calculate the expected number of triggering points an SDOF system is considered. The system is loaded by white noise. The natural eigenfrequency and the damping ratio are f=1 Hz and ζ=1%. The expected number of triggering points can be calculated using eq. (A.70). The variance of different combinations of the triggering levels $[a_1\ a_2]$ are calculated for each time lag of the correlation functions. The triggering levels which minimize eq. (3.65) are taken as the optimal choice. Figure 3.65 shows the optimal upper triggering level and the lower optimal triggering level as a function of the time lag.

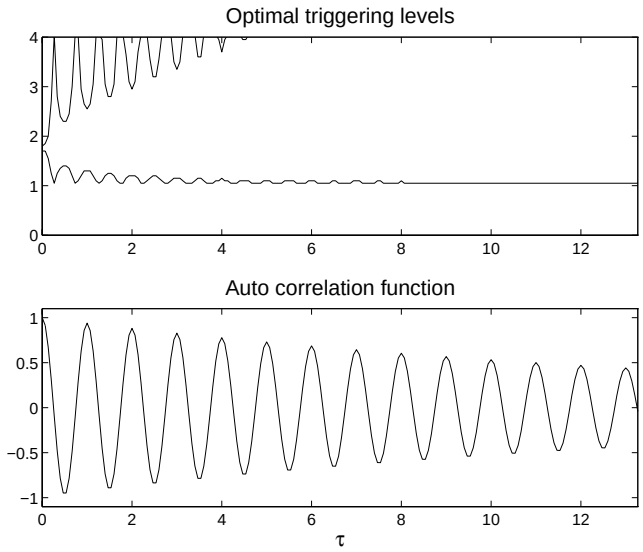

Figure 3.23: *Theoretically predicted optimal lower and upper triggering level ($_X$) for an SDOF system using local extremum triggering and the corresponding correlation function.*

Figure 3.23 illustrates a new result. It is not always that the optimal choice of triggering levels is those which maximize the number of triggering points. Theoretically, is it predicted that the triggering levels should be chosen as $[a_1\ a_2] = [\sigma_X\ \infty]$. The above result can only be a guideline to the user, since the result is dependent of the correlation function and thereby the physical system. The conclusion is that the triggering levels for the local extremum triggering condition should not uncritically be chosen as $[a_1\ a_2] = [0\ \infty]$, which maximizes the number of triggering points.

The above theoretical prediction does not take the correlation between the time segments in the averaging process into account. The prediction assumes uncorrelated time segments. In order to check the above result a simulation study is performed. 500 responses of the SDOF system loaded by Gaussian white noise are simulated. Each time series contains 5000 points and is sampled with 15 Hz. Estimates of the correlation function are calculated for each response using the local extremum triggering condition with different triggering levels. The triggering levels are chosen as all possible combinations of $a_1 = [0, 0.2, ..., 3] \cdot \sigma_X$, $a_2 = [0, 0.2, ..., 3] \cdot \sigma_X$ under the constraint that $a_2 > a_1$. The maximum upper level is chosen to $3\sigma_X$, since it is very unlike to find realizations of the response beyond $3\sigma_X$. A higher maximum upper level would demand simulation of extremely long time series. A similar argument is used to select the resolution of the triggering levels to 0.2. A higher resolution would also demand simulation of extremely long time series. The

optimal triggering levels are chosen as the levels with minimum error calculated as the sum of the absolute values of the difference between the simulated and theoretical correlation functions. The result of the simulation study is shown in figure 3.24.

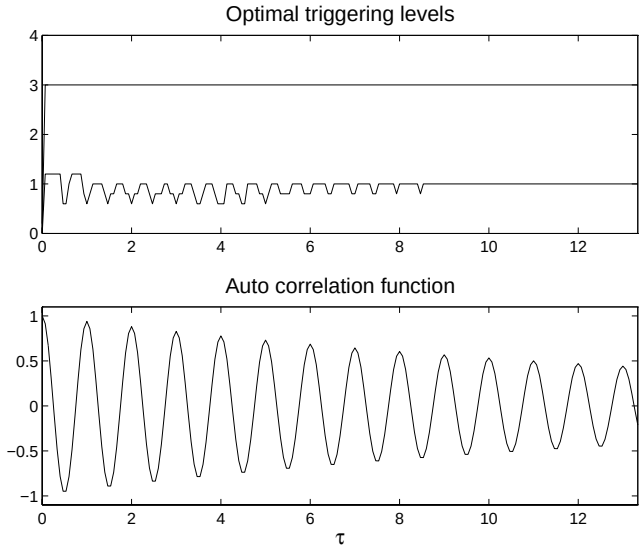

Figure 3.24: *Simulated optimal lower and upper triggering level ($\times\sigma_X$) for an SDOF system using local extremum triggering and the corresponding correlation function.*

The results of fig. 3.24 show good agreement with the theoretical predictions in fig. 3.23. It is recommended that the triggering levels for the local extremum triggering condition should be chosen around $[a_1\ a_2] = [\sigma_X\ \infty]$. The best way to select the optimal triggering levels is to perform a sensitivity study. The lower triggering level could be chosen as e.g. $[0\ 0.5\ 1\ 1.5]\cdot\sigma_X$ and the upper triggering level as infinity and the RD functions with lowest errors calculated using the symmetry relations decide which triggering levels are optimal.

A simulation study corresponding to the above is performed using the positive point triggering condition. The aim is to investigate how the triggering levels should be chosen. A theoretical prediction can be calculated, but the assumption of uncorrelated time segments is highly violated so the prediction is excluded. The results are shown in fig. 3.25.

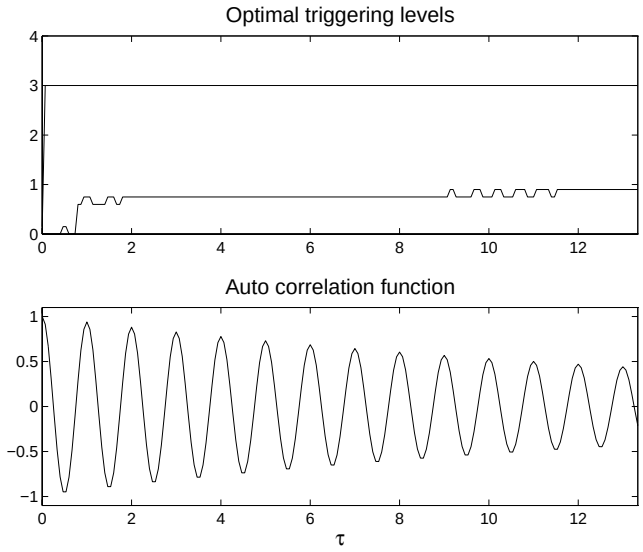

Figure 3.25: *Optimal triggering levels for positive point triggering for an SDOF system estimated by simulation together with the corresponding correlation function.*

The simulation study indicates that the triggering levels for the positive point triggering condition should be chosen as about $[a_1\ a_2] = [\sigma_X\ \infty]$.

During this section new information how to select the triggering levels for the different triggering conditions is obtained. It is shown that it can be appropriate to exclude the triggering points between 0 and σ_X. Although this is only a guideline it is important new information. The reason is that the accuracy of the estimates is increased and at the same time the estimation time is decreased since triggering points are excluded.

3.9 Comparison of Different Approaches

The purpose of this section is to compare the RD technique with other unbiased methods for estimation of correlation functions. Results shown in this section are parts of a study presented in Asmussen et al. [11]. The study will illustrate the advantages and the disadvantages of the RD technique. The comparison of the different techniques are based on simulations of the displacement response of a 2DOF system loaded by independent white noise at each mass. The modal parameters of the system are listed in table 3.3.

	f [Hz]	ζ [%]	$\lvert\phi\rvert^1$	$\lvert\phi\rvert^2$	$\angle\phi^1$	$\angle\phi^2$
Mode 1	3.17	1.22	1	1.62	0	1.5
Mode 2	4.92	3.50	1	0.62	0	178

Table 3.3: *Modal parameters of 2DOF system.*

The accuracy of the estimates of the (double sided) correlation functions is defined by the

error, $\mathcal{E}$

$$\mathcal{E} = \frac{1}{2 \cdot M + 1} \cdot \sum_{i=-M}^{M} (R(i \cdot \Delta t) - \hat{R}(i \cdot \Delta T))^2 \tag{3.68}$$

where R and $\hat{R}$ denote the theoretical correlation function and the estimate of the correlation function, respectively. The accuracy calculated using eq. (3.68) contains contributions from both random and bias errors. To reduce simulation errors all results are based on 250 averages (or simulations).

Section 3.9.1 describes the two traditional approaches which are used to estimate the correlation functions. Section 3.9.2 describes the chosen triggering conditions and levels for the RD technique. Section 3.9.3 presents the results of the simulation study. The simulation study is finished with a conclusion in section 3.9.4.

3.9.1 Traditional Approaches

The RD technique will be compared with two other traditionally and well-known approaches: The direct approach and an approach based on Fourier and inverse Fourier transforms. For the direct approach (or the sample estimate) the cross correlation functions in a finite continuous time interval are estimated by:

$$\hat{R}_{YX}(\tau) = \begin{cases} \frac{1}{T-\tau} \int_0^{T-\tau} y(t+\tau)x(t) & 0 \leq \tau < T \\ \\ \frac{1}{T-|\tau|} \int_{|\tau|}^{T} y(t+\tau)x(t) & -T < \tau \leq 0 \end{cases} \tag{3.69}$$

In a finite discrete time interval consisting of N points the cross correlation functions are estimated by

$$\hat{R}_{YX}(r\Delta T) = \begin{cases} \frac{1}{N-r} \sum_{i=0}^{N-r} y((i+r)\Delta T)x(i\Delta T) & 0 \leq r < N \\ \\ \frac{1}{N-|r|} \sum_{i=r}^{N} y((i-r)\Delta T)x(i\Delta T) & -N \leq r < 0 \end{cases} \tag{3.70}$$

The correlation functions estimated by the direct approach are unbiased. The second approach is based on Fourier and inverse Fourier transformations. The estimation procedure is unbiased and described in Bendat & Piersol [10] and Brincker et al. [2]. The computational steps are

- Divide the measurements into a number of sub-segments.
- Pad each sub-segment with zeroes to obtain double length.
- Calculate a subestimate of the cross spectral density by performing Fourier transformations of the sub-segments and multiply.
- Average all sub-cross spectral densities.

- Perform an inverse Fourier transformation of the averaged cross spectral density to obtain a biased estimate of the correlation function.
- Remove bias by division of the basic lag window.

The estimation time of both methods is of course dependent of size of the time series, T (N), and the maximum time lag, τ_{max}. But the estimation time of any of the methods is not dependent on the statistical nature of the time series. This is a significant difference compared to the RD technique.

3.9.2 Triggering conditions

For the RD technique 3 different triggering conditions are used: Level crossing, local extremum and positive point triggering. The triggering level for the level crossing condition is chosen as $\sqrt{2} \cdot \sigma_X$, where X is the triggering time series. This triggering level minimizes the variance of the estimate of the RD functions in eq. (3.24). For the local extremum triggering condition the triggering levels are chosen as $[a_1 \ a_2] = [1.5\sigma_X \ \infty]$. For the positive point triggering condition the triggering levels are also chosen as $[a_1 \ a_2] = [0 \ \infty]$. This assures that the maximum number of triggering points is obtained.

It is important that the estimation time of the RD functions using level crossing and local extremum triggering condition depends on the statistical nature of the time series. Two processes with different correlation structures would result in different estimation times. So the results for these two triggering conditions can only be guidelines. But the estimation time for the positive point triggering condition is independent of the statistical nature of the measurement. The results for the estimation time of this condition can be considered to be as general as the results for the direct and the Fourier-inverse Fourier approach. Since the triggering levels are $[0 \ \infty]$ the estimation times for the positive point condition will be the slowest possible for the RD technique. This is the reason for choosing these levels instead of e.g. $[\sigma_x \ \infty]$, which might result in more accurate RD functions.

3.9.3 Results of Simulation Study

Figure 3.26 shows the computational time of the different approaches used to estimate the correlation functions with a varying number of points in the time series. The number of time lags in the correlation functions is 128.

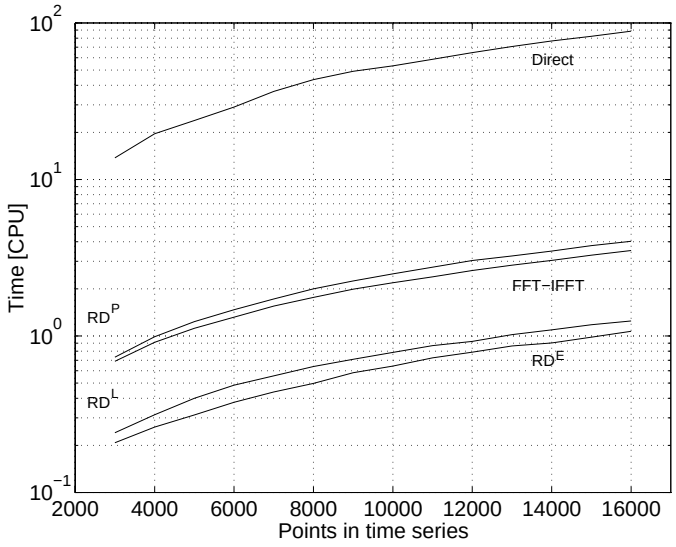

Figure 3.26: *Total estimation time of the 4 correlation functions with varying number of points in the time series and 128 time lags in the correlation functions. Direct: The direct approach. FFT-IFFT: The approach based on Fourier and inverse Fourier transformations.* RD^P*: Positive point triggering.* RD^E*: Local extremum triggering.* RD^L*: Level crossing triggering.*

As expected, the direct approach is clearly the slowest approach. The reduced estimation time by using the FFT-IFFT approach is obvious. The estimation time obtained using the positive point triggering condition is nearly equal to the estimation time obtained using the FFT-IFFT approach. Level crossing and local extremum triggering results in shorter estimation times compared to the FFT-IFFT approach. The estimation times of these two formulations depend on the chosen triggering levels and the correlation structure of the processes. Even though the estimation time would differ by using other triggering levels or a different physical system, the results indicate how fast the RD technique can be compared to the FFT-IFFT approach if a strict triggering condition is chosen.

Figure 3.27 shows the estimation time of the correlation functions with varying number of time lags in the correlation functions. The number of points in the time series is 8000.

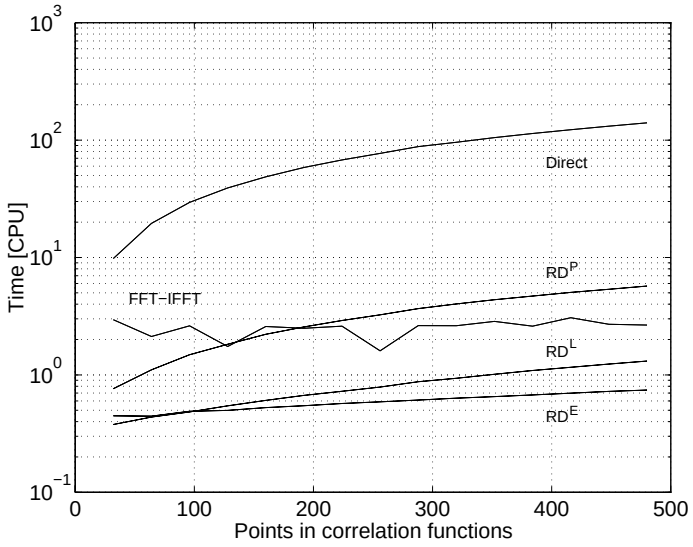

Figure 3.27: *Total estimation time of the 4 correlation functions with varying number of time lags and 8000 points in the time series. Direct: The direct approach. FFT-IFFT: The approach based on Fourier and inverse Fourier transformations.* RD^P*: Positive point triggering.* RD^E*: Local extremum triggering.* RD^L*: Level crossing triggering.*

Figure 3.27 shows the same tendency as figure 3.26. If a strict RD formulation, such as level crossing or local extremum triggering is used, the RD technique becomes faster than the FFT-IFFT approach. If only a small number of time lags is needed, the RD technique becomes significantly faster than the FFT-IFFT approach. The difference in the estimation time between the different triggering conditions reduces with a decreasing number of time lags in the correlation functions. This can be explained by the fact that the averaging process and the detection of triggering points both contribute to the total estimation time. For estimates with a large number of time lags the averaging process is dominant. With a decreasing number of time lags in the estimates, the detection of triggering points becomes correspondingly more dominant. On average the the number of triggering points for local extremum was 224 and for level crossing 430. For a large number of time lags local extremum triggering is faster. But for a small number of time lags level crossing triggering is faster. This is expected, since detecting a local extremum is more time consuming than detecting a level crossing.

Figure 3.28 shows the accuracy (see eq. (3.68)) of the different methods as a function of the number of points in the time series. Figure 3.29 shows the results of the same investigations performed on the time series with 20 % noise added. 20 % is the ratio between the standard deviation of the noise and the standard deviation of the time series. The direct approach has been omitted due to the high estimation times.

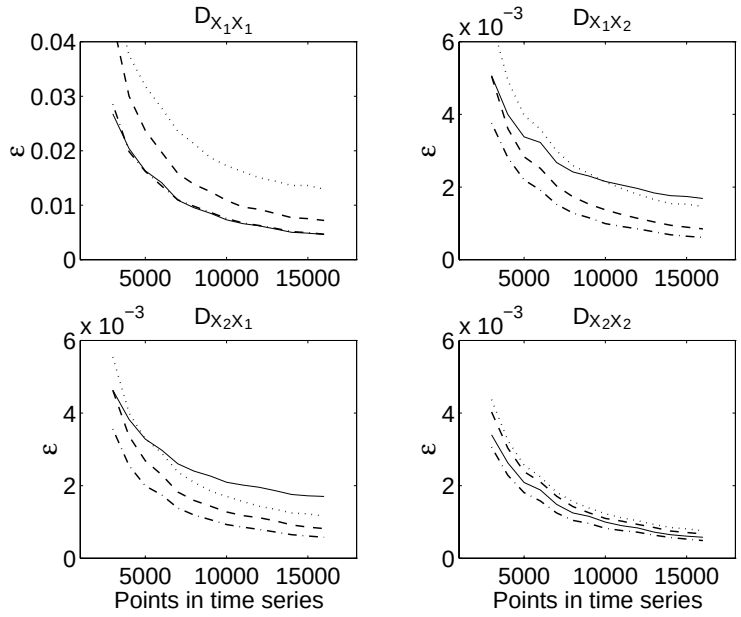

Figure 3.28: *Accuracy, $\mathcal{E}$, of correlation functions with varying time series length. 128 points in the correlation functions. [———] =FFT-IFFT, [· · · ·]=Local extremum, [– · – ·]=Positive point, [– – –]=Level crossing.*

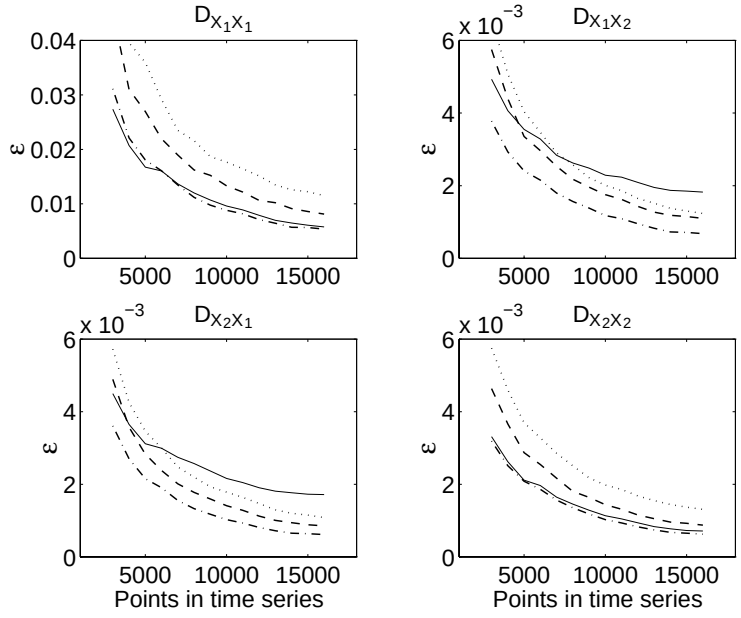

Figure 3.29: *Accuracy, $\mathcal{E}$, of correlation functions with varying time series length. 128 points in the correlation functions. 20 % noise independent Gaussian white noise added. [———] =FFT-IFFT, [· · · ·]=Local extremum, [– · – ·]=Positive point, [– – –]=Level crossing.*

As expected, the results show that the error of all four approaches converges towards zero with increasing length of the time series. The effect of adding noise is a slower convergence rate, but the results still have a high accuracy compared with the noise free analysis. The positive point triggering condition gives the lowest error, whereas the local extremum triggering condition has the highest error.

Figures 3.30 and 3.31 show the quality of the 4 approaches as a function of the number of points in the correlation functions. The results are based on 8000 points in the time series.

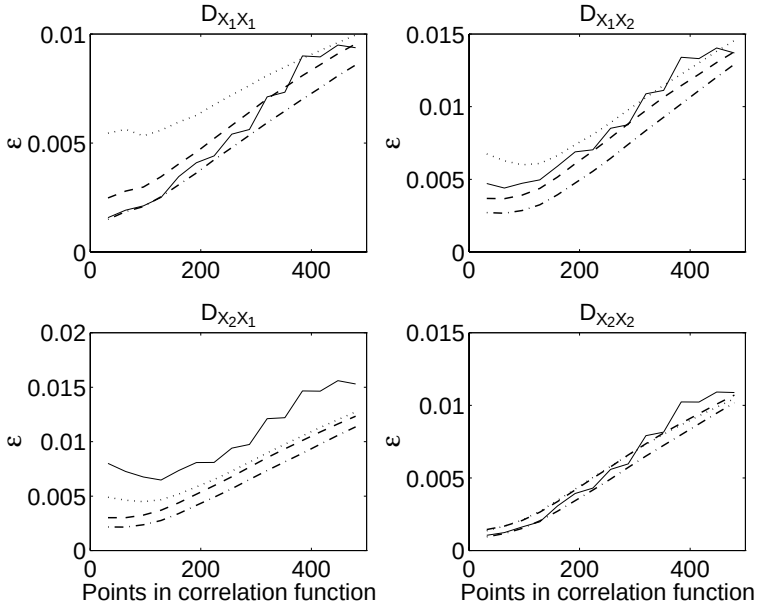

Figure 3.30: *Accuracy, $\mathcal{E}$, of correlation functions with increasing number of time lags. 8000 points in the time series. [−−−−−] =FFT-IFFT, [· · · ·]=Local extremum, [− · − ·]=Positive point, [− − −]=Level crossing.*

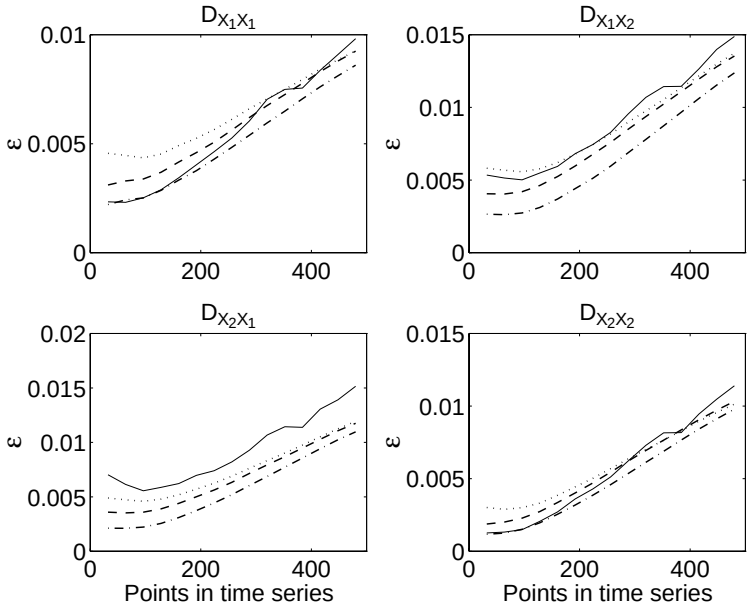

Figure 3.31: *Accuracy, $\mathcal{E}$, of correlation functions with increasing number of time lags. 8000 points in the time series. 20 % independent Gaussian white noise added. [———] =FFT-IFFT, [· · ·]=Local extremum, [– · – ·]=Positive point, [– – –]=Level crossing.*

All 4 approaches have increasing accuracy with an increasing number of points in the time series. In general the RD technique with local extremum triggering condition gives the highest error. The general difference between the results from the noise free responses and the responses with 20% noise added is only a slight increase in the error. It is interesting that although the absolute error is different for the 4 approaches, the rate of increase in the errror with increasing number of points in the correlation functions is the same.

3.9.4 Conclusions

Three different unbiased approaches for non-parametric estimation of correlation functions have been investigated: The direct approach, The FFT-IFFT approach and the RD technique. The main issue was illustration of advantages and disadvantages of different formulation of the RD technique. The investigations are based on simulated response of a 2DOF system loaded by Gaussian white noise.

The direct approach was clearly the most time-consuming approach. For a small number of points in the correlation functions the RD technique is the fastest approach no matter how this approach is formulated. For a large number of points only a strict formulation of the RD technique is faster than the FFT-IFFT approach.

Triggering using positive points and the FFT-IFFT produces the most accurate estimates of the modal parameters compared to the level crossing and the local extremum triggering condition. More information about the influence of applying bounds to the positive point triggering condition is needed. Applying bounds will decrease the estimation time and most probably also decrease the uncertainty.

3.10 Summary

The purpose of this chapter is to present and illustrate the RD technique. The main assumptions of the results are that the stochastic processes are stationary zero mean Gaussian distributed processes. In section 3.1 the RD functions are defined and the estimation procedure is presented. It is shown that the estimates of the RD functions are unbiased.

Section 3.2 introduces the applied general triggering condition. It is shown that using this triggering condition the RD functions become a weighted sum of the correlation functions and the time derivative of the correlation functions. Furthermore, an approximate equation for calculation of the variance of the RD functions is given. The applied general triggering condition is introduced, since the results for the four most well known triggering conditions can be derived directly from the results of the applied general triggering condition. These four conditions, level crossing, local extremum, positive point and zero crossing with positive slope are presented in sections 3.3 - 3.6. The relation between the RD functions and the correlation functions is given and an approximate relation for the variance of the RD functions is stated. The triggering conditions are illustrated by a simulation study.

Section 3.7 introduces the concept of quality assessment of RD functions. It is illustrated how the shape invariance relation of RD functions and the symmetry relations of correlation functions of stationary processes can be used as a basis for quality assessment. Section 3.8 indicates how the triggering levels of RD functions should be chosen. Guidelines for the user are given.

The chapter is concluded with a comparison of the speed and quality of different unbiased methods for estimation of correlation functions of stationary processes. It is shown that the RD technique can be superior in speed and/or quality if the triggering conditions and levels are selected carefully.

Bibliography

[1] Vandiver, J.K., Dunwoody, A.B., Campbell, R.B. & Cook, M.F. *A Mathematical Basis for the Random Decrement Vibration Signature Analysis Technique.* Journal of Mechanical Design, Vol. 104, April 1982, pp. 307-313.

[2] Brincker, R., Krenk, S., Kirkegaard, P.H. & A. Rytter. *Identification of Dynamical Properties from Correlation Function Estimates.* Bygningsstatiske Meddelelser, Vol. 63, No. 1, 1992, pp. 1-38.

[3] Brincker, R., Krenk, S. & J.L. Jensen *Estimation of Correlation Functions by the Random Dec Technique.* Proc. Skandinavisk Forum for Stokastisk Mekanik, Lund, Sweden, Aug. 30-31, 1990.

[4] Ditlevsen, O. *Uncertainty Modelling.* McGraw-Hill Inc. 1981. ISBN: 0-07-010746-0.

[5] Melsa, J.L. & Sage, A.P. *An Introduction to Probability and Stochastic Processes.* Prenctice-Hall, Inc. Englewood Cliffs, N.J., 1973. ISBN: 0-13-034850-3.

[6] Søderstrøm, T. & Stoica, P. *System Identification.* Prentice Hall International (UK) Ltd, 1989. ISBN: 0-13-881236.

[7] Rice, S.O. *Mathematical Analysis of Random Noise.* Bell Syst. Tech. J., Vol. 23, pp. 282-332; Vol 24, pp. 46-156. Reprinted in N. Wax, Selected Papers on Noise and stochastic Processes.

[8] Hummelshøj, L.G., Møller, H. & Pedersen, L. *Skadesdetektering ved Responsmåling.* M.Sc. Thesis (In Danish), Aalborg University, 1991.

[9] Brincker, R., Jensen, J.L. & Krenk, S. *Spectral Estimation by the Random Dec Technique.* Presented at the 9th International Conference on Experimental Mechanics, Lyngby, Copenhagen, August 20-24, 1990.

[10] Bendat, J.S. & Piersol, A.G. *Random Data - Analysis and Measurement Procedures.* 1986 John Wiley & Sons, Inc. ISBN 0-471-0400-2.

[11] Asmussen, J.C. & Brincker, R. *Estimation of Correlation Functions by Random Decrement.* Proc. ISMA-21, Noise and Vibration Engineering, Leuven, Belgium, Sept. 18-20, 1996, Vol. II, pp. 13-19.

[12] Allemang, R.J. & Brown, D.L. *A Correlation Coefficient for Modal Vector Analysis.* Proc. 1st International Modal Analysis Conference, Orlando, Florida, USA, 1982.

Chapter 4

Vector Triggering Random Decrement

This chapter introduces a new concept: Vector triggering Random Decrement (VRD). The argumentation for developing this technique is that experience has discovered some problems with the RD technique applied to a large number of measurements (e.g. >4) collected simultaneously. This is often the situation in ambient testing of bridges.

- If all measurements are used as the reference measurement, which will result in the maximum number of RD functions (full correlation matrix estimated), the estimation time will increase proportionally to the number of measurements compared to the situation where only a single measurement is used as reference measurement. Since the speed is one of the main advantages of this technique a decision of estimating all possible RD setups should be reconsidered. On the other hand if not all possible RD functions are estimated, valuable information can be lost.
- If only some of the RD setups are estimated, how should the actual reference measurements be chosen. By assuming the signal-to-noise ratio to be highest at the measurements with highest standard deviation, the standard deviation could be used as a criterion. But this is only a guideline, not a full solution.
- Usually the uncertainty of the cross RD functions is higher than the uncertainty of the auto RD functions. So auto RD functions should only be used for modal parameter estimation. But this excludes the possibility to estimate mode shapes.

The above problems are the motivation for developing the VRD technique. The target is somehow to estimate equivalent auto RD functions, which contains phase information and thus the possibility to estimate mode shapes, in contrast to auto RD functions only. The solution is to apply a vector triggering condition instead of the scalar triggering conditions used in chapter 3. The VRD concept is first presented in Ibrahim et al. [1], [2] and Asmussen et al. [3]. The purpose of this chapter is to present and illustrate the VRD technique.

VRD functions are defined in section 4.1 corresponding to the definition of the RD functions in section 3.1. A mathematical basis of the VRD technique is presented in section 4.2. In Ibrahim et al. [1], [2] a mathematical basis is presented, where the VRD functions are interpreted as free decays. In section 4.2 the VRD functions are interpreted in term

of correlation function. The link between the correlation functions and VRD functions is derived for the first time. The results will be equivalent to the results of chapter 4. In section 4.3 the variance of the VRD functions are derived. Section 4.4 discusses quality assessment of VRD functions. Sections 4.5 and 4.6 present simulation studies of the VRD technique. The purpose is to investigate the performance of the VRD technique compared to the traditional RD technique. The examples illustrate the advantage of the VRD technique.

4.1 Definition of VRD functions

Consider an n-dimensional stochastic vector process, $\mathbf{X}(t)$. The VRD functions are defined equivalently to traditional RD functions

$$\mathbf{D_X}(\tau) \;=\; \mathrm{E}[\mathbf{X}(t+\tau)|T^v_{\mathbf{X}(t+\mathbf{\Delta t})}] \tag{4.1}$$

where the vector triggering condition, $T^v_{\mathbf{X}(t+\mathbf{\Delta t})}$, is defined as

$$T^v_{\mathbf{X}(t+\mathbf{\Delta t})} \;=\; T^v_{X_1(t+\Delta t_1),X_2(t+\Delta t_2),...,X_m(t+\Delta t_m)}\;, \quad 2 \le m \le n \tag{4.2}$$

The size of the vector triggering condition has to be in between 2 and n. If the condition is scalar, a traditional RD triggering condition is formulated. A triggering point is detected if several of the elements (m) in the stochastic vector process fulfil individually formulated triggering conditions at any time t plus the individual time shifts Δt_i, $\mathbf{\Delta t} = [\Delta t_1, \Delta t_2, ..., \Delta t_m]$. At this stage the triggering conditions could be any of the conditions discussed in chapter 4. But as explained in section 4.2 only the positive point triggering condition is of practical interest.

The VRD functions are estimated as the empirical mean by assuming the processes to be ergodic

$$\hat{\mathbf{D}}_{\mathbf{X}}(\tau) \;=\; \frac{1}{N}\sum_{i=1}^{N} \mathbf{X}(t_i+\tau)|T^v_{\mathbf{X}(t_i+\mathbf{\Delta t})} \tag{4.3}$$

Another way of estimating the VRD functions is

$$\hat{\mathbf{D}}_{\mathbf{X}}(\tau+\mathbf{\Delta t}) \;=\; \frac{1}{N}\sum_{i=1}^{N} \mathbf{X}(t_i+\tau+\mathbf{\Delta t})|T^v_{\mathbf{X}(t_i+\mathbf{\Delta t})} \tag{4.4}$$

Of course the VRD functions $\hat{\mathbf{D}}_{\mathbf{X}}(\tau+\mathbf{\Delta t})$ should be shifted backwards according to the time shift vector, $\mathbf{\Delta t}$. Which of these implementation possibilities to use is for the user to decide. In the implementation performed during this work eq. (4.3) is preferred, since the time shift problem is solved during the estimation process. The time shift problem is thereby solved once and for all. Estimation of the VRD functions using eqs. (4.3) or (4.4) provides unbiased estimates, corresponding to the RD technique.

The following examples illustrate the VRD technique and some of the possibilities in formulation of the triggering condition, $T^v_{\mathbf{X}(t+\mathbf{\Delta t})}$, are discussed. The latter example illustrates the algorithm on a simple system corresponding to the examples in chapter 3.

Example - Situation with 2 Measurements

Consider a 2×1-dimensional stochastic vector process, $\mathbf{X}(t)$. The VRD functions obtained from a vector triggering condition of size two are given by

$$\begin{bmatrix} D_{X_1}(\tau) \\ D_{X_2}(\tau) \end{bmatrix} = \mathrm{E}[\begin{bmatrix} X_1(t+\tau) \\ X_2(t+\tau) \end{bmatrix} | T^v_{X_1(t+\Delta t_1),X_2(t+\Delta t_2)}] \tag{4.5}$$

The estimate of the VRD functions is calculated as

$$\begin{bmatrix} \hat{D}_{X_1}(\tau) \\ \hat{D}_{X_2}(\tau) \end{bmatrix} = \frac{1}{N}\sum_{i=1}^{N} \begin{bmatrix} x_1(t_i+\tau) \\ x_2(t_i+\tau) \end{bmatrix} | T^v_{x_1(t_i+\Delta t_1),x_2(t_i+\Delta t_2)} \tag{4.6}$$

where $x_i(t)$ is a realization of $X_i(t)$.

$\diamond$

Example - Situation with 4 Measurements

Consider a 4×1-dimensional stochastic vector process, $\mathbf{X}(t)$. The VRD functions obtained from a vector triggering condition of size four are given by

$$\begin{bmatrix} D_{X_1}(\tau) \\ D_{X_2}(\tau) \\ D_{X_3}(\tau) \\ D_{X_4}(\tau) \end{bmatrix} = \mathrm{E}[\begin{bmatrix} X_1(t+\tau) \\ X_2(t+\tau) \\ X_3(t+\tau) \\ X_4(t+\tau) \end{bmatrix} | T^v_{X_1(t+\Delta t_1),X_2(t+\Delta t_2),X_3(t+\Delta t_3),X_4(t+\Delta t_4)}] \tag{4.7}$$

The estimation of the VRD functions is calculated as

$$\begin{bmatrix} \hat{D}_{X_1}(\tau) \\ \hat{D}_{X_2}(\tau) \\ \hat{D}_{X_3}(\tau) \\ \hat{D}_{X_4}(\tau) \end{bmatrix} = \frac{1}{N}\sum_{i=1}^{N} \begin{bmatrix} x_1(t_i+\tau) \\ x_2(t_i+\tau) \\ x_3(t_i+\tau) \\ x_4(t_i+\tau) \end{bmatrix} | T^v_{x_1(t_i+\Delta t_1),x_2(t_i+\Delta t_2),x_3(t_i+\Delta t_3),x_4(t_i+\Delta t_4)} \tag{4.8}$$

where $x_i(t)$ are realizations of $X_i(t)$. It is obvious that the number of triggering points N will always decrease with an increasing number of measurements or elements in the vector triggering condition. With a high number of measurements, e.g. four, it is not obvious that the triggering condition should be applied to all measurements. This could lead to a low number of triggering points, resulting in an estimate of the VRD functions, which has not converged sufficiently.

The solution to this problem is to estimate one or several sets of VRD functions, each containing a number of VRD functions corresponding to the number of measurements. This is illustrated in the situation with four measurements by defining two sets of VRD functions.

$$\begin{bmatrix} D^1_{X_1}(\tau) \\ D^1_{X_2}(\tau) \\ D^1_{X_3}(\tau) \\ D^1_{X_4}(\tau) \end{bmatrix} = \mathrm{E}[\begin{bmatrix} X_1(t+\tau) \\ X_2(t+\tau) \\ X_3(t+\tau) \\ X_4(t+\tau) \end{bmatrix} | T^v_{X_1(t+\Delta t_1),X_2(t+\Delta t_2)}] \tag{4.9}$$

$$\begin{bmatrix} D^2_{X_1}(\tau) \\ D^2_{X_2}(\tau) \\ D^2_{X_3}(\tau) \\ D^2_{X_4}(\tau) \end{bmatrix} = \mathrm{E}[\begin{bmatrix} X_1(t+\tau) \\ X_2(t+\tau) \\ X_3(t+\tau) \\ X_4(t+\tau) \end{bmatrix} | T^v_{X_3(t+\Delta t_3),X_4(t+\Delta t_4)}] \tag{4.10}$$

In the general case with n measurements the maximum number of VRD setups which can be estimated is the lowest integer of $n/2$. Furthermore, the size of the vector triggering condition does not have to be equal for every setup. Consider e.g. five simultaneously recorded measurements. Two VRD setups could be calculated by the triggering conditions

$$T^v_{X_1(t+\Delta t_1),X_2(t+\Delta t_2)} \ , \quad T^v_{X_3(t+\Delta t_3),X_4(t+\Delta t_4),X_5(t+\Delta t_5)} \tag{4.11}$$

or alternatively

$$T^v_{X_1(t+\Delta t_1),X_2(t+\Delta t_2),X_3(t+\Delta t_3)} \ , \quad T^v_{X_4(t+\Delta t_4),X_5(t+\Delta t_5)} \tag{4.12}$$

$\diamond$

Example - Illustration of the Algorithm

The purpose of this example is to illustrate the VRD algorithm applied to a simple system. The resulting VRD function does not have any interpretation. Consider two continuous-time processes, $X_1(t)$ and $X_2(t)$. The continuous-time processes are shown i fig. 4.1 together with two discrete-time processes corresponding to sampling $X_1(t)$ and $X_2(t)$ simultaneously at equidistant time points.

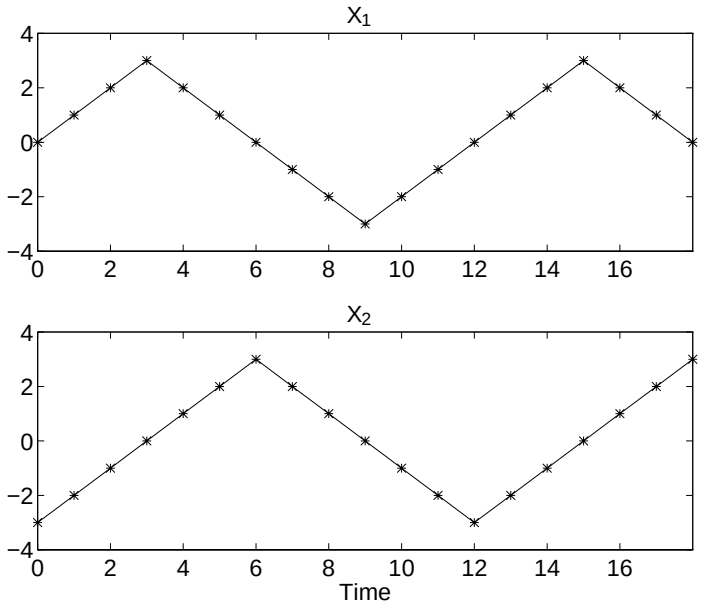

Figure 4.1: *The continuous-time processes and the corresponding discrete-time process.*

The VRD functions of the two processes are calculated using the following vector triggering condition and the following size of the time segments.

$$T^v_{\mathbf{X}(t+\boldsymbol{\Delta} t)} \ = \ \{X_1(t) > 0, \ X_2(t) > 0\} \tag{4.13}$$

$$\mathbf{D}_{\mathbf{X}}(\tau) = E[\mathbf{X}(t+\tau)|T^{v}_{\mathbf{X}(t+\mathbf{\Delta t})}] \qquad -1 \leq \tau \leq 1 \tag{4.14}$$

where $\mathbf{X}(t) = [X_1(t)\ X_2(t)]$. As seen the time shift vector is $\mathbf{\Delta t} = [0\ 0]$. Four triggering points are detected in the two processes. Figures 4.2 and 4.3 show the time segments at each triggering point and the resulting VRD functions. The time axis of the time segments corresponds to the time segments of the processes in fig. 4.1.

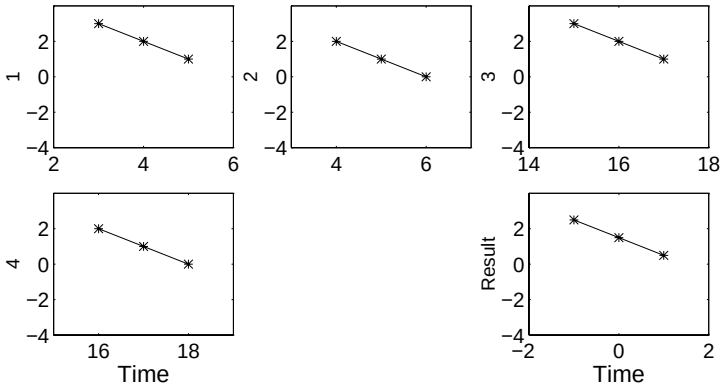

Figure 4.2: *The time segments picked out in the averaging process and the resulting VRD functions for* $X_1(t)$.

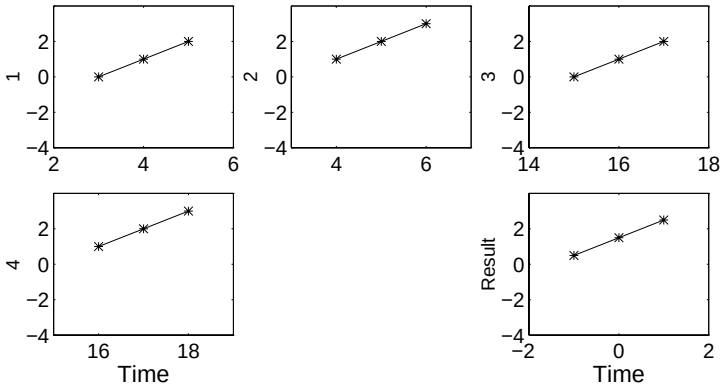

Figure 4.3: *The time segments picked out in the averaging process and the resulting VRD functions for* $X_2(t)$.

Figures 4.2 and 4.3 show that the VRD functions of the discrete-time process correspond to the VRD functions of the continuous-time process at the discrete-time points. The vector triggering condition could also have been formulated as

$$T^{v}_{\mathbf{X}(t+\mathbf{\Delta}t)} \ = \ \{X_1(t) > 0,\ X_2(t) < 0\} \tag{4.15}$$

where the time shift vector still is $\mathbf{\Delta}t = [0\ 0]$. Figures 4.4 and 4.5 show the the time segments picked out by the triggering condition and the corresponding resulting VRD functions.

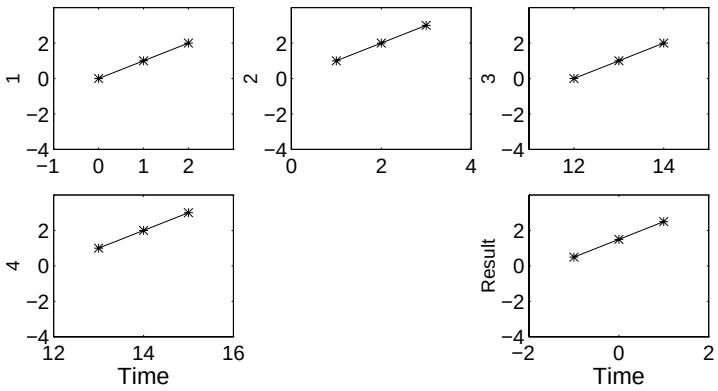

Figure 4.4: *The time segments picked out in the averaging process and the resulting VRD functions for* $X_1(t)$.

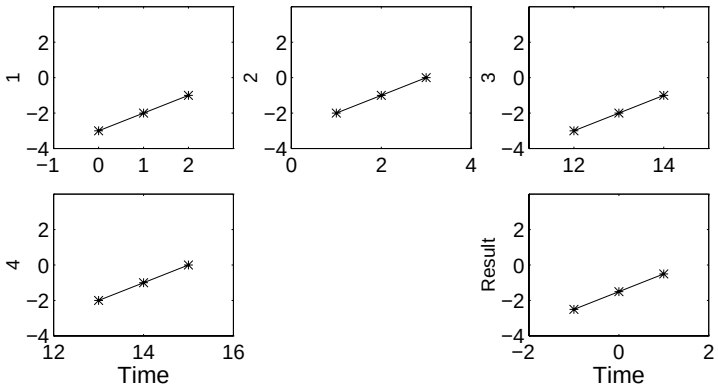

Figure 4.5: *The time segments picked out in the averaging process and the resulting VRD functions for* $X_2(t)$.

Four triggering points are detected using this triggering condition. In order to increase the number of triggering points the time shift vector can be chosen to be different from $\mathbf{\Delta}t = [0\ 0]$. A new triggering condition is formulated as

$$T^v_{\mathbf{X}(t+\mathbf{\Delta}t)} \;=\; \{X_1(t) > 0 \;\wedge X_2(t+3) > 0\} \tag{4.16}$$

A time shift has been introduced at $X_2(t)$, since $\mathbf{\Delta t} = [0\ 3]$. Figures 4.6 and 4.7 show the time segments picked out for the averaging process and the resulting VRD functions.

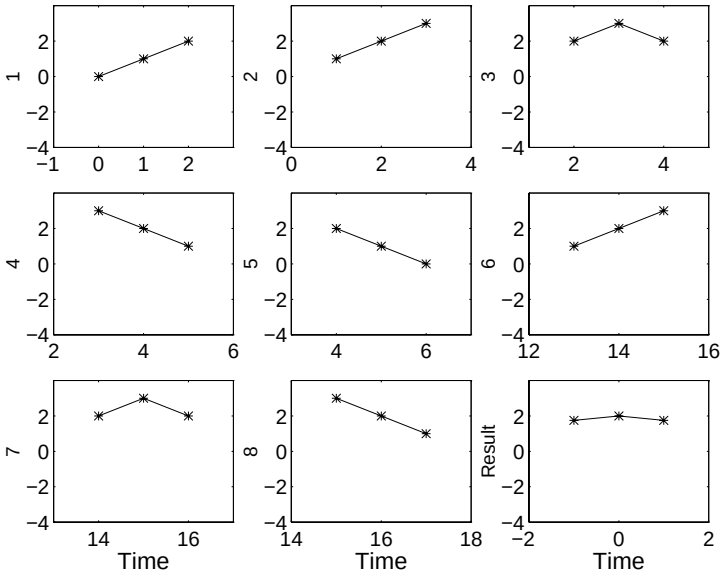

Figure 4.6: *The time segments picked out in the averaging process and the resulting VRD functions for* $X_1(t)$.

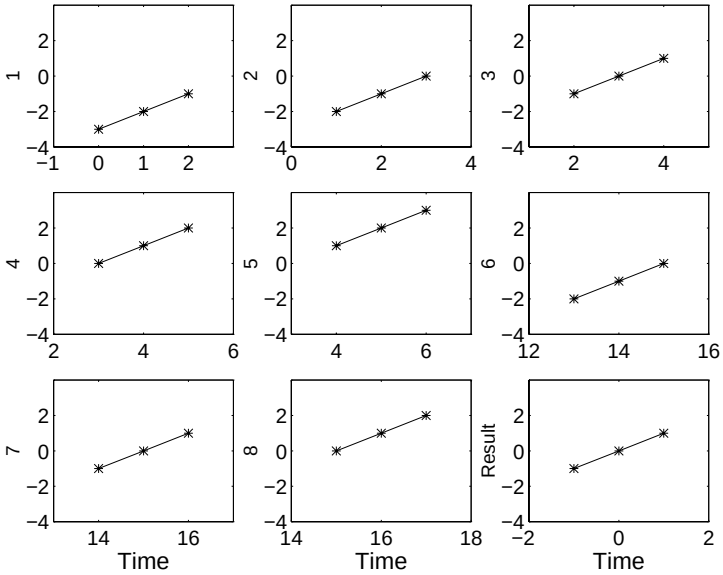

Figure 4.7: *The time segments picked out in the averaging process and the resulting VRD functions for* $X_2(t)$.

By introducing a proper time shift the number of triggering points has been increased from four to eight. This illustrates how versatile the VRD technique is. The number of triggering points is not only controlled by the triggering bounds but also by the choice of time shift vector. Notice that in figs. 4.6 and 4.7 the time segments are all picked out at the time t although the triggering condition is fulfilled at the time t for $X_1(t)$ and at time $t+3$ for $X_2(t)$.

4.2 Mathematical Basis of VRD

This section develops the relation between the VRD functions and the correlation functions of stationary zero mean Gaussian distributed processes. Consider an $n \times 1$-dimensional stochastic vector process, $\mathbf{X}(t)$

$$\mathbf{X}(t) \;=\; [X_1(t),\; X_2(t),\; \ldots, X_n(t)]^T \tag{4.17}$$

The correlation matrix of $\mathbf{X}$ at any time difference τ is given by

$$\begin{aligned} \mathbf{R_{XX}}(\tau) \;&=\; \mathrm{E}[\mathbf{X}(t+\tau)\mathbf{X}^T(t)] \\ &= \begin{bmatrix} R_{X_1X_1}(\tau) & R_{X_1X_2}(\tau) & .... & R_{X_1X_n}(\tau) \\ R_{X_2X_1}(\tau) & R_{X_2X_2}(\tau) & .... & R_{X_2X_n}(\tau) \\ : & : & : & : \\ R_{X_nX_1}(\tau) & R_{X_nX_2}(\tau) & .... & R_{X_nX_n}(\tau) \end{bmatrix} \end{aligned} \tag{4.18}$$

For simplicity the correlation matrix can be written as follows

$$\mathbf{R_{XX}}(\tau) \;=\; [\mathbf{R}_{X_1}(\tau)\; \mathbf{R}_{X_2}(\tau)\; \ldots\; \mathbf{R}_{X_n}(\tau)] \tag{4.19}$$

where the correlation vectors $\mathbf{R}_{X_i}$ are given by

$$\mathbf{R}_{X_i} \;=\; [R_{X_1X_i}(\tau)\; R_{X_2X_i}(\tau)\; \ldots\; R_{X_nX_i}(\tau)]^T \tag{4.20}$$

To describe the VRD technique two vector processes, $\mathbf{X}_v(t)$ and $\mathbf{Y}_v(t)$, are defined

$$\mathbf{X}_v(t) \;=\; \begin{bmatrix} X_1(t+\tau+\Delta t_1) \\ X_2(t+\tau+\Delta t_2) \\ X_3(t+\tau+\Delta t_3) \\ : \\ : \\ X_n(t+\tau+\Delta t_n) \end{bmatrix} \qquad \mathbf{Y}_v(t) \;=\; \begin{bmatrix} X_1(t+\Delta t_1) \\ X_2(t+\Delta t_2) \\ X_3(t+\Delta t_3) \\ : \\ X_m(t+\Delta t_m) \end{bmatrix} \tag{4.21}$$

where X_i refers to elements in the vector process defined in eq. (4.17). The time shifts Δt_i could be both positive and negative. The stochastic vector process $\mathbf{Y}_v(t)$ is of course restricted by $m \leq n$. It is important that $\mathbf{Y}_v$ is contained as the first m elements of $\mathbf{X}_v$ with $\tau = 0$. This is only a question of rearranging the elements in $\mathbf{X}_v$ and does not influence the final result or any application.

The auto correlation matrix of $\mathbf{Y}_v$ is given by

$$\mathbf{R}_{\mathbf{Y}_v\mathbf{Y}_v} \;=\; \mathrm{E}[\mathbf{Y}_v(t)\mathbf{Y}_v^T(t)] \;=$$

$$\begin{bmatrix} R_{X_1X_1}(0) & R_{X_1X_2}(\Delta t_1 - \Delta t_2) & .... & R_{X_1X_m}(\Delta t_1 - \Delta t_m) \\ R_{X_2X_1}(\Delta t_2 - \Delta t_1) & R_{X_2X_2}(0) & .... & R_{X_2X_m}(\Delta t_2 - \Delta t_m) \\ : & : & : & : \\ R_{X_mX_1}(\Delta t_m - \Delta t_1) & R_{X_mX_2}(\Delta t_m - \Delta t_2) & .... & R_{X_mX_m}(0) \end{bmatrix} \tag{4.22}$$

The cross correlation matrix between $\mathbf{X}_v$ and $\mathbf{Y}_v$ is given by:

$$\mathbf{R}_{\mathbf{X}_v\mathbf{Y}_v} = \mathrm{E}[\mathbf{X}_v(t)\mathbf{Y}_v^T(t)] =$$

$$\begin{bmatrix} R_{X_1X_1}(\tau) & R_{X_1X_2}(\tau+\Delta t_1-\Delta t_2) & .... & R_{X_1X_m}(\tau+\Delta t_1-\Delta t_m) \\ R_{X_2X_1}(\tau+\Delta t_2-\Delta t_1) & R_{X_2X_2}(\tau) & .... & R_{X_2X_m}(\tau+\Delta t_2-\Delta t_m) \\ : & : & : & : \\ R_{X_nX_1}(\tau+\Delta t_n-\Delta t_1) & R_{X_nX_2}(\tau+\Delta t_n-\Delta t_2) & .... & R_{X_nX_m}(\tau+\Delta t_n-\Delta t_m) \end{bmatrix} \quad (4.23)$$

The definition of the VRD functions is now restricted to be the mean value of $\mathbf{X}_v$ on condition that $\mathbf{Y}_v = \mathbf{y}_v$ (see eq. (4.1) for the general definition). This could be interpreted as a vector level crossing triggering condition

$$T_{\mathbf{Y}_v(t+\boldsymbol{\Delta}\mathbf{t})} = \{X_1(t+\Delta t_1) = y_1,\ \ldots\ , X_m(t+\Delta t_m) = y_m\} \quad (4.24)$$

Since $\mathbf{X}(t)$ has been assumed to have a zero mean vector (see eq. (4.17)) the conditional mean value can be calculated from eq. (A.5)

$$\mathrm{E}[\mathbf{X}_v|T_{\mathbf{Y}_v(t+\boldsymbol{\Delta}\mathbf{t})}] = \mathrm{E}[\mathbf{X}_v|\mathbf{Y}_v = \mathbf{y}_v] = \mathbf{R}_{\mathbf{X}_v\mathbf{Y}_v} \cdot \mathbf{R}^{-1}_{\mathbf{Y}_v\mathbf{Y}_v} \cdot \mathbf{y}_v \quad (4.25)$$

A triggering level vector, $\tilde{\mathbf{a}}$, is defined as

$$\tilde{\mathbf{a}} = \mathbf{R}^{-1}_{\mathbf{Y}_v\mathbf{Y}_v} \cdot \mathbf{y}_v\ , \qquad \tilde{\mathbf{a}} = [\tilde{a}_1\ \tilde{a}_2\ \ldots\ \tilde{a}_m]^T \quad (4.26)$$

The VRD functions can be rewritten using eq. (4.26)

$$\mathbf{D}^v_{\mathbf{X}}(\tau+\boldsymbol{\Delta}\mathbf{t}) = \mathrm{E}[\mathbf{X}_v|T^v_{\mathbf{Y}_v(t+\boldsymbol{\Delta}\mathbf{t})}] = \mathbf{R}_{\mathbf{X}_v\mathbf{Y}_v} \cdot \tilde{\mathbf{a}} \quad (4.27)$$

Before any attempt is made to extract the modal parameters each VRD function is shifted $-\Delta t_i$. This leads to the shifted VRD functions

$$\mathbf{D}^v_{\mathbf{X}_v}(\tau) =$$

$$\begin{bmatrix} R_{X_1X_1}(\tau-\Delta t_1) & R_{X_1X_2}(\tau-\Delta t_2) & .... & R_{X_1X_m}(\tau-\Delta t_m) \\ R_{X_2X_1}(\tau-\Delta t_1) & R_{X_2X_2}(\tau-\Delta t_2) & .... & R_{X_2X_m}(\tau-\Delta t_m) \\ : & : & : & : \\ R_{X_nX_1}(\tau-\Delta t_1) & R_{X_nX_2}(\tau-\Delta t_2) & .... & R_{X_nX_m}(\tau-\Delta t_m) \end{bmatrix} \begin{bmatrix} \tilde{a}_1 \\ \tilde{a}_2 \\ : \\ \tilde{a}_m \end{bmatrix} \quad (4.28)$$

The same result would have been obtained if $\mathbf{X}_v(t)$ in eq. (4.21) had been defined without the $\boldsymbol{\Delta}\mathbf{t}$ time shift vector. The computational effort in the estimation procedure is independent of the chosen formulation. Using eq. (4.19), eq. (4.28) can be rewritten as

$$\mathbf{D}^v_{\mathbf{X}}(\tau) = \mathbf{R}_{X_1}(\tau-\Delta t_1)\cdot\tilde{a}_1 + \mathbf{R}_{X_2}(\tau-\Delta t_2)\cdot\tilde{a}_2 + \ \ldots\ + \mathbf{R}_{X_m}(\tau-\Delta t_m)\cdot\tilde{a}_m \quad (4.29)$$

Notice that if $m = 1$ and $\Delta t_i = 0$ the traditional RD formulation for the level triggering condition is obtained

$$D_{X_1X_1}(\tau) = R_{X_1X_1}(\tau)\cdot\tilde{a}_1 = \frac{R_{X_1X_1}(\tau)}{\sigma^2_{X_1}} \cdot y_1 \quad (4.30)$$

The probability that $\mathbf{Y}_v = \mathbf{y}_v$ occurs is very small. This means that the expected number of triggering points can easily be too small to achieve a VRD function, which has converged acceptably. Instead a vector positive point triggering condition is used

$$T^v_{\mathbf{Y}_v(t+\mathbf{\Delta t})} = \{a_1 \leq X_1(t+\Delta t_1) \leq b_1, \ \ldots, a_m \leq X_m(t+\Delta t_m) \leq b_m\} \tag{4.31}$$

The maximum number of triggering points is always obtained by choosing $\mathbf{a} = \mathbf{0}$ and $\mathbf{b} = |\infty|$. In order to link this triggering condition with the results from eq. (4.25) or eq. (4.27), eq. (A.8) is used

$$\begin{aligned}
\mathbf{D_X}(\tau + \mathbf{\Delta t}) &= \mathrm{E}[\mathbf{X}_v | T^v_{Y_v(t+\mathbf{\Delta t})}] = \mathrm{E}[\mathbf{X}_v | \mathbf{a} < \mathbf{Y}_v \leq \mathbf{b}] \\
&= \int_{-\infty}^{\infty} \mathbf{x}_v p_{\mathbf{X_v}|T^v_{\mathbf{Y}_v(t+\mathbf{\Delta t})}}(\mathbf{x}_v | T_{\mathbf{y}_v(t+\mathbf{\Delta t})}) d\mathbf{x}_v \\
&= \frac{1}{k_1} \int_{\mathbf{a}}^{\mathbf{b}} \int_{-\infty}^{\infty} \mathbf{x}_v p_{\mathbf{X}_v|\mathbf{Y}_v}(\mathbf{x}_v|\mathbf{y}_v) p_{\mathbf{Y}_v}(\mathbf{y}_v) d\mathbf{x}_v d\mathbf{y}_v \\
&= \mathbf{R}_{\mathbf{X}_v\mathbf{Y}_v} \cdot \mathbf{R}^{-1}_{\mathbf{Y}_v\mathbf{Y}_v} \cdot \frac{1}{k_1} \cdot \int_{\mathbf{a}}^{\mathbf{b}} \mathbf{y}_v p_{\mathbf{Y}_v}(\mathbf{y}_v) d\mathbf{y}_v \\
&= \mathbf{R}_{\mathbf{X}_v\mathbf{Y}_v} \cdot \tilde{\mathbf{a}}
\end{aligned} \tag{4.32}$$

where the triggering level $\tilde{\mathbf{a}}$ is now defined as

$$\tilde{\mathbf{a}} = \frac{\mathbf{R}^{-1}_{\mathbf{Y}_v\mathbf{Y}_v}}{k_1} \int_{\mathbf{a}}^{\mathbf{b}} \mathbf{y}_v \cdot p(\mathbf{y}_v) d\mathbf{y_V} \qquad k_1 = \int_{\mathbf{a}}^{\mathbf{b}} p_{\mathbf{Y}_v}(\mathbf{y}_v) d\mathbf{y}_v \tag{4.33}$$

So the vector positive point triggering condition gives results equivalent to the vector level crossing triggering condition

$$\mathbf{D}^v_{\mathbf{X}}(\tau) = \mathbf{R}_{X_1}(\tau - \Delta t_1) \cdot \tilde{a}_1 + \mathbf{R}_{X_2}(\tau - \Delta t_2) \cdot \tilde{a}_2 + \ldots + \mathbf{R}_{X_m}(\tau - \Delta t_m) \cdot \tilde{a}_m \tag{4.34}$$

Only the weights, $\tilde{a}_i$, of the correlation functions have changed. In practice only the vector positive point triggering condition is of interest, since this is the only triggering condition, which results in a reasonable number of triggering points.

In conclusion the VRD functions are a sum of a number of correlation functions corresponding to the size of the vector condition. The result in eq. (4.34) is important since the modal parameters can be extracted from the VRD functions using the methods described in chapter 2.

A single problem arises when methods developed to extract modal parameters from free decays are used to extract modal parameters from VRD functions. These methods can only deal with positive time lag correlation functions. The *decays* should dissipate with increasing time lags. This is not the case for the part of the correlation functions which has negative time lags. This also means that the VRD functions cannot be used directly as input to ITD or PTD. First of all, only the part of the VRD functions with $\tau \geq 0$ can be used. Furthermore, a number of points corresponding to $\max(\Delta t_i)$ should be removed from all functions. Otherwise, a part from the correlation functions with negative time lags is used in the modal parameter extraction procedure. This can result in highly erroneous damping ratios.

4.2.1 Choice of Time Shifts

Another problem is to choose the time shifts Δt_1, Δt_2, ... Δt_m in a way to obtain the maximum number of triggering points. The obvious possibility is to estimate a column in the correlation matrix at several positive as well as negative time points using the traditional RD technique. To obtain the maximum number of triggering points for the VRD technique the time shifts Δt_i can be chosen from

$$\max(|D_{X_iX_j}(\tau)|) \quad \Rightarrow \quad \Delta t_i \ = \tau \tag{4.35}$$

Notice that the time shift corresponding to $i = j$ will always be $\Delta t_i = 0$ which is always the time lag with maximum value for the auto correlation functions of a stationary process. If $D_{X_iX_j}(\Delta t_i)$ is negative, the triggering levels a_i and b_i should also be negative.

4.3 Variance of VRD Functions

The variance of the VRD functions is derived corresponding to the principles used to derive the variance of the RD functions, see appendix A. Two vector processes $\mathbf{X}_v(t)$ and $\mathbf{Y}_v(t)$ are constructed from the stationary Gaussian distributed zero mean vector process $\mathbf{X}(t)$ corresponding to eq. (4.21)

$$\mathbf{X}_v(t) \ = \ \begin{bmatrix} X_1(t+\tau+\Delta t_1) \\ X_2(t+\tau+\Delta t_2) \\ X_3(t+\tau+\Delta t_3) \\ : \\ : \\ X_n(t+\tau+\Delta t_n) \end{bmatrix} \qquad \mathbf{Y}_v(t) \ = \ \begin{bmatrix} X_1(t+\Delta t_1) \\ X_2(t+\Delta t_2) \\ X_3(t+\Delta t_3) \\ : \\ X_m(t+\Delta t_m) \end{bmatrix} \tag{4.36}$$

By assuming that the stochastic vector process $\mathbf{X}(t)$ is ergodic and that the individual time segments in the averaging process (see eq. (4.3)) are uncorrelated, the variance of the VRD functions can be calculated from

$$\mathrm{Var}[\hat{\mathbf{D}}^v_{\mathbf{X}}(\tau)] \ = \ \frac{1}{N}\mathrm{Var}[\mathbf{X}_v|T^v_{\mathbf{Y}_v(t+\boldsymbol{\Delta}\mathbf{t})}] \tag{4.37}$$

where N is the number of triggering points. $\mathrm{Var}[\mathbf{X}_v|T^v_{\mathbf{Y}_v(t+\boldsymbol{\Delta}\mathbf{t})}]$ are the diagonals of the covariance functions $\mathrm{Cov}[\mathbf{X}_v|T^v_{\mathbf{Y}_v(t+\boldsymbol{\Delta}\mathbf{t})}]$.

$$\begin{aligned} \mathrm{Cov}[\mathbf{X}_v|T^v_{\mathbf{Y}_v(t+\boldsymbol{\Delta}\mathbf{t})}] \ &= \ \int_{-\infty}^{\infty} \mathbf{x}_v\mathbf{x}_v^T p_{\mathbf{X}_v|T^v_{\mathbf{Y}_v(t+\boldsymbol{\Delta}\mathbf{t})}}(\mathbf{x}_v|T^v_{\mathbf{y}_v(t+\boldsymbol{\Delta}\mathbf{t})})d\mathbf{x}_v \ - \\ &\quad \mathrm{E}[\mathbf{X}_v|T^v_{\mathbf{Y}_v(t+\boldsymbol{\Delta}\mathbf{t})}]\mathrm{E}[\mathbf{X}_v|T^v_{\mathbf{Y}_v(t+\boldsymbol{\Delta}\mathbf{t})}]^T \end{aligned} \tag{4.38}$$

Using the results in appendix A, see eq. (A.8), the above integral can be calculated.

$$\begin{aligned} \mathrm{Cov}[\mathbf{X}_v|T^v_{\mathbf{Y}_v(t+\boldsymbol{\Delta}\mathbf{t})}] \ &= \ \mathbf{R}_{\mathbf{X}_v\mathbf{X}_v} \ - \ \mathbf{R}_{\mathbf{X}_v\mathbf{Y}_v}\mathbf{R}^{-1}_{\mathbf{Y}_v\mathbf{Y}_v}\mathbf{R}^T_{\mathbf{X}_v\mathbf{Y}_v} \ - \\ &\quad \frac{1}{k_1^2}\mathbf{R}_{\mathbf{X}_v\mathbf{Y}_v}\mathbf{R}^{-1}_{\mathbf{Y}_v\mathbf{Y}_v}\int_{\mathbf{a}}^{\mathbf{b}} \mathbf{y}_v p_{\mathbf{Y}_v}(\mathbf{y}_v)d\mathbf{y}_v \cdot \end{aligned}$$

$$\left(\int_{\mathbf{a}}^{\mathbf{b}} \mathbf{y}_v p_{\mathbf{Y}_v}(\mathbf{y}_v) d\mathbf{y}_v\right)^T \mathbf{R}^{-1,T}_{\mathbf{Y}_v\mathbf{Y}_v} \mathbf{R}^T_{\mathbf{X}_v\mathbf{Y}_v} \; + \tag{4.39}$$

$$\frac{1}{k_1} \mathbf{R}_{\mathbf{X}_v\mathbf{Y}_v} \mathbf{R}^{-1}_{\mathbf{Y}_v\mathbf{Y}_v} \int_{\mathbf{a}}^{\mathbf{b}} \mathbf{y}_v \mathbf{y}_v^T p_{\mathbf{Y}_v}(\mathbf{y}_v) d\mathbf{y}_v \mathbf{R}^{-1,T}_{\mathbf{Y}_v\mathbf{Y}_v} \mathbf{R}^T_{\mathbf{X}_v\mathbf{Y}_v}$$

This allows the variance of the VRD functions to be calculated. The variance is not only a function of the VRD functions but a function of the correlation functions. This means that eq. (4.37) can only be used in theoretical applications, e.g. to investigate the significance of the number of triggering points. It is also seen to be a more complicated expression compared to the results for the RD technique.

4.4 Quality Assessment

In application of the RD technique the RD functions are assumed to be proportional to the correlation functions. For e.g. the positive point triggering condition the following relation is valid

$$D_{XY}(\tau) \;=\; \frac{R_{XY}(\tau)}{\sigma_Y^2} \cdot a \quad , \qquad a \;=\; \frac{\int_{a_1}^{b_1} y p_Y(y) dy}{\int_{a_1}^{b_1} p_Y(y) dy} \tag{4.40}$$

The proportionality relation is independent of any choice of the triggering levels a_1 and a_2. This is denoted shape invariance. By choosing different triggering levels a number of different RD functions can be calculated. By normalizing these functions properly a number of theoretical identical RD functions can be obtained. A quality measure based on eq. (4.40) can be defined on the basis of the difference between the estimated RD functions. This approach were developed for the RD technique in section 1.7.

It would be obvious to extend this approach to the VRD technique. The VRD functions corresponding to eq. (4.40) given by are

$$\mathbf{D}^v_{\mathbf{X}}(\tau) \;=\; \mathbf{R}_{X_1}(\tau - \Delta t_1) \cdot \tilde{a}_1 + \mathbf{R}_{X_2}(\tau - \Delta t_2) \cdot \tilde{a}_2 + ... + \mathbf{R}_{X_m}(\tau - \Delta t_m) \cdot \tilde{a}_m \tag{4.41}$$

$$\tilde{\mathbf{a}} \;=\; \mathbf{R}^{-1}_{\mathbf{Y}_v\mathbf{Y}_v} \frac{\int_{\mathbf{a}}^{\mathbf{b}} \mathbf{y}_v p_{\mathbf{Y}_v}(\mathbf{y}_v) d\mathbf{y}_v}{\int_{\mathbf{a}}^{\mathbf{b}} p_{\mathbf{Y}_v}(\mathbf{y}_v) d\mathbf{y}_v} \tag{4.42}$$

If VRD functions are shape invariant, the following relation should be fulfilled

$$\tilde{\mathbf{a}}(\mathbf{a}_1, \mathbf{b}_1) \;=\; k \cdot \tilde{\mathbf{a}}(\mathbf{a}_2, \mathbf{b}_2) \tag{4.43}$$

where k is an arbitrary constant. This demand can be reformulated using eq. (4.42)

$$\int_{\mathbf{a}_1}^{\mathbf{b}_1} \mathbf{y}_v p_{\mathbf{Y}_v}(\mathbf{y}_v) d\mathbf{y}_v \;=\; k \int_{\mathbf{a}_2}^{\mathbf{b}_2} \mathbf{y}_v p_{\mathbf{Y}_v}(\mathbf{y}_v) d\mathbf{y}_v \tag{4.44}$$

This relation cannot in general lead to a guideline to show how the choices of $\mathbf{a}_i$ and $\mathbf{b}_i$ can secure shape invariance of VRD functions.

Another method to assess the quality of RD functions is based on the following relation for stationary processes

$$R_{XY}(\tau) \;=\; R_{YX}(-\tau) \tag{4.45}$$

Which leads to the error function

$$\mathcal{E} \;=\; \hat{D}_{XY}(\tau) - \hat{D}_{YX}(-\tau) \tag{4.46}$$

where the error function contains information about the quality of the RD functions. This approach was also developed in section 1.7 for the RD technique. Again, it would be obvious to extend this approach for VRD functions. The VRD functions are a sum of correlation functions, see eq. (4.34)

$$D^{v}_{X_i}(\tau) \;=\; \sum_{j=1}^{m} R_{X_iX_j}(\tau - \Delta t_j) \cdot \tilde{a}_j \tag{4.47}$$

First of all it is clear that in general the VRD functions are not symmetric since

$$\sum_{j=1}^{m} R_{X_iX_j}(\tau - \Delta t_j) \cdot a_i \;-\; \sum_{j=1}^{m} R_{X_iX_j}(\Delta t_j - \tau) \cdot a_i \;\neq\; 0 \tag{4.48}$$

This holds even for $\Delta t_j = 0,\ j = 1, ..., m$, since the cross correlation functions in eq. (4.48) are not symmetric. Next attempt would be to combine (add or subtract) the n VRD functions, so that the final result is theoretically zero. This can be done if and only if $m = n$, since both $R_{X_iX_j}$ and $R_{X_iX_j}$ should be represented in the VRD functions. If $m \leq n$ only the first m VRD functions can be used. Next assume that $m = n$. Then the following relation should hold

$$R_{X_iX_j}(\tau - \Delta t_j) \cdot a_i \;=\; R_{X_jX_i}(\tau - \Delta t_i) \cdot a_j \tag{4.49}$$

In general this cannot be fulfilled since $\Delta t_i \neq \Delta t_j$ and $a_i \neq a_j$ are both unknown. So in general the relation eq. (4.45) does not constitute a basis for quality assesment of VRD functions.

It is a disadvantage of the VRD technique, that the quality assesment cannot be performed using the methods developed for the RD technique. The only approach to quality assessment of VRD functions is to choose two triggering conditions, where the only difference is the sign of the triggering levels.

$$T^{v_1}_{\mathbf{Y}_v(t+\boldsymbol{\Delta}\mathbf{t})} \;=\; [a_1 \leq Y_1(t + \Delta t_1) < b_1, ..., a_m \leq Y_m(t + \Delta t_m) < b_m] \tag{4.50}$$

$$T^{v_2}_{\mathbf{Y}_v(t+\boldsymbol{\Delta}\mathbf{t})} \;=\; [-b_1 < Y_1(t + \Delta t_1) \leq -a_1, ..., -b_m < Y_m(t + \Delta t_m) \leq -a_m] \tag{4.51}$$

The estimated VRD functions have the following relations

$$\hat{\mathbf{D}}^{v_1}_{\mathbf{X}_v} \;=\; -\hat{\mathbf{D}}^{v_2}_{\mathbf{X}_v} \tag{4.52}$$

This can be used to define an error function, which should theoretically be zero and thereby constitute a basis for quality assessment.

4.5 Examples - 2DOF Systems

In order to test the performance of the VRD technique a simulation study of two 2 DOF systems loaded by independent white noise at each mass is performed in section 4.5.1 and section 4.5.2. Since these are the first results obtained using the VRD technique, it is natural to have a starting point with a simple system such as a 2 DOF-system. The efficiency of the VRD technique is compared with the RD technique by comparing modal parameters estimated from the VRD functions with modal parameters estimated from the RD functions. Modal parameters are extracted from the RD and VRD functions using the ITD technique, see chapter 2.

Three different quality measures are defined in order to compare the accuracy of the different approaches: $\mathcal{E}_1$, $\mathcal{E}_2$ and $\mathcal{E}_3$. θ is the theoretical parameter (frequencies or damping ratios or mode shape components) and $\hat{\theta}$ is the estimated parameter.

$$\mathcal{E}_1 = \sum_{i=1}^{2} \frac{|\theta_i - \hat{\theta}_i|}{\sigma_{\hat{\theta}_i}} \tag{4.53}$$

$$\mathcal{E}_2 = \sum_{i=1}^{2} \frac{\sigma_{\hat{\theta}_i}}{\theta_i} \tag{4.54}$$

$$\mathcal{E}_3 = \sum_{i=1}^{2} \frac{|\theta_i - \hat{\theta}_i|}{\hat{\theta}_i} \tag{4.55}$$

10% independent Gaussian white noise is added to each response (10% is the standard deviation of the noise divided by the standard deviation of the noise free response). The purpose is to model a real life situation.

4.5.1 Example 1

The modal parameters of the system are shown in table 4.1

	f [Hz]	ζ	$\lvert\Phi\rvert^1$	$\lvert\Phi\rvert^2$	$\angle\Phi^1$	$\angle\Phi^2$
Mode 1	1.29	3.39	1.00	0.68	0.00	1
Mode 2	2.10	1.09	1.00	1.48	0.00	179

Table 4.1: *Modal parameters of the 2 DOF system for example 1.*

The quality measures in eqs. (4.53) - (4.55) are calculated on the basis of 200 independent simulations of the response of the system by estimating VRD and RD functions from each simulated response and extract the modal parameters using ITD. The final quality measures are the mean values of the measures obtained from each of the simulations. 500 points are generated in each response time series and the sampling frequency is 10 Hz. The system is simple, so no more than 500 points are necessary in order to estimate reasonable modal parameters.

Figure 4.8 shows typical RD functions using triggering at a single measurement. Positive point triggering has been used with $a = 0.5\sigma_X$ and $b = \infty$. These triggering levels are

chosen for all RD and VRD functions. The (*) and the (o) on the cross RD functions indicate optimum time delays for vector triggering if the triggering levels are selected to be positive for (*) and negative for (o).

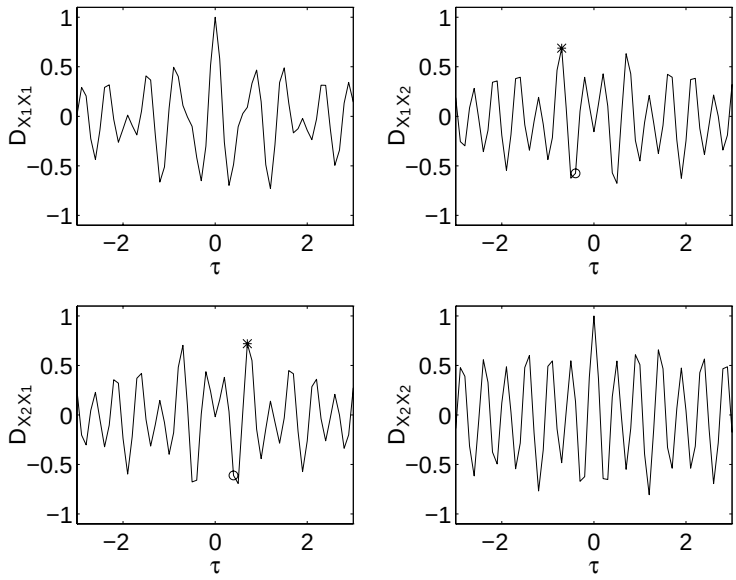

Figure 4.8: *RD functions using measurement 1 (left) and measurement 2 (right) for triggering. The (*) and (o) on the cross RD functions designate optimum time delays for VRD estimation. The RD functions have been normalized column wise so the auto RD functions are correlation coefficient functions.*

Figure 4.9 shows typical VRD functions of the simulated response based on $\Delta t_1 = 0$, $\Delta t_2 =$ $(*)$. The VRD functions are not symmetric around $\tau = 0$, which illustrates the difference between auto RD functions and VRD functions.

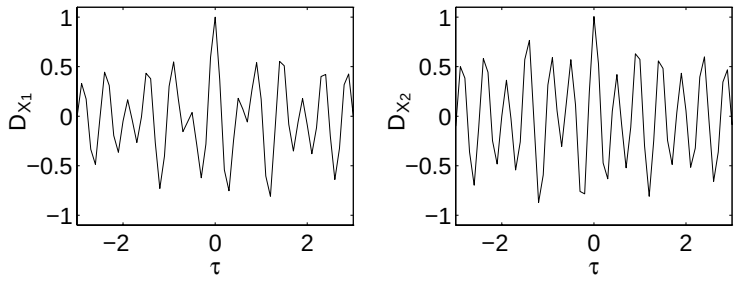

Figure 4.9: *VRD functions estimated using the (*) time delay from fig. 5.1.*

The quality measures calculated from the 200 independent simulations are shown in fig. 4.10. Five different bars are plotted in each sub-figure. Bars 1 and 2 correspond to results, where the modal parameters have been extracted from RD functions using triggering only at the response of the first and second masses, respectively (or results based on the first column in fig. 4.8 and the second column in fig. 4.8 only). Bar 3 corresponds to results where all four RD functions have been used in the modal parameter extraction

procedure. Bars 4 and 5 correspond to results from VRD functions using the time shifts $\Delta t_1 = 0,\ \Delta t_2 = (*)$ and $\Delta t_1 = 0,\ \Delta t_2 = (o)$, see fig. 4.8.

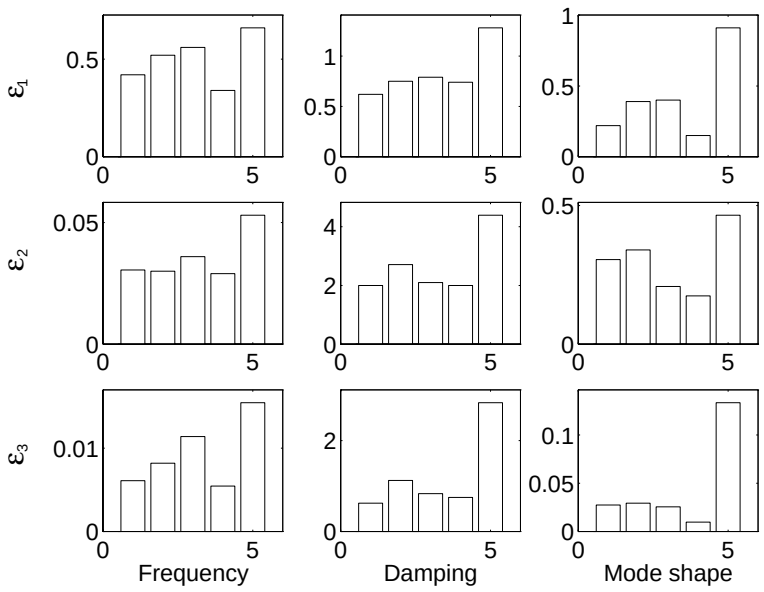

Figure 4.10: *Bias, variance and relative error for different RD functions (bar 1-3) and different VRD functions (bar 4-5).*

The results indicate the importance of choosing the time shifts for triggering with high positive correlation and positive triggering levels or with high negative correlation and negative correlation. Bar 5 shows that a time shift with high negative correlation and positive triggering levels results in poor quality measures. The results for a correct choice of time shifts and triggering levels (bar 4) document the mathematical basis. On average the VRD technique can produce results with the same high accuracy as the RD technique according to the quality measures.

If the VRD technique should be a genuine alternative to the traditional RD technique, the difficulties in choosing proper time shifts have to be paid off with either a high accuracy or a low computational time compared to the RD technique.

4.5.2 Example 2

The purpose of this example is to document that under certain observable and realistic conditions the VRD technique can be more accurate than the RD technique. The modal parameters of the system are shown in table 4.1.

	f [Hz]	ζ	$\lvert\Phi\rvert^1$	$\lvert\Phi\rvert^2$	$\angle\Phi^1$	$\angle\Phi^2$
Mode 1	1.56	2.19	1.00	0.08	0.00	2
Mode 2	4.22	1.83	1.00	12.0	0.00	174

Table 4.2: *Modal parameters of a 2DOF system for example 2.*

The major difference from example 1 is that there is practically no information between the two masses (the cross mode shape component is relatively small). The results are based

on 200 independent simulations of the response of the system with the modal parameters in table 4.2 loaded by independent Gaussian white noise. 2000 points are generated in each time series and the sampling frequency is 20 Hz. 10 % independent Gaussian white noise is added (standard deviation of the noise divided by the standard deviation of the noise-free process). Figure 4.11 shows typical RD functions.

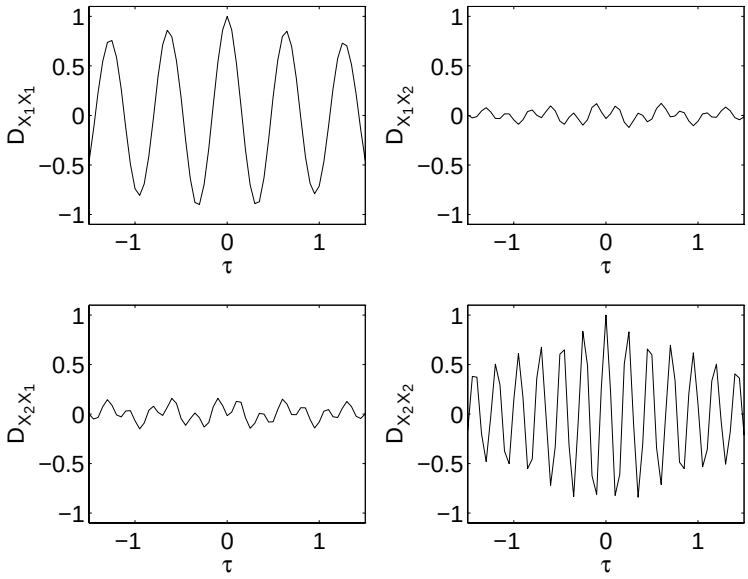

Figure 4.11: *RD functions using measurement 1 (left) and measurement 2 (right) for triggering. The RD functions have been normalized column wise so the auto RD functions are correlation coefficient functions.*

Figure 4.12 shows the VRD functions. The time shifts are chosen as $\Delta t_1 = 0,\ \Delta t_2 = 0.05$ s, which are the time shifts with maximum correlation, see fig. 4.11.

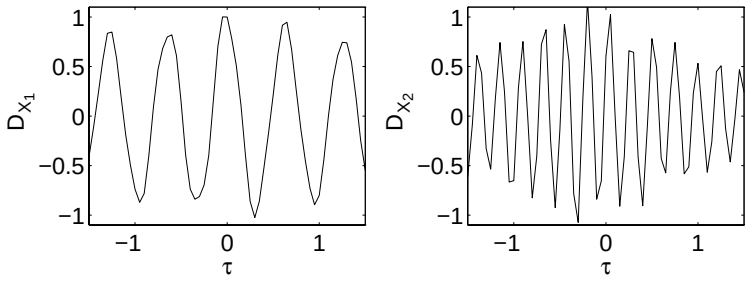

Figure 4.12: *VRD functions estimated using the time shift vector* $\boldsymbol{\Delta}t = [00.05]$ *s.*

Figure 4.13 shows the quality measures calculated on the basis of the 200 independent simulations. Bars 1 and 2 correspond to RD functions using triggering only at the first and second mass, respectively. Bar 3 corresponds to results from all four RD functions and bar 4 corresponds to results from VRD functions.

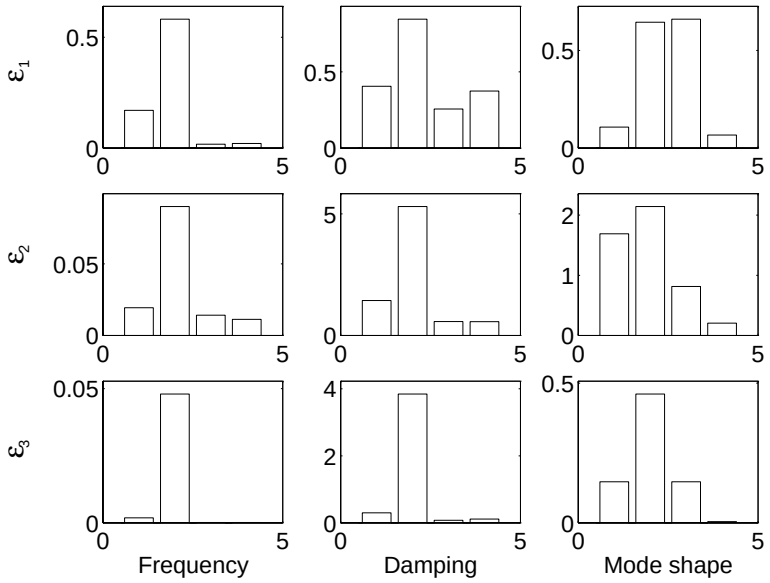

Figure 4.13: *Bias, variance and relative error for different RD functions (bar 1-3) and different VRD functions (bar 4).*

These results illustrate that the VRD technique is superior with respect to the accuracy compared to the RD technique, when only a single setup is used in the modal parameter extraction procedure. The VRD technique should be compared with the RD technique where all RD setups are used to extract the modal parameters.

4.6 Example - 4DOF System

The purpose of this example is further documentation of the applicability of the VRD technique by performing a simulation study on a more complicated system compared to the 2 DOF systems used in section 4.5. The eigenfrequencies and the damping ratios of the chosen system are shown in table 4.3.

Mode	1	2	3	4
f [Hz]	1.62	4.61	6.86	9.00
ζ [%]	3.70	2.07	1.16	1.52

Table 4.3: *Modal parameters of 4-DOF system.*

The mode shapes of the system are illustrated by plotting their absolute value in fig. 4.14. The mode shapes are approximately in or out of phase.

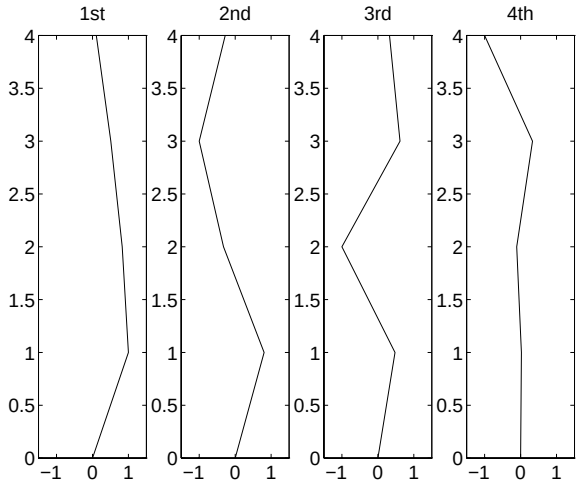

Figure 4.14: *Absolute value of mode shape of 4-DOF system.*

In order to describe the accuracy of the different methods statistically the simulation and estimation process are repeated 500 times. The sampling frequency is 50 Hz and 8000 points are simulated in each time series. 10 % independent Gaussian white noise is added to each response. The quality measures in eqs. (4.53) - (4.55) are calculated on the basis of the 500 simulations.

Four different approaches are compared:

- **Approach 1:** RD using positive point triggering at the measurement with the highest standard deviation. So only a single RD setup is estimated. The triggering levels are chosen as: $a = 0,\ b = \infty$
- **Approach 2:** RD using level triggering estimating the full correlation matrix. The triggering levels are chosen as: $a = 1.4\sigma_X$.
- **Approach 3:** RD using positive point triggering estimating the full correlation matrix. The triggering levels are all chosen as: $a_i = 0,\ b_i = \infty\ i = 1, ..., 4$.
- **Approach 4:** VRD using a vector triggering condition of size four. The triggering levels are chosen as: $a_i = 0,\ b_i = \infty\ i = 1, ..., 4$.

Figure 4.15 shows typical RD functions estimated by approach 1. The RD functions are an estimate of a single column in the correlation functions.

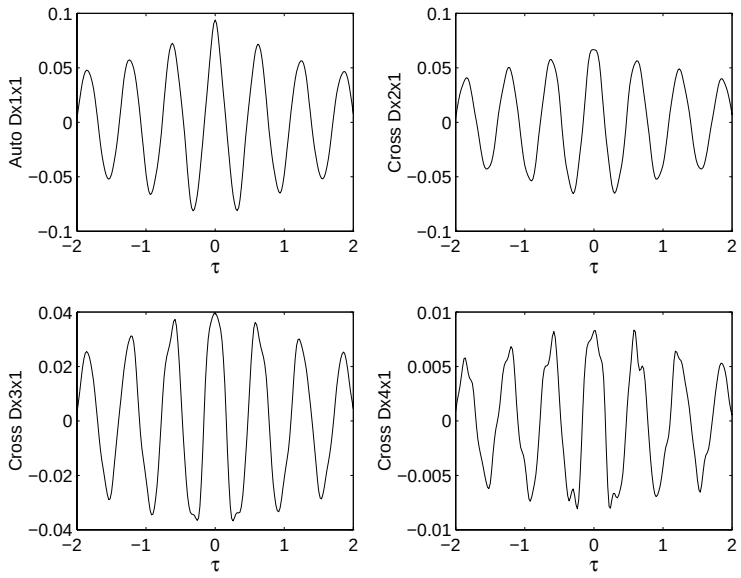

Figure 4.15: *RD functions estimated using approach 1.*

From fig. 4.15 it is seen that a choice of VRD time shifts of $\Delta t_i = 0$, $i = 1, ..., 4$ have maximum correlation. Figure 4.16 shows typical VRD functions.

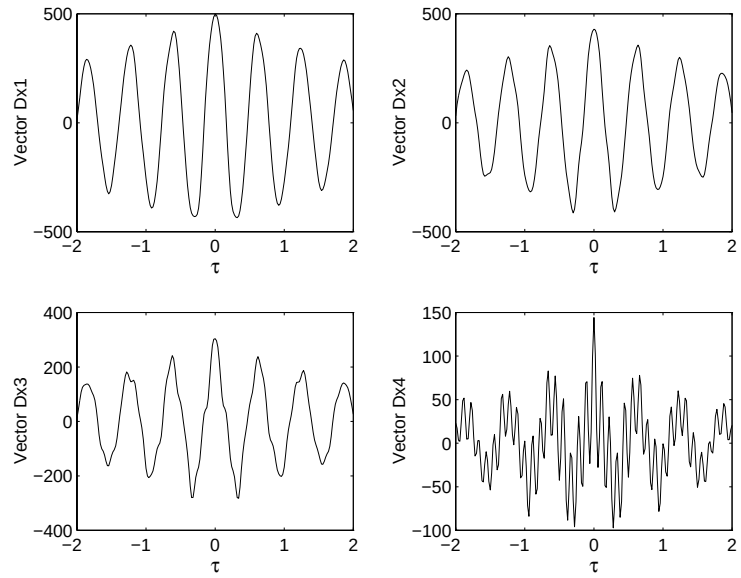

Figure 4.16: *VRD functions estimated using time shifts* $\Delta t_i = 0,\ i = 1, ..., 4$.

The VRD functions are not symmetric around $\tau = 0$. Figure 4.17 shows the quality measures. The four bars correspond to the 4 different approaches in the order they were described previously.

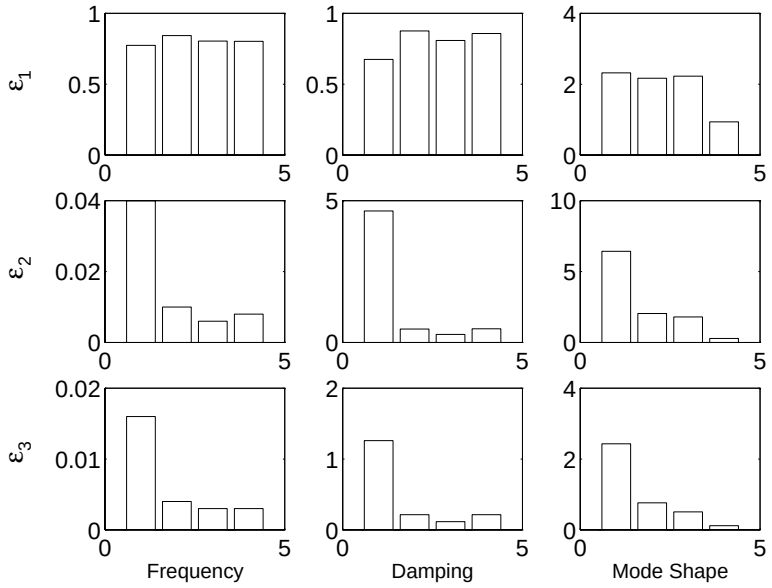

Figure 4.17: *Bias, variance and relative error for different RD (bar 1-3) and VRD (bar 4) approaches.*

The quality measures show that the VRD and the RD technique (approach 3) using positive point triggering estimating the full correlation matrix, in general has higher quality compared to RD approach 1 and 2. The result is expected, since approaches 1 and 2 can be interpreted as *sub*-approaches to the more general approach 3. The estimation times and the number of triggering points of the 4 different approaches are shown in table 4.4. Column 5 shows the results from the necessary initial estimation time using level crossing triggering.

Approach	1	2	3	4	5
Time	1.39	1.40	5.56	1.05	0.31
N	3950	470	3950	1590	470

Table 4.4: *Estimation time [CPU] and number of triggering points, N*

As seen the VRD technique has the same estimation time as approaches 1 and 2 and it is about 4-5 times faster than approach 3. The results of this section are summarized in table 4.5 by giving the different approaches grades in the form of a number of + signs.

Approach	1	2	3	4
Quality	+	++	++++	+++
CPU Time	++	++	+	++

Table 4.5: *Evaluation of different approaches.*

The simulation study indicates that the VRD approach is efficient in the sense of having low estimation and high accuracy. The VRD technique can replace the traditional RD technique. Only in the case of measurements with a high content of noise, it is recommended to use the traditional RD technique with all possible RD setups.

4.7 Summary

In this chapter a new concept has been introduced: Vector triggering Random Decrement. The VRD technique differs from the RD technique in the formulation of the triggering condition. In formulation of the traditional RD technique the triggering condition should only be fulfilled in a single process, whereas in formulation of the VRD technique the triggering condition should be fulfilled in several processes. This makes it a vector triggering condition.

In section 4.1 the VRD functions are defined and the estimation process, which provides unbiased estimates, is described. The relation between the VRD functions and the correlation functions of stationary zero mean Gaussian distributed vector process is derived in section 4.2 for the first time. The VRD functions are a weighted sum of the correlation functions of the vector process. The number of correlation functions is equal to the size of the vector triggering condition. In section 4.3 an approximate relation for the variance of the estimate of the VRD functions is derived, corresponding to the relations for the estimate of the RD functions. Section 4.4 discusses quality assessment of VRD functions. It is shown that the VRD functions are not shape invariant and that the symmetry relations for correlation functions of stationary processes can only be used in a very special situation. Instead quality assessment is suggested to be based on the difference between the VRD functions estimated by shifting the sign of the processes.

Sections 4.5 and 4.6 describe different simulation studies, which document the applicability of the VRD technique. Section 4.5 illustrates that the VRD technique is superior in accuracy compared to the RD technique using a single set of RD functions, if a physical system with low correlation between the measurements is analysed. In section 4.6 it is illustrated that the accuracy or the speed of the VRD technique can be superior to the RD technique. In conclusion the VRD technique can be used with a lower estimation time and as high accuracy as the RD technique, unless measurements with a high noise content are considered. The VRD tehcnique is an attractive alternative to the RD technique.

A final comparison between the RD and the VRD technique is performed in chapter 7, where a laboratory bridge model loaded by Gaussian white noise through a shaker has been analysed.

Bibliography

[1] Ibrahim, S.R., Asmussen, J.C. & Brincker, R. *Theory of Vector Triggering Random Decrement Technique.* Proc. 15th International Modal Analysis Conference, Orlando, Florida, USA, 1997, Vol. I, pp. 502-510.

[2] Ibrahim, S.R., Asmussen, J.C. & Brincker, R. *Vector Triggering Random Decrement for High Identification Accuracy.* Accepted for publication in Journal of Vibration and Acoustics.

[3] Asmussen, J.C., Ibrahim, S.R. & Brincker, R. *Application of the Vector Triggering Random Decrement Technique.* Proc. 15th International Modal Analysis Conference, Orlando, Florida, USA, 1997, Vol. II, pp. 1165-1171.

Chapter 5

Variance of RD Functions

The purpose of this chapter is to investigate the variance of RD functions. Knowledge of the variance of RD functions could be used in the modal parameter extraction procedure or to indicate the duration of the RD functions which are not too uncertain.

The relations for the variance of the estimate of the RD functions given in chapter 3 are considered. The decisive assumption for these relations is that the different time segments in the averaging proces are uncorrelated. This assumption can be violated in such a degree that the relations shown in chapter 3 are unusable. Instead a new approach for obtaining more accurate estimates of the variance of RD functions is suggested. This new approach takes the correlation between the different time segments into account by considering the relative time distribution of the triggering points.

5.1 Variance of RD Functions

This section investigates how the variance of the estimates of the RD functions can be calculated. In chapter 3 approximate equations for the variance of the estimates of the RD functions are given for all triggering conditions. The strength of these relations is that the approximate variance can be calculated from the estimated RD functions and the number of triggering points only. A simpler and faster approach is impossible. The important assumption of the relations is that the time segments in the averaging process are uncorrelated. This assumption is in theory always violated. In practice the consequence is that the relations for the variance of the RD functions cannot be used for e.g. the positive point triggering condition, since it is obvious that the time segments are not uncorrelated for this triggering condition. It can only be a guideline, also for other conditions than positive point triggering.

The purpose of this section is to introduce a new method for estimating the variance of the RD functions. It will be assumed that the measurements are realizations of stationary zero mean Gaussian distributed processes. A new method should fulfil the following demands.

- The method should be valid for all triggering conditions. This means that the correlation between the time segments should be taken into account and that the method is independent of the chosen triggering condition.
- The method should be accurate and consistent. Consistent means that the accuracy

of the method should be independent of the physical system describing the measured responses.

- The method should be fast, otherwise the absolute main advantage of the RD technique is vasted and the method will only have theoretical interest.
- The requirement for the speed of the method is fulfilled if the variance can be predicted by the RD functions only.

In the following a new method is proposed and it is investigated if it fulfils the above demands. Only cross RD functions and the variance of the estimated cross RD functions are considered, in order to simplify the derivations and still preserve generality. The RD functions are always estimated as the empirical mean

$$\begin{aligned}
\hat{D}_{YX}(\tau) &= \frac{1}{N}\sum_{i=1}^{N} y(t_i+\tau)|T^{G_A}_{x(t_i)} \\
&= \frac{1}{N}\sum_{i=1}^{N} y(t_i+\tau)|x(t_i)=x_i, \dot{x}(t_i)=\dot{x}_i \\
&= \frac{1}{N}\sum_{i=1}^{N} y(t_i+\tau|T_{x_i}) \qquad (5.1)
\end{aligned}$$

where the applied general triggering condition is used to preserve generality, since this condition contains any particular condition. When the RD functions have been estimated the applied general triggering condition can be replaced by N alternative triggering conditions, which are formulated from the observable values of x and $\dot{x}$ at the already detected time points t_i. If these triggering conditions are applied to the measurements exactly the same RD functions would be estimated, since the same triggering points are detected. Although this is impossible in practice, since the values of $x(t_i)$ and $\dot{x}(t_i)$ and the corresponding time points, t_i, are unknown in advance, the conditions will be used as a basis for the model presented in the following. The idea is that the information of $x(t_i)$, $\dot{x}(t_i)$ at the triggering time points t_i can be obtained from the estimation procedure of the RD functions and used in an estimation method for the variance of the RD functions.

The variance of the estimated RD functions can be calculated as

$$\begin{aligned}
\mathrm{Var}[\hat{D}_{YX}(\tau)] &= \frac{1}{N^2}\mathrm{Var}[\sum_{i=1}^{N} y(t_i+\tau)|T^{G_A}_{x(t_i)}] \\
&= \frac{1}{N^2}\sum_{i=1}^{N}\sum_{j=1}^{N}\mathrm{Cov}[y(t_i+\tau)|T^{G_A}_{x(t_i)}; y(t_j+\tau)|T^{G_A}_{x(t_j)}] \qquad (5.2)
\end{aligned}$$

If all cross terms in eq. (5.2) are neglected then the relations for the variance of the estimated RD functions described in chapter 3 are obtained. The variance of the RD function could as well be calculated on the basis of the alternative triggering condition introduced in parts 2 and 3 of eq. (5.1).

$$\begin{aligned}\mathrm{Var}[\hat{D}_{YX}(\tau)] &= \frac{1}{N^2}\mathrm{Var}[\sum_{i=1}^{N} y(t_i+\tau)|T_{x_i}] \\ &= \frac{1}{N^2}\sum_{i=1}^{N}\sum_{j=1}^{N}\mathrm{Cov}[y(t_i+\tau)|T_{x_i}; y(t_j+\tau)|T_{x_j}] \end{aligned} \tag{5.3}$$

By keeping track of the real time points, t_i, $i = 1, 2, \ldots, N$ in the estimation of the RD functions, the variance of the RD functions can be rewritten using this information without the loss of generality

$$\begin{aligned}\mathrm{Var}[\hat{D}_{YX}(\tau)] &= \frac{1}{N^2}\cdot\Bigg(\sum_{i=1}^{N}\mathrm{Cov}[y(t_i+\tau)|T_{x_i}; y(t_i+\tau)|T_{x_i}] \\ &+ \sum_{j=1}^{m}\sum_{i=1}^{N_j}\mathrm{Cov}[y(t_i+\tau)|T_{x_i}; y(t_i+j\Delta T+\tau)|T_{x_{i+j}}] \\ &+ \sum_{j=1}^{m}\sum_{i=1}^{N_j}\mathrm{Cov}[y(t_i+j\Delta T+\tau)|T_{x_{i+j}}; y(t_i+\tau)|T_{x_i}]\Bigg) \end{aligned} \tag{5.4}$$

where m is the maximum number of time lags between any triggering points. In eq. (5.4) some of the N_i can be zero. The general requirement for the number of the covariance terms at each time step is

$$N + 2\cdot N_1 + 2\cdot N_2 + \ldots + 2\cdot N_m = N^2 \tag{5.5}$$

Since the covariance of the conditional processes is independent of the chosen initial conditions, T_{x_i}, which will be shown later, eq. (5.4) can be rewritten as

$$\begin{aligned}\mathrm{Var}[\hat{D}_{YX}(\tau)] &= \frac{1}{N^2}\cdot\Bigg(\sum_{i=1}^{N}\mathrm{Cov}[Y(t+\tau)|T_{X(t)}^{G_T}; Y(t+\tau)|T_{X(t)}^{G_T}] \\ &+ \sum_{j=1}^{m} N_j\mathrm{Cov}[Y(t+\tau)|T_{X(t)}^{G_T}; Y(t+j\Delta T+\tau)|T_{X(t+j\Delta T)}^{G_T}] \\ &+ \sum_{j=1}^{m} N_j\mathrm{Cov}[Y(t+j\Delta T+\tau)|T_{X(t+j\Delta T)}^{G_T}; Y(t+\tau)|T_{X(t)}^{G_T}]\Bigg) \end{aligned} \tag{5.6}$$

where $T_{X(t)}^{G_T}$ is of the same form as the theoretical general triggering condition.

$$T_{X(t)}^{G_T} = \{X(t) = a, \dot{X}(t) = b\} \tag{5.7}$$

The major problem is to calculate the general covariance between $Y(t+\tau)|T_{X(t)}^{G_T}$ and $Y(t+j\Delta T+\tau)|T_{X(t+j\Delta T)}^{G_T}$. Consider the following two Gaussian distributed stochastic vectors

$$\mathbf{X}_1 = [Y(t+\tau)\; Y(t+t_1+\tau)]^T \tag{5.8}$$

$$\mathbf{X}_2 \;=\; [X(t)\; X(t+t_1)\; \dot{X}(t)\; \dot{X}(t+t_1)]^T \tag{5.9}$$

The covariance of $\mathbf{X}_1$ on condition of $\mathbf{X}_2$ is calculated using eq. (A.4).

$$\mathrm{Cov}[\mathbf{X}_1|\mathbf{X}_2] \;=\; \mathbf{R}_{\mathbf{X}_1\mathbf{X}_1} \;-\; \mathbf{R}_{\mathbf{X}_1\mathbf{X}_2}\mathbf{R}^{-1}_{\mathbf{X}_2\mathbf{X}_2}\mathbf{R}^{T}_{\mathbf{X}_1\mathbf{X}_2} \tag{5.10}$$

Using the definition of the correlation functions in eq. (2.55) the correlation matrices in (5.10) can be calculated from eqs (5.11) - (5.13) ($\mathbf{X}$ and $\mathbf{Y}$ are assumed to have zero mean value).

$$\mathbf{R}_{\mathbf{X}_1\mathbf{X}_1} \;=\; \begin{bmatrix} R_{YY}(0) & R_{YY}(-t_1) \\ R_{YY}(t_1) & R_{YY}(0) \end{bmatrix} \tag{5.11}$$

$$\mathbf{R}_{\mathbf{X}_2\mathbf{X}_2} \;=\; \begin{bmatrix} R_{XX}(0) & R_{XX}(-t_1) & -R'_{XX}(0) & -R'_{XX}(t_1) \\ R_{XX}(t_1) & R_{XX}(0) & -R'_{XX}(t_1) & -R'_{XX}(0) \end{bmatrix} \tag{5.12}$$

$$\mathbf{R}_{\mathbf{X}_1\mathbf{X}_2} \;=\; \begin{bmatrix} R_{YX}(\tau) & R_{YX}(\tau-t_1) & -R'_{YX}(\tau) & -R'_{YX}(\tau-t_1) \\ R_{YX}(\tau+t_1) & R_{YX}(\tau) & -R'_{YX}(\tau+t_1) & -R'_{YX}(\tau) \\ R'_{YX}(\tau) & R_{YX}(\tau-t_1) & -R''_{YX}(\tau) & -R''_{YX}(\tau-t_1) \\ R'_{YX}(\tau+t_1) & R_{YX}(\tau) & -R''_{YX}(\tau+t_1) & -R''_{YX}(\tau) \end{bmatrix} \tag{5.13}$$

The covariance between the $Y(t+\tau)|T^{G_T}_{X(t)}$ and $Y(t+n\Delta T+\tau)|T^{G_T}_{X(t+n\Delta T)}$, can be calculated by inserting the results of eqs. (5.11), (5.12) and (5.13) in eq. (5.10). The covariance is taken as the element [1,2] of the 4×4 dimensional covariance matrix $\mathrm{Cov}[\mathbf{X}_1|\mathbf{X}_2]$.

It is important that the only information which should be available is $R_{YX}(\tau)$, $R'_{YX}(\tau)$ and $R''_{YX}(\tau)$. Since the estimated RD functions are proportional to the correlation functions the information can be obtained by scaling the RD functions and then calculate the time derivative and double time derivative of the correlation functions using numerical differentiation. This is considered to be a simple and computationally fast requirement. The disadvantage is that numerical differentiation of the correlation functions demands that the measurements are oversampled. Otherwise the terms $R'_{YX}(\tau)$ and $R''_{YX}(\tau)$ should be obtained by differentiating the measurements and then estimating the corresponding correlation functions using the RD technique. This might be the best solution if the system is not sufficiently oversampled for numerical differentiation of the RD functions.

What now remains is somehow to make the number of the different correlation functions, $N_1, N_2, \ \ldots\ , N_m$, available. Instead of somehow making theoretical consideration of the distribution of the triggering points it is decided to use the *sample* distribution. This means that the weighting numbers, $N_1, N_2, \ \ldots\ , N_m$, are obtained by picking out the time for each triggering point in the estimation of the RD functions. By sorting the time differences between the triggering points the weighting numbers are obtained.

The estimate of the variance of the RD functions involves the following computational steps.

- Sampling the time for each triggering point in estimation of the RD functions.
- Sorting the time differences between the triggering points.

- Numerical (two-time) differentiation of the RD functions (scaled to be the correlation functions).
- Calculating the variance estimate according to eq. (5.6).

None of these computational steps are extremely time consuming. The sampling of the time points for each triggering point is free, since these time points are identified in the estimation process of the RD functions. In the following sections the accuracy of the method for estimating the variance of RD functions are investigated by different simulation studies.

5.2 Example 1: Level Crossing - SDOF

An SDOF system loaded by Gaussian white noise is considered. The system has an eigenfrequency of 1 Hz and a damping ratio of 5 %. The response is sampled with $\Delta T = \frac{1}{30f}$ at 5000 time points. 30000 simulations of this system are performed. For each simulated response an RD function with 601 points corresponding to $-10/f \leq \tau \leq 10/f$ is estimated using level crossing triggering with a triggering level of $a = \sqrt{2}\sigma_X$. The time points for each triggering point are picked out and the distribution of the time points is obtained by sorting the time differences. The response has unit standard deviation. The average number of triggering points was 185.

Figure 5.1 shows the average distribution of the triggering points for all simulations. The distribution is taken as the true distribution of triggering points for the system considered. The distribution corresponds to the weighting numbers in eq. (5.6).

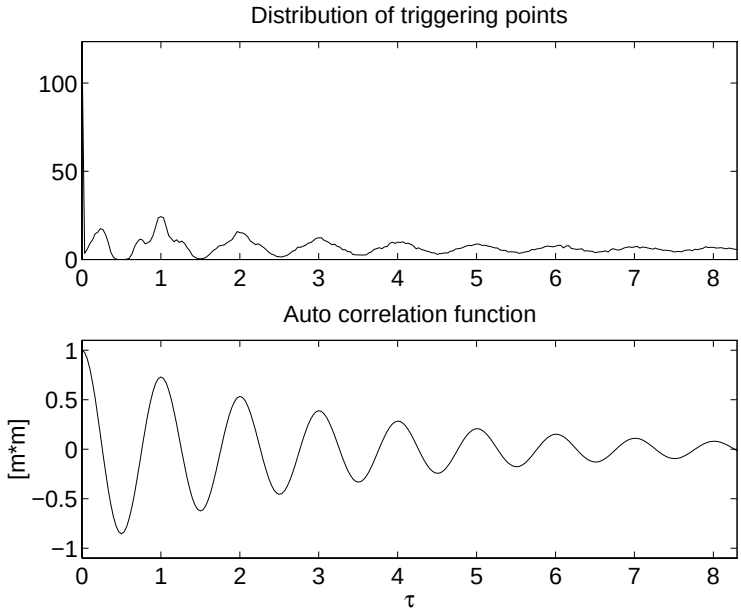

Figure 5.1: *Average distribution of triggering points using level crossing triggering obtained from simulations and the theoretical auto correlation function of the system.*

The figure illustrates that it is not correct to assume that the time segments in the averaging process are uncorrelated, since many triggering points are within the correlation

length, $\tau_{\max}$, of the system. The correlation length is defined as $|R_{XX}(\tau_{\max})| \leq \delta$, where δ is a small number, say e.g. 0.1. The true variance of the RD functions is calculated on basis of the 30000 independently estimated RD functions. Furthermore, the variance of the RD function estimated using the new method is calculated. The true distribution from fig. 5.1 is used together with the theoretical correlation functions. This means that the variance predicted by the method is as accurate as possible, since the true distributions and not the sample distributions are used. This procedure is used in order to control the validity of the method.

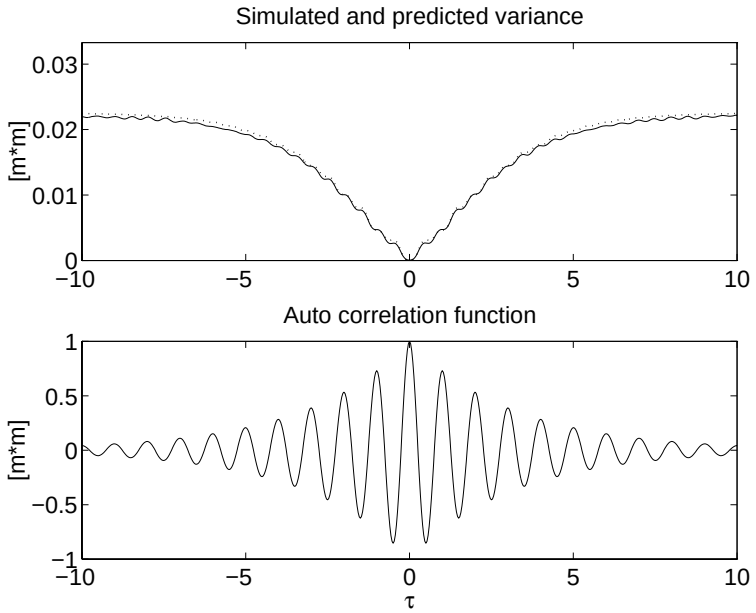

Figure 5.2: *The simulated and the predicted variance of the RD functions using level crossing triggering $a = 2^{0.5}\sigma_X$ and the auto correlation function of the system. [——]: Theoretical (simulated) variance of the RD function. [· · · ·]: Predicted variance of the RD function using the new method.*

As seen the method predicts the variance of the estimated RD functions extremely well. The next step is to investigate how well the variance of the RD functions are predicted by the method if a sample distribution of the triggering points and the estimated correlation functions from a single realization of the response are used.

Figure 5.3 shows simulated variance of the RD functions together with the variance predicted by the new method and the variance predicted by the relation in eq. (3.24).

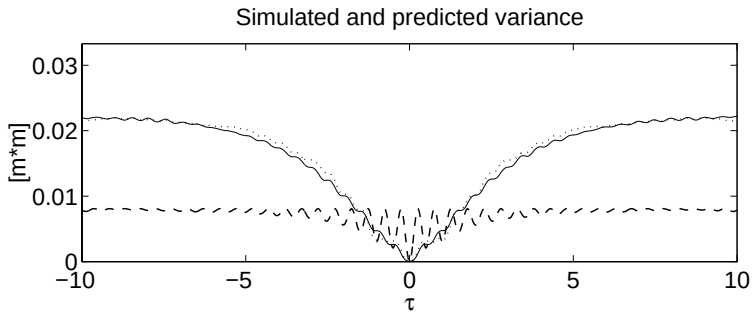

Figure 5.3: *Simulated and predicted variance of the RD functions using level crossing triggering* $a = 2^{0.5}\sigma_X$. *[——]: Theoretical (simulated) variance of the RD function. [· · · ·]: Predicted variance of the RD function using the new method. [- - - -]: Predicted variance using eq. (3.24).*

The situation where only a single realization of the response is available corresponds to the real life situation. So it is very important that the method predicts the true variance as well as shown in figure 5.3 from a single realization. The estimated RD function, the theoretical RD function and the distribution of the triggering points for the single realization are shown in fig. 5.4.

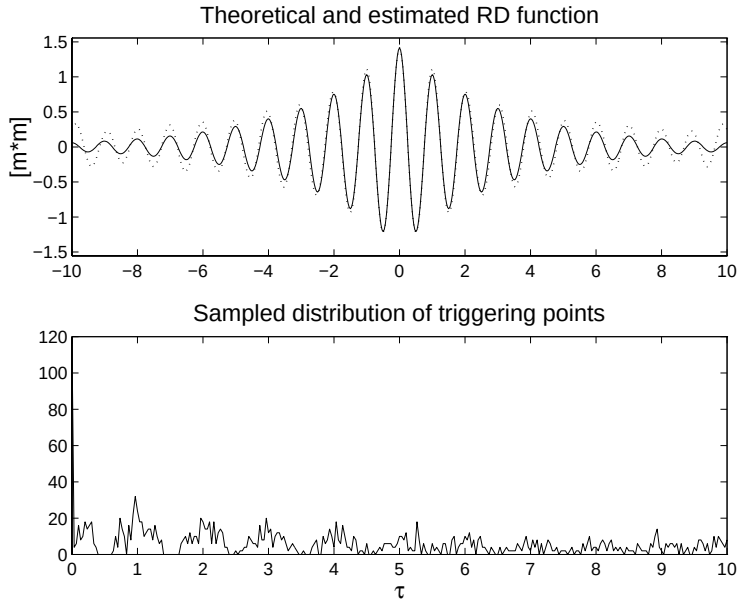

Figure 5.4: *The theoretical and the estimated RD function using level crossing triggering* $a = 2^{0.5}\sigma_X$ *and the sample distribution of the triggering points. [——]: Theoretical RD function. [· · · ·]: Estimated RD function.*

Even though the accuracy of the estimated RD function is not excellent and that the distribution of the triggering points differs significantly from the true distribution shown in fig. 5.1 the new method shows a promising result.

5.3 Example 2: Positive Point - SDOF

In order to investigate further the accuracy of the method to predict the variance of the estimated RD functions and thereby further document the validity of the method the positive point triggering condition is considered. The system is the same as in section 5.2. The distribution of the triggering points is estimated on the basis of 30000 simulations of the response followed by the identification and sorting of the triggering points for each response. Correspondingly the variance of the RD function is obtained on the basis of the simulations. Two different sets of triggering levels are investigated. First $[a_1\ a_2] = [0\ \infty]$ is used since this maximizes the number of triggering points and there is a high correlation between the triggering points.

Figure 5.5 shows the distribution of the triggering points and the theoretical auto correlation function.

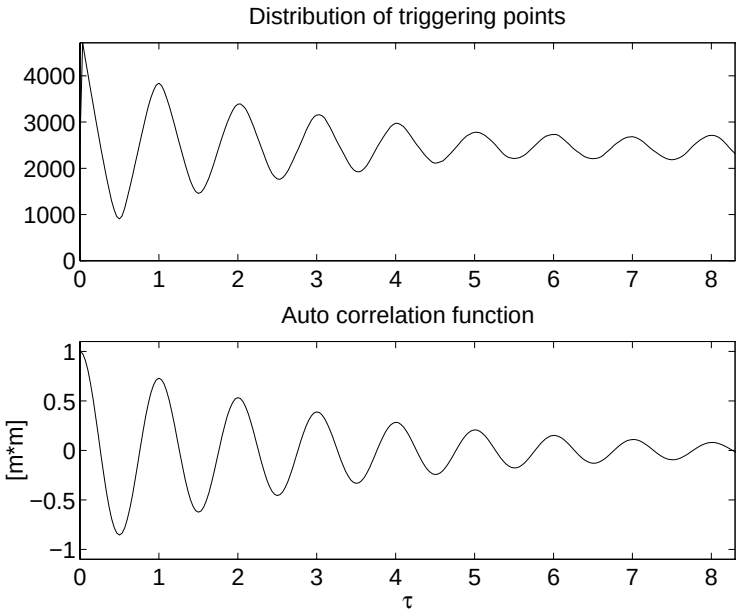

Figure 5.5: *Average distribution of triggering points using positive point triggering* $[a_1\ a_2] = [0\ \infty]\sigma_X$ *obtained by simulations and the auto correlation function of the system.*

The difference in the distribution of the triggering points in comparison with the result in fig. 5.1 is obvious. Figure 5.10 shows the simulated and the predicted variance obtained using the theoretical values.

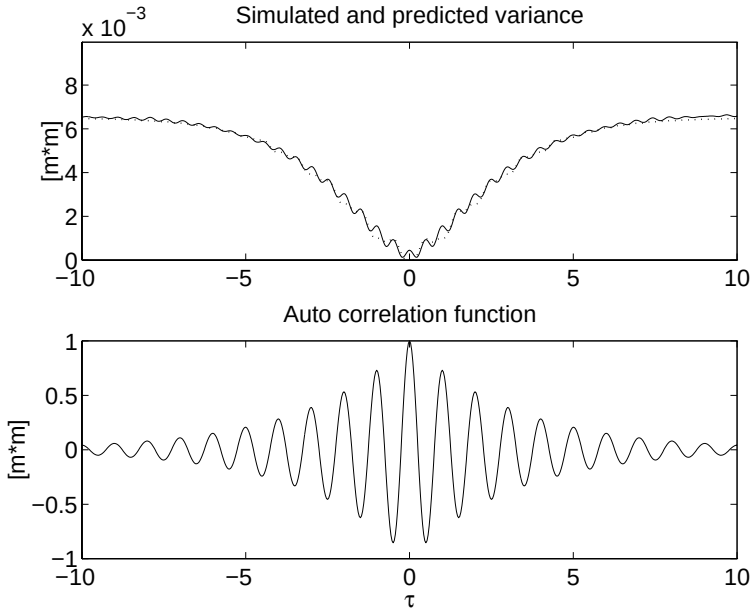

Figure 5.6: *The simulated and the predicted variance of the RD functions using positive point triggering* $[a_1\ a_2] = [\sigma_X\ \infty]$ *and the auto correlation function of the system. [——]: Theoretical (simulated) variance of the RD function. [· · · ·]: Predicted variance of the RD function using the new method.*

The variance predicted using eq. (3.46) and the variance predicted by the new method are shown in fig. 5.7 where a single estimate of the RD function and the distribution of the triggering point have been used.

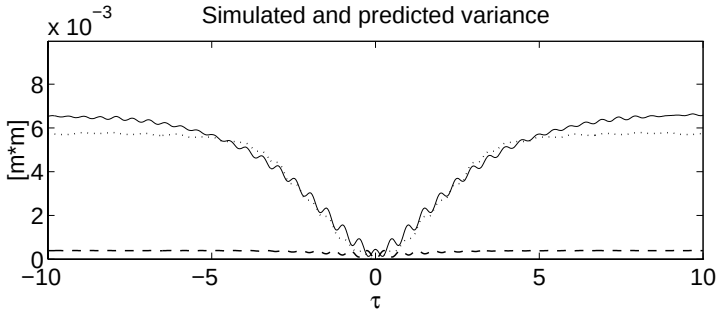

Figure 5.7: *The simulated and the predicted variance of the RD functions using positive point triggering* $[a_1\ a_2] = [0\ \infty]$. *[——]: Theoretical (simulated) variance of the RD function. [· · · ·]: Predicted variance of the RD function using the new method. [- - -]: Predicted variance using eq. (3.46).*

The estimated RD function, the theoretical RD function and the distribution of the triggering points for the single realization are shown in fig. 5.8.

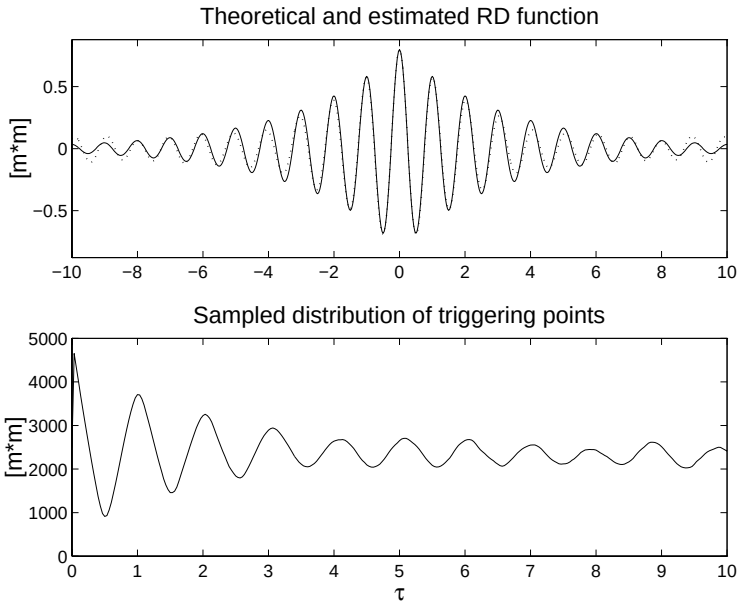

Figure 5.8: *The theoretical and the estimated RD function using positive point triggering* $[a_1\ a_2] = [0\ \infty]$ *and the sample distribution of the triggering points. [——]: Theoretical RD function. [· · · ·]: Estimated RD function.*

The results of the simulations show that the method can be used also for the positive point triggering condition. Usually the triggering levels for this condition are not chosen as $[a_1\ a_2] = [0\ \infty]$. As shown in chapter 3 $[a_1\ a_2] = [\sigma_X\ \infty]$ can increase the accuracy of the RD functions and decrease the computational time. In the following the system described above is investigated again using the positive point triggering condition with $[a_1\ a_2] = [\sigma_X\ \infty]$. Figure 5.9 shows the distribution of the triggering points obtained by simulations together with the auto correlation function.

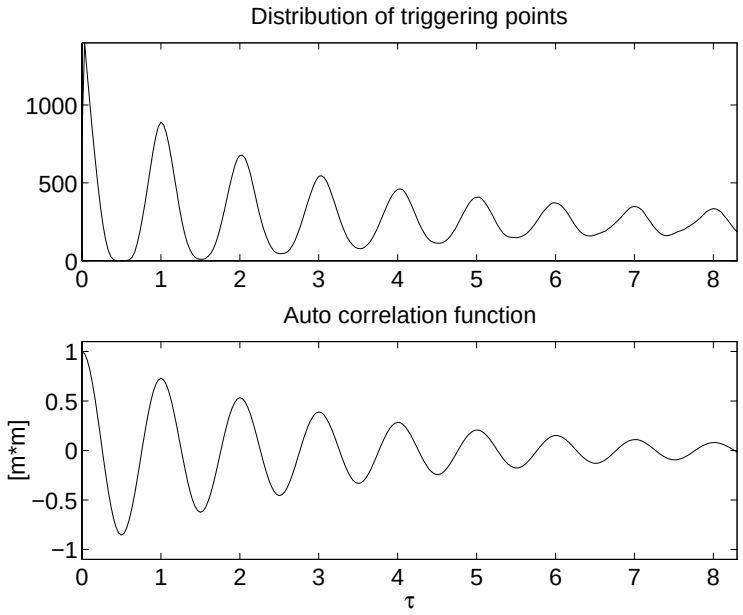

Figure 5.9: *Average distribution of triggering points obtained by simulation using positive point triggering* $[a_1\ a_2] = [\sigma_X\ \infty]$ *and the auto correlation function of the system.*

Figure 5.10 shows the simulated and predicted variance obtained using the theoretical values.

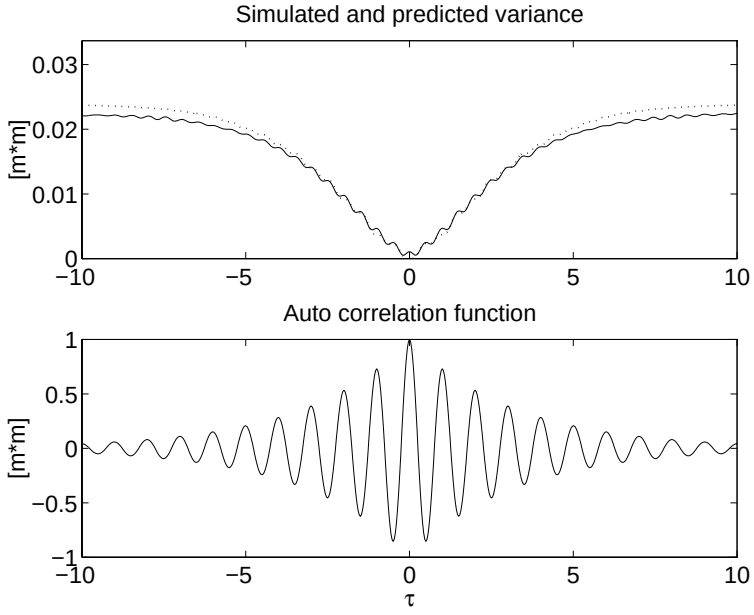

Figure 5.10: *The simulated and the predicted variance of the RD functions using point triggering* $[a_1\ a_2] = [\sigma_X\ \infty]$ *and the auto correlation function of the system. [——]: Theoretical (simulated) variance of the RD function. [· · · ·]: Predicted variance of the RD function using the new method.*

The variance predicted using eq. (3.46) and the variance predicted by the new method are shown in fig. 5.11, where the RD function and the distribution of triggering point from a single realization have been used.

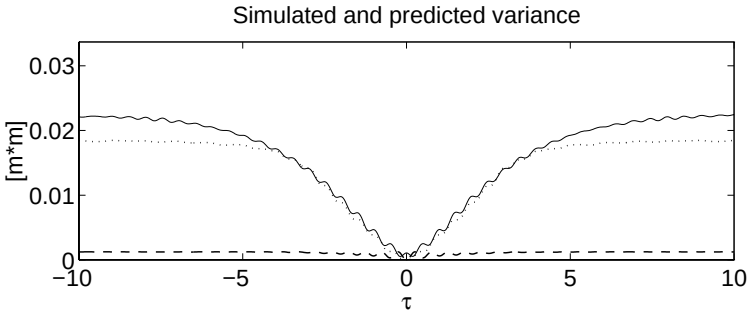

Figure 5.11: *The simulated and the predicted variance of the RD functions using positive point triggering* $[a_1\ a_2] = [\sigma_X\ \infty]$. *[——]: Theoretical (simulated) variance of the RD function. [· · · ·]: Predicted variance of the RD function using the new method. [- - - -]: Predicted variance using the relation from chapter 3.*

The estimated RD function, the theoretical RD function and the distribution of the triggering points for the single realization are shown in fig. 5.12.

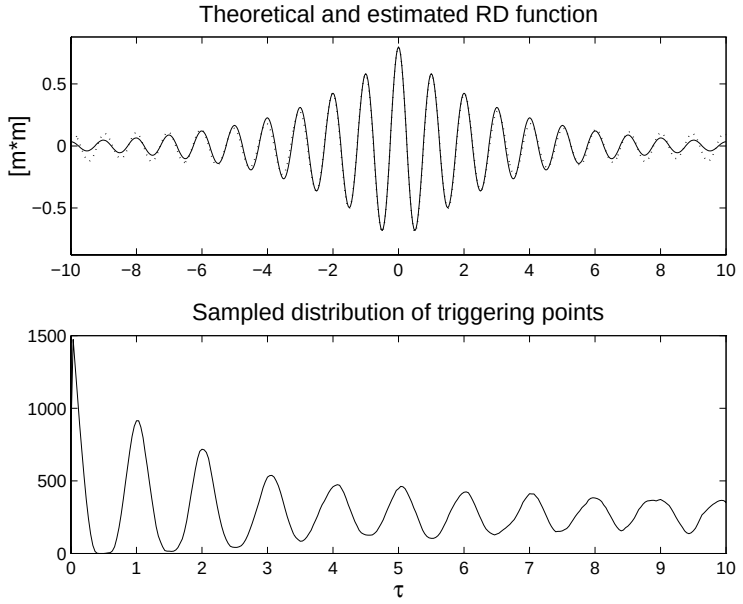

Figure 5.12: *The theoretical and the estimated RD function using positive point triggering* $[a_1\ a_2] = [\sigma_X\ \infty]$ *and the sample distribution of the triggering points. [——]: Theoretical RD function. [· · · ·]: Estimated RD function.*

5.4 Example 3: Positive Point - 2DOF

This section investigates how the model works on a 2DOF system loaded by uncorrelated white noise at each mass. It is a natural continuation of the work performed with an SDOF system. The modal parameters are printed in table 5.1.

	f [Hz]	ζ [%]	$\lvert\Phi\rvert^1$	$\lvert\Phi\rvert^2$	$\angle\Phi^1$	$\angle\Phi^2$
Mode 1	3.74	4.10	1.000	1.005	0.00	177.7
Mode 2	6.27	4.50	1.000	0.995	0.00	1.3

Table 5.1: *Modal parameters of a 2DOF system.*

The theoretical correlation (scaled RD) functions of the 2DOF system is shown in figure 5.13.

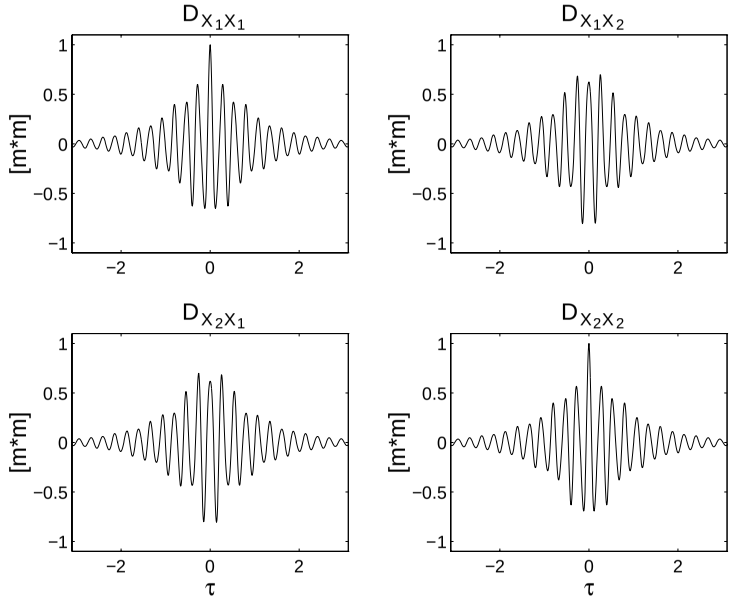

Figure 5.13: *Theoretical correlation (scaled RD) functions of 2DOF system.*

The investigations are based on 50000 simulations of the response of the system loaded by white noise followed up by an estimation of the RD functions using the positive point triggering condition with the triggering levels $[a_1\ a_2] = [\sigma_X\ \infty]$. Figure 5.14 shows the simulated distribution of the triggering points and a single realization of the distribution of triggering points. This realization is used later to predict the variance of RD functions from a single set of measurements only.

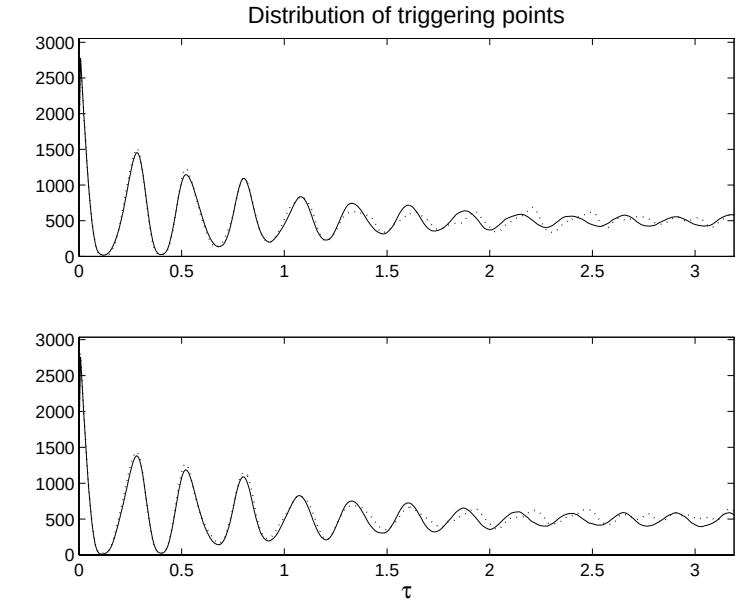

Figure 5.14: *Simulated distribution of triggering points and distribution of triggering points from a single realization.*

Figure 5.14 illustrates that the distribution of the triggering points is well described by a single realization of the measurements.

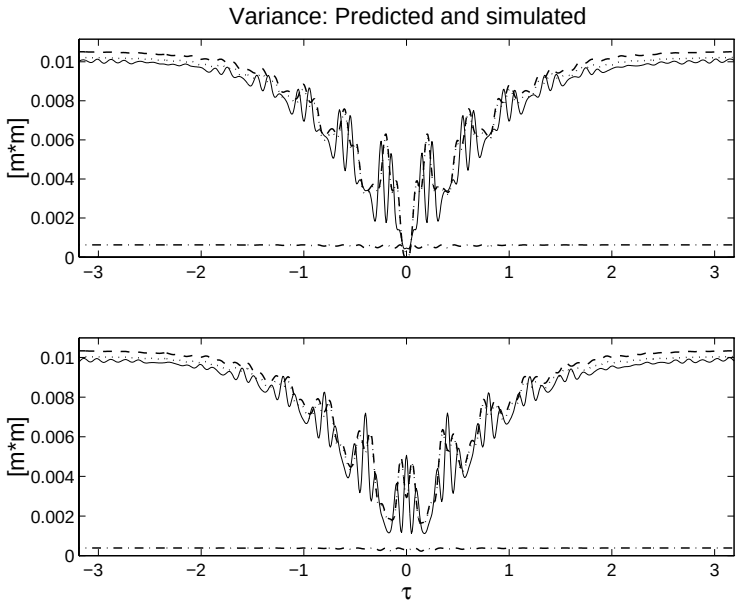

Figure 5.15: *Variance of RD functions. [——]: Simulated variance. [- - - -]: Variance predicted from a single realization. [·····]: Variance predicted from theoretical RD function and simulated distribution of triggering points. [—·—·—]: Variance predicted by eq. (3.46).*

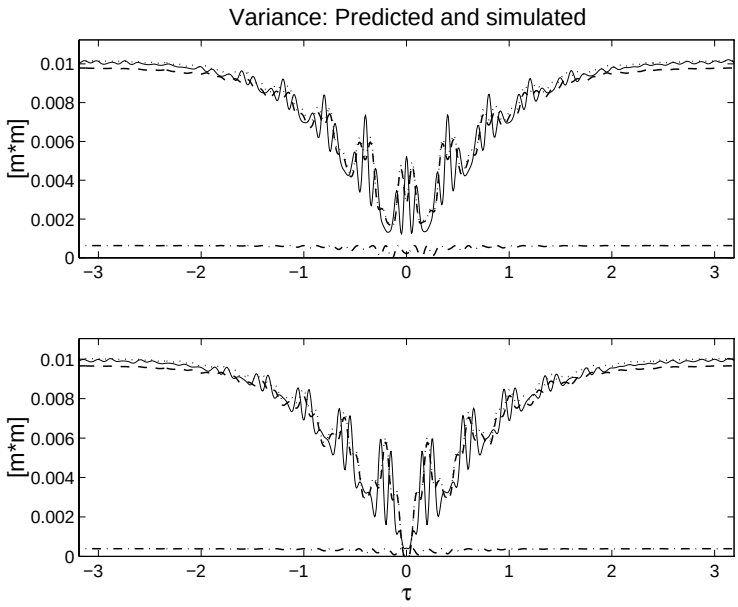

Figure 5.16: *Variance of RD functions. [——]: Simulated variance. [- - - -]: Variance predicted from a single realization. [·····]: Variance predicted from theoretical RD function and simulated distribution of triggering points. [·–·–·–]: Variance predicted by eq. (3.46).*

The investigation of this 2 DOF system show that the new method is superior to the predictions by eq. (3.46). Whether or not the new method is accurate enough to pay off the extra computational time is an open question. The accuracy of the method is highest around the zero time lag and especially for higher time lags.

5.5 Example 4: Positive Point - 5 DOF

The investigation is concluded with the analysis of a lumped mass parameter system with 5 DOF loaded by white noise. The eigenfrequencies and the damping ratios of the system are listed in table 5.2 and the auctocorrelation function for the response of the first mass is shown in fig. 5.17.

Mode	1	2	3	4	5
f [Hz]	2.18	4.18	5.81	6.69	7.73
ζ [%]	3.46	3.57	3.72	3.80	4.70

Table 5.2: *Modal parameters of the 5 DOF system.*

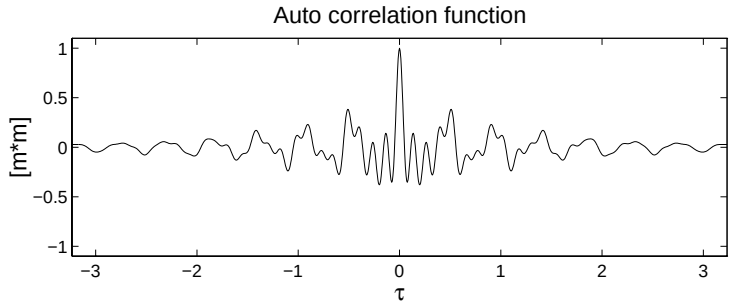

Figure 5.17: *The auto correlation function of the response of the first mass.*

It is a very time-consuming process to investigate the performance of the method for all 25 RD funtions. Instead only the response of a single mass is considered. Figure 5.18 shows the distribution of triggering points obtained from simulation and a single realization.

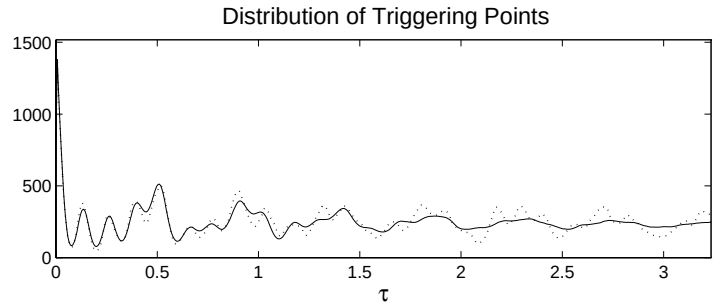

Figure 5.18: *[——]: Simulated distribution of triggering points. [· · · ·]: Distribution of triggering points from a single realization.*

Figure 5.19 shows the variance calculated by simulation, eq. (3.46), theoretical RD function with simulated distribution of triggering points and RD function and distribution of triggering points obtained from a single realization.

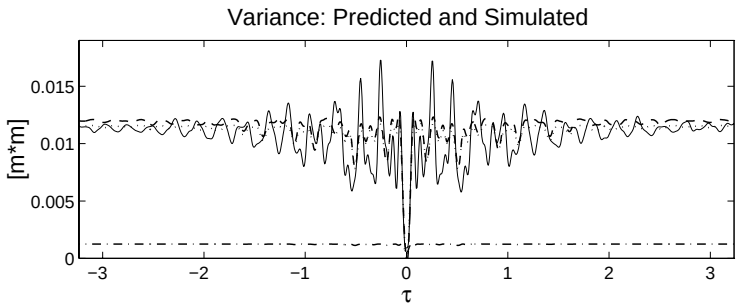

Figure 5.19: *Variance of RD functions. [——]: Simulated variance. [- - - -]: Variance predicted from a single realization. [·····]: Variance predicted from theoretical RD function and simulated distribution of triggering points. [·—·—·—]: Variance predicted by eq. (3.46).*

Again it is concluded that the method predicts the variance well, especially around zero time lag and for time lags where the variance becomes constant.

5.6 Summary

An approach to estimate the variance of RD functions has been suggested. The method takes the correlation between the time segments into account by using the sampled time points of the triggering points. The method has been tested by simulation of different systems. The method seems to predict the variance well at the zero time lag and for time lags where the variance have converged. It is superior to the method for predicting the variance, which is based on uncorrelated time segments in the averaging process. It is an open question if this increase in accuracy can pay off the increasing computational time. Further investigations in order to understand the approach are recommended.

Bibliography

[1] Asmussen, J.C. & Brincker, R. *A New Approach for Predicting the Variance of Random Decrement Functions.* Proc. 16th International Modal Analysis Conference, Santa Barbara, California, USA, February 2-5 1998.

[2] Asmussen, J.C. & Brincker, R. *A New Approach for Predicting the Variance of Random Decrement Functions.* Submitted for publication in Journal of Mechanical Systems and Signal Processing.

Chapter 6

Bias Problems and Implementation

The purpose of this chapter is to discuss the practical problems, which arise in applications and implementations of the RD technique. Most of these problems are due to the sampling of continuous-time processes into discrete-time processes. The aim is to point out these problems and describe when and how to be attentive to these practical problems.

Section 6.1 describes different bias problems, which arise in application of the RD technique. The bias problems are discussed and illustrated. Special attention is given to their importance towards both the estimated correlation functions and the modal parameters extracted from these correlation functions. The solutions to the bias problems are explained and it is described when to be attentive to these problems.

Section 6.2 illustrates the different implementations of the RD technique, which has been programmed and used during this work. The RD functions have been programmed in HIGH-C, see the reference manual [1] and linked to MATLAB, see the user guide [2], using MATLAB's external interface opportunities, see MATLAB [3].

6.1 Bias of RD Functions

Theoretically, the RD functions are unbiased as described in chapter 3. In applications of the RD technique 3 different types of bias are introduced. These are:

- Bias due to the discretization of the continuous-time processes.
- Bias due to false sorting of triggering points.
- Bias due to high damping.

In the following sections these three types of bias are discussed and illustrated.

6.1.1 Bias due to Discretization

Since the measured responses of any structure are always converted from an analog to a digital signal, bias is introduced in the RD functions. This bias problem is dominant if

any triggering condition corresponding to the theoretical general triggering condition is used

$$T_{X(t)}^{G_T} \;=\; \{X(t) = a, \dot{X}(t) = b\} \tag{6.1}$$

In continuous-time it is not a problem to use the above triggering condition, but if the sampled measurements are considered the event that $x(t_i) = a$ and/or $\dot{x}(t_i) = b$ will in general never occur. This introduces bias. The effect is illustrated using the level crossing triggering condition. Figure 6.1 shows a realization of a continuous-time process and the corresponding discrete-time process sampled at equidistant time points at the sampling interval ΔT.

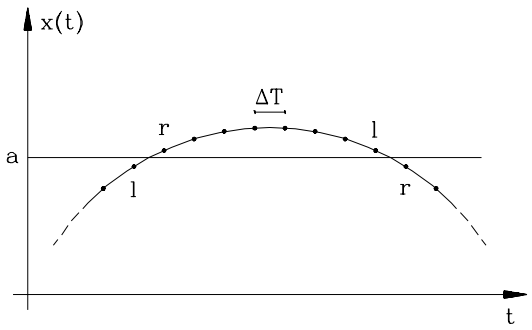

Figure 6.1: *Illustration of the effect of sampling a continuous process at equidistant time points.*

The triggering level a is indicated with the horizontal line. As seen the continuous-time process fulfils the condition $X(t) = a$ at two time points. But the sampled process never fulfils this condition. In order to detect the triggering points it is necessary to use a crossing condition. An implementation of a level crossing triggering condition in MATLAB could be like

```
if ((x(k+1)>a & x(k)<a) | (x(k+1)<a & x(k)>a)), ...
```

The discrete time process fulfils this condition twice corresponding to the continuous-time process. The problem is: Which time point should be used as centre of the time segment picked out and used in the averaging process? Three possibilities exist. The left-hand point (y(k)) could be used, the right-hand point (y(k+1)) could be used or both points could be used corresponding to using the average of the two time segments. In Brincker et al. [1] the latter approach is denoted a symmetric window. The left-hand (l) and right-hand (r) points are shown in fig. 6.1.

In order to illustrate the different possibilities an SDOF system loaded by Gaussian white noise is considered. The eigenfrequency is $f = 1$ Hz and the damping ratio is $\zeta = 1\%$. The response of this system is simulated at a sampling interval of $\Delta T = \frac{1}{5f}$ at 8000 time points. Figure 6.2 show the estimated RD functions (level crossing) using the left-hand point, the right-hand point and both points as triggering points.

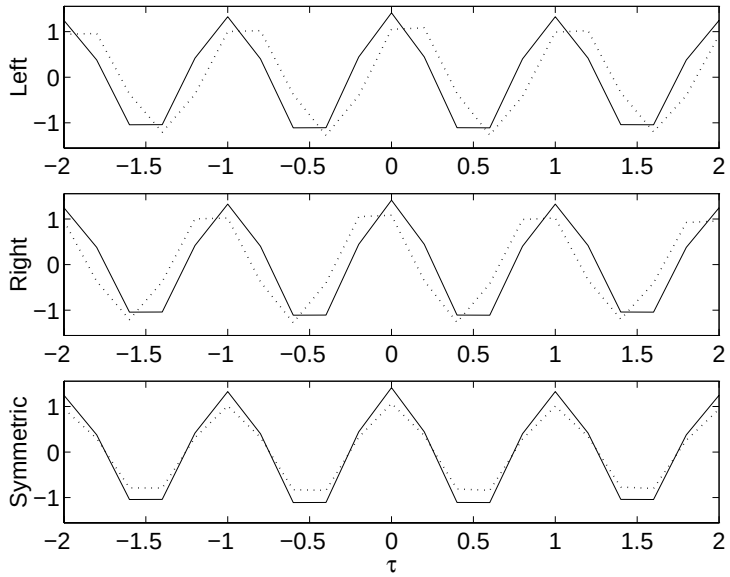

Figure 6.2: *Illustration of bias problems. RD functions of an SDOF system with* $\Delta T = \frac{1}{5f}$. *[——]: Theoretical RD function. [· · · ·]: Estimated RD function.*

The bias introduced from the sampling of the continuous process is illustrated in figure 6.2. If the left-hand point is used as triggering point the estimate of the RD function is shifted to the right and if the right-hand point is used the estimate of the RD function is shifted to the left. If the left-hand and the right-hand point is used as triggering points, the estimated RD functions is not shifted only scaled.

If the aim is to estimate modal parameters the above bias problems can almost always be neglected. It is assumed that the methods such as ITD and PTD are used to extract the modal parameters from the RD functions. These methods are only capable of extracting correct modal parameters from either the positive time lags or the negative time lags of the correlation functions. Assume that only the positive time lags of the estimated RD functions in fig. (6.1) are used. The RD functions estimated using the right-hand point or using both the right-hand and the left-hand point will result in correct modal parameters. But the RD functions estimated using the left-hand point will result in erroneous modal parameters, unless a number of points corresponding to the time shift is omitted. The reason is that the part of the RD function from zero to the time shift corresponds to the part of the true RD function from minus the time shift to zero. The discontinuity at time lag zero cannot be described using the methods to extract modal parameters from free decays introduced in chapter 3.

The ratio between the natural eigenfrequency and the sampling frequency influences the bias problem. The system used above is considered again. The response of the system is sampled at a lower sampling interval, $\Delta T = \frac{1}{15f}$, again at 8000 time points. Figure 6.3 shows the estimated RD functions using the left-hand point, right-hand point and left-hand and right-hand point as triggering points. The triggering level is $a = \sqrt{2}\sigma_X$.

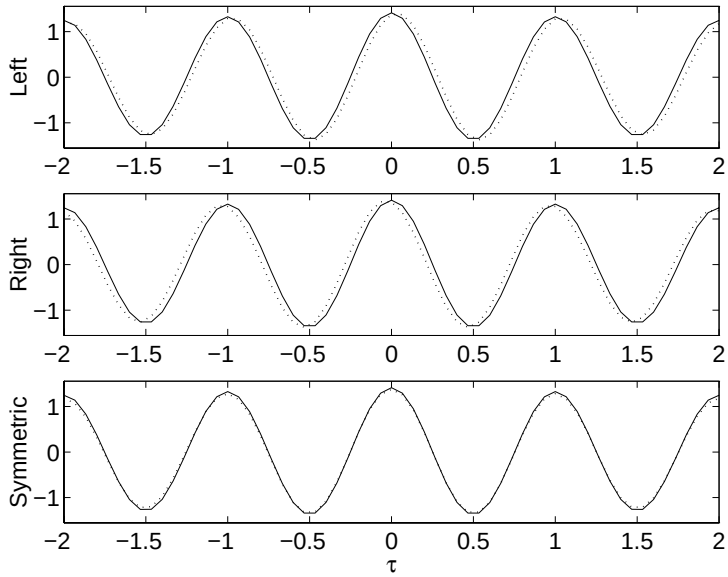

Figure 6.3: *Illustration of bias problems. RD functions of a SDOF system with* $\Delta T = \frac{1}{15f}$. *[——]: Theoretical RD function. [· · · ·]: Estimated RD function.*

As seen the bias problem cannot be neglected, but it has decreased with increasing sampling frequency. This means that for highly oversampled systems the bias problem can be neglected.

The above bias problems have been discussed in detail by Brincker et al. [5], [6] and [7]. If the level crossing triggering condition or the zero crossing with positive slope triggering condition is used the above problems should be considered. If the positive point or the local extremum triggering condition is used, the above problems do not exists. Only if the triggering levels a_1 and a_2 are formulated so that $a_1 \approx a_2$ the above problems can arise in application of these conditions.

6.1.2 Bias due to Sorting of Triggering Points

Another bias problem is sorting of triggering points. If long records are analysed, it might be tempting to perform some kind of selection among all the detected triggering points in order to keep a low estimation time. It is very difficult to exclude some of the triggering points without introducing bias. This is illustrated in the following two examples.

Consider an SDOF system loaded by Gaussian white noise. The natural eigenfrequency is $f = 1$ Hz and the damping ratio is $\zeta = 3\%$. The system is sampled with $\Delta T = \frac{1}{15f}$ at 40000 time points. In order to restrict the number of triggering points a time jump of $100 \cdot \Delta T$ is performed each time a triggering point is detected, before detection of the next triggering point starts. The theoretical RD function and the RD function estimated using level crossing with $a = \sqrt{2}\sigma_X$ and the time jump are shown in fig. 6.4.

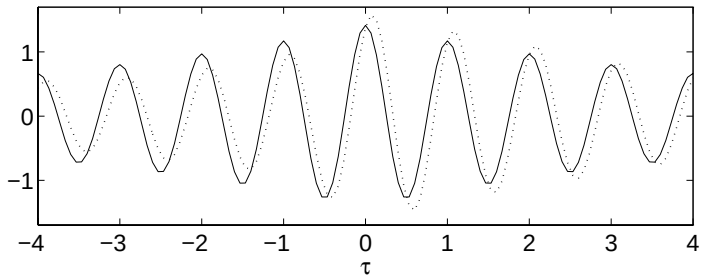

Figure 6.4: *Illustration of bias due to false triggering point sorting using the level crossing triggering condition. Every time a triggering point is detected a jump of 100 points is performed before the search for a new triggering point continues. [——]: Theoretical RD function. [· · · ·]: Estimated RD function.*

As seen this makes the RD functions highly biased. The bias consists of a time shift of the RD functions and an underestimation of the damping ratio for the positive time lags and an overestimation of the damping ratio for negative time lags. The explanation is that the probability of an upcrossing after a time jump is much higher than the probability of a downcrossing. So a hidden condition stating that the velocity of the process is positive is introduced. If the average of the negative and positive time lags are used this bias does not influence the modal parameters.

Consider another SDOF system loaded by Gaussian white noise. The natural eigenfrequency is $f = 1$ Hz and the damping ratio is $\zeta = 10\%$. The system is sampled with $\Delta T = \frac{1}{10f}$ at 10000 time points. The local extremum triggering condition is used to estimate the RD function from the response. The damping ratio is chosen high in order to ensure that the response contains both local minima and local maxima for positive response levels. The RD functions are estimated using the local maxima as triggering points only. The result is shown in figure 6.5. The top figure shows the non-normalized estimated RD functions and the bottom figure shows the normalized RD functions with the theoretical RD function.

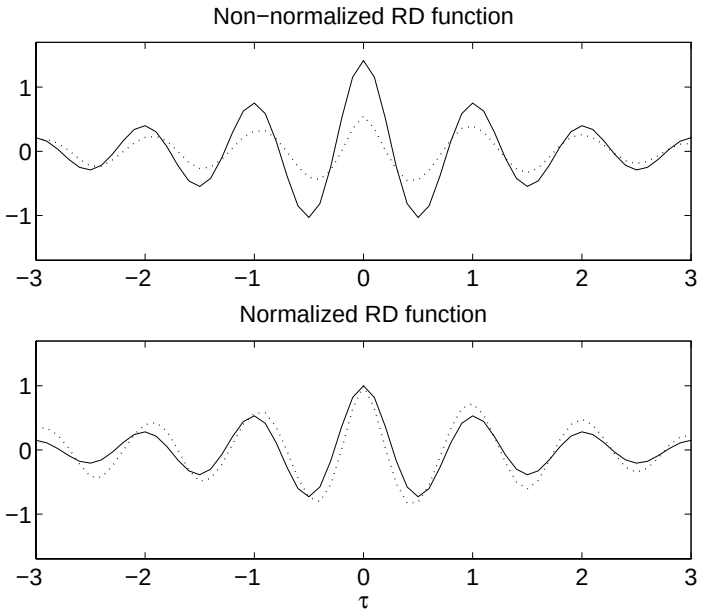

Figure 6.5: *Illustration of bias due to false triggering point sorting using the local extremum triggering condition. Only local maxima are used in the averaging process. [——]: Theoretical RD function. [· · · ·]: Estimated RD function.*

As seen the difference is not only a simple scaling factor but also extensive bias. Even the frequency of the RD function is changed. The explanation is that since only local maxima are used a hidden condition is made on the acceleration of the process ($\ddot{X}(t) \leq 0$). The acceleration of the process is not independent of the process itself and thereby extensive bias is introduced. This bias cannot be removed. The example illustrates that sorting or selection of triggering points is very difficult. It is recommended to avoid selection of triggering points and instead choose another triggering condition if the estimation time is too high.

6.1.3 Bias due to High Damping

The last-mentioned bias problem is due to high damping. High levels of damping seldom occur in mechanical systems or civil engineering structures so this phenomenon is only illustrated and not discussed in detail. In section 6.1.1, it is illustrated how the discretization of a continuous-time process introduces bias into the RD functions. The solution to these bias problems is to use a symmetric window, which means that the average of the left-hand and right-hand triggering point is used. If the system is heavily damped it is not possible to remove the bias by using the average of two time segments. The reason is that a typical upcrossing and a typical downcrossing are not symmetric. A downcrossing is not a *mirror* of the upcrossing. This introduces bias.

Consider an SDOF system loaded by Gaussian white noise. The natural eigenfrequency is $f = 1$ Hz and the damping ratio is $\zeta = 20\%$. The system is sampled with $\Delta T = \frac{1}{3f}$ at 40000 time points. The RD function is calculated from the response using the level crossing triggering condition. All three different choices of the triggering condition described in section 6.1.1 are used.

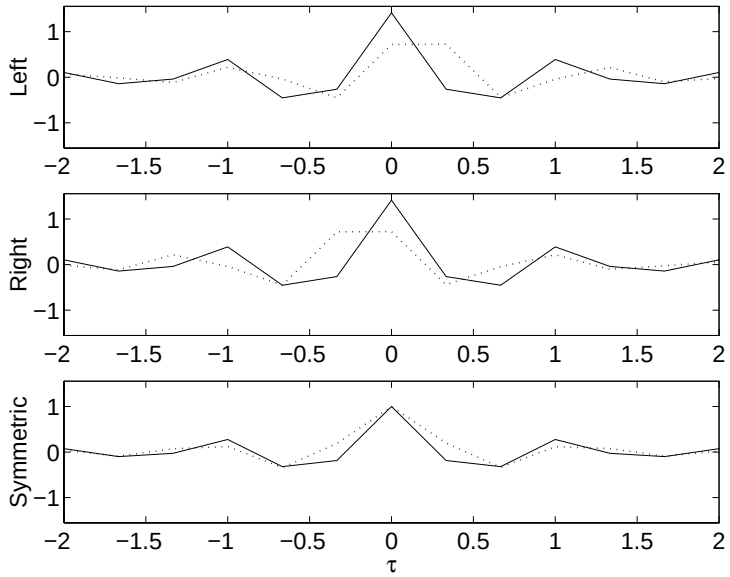

Figure 6.6: *Illustration of bias due to heavy damping using the level crossing triggering condition.* $\Delta T = \frac{1}{3f}$. *[——]: Theoretical RD function. [· · · ·]: Estimated RD function.*

The RD functions become biased. The bias is reduced by choosing a higher sampling frequency. This is illustrated in fig. 6.7 where the RD function is calculated from the response which has been sampled with $\Delta T = \frac{1}{10f}$ at 40000 time points.

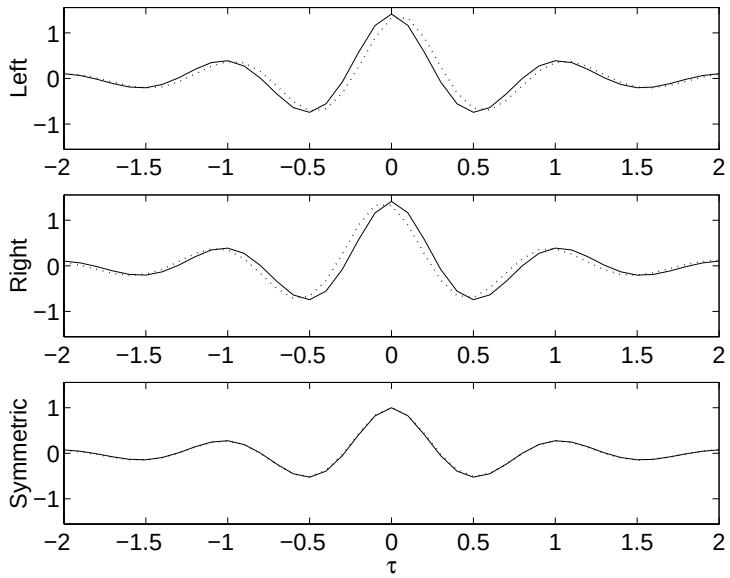

Figure 6.7: *Illustration of bias due to high damping using the level crossing triggering condition.* $\Delta T = \frac{1}{10f}$. *[——]: Theoretical RD function. [· · · ·]: Estimated RD function.*

The figure illustrates that a high sampling rate removes the bias for highly damped systems.

6.2 Implementation of RD Functions

This section describes implementation of the RD technique in MATLAB. The functions described here have been used throughout this thesis for estimation of RD functions. One of the disadvantages of MATLAB is that *for-do-end* loops are performed extremely slowly compared to most other programming languages. The reason is that MATLAB is a programming language constructed specially for matrix operation. In a *for-do-end* loop the purpose is to perform operations at index level. Loops with operation at index level should not be programmed in MATLAB, since they are extremely slow, see the MATLAB Userguide [2]. For this reason all RD functions have been implemented in HIGH-C [1] and linked to MATLAB using MATLAB's external interface opportunities, see MATLAB [3]. Using this approach the RD function can be used as if they were programmed in MATLAB. The HIGH-C language has been chosen, since it does not give any restriction on the size of vectors and matrices. This is equivalent to MATLAB and is convenient for time series analysis.

6.2.1 RD and VRD Functions in HIGH-C

For each triggering condition eight different implementations of the four triggering conditions described in chapter 3 have been programmed. The purpose of programming eight different functions for each condition instead of programming a single general function for each condition is to ensure the highest possible speed of the technique for user application. In the following the name of the functions for the different triggering condition is given together with an example of a function call in MATLAB.

Level crossing triggering condition (lev)

$RD1alev$	$RD2alev$	$RD3alev$	$RD4alev$
$RD1plev$	$RD2plev$	$RD3plev$	$RD4plev$

```
>>[Ntrig RD]=RD1alev(X,n,no,a);
```

The input/output variables, which are common to all the above RD functions, are

Input	X	The measurement matrix.
	n	The number of points in the RD functions.
	no	The number of the triggering measurement.
	a	The triggering level.
Output	$Ntrig$	The number of triggering points.
	RD	The RD functions (not normalized with $Ntrig$).

Local extremum triggering condition (loc)

*RD*1*aloc* *RD*2*aloc* *RD*3*aloc* *RD*4*aloc*
*RD*1*ploc* *RD*2*ploc* *RD*3*ploc* *RD*4*ploc*

>>[Ntrig RD]=RD3aloc(X,n,no,a1,a2);

The input/output variables, which are common to all the above RD functions, are

Input	X	The measurement matrix.
	n	The number of points in the RD functions.
	no	The number of the triggering measurement.
	$a1$	The lower triggering level.
	$a2$	The upper triggering level.
Output	$Ntrig$	The number of triggering points.
	RD	The RD functions (not normalized with $Ntrig$).

Positive point triggering condition (pos)

*RD*1*apos* *RD*2*apos* *RD*3*apos* *RD*4*apos*
*RD*1*ppos* *RD*2*ppos* *RD*3*ppos* *RD*4*ppos*

>>[Ntrig RD]=RD3apos(X,n,no,a1,a2);

The input/output variables, which are common to all the above RD functions, are

Input	X	The measurement matrix.
	n	The number of points in the RD functions.
	no	The number of the triggering measurement.
	$a1$	The lower triggering level.
	$a2$	The upper triggering level.
Output	$Ntrig$	The number of triggering points.
	RD	The RD functions (not normalized with $Ntrig$).

Zero Crossing triggering condition (zer)

*RD*1*azer* *RD*2*azer* *RD*3*azer* *RD*4*azer*
*RD*1*pzer* *RD*2*pzer* *RD*3*pzer* *RD*4*pzer*

>>[Ntrig RD]=RD3azer(X,n,no);

The input/output variables, which are common to all the above RD functions, are

Input	X	The measurement matrix.
	n	The number of points in the RD functions.
	no	The number of the triggering measurement.
Output	$Ntrig$	The number of triggering points.
	RD	The RD functions (not normalized with $Ntrig$).

The different triggering conditions have been implemented so that the only difference in the input to these functions is the triggering levels. The argument for not normalizing the RD functions is that if the aim is to estimate modal parameters from a single set of RD functions it is not unnecessary to normalize the RD functions. This means less computational time.

The difference between e.g. *RD1apos* and *RD1ppos* is that *RD1apos* estimates RD functions with both positive and negative time lags, whereas *RD1ppos* only uses positive time lags. The difference between *RD1apos* - *RD4apos* and *RD1ppos* - *RD4ppos* is the speed and accuracy of the different implementations. The numbers refer to the following restrictions of the data matrix X.

1: X in double precision. No restriction on the size of X.
2: X in single precision. Maximum size of X is 65535 points.
3: X in double precision. No restriction on the size of X.
4: X in single precision. Maximum size of X is 65535 points.

The fastest functions are *RD4a???* or *RD4p???* and the slowest functions are *RD1a???* or *RD1p???*. For all of the above functions the uncompiled file name has extension *.c* and the compiled version of the functions have extension *.mex* (Matlab Executable), since they can be called directly from the MATLAB evironment. Common to all functions is that online help is available by typing the function name in the MATLAB environment. The help functions have extension *.m* and are simple editable files. The online help utility is simple to use. If the following command is given in the MATLAB environment the help file will respond as shown below.

>>RD1apos

will result in the following help statement.

```
**********************************************************************
**    RD1aPOS.C    :  Random Decrement Function                       **
*                     Positive Point Triggering Condition            **
*                                                                    **
*     Purpose      :  To calculate the Random Decrement functions using **
*                     triggering at positive points. The function uses **
*                     both positive and negative time delays. This   **
*                     function can deal with infinitely many points in **
*                     the data matrix and works with DOUBLE precision. **
*                     Remember to use an unequal number of points in **
*                     the functions.                                 **
*                                                                    **
*     Call         :  RD1aPOS(X,n,no,a1,a2)                          **
*                     X: Matrix with time series. Time series must be **
*                     at the columns.                                **
*                     n: Number of points in RD functions. Choose an **
*                     unequal number.                                **
*                     no: Number of the reference (triggering) measure- **
*                     ment.                                          **
*                     a1: Trig level lower bound. Lower triggering le- **
*                     vel.                                           **
*                     a2: Trig level upper bound. Upper triggering le- **
*                     vel.                                           **
*                                                                    **
*     Return       :  1: Number of triggering points.                **
*                     2: Estimated RD functions from matrix.         **
*                                                                    **
*     Computed     :  JCA 1/06-96                                    **
*     Edited       :  JCA 1/06-96                                    **
**********************************************************************
```

This finishes the description of the computational RD algorithms in HIGH-C. For the VRD technique the computational algorithm has also been programmed in HIGH-C and linked to MATLAB using MATLABs external interface possibilities. Only the positive point triggering condition has been implemented, since this is the only triggering condition which gives sufficient triggering points. Furthermore, only a single type, which corresponds to type three of the RD functions, has been implemented.

Vector triggering condition

vectora vectorp

>>[Ntrig VRD]=vectora(X,n,a1,a2,vec1,m,k);

The input/output variables are

Input	X	The measurement matrix.
	n	The number of points in the RD functions.
	$a1$	The lower triggering level.
	$a2$	The upper triggering level.
	$vec1$	Time shift for vector triggering.
	m	Size of vector triggering condition.
	k	Maximum time shift of the vector condition.
Output	$Ntrig$	The number of triggering points.
	VRD	The VRD functions (Not normalized with Ntrig).

The difference between *vectora* and *vectorp* is that *vectorp* only estimates positive time lags in the VRD functions, whereas *vectora* estimates positive and negative time lags. The uncompiled versions of the functions has extension *.c* and the compiled version have extension *.mex*. There is also online help available for the VRD functions. The following MATLAB command will result in the help statement

>>vectora

```
**********************************************************************
**    VECTORa.C     :  Vector Random Decrement Function              **
*                      Positive point triggering condition          **
*                                                                   **
*     Purpose        :  To the estimate the Vector Random Decrement func-  **
*                       tions using positive point triggering. The function  **
*                       uses both positive and negative time delays. All     **
*                       variables are of size DOUBLE. Remember to use an     **
*                       unequal number of points in the functions.           **
*                                                                   **
*     Call           :  vectora(X,n,a1,a2,vec1,m,k)                **
*                       x: Data matrix with measurements.           **
*                       n: Number of points in RD functions. Choose an un-   **
*                       equal number.                               **
*                       a1: Lower triggering level vector.          **
*                       a2: Upper triggering level vector. au¿al¿0. **
*                       vec1: Vector with triggering time shifts.   **
*                       m: Size of vector condition.                **
*                       k: Maximum time shift.                      **
*                                                                   **
*     Return         :  1 : Number of triggering points.           **
*                       2 : Estimated VRD functions from matrix.    **
*                                                                   **
*     Computed by    :  JCA 01/06-96                               **
*     Edited by      :  JCA 01/09-96                               **
**********************************************************************
```

6.2.2 MATLAB Utility Functions

This section describes functions programmed in MATLAB, which uses the basic **.mex* functions or the RD/VRD functions for further analysis. Usually in the analysis of several simultaneously recorded measurements the full covariance (correlation) matrix is estimated. This means that the above functions have to be used several times, since each function call only results in an estimated set of RD functions corresponding to a column

of the correlation matrix. In order to standardize this computational routine two MATLAB functions, *fullcova.m* and *fullcovp.m* have been programmed. These functions return the full covariance matrix at positive and negative time lags, (a), or positive time lags (p) only. The online help for *fullcova* is

```
**************************************************************************
**    FULLCOVA.M   :   Random Decrement utility functions                 **
*                                                                         **
*     Purpose          Estimation of FULL COVariance matrices using RD    **
*                      functions. Both positive and negative time lags are**
*                      used. Notice that the RD functions are scaled so   **
*                      that the true covariance matrix are returned.      **
*                                                                         **
*     Call         :   fullcova(X,Type1,Type2,n,a1,a2)                    **
*                      X: Data matrix with measurements.                  **
*                      Type1: Type of implementation of the RD technique. **
*                      1: Double precision, 0-4294967925 points.          **
*                      2: Single precision, 0-4294967925 points.          **
*                      3: Double precision, 0-65535 points.               **
*                      4: Single precision, 0-65355 points.               **
*                      Type2: Type of triggering condition used for esti- **
*                      mation of covariance functions.                    **
*                      1: Level crossing triggering condition.            **
*                      2: Local extremum triggering condition.            **
*                      3: Every positive point triggering condition.      **
*                      4: Zero crossing with positive slope trig condition.**
*                      !!This triggering condition estimates the time deriva-**
*                      tive of the covariance functions.                  **
*                      N: Number of points in correlation functions. Must **
*                      be unequal in order to take the zero time lag into **
*                      account.                                           **
*                      a1: If Type2=1, a1 is the triggering level.        **
*                      If Type2=2,3 a1 is the lower triggering bound      **
*                      a2: If Typ2e=1, a2 is not used.                    **
*                      If Type2=2,3 a2 is the upper triggering bound.     **
*                                                                         **
*     Return       :   Ntrig: Vector with number of triggering points.    **
*                  :   Cfull: Covariance matrix. C11=row1. C21=Row2.      **
*                      Cn1=Rown. C12=rown+1. C22=Rown+2 ...               **
*                                                                         **
*     Computed by  :   JCA 01/09-96                                       **
*     Edited by    :   JCA 01/09-96                                       **
**************************************************************************
```

Although the above functions make it easy to estimate the correlation matrix of the measurements the triggering level and triggering condition should be chosen carefully as described in chapter 3. Furthermore, the positive point triggering condition and the local extremum triggering condition are implemented so that the triggering levels a_1 a_2 should not be chosen as $a_1 \approx a_2$. Consider the function *RD1apos*. The computational code for the detection of triggering points and the averaging process in HIGH-C looks like

```
for (i = N1; i < Row - N1; i++) {
 if (*(X+(No-1)*Row+i)>*Al && *(X+(No-1)*Row+i)<*Au) {
  (*Po_trig)++;
  for (j=0; j<Col; j++){
   p=X+j*Row+i-N1;
   for (k=0; k<N; k++){
     *(RD+j*N+k)+=*(p+k);
} } } }
```

where X is the measurement matrix with Row points and Col measurements, Al and Au are the lower and upper triggering level, respectively and Po_trig is the number of triggering points. If $a_1 \rightarrow a_2$ then a bias problem arises since the discrete process might be sampled so that $X(k) < a_1$ and $X(k+1) > a_2$. This will occur for high levels of the time derivative. In order to take this situation into account the condition in the above code should be combined with a crossing condition. So in conclusion for the positive point triggering condition and the local extremum triggering condition the triggering levels should not be chosen as $a_1 \approx a_2$.

In order to use information from both positive and negative time lags and to obtain a quality measure of the RD functions a MATLAB function, which uses the symmetry relations for correlation/covariance functions of stationary processes, see chapter 2, has been programmed. The name of the function is *avgcov.m* and returns the average estimated covariance functions and the error for the average covariance functions. *avgcov.m* can only be used in combination with the output of *fullcova.m*. The online help for *avgcov.m* is

```
**********************************************************************
**    AVGCOV.M     :  Random Decrement utility function.              **
*                                                                    **
*     Purpose      :  From a full covariance matrix with both positive **
*                     and negative time lags an averaged covariance ma- **
*                     trix with only positive time lags is returned. Fur- **
*                     thermore, an error matrix with the difference be- **
*                     tween positive and negative time lags is returned. **
*                     The averaging process is based on the validity of **
*                     the following eqs. for the covariance matrices for **
*                     stationary processes.                          **
*                     Cxy(t)=Cyx(-t) Cyx(t)=Cxy(-t)                  **
*     Call            avgcov(Cfull);                                 **
*                     Cfull: Full covariance matrix with positive and **
*                     negative time lags (output from fullcova.m).   **
*     Return          CfullP: Averaged covariance matrix. All negative **
*                     time lags averaged with corresponding positive time **
*                     lags after Cxy(t)=Cyx(-t)                      **
*                     Cerror: Error matrix with difference between posi- **
*                     tive and negative time lags, theoretically zero **
*                     matrix.                                        **
*                                                                    **
*     Computed by  :  JCA 22/3-1996                                  **
*     Edited by    :  JCA 22/3-1996                                  **
**********************************************************************
```

The matrix CfullP can be used as input to ITD or PTD and the matrix Cerror can be used for quality assessment of CfullP.

For the VRD technique a general MATLAB function has been programmed. The function uses *vectora.mex* and *vectorp.mex*. The online help for this function is

```
**************************************************************************
**    VECTRICA.M    :  Random Decrement utility function.                 **
*                                                                         **
*     Purpose       :  To calculate the Random Decrement functions using  **
*                      vector positive point triggering. Assuming more mea-**
*                      surements than channels. The vector triggering con-**
*                      dition is assumed to be applied to the first n mea-**
*                      surements.                                         **
*                                                                         **
*     Call          :  VECTRICA(X,n,a1,a2,Type,Vec1,Vec2)                 **
*                      X: Data matrix with measurements.                  **
*                      n: Number of points in the RD functions. If positive**
*                      and negative time lags are used (Type=1) n is unequal**
*                      a1: Lower triggering level vector (which are multi-**
*                      plied by the standard deviation of the corresponding**
*                      measurement.                                       **
*                      a2: Upper triggering level vector (which are multi-**
*                      plied by the standard deviation of the corresponding**
*                      measurement.                                       **
*                      Type: If Type=1, both positive and negative time de-**
*                      lays are used in the RD functions. If Type=2, only **
*                      positive time delays are used.                     **
*                      Vec1: Vector with time delays for the triggering   **
*                      condition.                                         **
*                      Vec2: Vector with sign of the triggering condition.**
*                      1 or -1.                                           **
*                                                                         **
*     Return        :  Ntrig: Number of triggering points.                **
*                      VRD: Vector Random Decrement functions.            **
*                                                                         **
*     Computed by   :  JCA 01/09-96                                       **
*     Edited        :  JCA 01/09-96                                       **
**************************************************************************
```

The modal parameters of the system can be extracted from the output of either *vectrica*, *avgcov*, *fullcova*, *fullcovp* or the basic RD and VRD functions programmed in HIGH-C. For this purpose the ITD and the PTD algorithm have been programmed in MATLAB. The online help for the functions are as follows.

```
**********************************************************************
**    ITD_UHSM.M   :   Ibrahim Time Domain function.                  **
*                                                                     **
*     Purpose          To estimate eigenfrequencies, damping ratios and mode  **
*                      shapes from free decay measurements from an MDOF  **
*                      structural system.                             **
*                                                                     **
*     Call             ITD_UHSM(X,Dt,N1,N2,N3,N4,N5,Vecmeas,Avg,Name) **
*                      X: Data matrix containing the free decay measure-  **
*                      ments or the RD/VRD functions.                 **
*                      Dt: The sampling interval.                     **
*                      N1: The number of points omitted from the input ma-  **
*                      trix in the estimation procedure. The first points  **
*                      might be biased due to noise.                  **
*                      N2: Every N2 points is only used in the identifica-  **
*                      tion which increases the sampling interval to dt*N2.  **
*                      N3: The number of physical modes to be identified.  **
*                      N4: The matrix aspect ratio for linear regression.  **
*                      N5: The number of time delays for calculation of MCFs  **
*                      Vecmeas: Vector with information about the free de-  **
*                      cays or RD/VRD functions. The vector inform about  **
*                      rows of the reference measurements. The reference  **
*                      measurement should always be the top measurement.  **
*                      Avg: Indicates if the mode shapes from different set-  **
*                      ups should be averaged. Useful for e.g. RD func-  **
*                      tions corresponding to a full covariance matrix.  **
*                      This option can only be used if the setups have the  **
*                      same number of free decays.                    **
*                      Avg=1 averages, other numbers discards the averaging.  **
*                      Name: Name of file to which the results are written.  **
*                                                                     **
*     Return           RES: Matrix with results. Matrix has 2*N4 rows.  **
*                      Column 1: Estimated eigenfrequencies.          **
*                      Column 2: Estimated damping ratios.            **
*                      Column 3: Averaged MCF magnitude.              **
*                      Column 4: Averaged MCF phase.                  **
*                      Column 5: RMS ABS MPF.                         **
*                      Column 6:6+N Complex mode shapes.              **
*                      Column 6+N+1:6+2*N: MCF magnitude.             **
*                      Column 6+2*N+1:6+3*N MCF phase.                **
*                      Column 6+3*N+1:6+4*N Absolute Value of MPF     **
*                                                                     **
*     Computed by      JCA 1/7 1996                                   **
*     Edited by        JCA 1/7 1996                                   **
**********************************************************************
```

```
**********************************************************************
**    POLYREF.M   :   Polyreference Time Domain function.            **
*                                                                    **
*     Purpose         This is an implementation of the PTD technique. The **
*                     The results are modal parameters and modal confiden- **
*                     ce factors for magnitude and phase.            **
*                                                                    **
*     Call            polyref(X,Dt,N1,N2,N3,N4,N5,Vecmeas,Avg,Name); **
*                     X: Data matrix with free decays or RD/VRD func- **
*                     tions.                                         **
*                     Dt: The sampling interval.                     **
*                     N1: The number of points omitted from the input ma- **
*                     trix in the estimation procedure. The first couple **
*                     of points might be biased due to noise.        **
*                     N2: Every N2 point is only used in the identifica- **
*                     tion. Increasing the sampling interval to N2*Dt **
*                     N3: The number of physical modes to be identified. **
*                     N4: The number of time delays for MCFs.        **
*                     N5: The number of setups (inputs).             **
*                     N6: The number of measurement locations.       **
*                     Name: Name of file to which the results are written. **
*                                                                    **
*     Return          RES: Matrix with results. Matrix has 2*N4 rows. **
*                     Column 1: Estimated eigenfrequencies.          **
*                     Column 2: Estimated damping ratios.            **
*                     Column 3: Averaged MCF magnitude.              **
*                     Column 4: Averaged MCF phase.                  **
*                     Column 5: RMS ABS MPF.                         **
*                     Column 6:6+N Complex mode shapes.              **
*                     Column 6+N+1:6+2*N: MCF magnitude.             **
*                     Column 6+2*N+1:6+3*N MCF phase.                **
*                     Column 6+3*N+1:6+4*N Absolute Value of MPF     **
*                                                                    **
*     Computed by     JCA 1/9 1996                                   **
*     Edited by       JCA 1/9 1996                                   **
**********************************************************************
```

6.2.3 Example

Consider the 2DOF system from chapter 3 again. The system has the following modal parameters

	f [Hz]	ζ %	$\lvert\Phi\rvert^1$	$\lvert\Phi\rvert^2$	$\angle\Phi\rvert^1$	$\angle\Phi\rvert^2$
Mode 1	3.09	1.69	1.00	1.61	0	4.7
Mode 2	4.56	3.56	1.00	0.62	0	173.0

Table 6.1: *Modal parameters of the 2DOF system.*

The response of this system to Gaussian white noise is simulated and saved in the data matrix X. 10000 points are simulated at a sampling frequency of 120 Hz. In order to calculate the correlation matrix the following commands are given

>>Cfull=fullcova(X,3,3,501,1,80);

>>[Cavg Cerr]=avgcov(Cfull);

The number of points in the scaled RD functions in Cfull is 501. The positive point triggering condition has been used and the triggering levels are chosen as $[a_1\ a_2] = [\sigma_X\ \infty]$ ($\infty \approx 80$). In order to evaluate the estimate of the correlation functions the functions in *Cavg* are plotted together with *Cerr*.

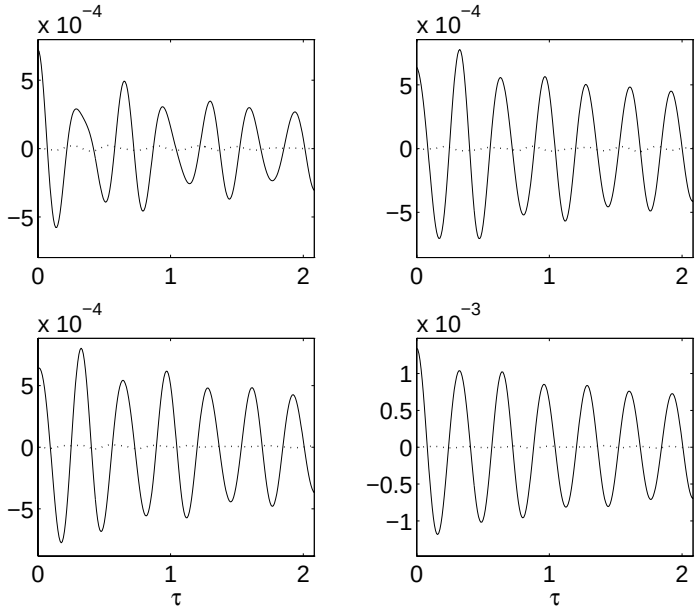

Figure 6.8: *[——]: Average correlation functions. [· · · · · · ·]: Errors of the average of the correlation functions.*

The figure illustrates that the errors of the average estimate of the correlation functions are small. In order to extract the modal parameters the PTD technique is used. The following command is given

>>RES=polyref(Cavg,1/120,5,1,2,1,2,2,'result')

The number of modes is 2, five points have been removed from the beginning of the correlation functions and a single time shift is used for the calculation of the MCFs. The RESult matrix is saved in the file 'result'. the absolute values of the first 7 columns of the RES matrix are

3.10	2.02	0.999	0.11	11.66	1.00	1.61
4.52	3.00	0.998	0.23	20.10	1.00	0.63

which can be compared with the theoretical values in table 6.1. The columns have the following estimates: 1: Frequencies, 2: Damping ratios, 3: MCF magnitude, 4: MCF phase, 5: MPFs, 6: Mode shape component 1, 7: Mode shape component 2.

This example shows how simple it is to estimate modal parameters using MATLAB in combination with the HIGH-C functions.

6.3 Summary

In this chapter considerations concerning the implementation of the RD technique have been discussed. Section 6.1 illustrates the bias problems, which can occur in application of the RD technique. In general the bias problems can be avoided by proper implementation. In the situation where the sampling frequency is much higher than the maximum eigenfrequency of the system the bias problems vanish.

In section 6.2 a description of the different implementation made during this work of the RD funcions is given, and it is illustrated how to use these functions. The RD functions are implemented in HIGH-C and linked to MATLAB using MATLAB's external interface opportunities in order to make the technique as fast as possible. Several different implementations of each triggering condition are made in order to be able to select the fastest and most accurate function dependent on the size and the precision of the available data.

Bibliography

[1] HIGH-C/C++ Tools, Library and Program manuals 1992. MetaWare Inc.

[2] MATLAB User's Guide (August 1992). MathWorks, Inc.

[3] MATLAB External Interface Guide (January 1992). MathWorks, Inc.

[4] Brincker, R., Jensen, J.L. & Krenk, S. *Spectral Estimation by the Random Dec Technique.* Proc. 9th International Conference on Experimental Mechanics, Lyngby, Copenhagen, Aug. 20-24, 1990.

[5] Brincker, Krenk, S. & R., Jensen, J.L. *Estimation of Correlation Functions by the Random Dec Technique.* Proc. Skandinavisk Forum for Stokastisk Mekanik, Lund, Sweden, Aug. 30-31, 1990.

[6] Brincker, R., Kirkegaard, P.H. & Rytter, A. *Identification of System Parameters by the Random Decrement Technique.* Proc. 16th International Seminar on Modal Analysis, Florence, Italy, Sept. 9-12, 1991.

[7] Brincker, R., Krenk, S. & Jensen, J.L. *Estimation of Correlation Functions by the Random Decrement Technique.* Proc. 9th International Modal Analysis Conference and Exhibit, Firenze, Italy, April 14-18, 1991.

[8] MATLAB Reference Guide (October 1992). MathWorks, Inc.

Chapter 7

Estimation of FRF by Random Decrement

In this chapter a new method for estimating FRF is tested. The method is based on the RD functions of the load to and the response from a linear system. It is assumed that the input is stochastic and stationary. Traditionally the measured response of and load to a linear system has been analysed using the FFT algorithm in order to obtain the FRFs. As described in the introduction to this thesis such an approach will in general always result in biased estimates of the FRM. Using the RD technique as basis for the estimation of the FRFs bias can under the right circumstances be removed. This is an important relation of the RD technique. This method was first tested in Brincker et al. [1] and Asmussen et al. [2].

Section 7.1 describes the traditional FFT based approaches for estimating the FRFs. The different approaches which are used to minimize bias and random errors are described. In section 7.2 the theoretical background for estimating FRFs using the RD technique is given together with a description of the expected advantages and disadvantages. Section 7.3 presents an illustrative simulation study and an experimental test performed in order to validate the performance of this method.

7.1 Traditional FFT Based Approach

This section gives a short review of the traditional FFT based approach for estimation of FRFs. As described in the introduction to this thesis the spectral densities can be defined using Fourier transformation, see e.g. Bendat & Piersol [3], Schmidt [4]. Consider two stationary stochastic processes $X(t)$ and $Y(t)$. The spectral densities are defined as

$$S_{XX}(\omega) = \lim_{T\to\infty} E[\frac{1}{T}X_k^*(\omega,T)X_k(\omega,T)] \tag{7.1}$$

$$S_{YX}(\omega) = \lim_{T\to\infty} E[\frac{1}{T}Y_k^*(\omega,T)X_k(\omega,T)] \tag{7.2}$$

$$S_{XY}(\omega) = \lim_{T\to\infty} E[\frac{1}{T}X_k^*(\omega,T)Y_k(\omega,T)] \tag{7.3}$$

$$S_{YY}(\omega) = \lim_{T\to\infty} E[\frac{1}{T}Y_k^*(\omega,T)Y_k(\omega,T)] \tag{7.4}$$

where superscript * denotes complex conjugate and

$$X(\omega,T) = \frac{1}{2\pi}\int_0^T X(t)e^{-i\omega t}dt \qquad Y(\omega,T) = \frac{1}{2\pi}\int_0^T Y(t)e^{-i\omega t}dt \tag{7.5}$$

The mean value operation in eqs. (7.1) - (7.4) is over the statistical ensemble of the different realizations, $x_k(t)$ and $y_k(t)$, of the processes $X(t)$ and $Y(t)$. In practice the limit $T \to \infty$ can never be obtained. This is modelled by multiplying the realizations of the processes by a window function, which delimits the time period of the realizations to be T.

$$\begin{aligned} x(t,T) &= W(t,T)\cdot x(t) \\ y(t,T) &= W(t,T)\cdot y(t) \end{aligned} \qquad W(t,T) = \begin{cases} w(t) & |t| < T/2 \\ 0 & |t| < T/2 \end{cases} \tag{7.6}$$

If $w(t) = 1$ the boxcar or rectangular window is used. The limitations of the time period of the realizations, forces the frequency resolution to be finite, $\Delta\omega = \frac{2\pi}{T}$. The spectral densities in eqs. (7.1) - (7.4) can only be estimated as e.g. eq. (7.2)

$$\hat{S}_{YX}(\omega) = E[\frac{1}{T}Y_k^*(\omega,T)X_k(\omega,T)] \tag{7.7}$$

This estimate will always be biased due to the finite record period or window effects. These bias errors are usually denoted leakage errors since energy (or signal power) at a given frequency band is moved to the surrounding frequency band. Random errors can also be introduced if only a finite number of realizations of the processes $X(t)$ and $Y(t)$ are available. The bias errors can be reduced by using more complicated window functions than the boxcar window as the Hanning or the Hamming window, see e.g. Schmidt [4]. In a real life situation only a single realization of each process is available (the measurements). This problem is solved by assuming that the processes are ergodic. Then the realizations can be divided into a number of segments, which represent the statistical properties of the ergodic process. The above description follows Bendat & Piersol [3] and Schmidt [4].

The stochastic process $X(\omega)$ is interpreted as a load applied to a linear structure at the location i and $Y(\omega)$ is the stochastic process describing the corresponding response at the location j of the structure. The FRF which transfers $X(\omega)$ into $Y(\omega)$, $H_{ji}(\omega)$ will for simplicity be denoted $H(\omega)$ without any subscripts.

$$Y(\omega) = H(\omega)X(\omega) \tag{7.8}$$

Using the definition of the spectral densities in eqs. (7.1) - (7.4) the FRF can be expressed in terms of spectral densities.

$$S_{XY}(\omega) = H(\omega)S_{XX}(\omega) \tag{7.9}$$

$$S_{YY}(\omega) = H(\omega)S_{YX}(\omega) \tag{7.10}$$

Equations (7.9) and (7.10) constitute the basis of the two basic estimators of the FRF, $H_1(\omega)$ and $H_2(\omega)$.

$$\hat{H}(\omega) = H_1(\omega) = \frac{\hat{S}_{XY}(\omega)}{\hat{S}_{XX}(\omega)} \tag{7.11}$$

$$\hat{H}(\omega) \;=\; H_2(\omega) \;=\; \frac{\hat{S}_{YY}(\omega)}{\hat{S}_{YX}(\omega)} \tag{7.12}$$

Other more complicated estimators of the FRF exist such as H_3 and H_4, see e.g. Fabunmi et al. [5] and Yun et al. [6]. But the H_1 and the H_2 estimator is the basic estimators.

Assume that the input measurement or load $X(t)$ is measured without the introduction of any noise. The response or output $Y(t)$ is measured with an noise process added. If this noise process is uncorrelated with the response, the H_1 estimator will result in a true FRF, in the sense of being independent of the noise added to the response. On the other hand, assume that the input measurement is collected with a noise process added. The output measurement is noise free. If the noise process is independent of the input or load the H_2 estimator will result in a true FRF, in the sense of being independent of the noise added to the input. For more complicated noise situations other estimators have been developed as mentioned previously.

The ordinary coherence function is defined as

$$\gamma_{xy}^2(\omega) \;=\; \frac{|S_{XY}(\omega)|^2}{S_{XX}(\omega)S_{YY}(\omega)} \qquad\qquad 0 \leq \gamma_{xy}^2(\omega) \leq 1 \tag{7.13}$$

The estimate of the coherence function is calculated by using the estimates of the spectral densities. The coherence function can be used for quality assessment of the estimate of the FRF. A high coherence means a good estimate of the FRF at the corresponding frequency and a low coherence means a poor estimate of the FRF. Low coherence could also be interpreted to be an indicator of non-linearities. The coherence should be high (≈ 1) around the peaks of an FRF.

The problems with an approach to estimate the FRFs based on the FFT algorithm can be summarized to

- the choice of a proper window function.
- the choice of a proper estimator.

In the next section an approach for estimating FRFs based on the RD technique is introduced. The main difference to the traditional methods presented shortly in this section is that the averaging process, see e.g. eqs. (7.1) - (7.4), is performed in the time domain before the Fourier transformation is used. This makes it possible to obtain unbiased estimates of the FRF.

7.2 Random Decrement Based Approach

Two ergodic stochastic processes $X(t)$ and $Y(t)$ are considered. As in section 7.1, $X(t)$ will be interpreted as the load at point i on a structure and $Y(t)$ as the corresponding response of the structure at point j. The IRF and FRF will be abbreviated $h(t)$ and $H(\omega)$ instead of $h_{ji}(t)$ and $H_{ji}(\omega)$. The structure is assumed to be linear and time invariant as described in chapter 2. The response of the structure is given by the convolution integral.

$$Y(t) = \int_{-\infty}^{t} h(t-\eta)X(\eta)d\eta \tag{7.14}$$

where the influence of the initial conditions has been neglected. Substituting variables, $t = t + \tau$ and $\eta = \xi + t$, eq. (7.14) can be rewritten as

$$Y(t+\tau) = \int_{-\infty}^{\tau} h(\tau - \xi) X(t+\xi) d\xi \tag{7.15}$$

Taking the conditional mean value of eq. (7.15) yields

$$E[Y(t+\tau)|T_X^{G_A}(t)] = \int_{-\infty}^{\tau} h(\tau - \xi) E[X(t+\xi)|T_X^{G_A}(t)] d\xi \tag{7.16}$$

or

$$E[Y(t+\tau)|T_Y^{G_A}(t)] = \int_{-\infty}^{\tau} h(\tau - \xi) E[X(t+\xi)|T_Y^{G_A}(t)] d\xi \tag{7.17}$$

Using the definition of the RD functions introduced in chapter 3 eqs. (7.16) and (7.17) become

$$D_{YX}(\tau) = \int_{-\infty}^{\tau} h(\tau - \xi) D_{XX}(\tau) d\xi \tag{7.18}$$

$$D_{YY}(\tau) = \int_{-\infty}^{\tau} h(\tau - \xi) D_{XY}(\tau) d\xi \tag{7.19}$$

Equations (7.18) - (7.19) establish relations for estimating the IRF. The original processes are transformed into the RD functions, but the input-output relation is preserved. The advantage is that noise has been averaged out in the estimation process of the RD functions. Also, the size of the problem has been reduced, since RD functions contain a considerably smaller number of points corresponding to the original time series. If the response of a structure was measured at several points the relation in eq. (7.19) could be extended to cross RD functions only, by using the RD functions $D_{Y_i Y_j}(\tau)$ and $D_{XY_j}(\tau)$. By introducing the Fourier transform of an RD function as $Z_{XY}(\omega)$ defined as

$$Z_{XY}(\omega) = \frac{1}{2\pi} \int_{-\infty}^{\infty} e^{-i\omega\tau} D_{XY}(\tau) d\tau \tag{7.20}$$

eqs. (7.18) and (7.19) can be transformed into the frequency domain as

$$Z_{YX}(\omega) = H(\omega) Z_{XX}(\omega) \tag{7.21}$$

and

$$Z_{YY}(\omega) = H(\omega) Z_{XY}(\omega) \tag{7.22}$$

These two equations constitute a basis for estimating $H(\omega)$ corresponding to the H_1 and H_2 estimators in eqs. (7.11) and (7.12). The approach in eq. (7.21) is denoted H_1^{RD} and the approach in eq. (7.22) is denoted H_2^{RD}

$$H(\omega) = H_1^{RD} = \frac{Z_{YX}(\omega)}{Z_{XX}(\omega)} \tag{7.23}$$

$$H(\omega) = H_2^{RD} = \frac{Z_{YY}(\omega)}{Z_{XY}(\omega)} \tag{7.24}$$

Corresponding to eq. (7.13) a coherence function for the RD functions can be defined as

$$\gamma_{xy}^2 \;=\; \frac{H_1^{RD}}{H_2^{RD}} \;=\; \frac{Z_{XY}(\omega)Z_{YX}(\omega)}{Z_{XX}(\omega)Z_{YY}(\omega)} \tag{7.25}$$

There is a main difference between the two coherence functions defined in this chapter. In eqs. (7.13) the coherence function is based on the number of averages in the frequency domain, whereas eq. (7.25) is only based on two different estimates in the frequency domain. The averaging process is performed in time domain. Alternatively the coherence function for the estimates based on the RD technique could be based on several RD functions estimated with different triggering levels.

It will now be assumed that the load is Gaussian white noise. This means that the response will also be Gaussian distributed. It also means that the RD functions will be proportional to the correlation functions of the processes. Since $R_{YX}(\tau)$, $R_{XY}(\tau)$, $R_{YY}(\tau)$ and $R_{XX}(\tau)$ all satisfy $R \;\rightarrow\; 0$ for $|\tau| \rightarrow \infty$ it follows that all RD functions in eqs. (7.18) and (7.19) dissipate towards zero with increasing time distance from zero. The result of this relation is that the bounds in the Fourier transformation do not have to be $-\infty$ and ∞ and thereby no leakage errors will occur. This assumes that $R(\pm\tau_{\max}) \approx 0$, where $\tau_{\max}$ is the maximum time lag in the correlation function.

Assume that the input to the system is measured with a noise process, U(t), added. The noise process is assumed to be Gaussian distributed and uncorrelated with the measured output, which is free of noise. Subscript M denotes the measured realizations of the different processes

$$y_M \;=\; y(t)\,, \quad x_M \;=\; x(t) \;+ u(t) \tag{7.26}$$

The RD functions are proportional to the correlation functions, since the processes are Gaussian distributed

$$R_{Y_M Y_M}(\tau) \;=\; E[y_M(t+\tau)y_M(t)] \;=\; R_{YY}(\tau) \tag{7.27}$$

$$R_{X_M Y_M} \;=\; E[y_M(t+\tau)x_M(t)] \;=\; R_{XY}(\tau) + \; R_{UY}(\tau) \;=\; R_{XY}(\tau) \tag{7.28}$$

In this situation the estimation of the FRF should be based on eq. (7.22). Correspondingly if a Gaussian distributed noise process is added to the output of the system and the measured input is noise free the estimation of the FRF should be based on eq. (7.21).

Two main advantages are expected using the RD based method for estimation of FRF compared to the traditional method based on pure FFT. The computational time is expected to decrease, since the estimation of RD functions only involved averaging, whereas the estimation using pure FFT involves multiplication. In general this question can not be answered since the estimation time for the RD technique depends on the statistical description of the processes. This issue was discussed in chapter 3. RD functions are estimated unbiased and dissipate towards zero for increasing absolute time lags. This is an advantage since no leakage errors are introduced.

7.3 Case Studies

This method was first tested in an introductory simulation study of a 3DOF system loaded by white noise, see Asmussen & Brincker [2]. In Brincker & Asmussen [1] the method was tested and compared with the FFT based approach using experimentally obtained data.

This section starts with an illustrative example of an SDOF system. The purpose is to illustrate the advantages and disadvantages of the method and to describe the different problems, which arise in the application of this technique. The method is further investigated by analysing the vibrations of a laboratory bridge model loaded by Gaussian white noise through a shaker.

7.3.1 Basic Case - SDOF System

Consider an SDOF system with an eigenfrequency $f = 1$ Hz and a low damping ratio of $\zeta = 0.6\%$. The system is loaded by Gaussian white noise. Firstly, the measurements consist of 10000 points sampled at 5.8 Hz. The FRF is calculated using the traditional method based on the FFT algorithm and the H_1 estimator. 1024 points are used in each time segment for each Fourier transformation and each time segment is multiplied by the Hanning window. The FRF is also estimated using the H_1^{RD} estimator. The positive point triggering condition is used with 1025 points in each RD function and the triggering bounds are chosen as $[a_1\ a_2] = [0.5\sigma_X\ \infty]$. From the FRFs the IRFs are calculated using inverse FFT. The eigenfrequencies and the damping ratios are estimated from the IRFs using the ITD algorithm. In order only to have bias errors the modal parameters are estimated using the two approaches from 100 independent simulations of the Gaussian white noise load and the corresponding response. Figure 7.1 shows a typical auto and cross RD function for the Gaussian white noise load, $D_{XX}(\tau)$, and the response, $D_{YX}(\tau)$.

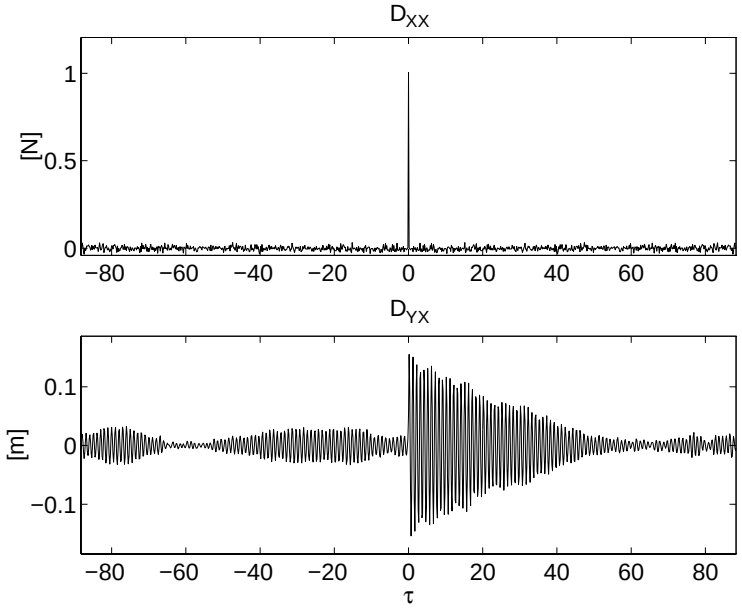

Figure 7.1: *Typical auto (load) and cross (response) RD functions estimated using positive point triggering.*

The RD functions in fig. 7.1 illustrate the idea of using the RD technique for estimation of FRFs. The auto RD function is seen to be almost identical to the auto correlation function of the white noise load. An appropriate choice window function can increase the accuracy of the RD functions. The window functions can be chosen to be e.g. symmetric exponentials or a force window for the auto RD functions according to the standard approach used in impact testing.

Figure 7.2 shows the RD functions from fig. 7.1, where a symmetric exponential window has been multiplied to both functions.

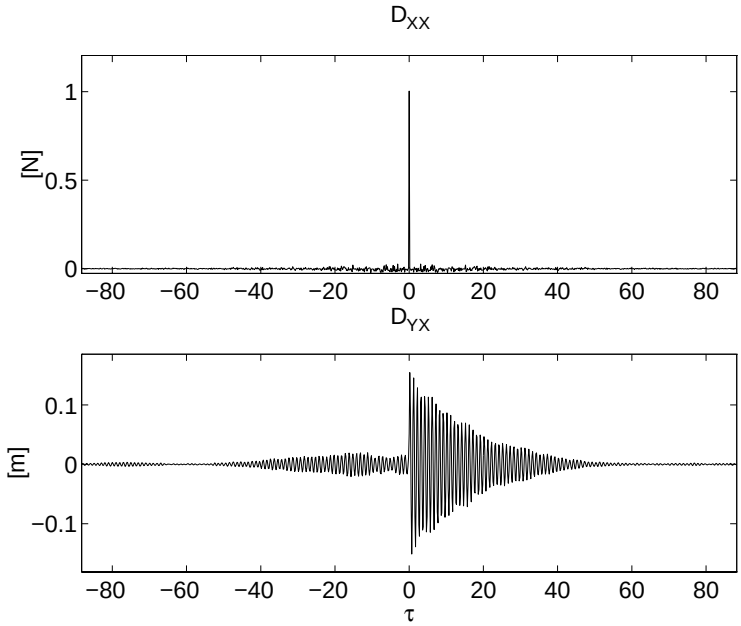

Figure 7.2: *Typical auto, $D_{XX}(\tau)$, and cross, $D_{YX}(\tau)$ RD functions estimated using positive point triggering and a symmetric exponential window.*

The effect of the exponential window is clear. The RD functions dissipate to zero more efficiently, which means that leakage errors are controlled by the exponential window.

Figure 7.3 shows the absolute value of a typical FRF calculated theoretically and using the H_1 and the H_1^{RD} estimators. The result for the H_1^{RD} estimator is based on the RD functions shown in fig. 7.1. The different estimates of the FRF are very alike except for the ragged curve, which is the FRF from the H_1^{RD} estimator without applying any window function, see fig. 7.1 (no windowing corresponds to using the boxcar window). The result of applying a symmetric exponential window is that the estimates become smooth on account of artificial introduced damping. The estimated modal parameters can be corrected for this artificially damping using principles developed for impact testing.

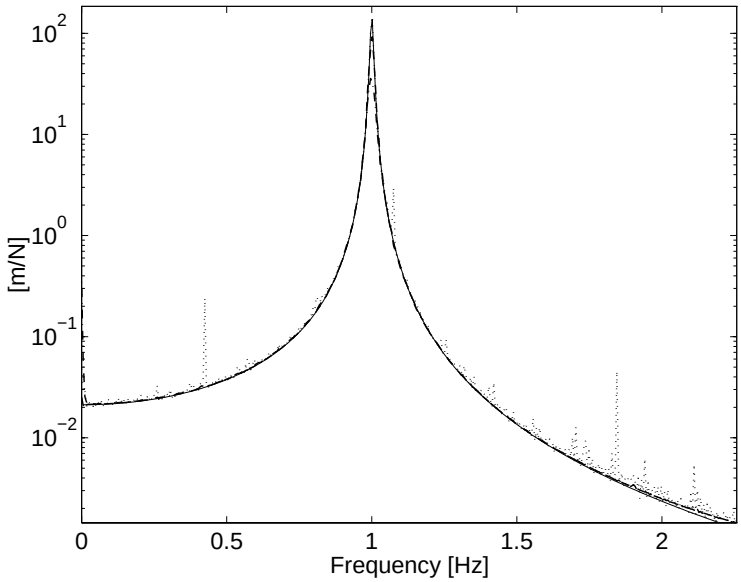

Figure 7.3: *Absolute value of FRFs. [------]: Theoretical. [- - - -]: FFT Hanning window, H_1. [· · · · ·]: RD-FFT, No windowing, H_1^{RD}. [· – · – ·]: RD-FFT, exponential window, H_1^{RD}.*

Figure 7.4 shows a zoom of fig. 7.3 around the resonance frequency.

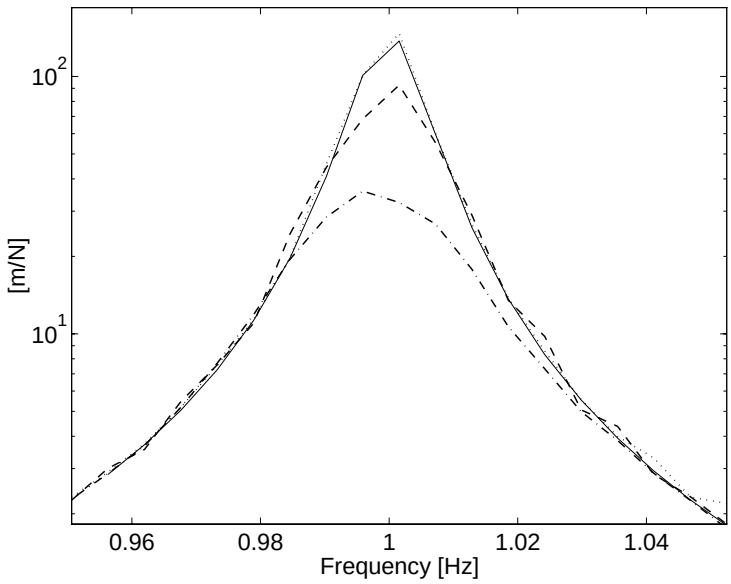

Figure 7.4: *Zoom of absolute value of the FRFs. [------]: Theoretical. [- - - -]: FFT Hanning window, H_1. [· · · · ·]: RD-FFT, No windowing, H_1^{RD}. [· – · – ·]: RD-FFT, exponential window, H_1^{RD}.*

The curve from the H_1^{RD} estimator from the RD function in fig. 7.1 (no windowing) is almost identical to the theoretical curve. If the symmetric exponential window is used the FRF is smooth in all the frequency band, but in the vicinity of f the artificial damping is very clear.

In order to investigate the influence of the length of the record period the number of measurement points is increased to 40000. Figure 7.2 shows the estimated RD functions without windowing.

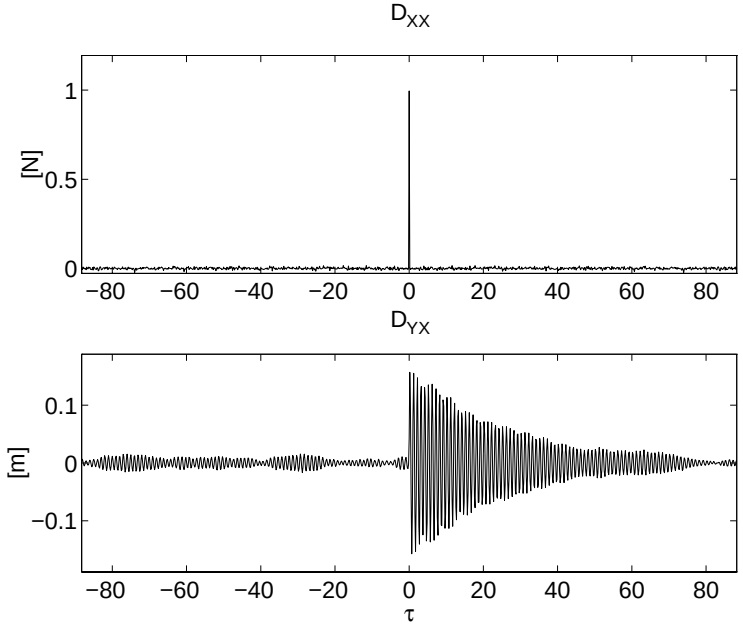

Figure 7.5: *No windowing 40000 points*

The figure illustrates that the increase of the record length has increased the accuracy of the RD functions. The noise content is lower and the RD functions dissipate more clearly towards zero with increasing time lags. Figure 7.6 shows the estimated FRFs.

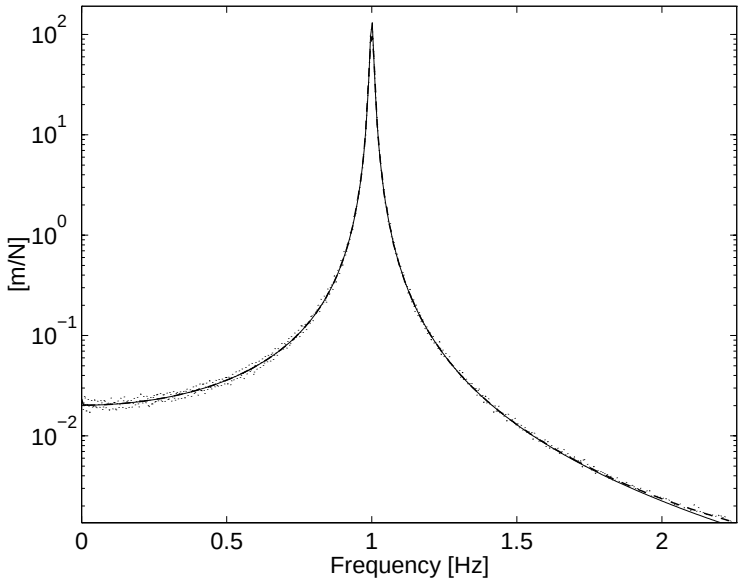

Figure 7.6: *FRFs estimated from a record length of 40000 points. [——]: Theoretical. [- - - -]: FFT Hanning window, H_1. [· · · ·]: RD-FFT, No windowing, H_1^{RD}.*

Figure 7.6 shows that the H_1^{RD} estimates become smooth with increasing record length,

even though no window is applied. Figure 7.7 shows a zoom of the FRFs in fig. 7.6 around the resonant frequency.

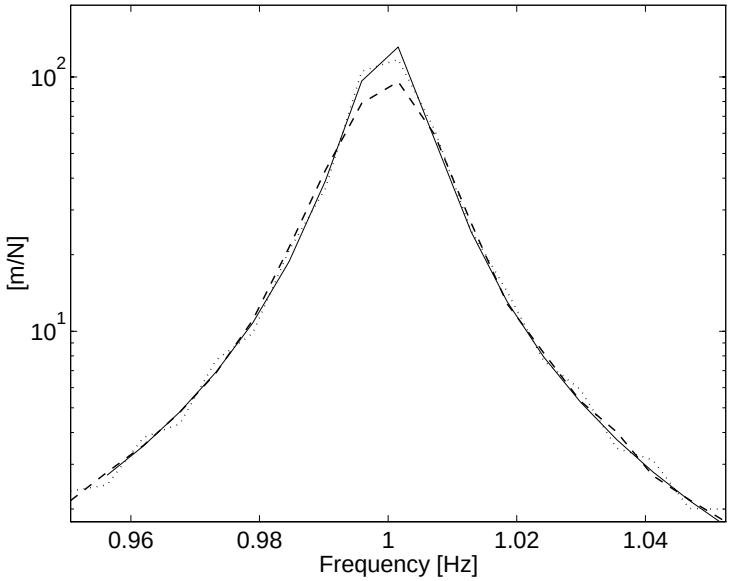

Figure 7.7: *Zoom of absolute value of the FRFs. [------]: Theoretical. [- - - -]: FFT Hanning window, H_1. [· · · · ·]: RD-FFT, No windowing, H_1^{RD}.*

The increase of the record length has increased the accuracy of the H_1^{RD} estimate, but the H_1 estimate is still biased (an increase in the length of the time segments from 1024 to 2048 would decrease the bias, but for illustration purposes this is omitted).

The estimation of the FRFs using the 5 different approaches is performed 100 times. The mean values and the standard deviations are shown in table 7.1.

	f [Hz]	σ_f	ζ [%]	σ_ζ
FFT - 10000 pts.	1.000	$1.14 \cdot 10^{-4}$	0.68	0.0054
FFT - 40000 pts.	1.000	$0.53 \cdot 10^{-4}$	0.67	0.0026
RD - 10000 pts.	1.000	$6.71 \cdot 10^{-4}$	0.59	0.0100
RD - 10000 pts., window	1.000	$4.97 \cdot 10^{-4}$	0.60	0.0073
RD - 40000 pts.	1.000	$2.69 \cdot 10^{-4}$	0.60	0.0032

Table 7.1: *Average values of the modal parameters and the corresponding standard deviations based on 100 simulations. The theoretical values are $f = 1$ Hz and ζ=0.6 %.*

The results show that all approaches provide unbiased estimates of the eigenfrequencies, but the FFT approach provides biased estimates of the damping ratio. On the other hand, the standard deviation of the estimates using the RD technique is higher than the estimates using the FFT approach. If no window function is applied and the system has low damping the ragged spectral densities will result in modal parameters affected by high random errors. The high standard deviations of the modal parameters estimated based on the RD technique is a result of the difficulties which arise in the Fourier transformation of the RD functions.

7.3.2 Experimental Study - Laboratory Bridge Model

This case study is based on a laboratory bridge model loaded by Gaussian white noise. The model consists of a simply supported steel plate with 3 spans. The steel plate has the dimensions 3.0 $\times$ 0.35 m. The length of each span is 1 m. A shaker is attached at the right-hand span. The shaker is exciting the bridge model with Gaussian white noise in the frequency span 0-60 Hz. The measurements consist of 32000 points sampled with 150 Hz. The measurements are analog and digital filtered to avoid aliasing and to suppress high frequency noise. Figure 7.8 shows an outline draft of the bridge and the sensor locations are also indicated.

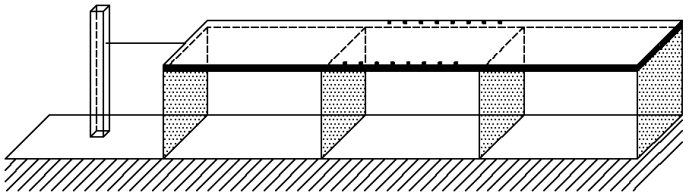

Figure 7.8: *Laboratory bridge model and sensor locations.*

The measurements are collected in 3 setups consisting of 7,7 and 6 response records in each setup and the corresponding record of the load. Two different approaches are used to estimate the FRFs of the structure. The approach based on the FFT algorithm with the H_1 estimator is used. Each time segment has a length of 1024 points and is multiplied by the Hanning window to reduce leakage errors. The second approach is based on the H_1^{RD} estimator. The positive point triggering condition is used with triggering levels chosen as $[0.5\sigma_X \ \infty]$. Each RD function has a length of 825 points. In common for both approaches is that the FRFs are transformed into IRFs using inverse FFT. The modal parameters are extracted from the IRFs using the PTD algorithm. Structural modes are separated from noise modes using the MCF, MPF and a requirement for low damping ratios as described in chapter 2. Table 7.2 shows the estimated eigenfrequencies and the corresponding damping ratios.

f [Hz] (RD)	f [Hz] (FFT)	ζ % (RD)	ζ % (FFT)
11.64	11.63	1.14	0.73
15.45	15.44	0.34	0.56
21.51	21.50	0.29	0.47
45.09	45.08	0.10	0.18
47.97	47.97	0.17	0.24
49.96	50.11	0.36	0.53
50.30	50.17	0.21	0.15
51.77	51.74	0.15	0.14
61.60	66.61	0.22	0.28
65.47	65.45	0.43	0.50

Table 7.2: *Modal parameters estimated using FFT and RD-FFT.*

There is a good agreement between the eigenfrequencies estimated using the two approaches. Only at the two closely spaced modes at about 50 Hz, there is a small disagreement. All the damping ratios are small and it seems that the damping ratios estimated using the RD approaches are generally smaller compared to the damping ratios estimated using the FFT approach. It is the experience obtained during this analysis that the modal parameters of the RD technique are far more sensitive to the choice of model order and the number of points used from the IRFs as input to the PTD algorithm. Compared to the RD technique the results of the FFT algorithm is more stable and not very sensitive to these choices.

The reason can be that the FRFs estimated using the RD technique is more ragged than the FRFs estimated using the FFT algorithm. It is very difficult to calculate the FFT of the RD functions with a satisfying result. The result is very sensitive to the number of points in the RD functions. Figures 7.9 and 7.10 show two typical FRFs estimated using the H_1^{RD} and the H_1 estimators, respectively.

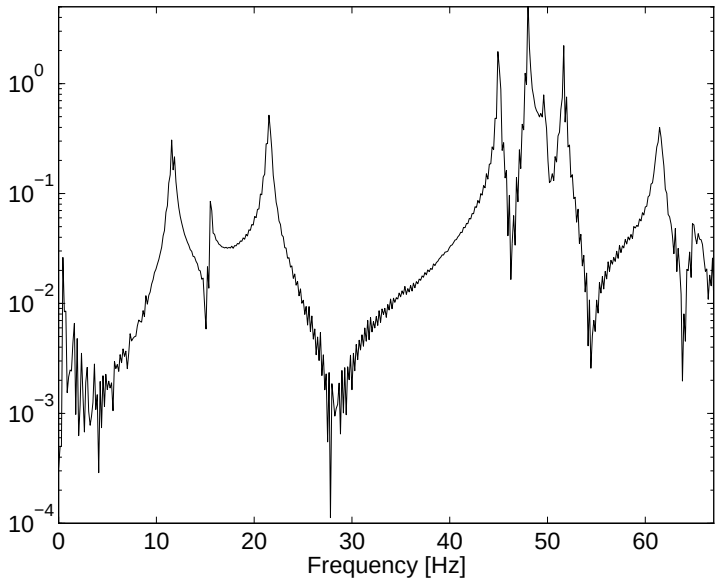

Figure 7.9: *Typical* $|H(\omega)|$ *estimated using* H_1^{RD}.

The figure illustrates that the FRFs estimated using H_1^{RD} is very ragged. Around the spikes the shape of the curve is very convincing, since the curve is smooth and it is clear that this system has low damping. The FRF shown in fig. 7.10 is on the other hand very smooth. The experience with this experimental study is that the modal parameters estimated based on the RD technique are more uncertain than the modal parameters estimated based on the FFT technique. The model order should be higher and the fluctuation of the modal parameters is also higher. This difference in the FRFs is believed to be the explanation for the high uncertainty (or higher random errors) of the modal parameters estimated using the RD technique.

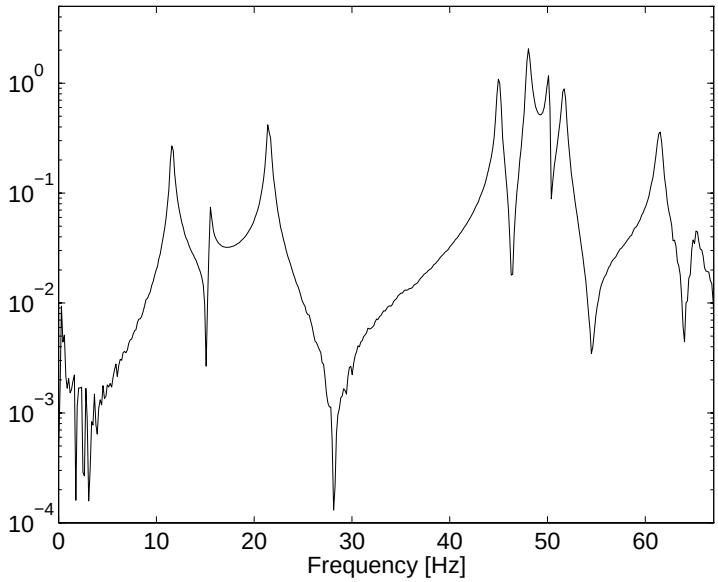

Figure 7.10: *Typical* $|H(\omega)|$ *estimated using* H_1.

The higher uncertainty of the modal parameters estimated from H_1^{RD} compared to the results from the H_1 estimator is supported by the estimated mode shapes, which are shown in figs. 7.11 - 7.15. Except for the two closely spaced modes at about 50 Hz, the absolute value of the mode shapes from the H_1 estimator is the most convincing result.

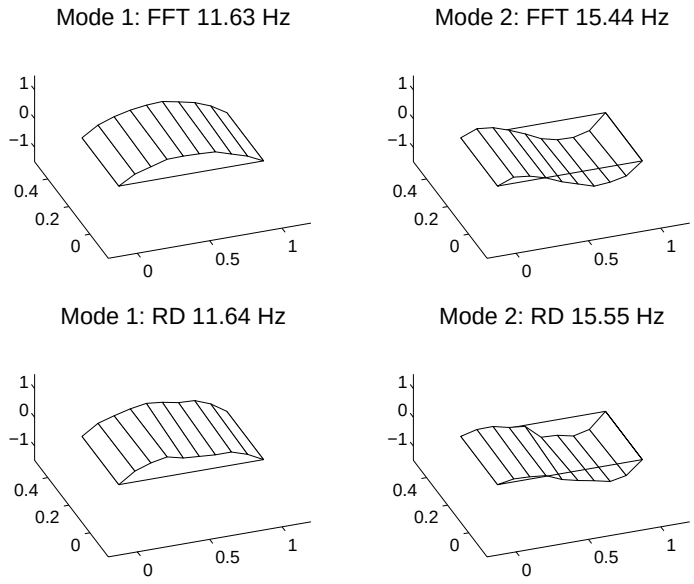

Figure 7.11: *Mode shapes 1 and 2 estimated using* H_1^{RD} *and* H_1. *MAC=0.98 and MAC=0.81, respectively.*

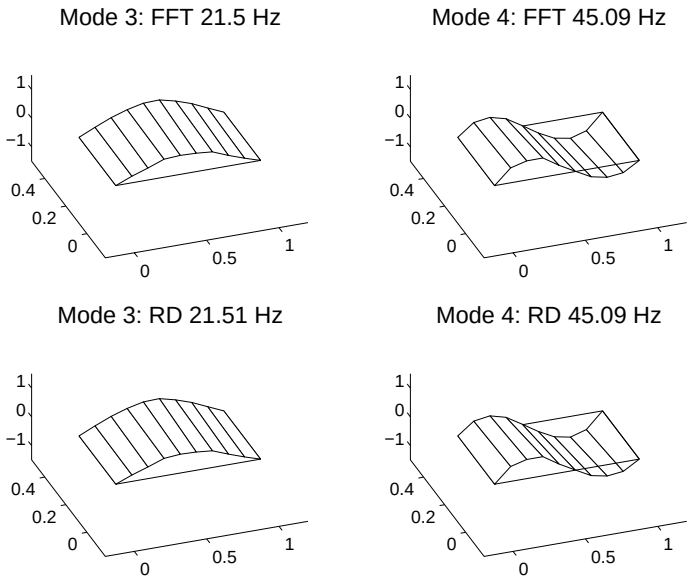

Figure 7.12: *Mode shapes 3 and 4 estimated using* H_1^{RD} *and* H_1. *MAC=1.00 and MAC=1.00, respectively.*

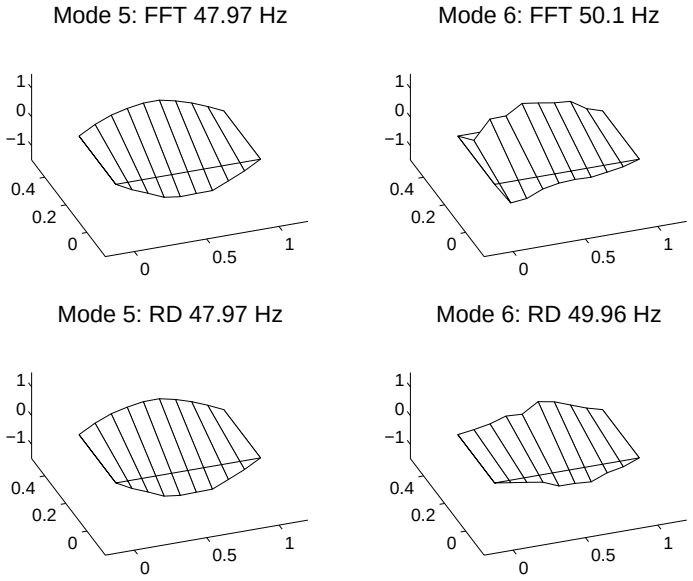

Figure 7.13: *Mode shapes 5 and 6 estimated using* H_1^{RD} *and* H_1. *MAC=1.00 and MAC=0.54, respectively.*

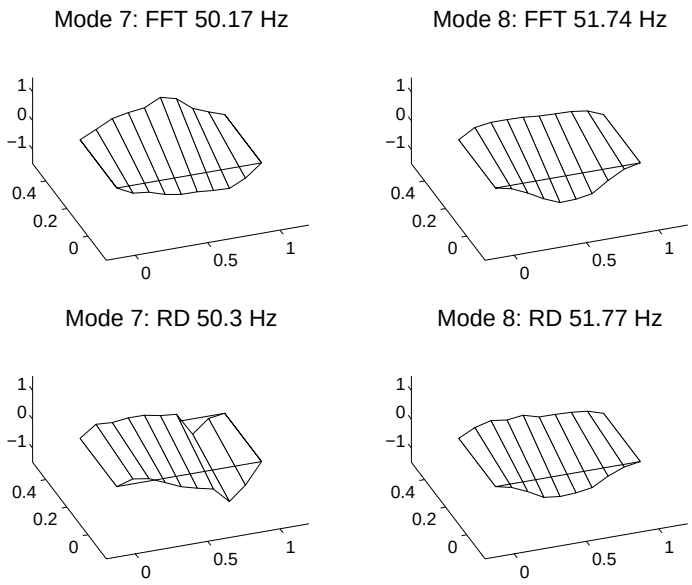

Figure 7.14: *Mode shapes 7 and 8 estimated using* H_1^{RD} *and* H_1*. MAC=0.56 and MAC=0.99, respectively.*

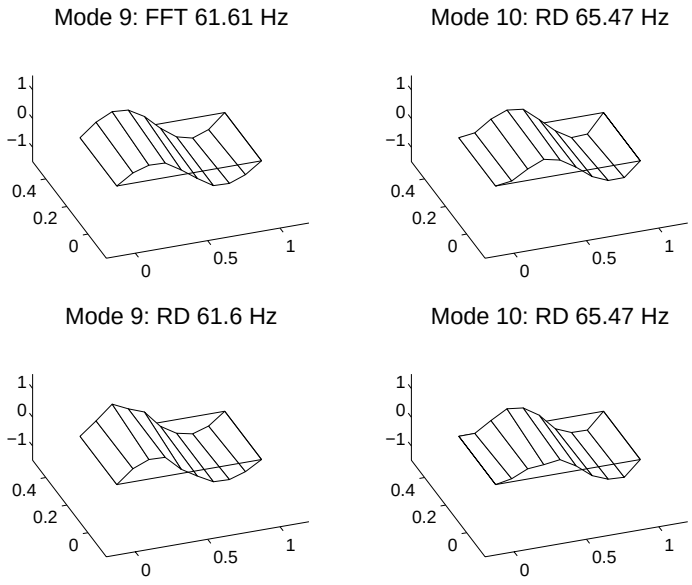

Figure 7.15: *Mode shapes 9 and 10 estimated using* H_1^{RD} *and* H_1*. MAC=0.96 and MAC=0.93, respectively.*

The MAC values show that in general there is a high correlation between the mode shapes. There is only major disagrement at the closely spaced modes. It is clear that the FFT based estimates are more convincing, since the mode shapes look very smooth.

The estimation time for the two approaches was almost equal. The reason is that the

RD functions contain relatively many points and that there is a high number of averages. 1025 points in an RD function is in general a very high number. For a system with lower damping ratios less points in the RD functions are necessary and the estimation time thereby decreases.

It is very difficult to use the RD technique for estimation of FRFs for ligthly damped systems. One of the major problems is that although the RD functions are estimated with high accuracy, it is very difficult to calculate the FRF from the RD functions. If systems with higher damping are considered, less points in the RD functions are needed. This will make the RD technique much faster than the FFT approach, and the accuracy will also increase. The RD functions are always more accurate close to the centre and the functions will dissipate towards zero more clearly if a system with higher damping is analysed.

7.4 Summary

A new method for estimating FRF based on the RD technique has been introduced. The idea is based on the fact that the RD functions of the input and output of a linear system are related, since the RD function of the response is the convolution integral of the RD function of the load and the IRF. This relation is always valid no matter what type of load has been subjected to the structure.

In this chapter it has been assumed that the load is Gaussian white noise. This means that the RD functions will dissipate to zero with increasing absolute time lags. Intuitively it will be perfect to Fourier transform the RD functions, since the restriction of finite time record length is insignificant. The influence of the load can be removed in the frequency domain using either the H_1^{RD} or H_2^{RD} estimator, both of which are based on plain division. Based on the experience with the simulation study and the analysis of the bridge model in section 7.3.2 and in Brincker et al. [1] it is recommended to use the H_1^{RD} estimator.

Compared with the traditional method based on the FFT algorithm the RD-FFT approach is not as stable. The auto and cross RD functions can be calculated with satisfactory accuracy if the guidelines given in chapter 3 are followed. It is the transformation of the RD functions into the frequency domain which creates trouble. The experience obtained in this study is that it is necessary to introduce a window function. Otherwise the FRFs will be dominated by the noise introduced with the Fourier transformation. Furthermore, the result is dependent on a proper choice of the length of the RD functions. If the RD functions contains too many points the FRFs will be dominated by noise.

The problems are particular dominant for lightly damped structures. If the damping ratio increases from $0.1\% - 1\% \rightarrow 3\% - 5\%$ the stability of the RD-FFT approach will improve, since the RD functions will dissipate faster. The result is that shorter and thereby more accurate RD functions are obtained.

Further work with this approach is recommended to focus on the relations in eqs. (7.18) and (7.19). The modal parameters can be extracted directly from these relations by using algorithms which are based on the input-output relation in the time domain. This approach would also not require that the input to the structure is white noise.

Bibliography

[1] Brincker, R. & Asmussen, J.C. *Random Decrement Based FRF Estimation.* Proc. 15th International Modal Analysis Conference, Orlando, Florida, USA, Feb. 3-6, 1997, Vol. II, pp. 1571-1576.

[2] Asmussen, J.C. & Brincker, R. *Estimation of Frequency Response Functions by Random Decrement.* Proc. 14th International Modal Analysis Conference, Dearborn, Michigan, USA, Feb. 12-15, 1996, Vol. I, pp. 246-252.

[3] Bendat, J. & Piersol, A. *Random Data: Analysis and Measurement Procedures.* John Wiley & Sons, Inc. 1986. ISBN 0-471-04000-2.

[4] Schmidt, H. *Resolution Bias Errors in Spectral Density, Frequency Response and Coherence Function Measurement, I: General Theory.* Journal of Sound and Vibration (1986) 101(3) pp. 347-362.

[5] Fabunmi, J.A. & Tasker, F.A. *Advanced Techniques for Measuring Structural Mobilities.* Journal of Vibration, Acoustics, Stress, and Reliability in Design. July 1988, Vol. 110, pp. 345-349.

[6] Yun, C.-B. & Hong, K.-S. *Improved Frequency Domain Identifications of Structures.* Structural Safety and Reliability, ICOSSAR '93, Vol. 2. 1994 Balkema, Rotterdam, ISBN 90 5410 357 4. pp. 859-865.

Chapter 8

Ambient Testing of Bridges

The main advantages of the RD technique is the low estimation time and the simple estimation algorithm. The advantage of a low estimation time can be utilized in identification of large structures, where the response of the structure is collected at many locations. In general this is the situation in ambient testing of bridges. The purpose of this chapter is to document the applicability of the RD technique for ambient testing of bridges. Ambient testing of bridges refers to measurements of the vibrations of bridges due to ambient loads such as traffic, wind, waves and micro tremors.

In ambient testing of bridges a special terminology is used. Usually the number of measurement locations is higher than the number of measurement channels available from the measurement system. The number of measurement channels available in a bridge measurement system is delimited by the number of cables available, the number of accelerometers available and the analog/digital conversion of the measurements. This means that the measurements have to be collected by applying the measurement system several times. A single set of these measurements is denoted a setup. It is necessary to have one or several measurement locations represented in each of the setups. Otherwise it is not possible to link the mode shapes estimated from the different setups together. The measurements collected at the locations, which are represented in all setups, are denoted reference measurements. In principle it is sufficient with a single reference measurement, but it is common to use two or more reference measurements. This ensures that the probability that all modes are well represented in one of the reference measurements is high.

Section 8.1 deals with identification of the Queensborough bridge from ambient vibrations. This work was a pre-investigation of the performance of the RD technique compared to other well-known techniques, such as FFT and ARMAV based approaches. The results of this study encouraged a continuation with the RD technique as a tool for analyzing ambient measurements of bridges.

In section 8.2, a laboratory bridge model is considered. The purpose of this work was to compare the speed and accuracy of the RD and the VRD technique. This study concluded the development and documentation of the VRD technique.

Ambient testing of the Vestvej bridge is reported in section 8.3. These measurements were collected using a bridge measurement system developed as a part of this Ph.D.-

project. The purpose of this work, besides testing the performance of the RD technique, is to check the bridge measurement system. The analysis is also a pre-investigation to a demonstration project of vibration based inspection using the RD technique.

8.1 Case Study 1: Queensborough Bridge

This case study presents the results of an application of the RD technique for identification of bridges. The modal parameters of the Queensborough bridge are estimated from ambient responses. The study was performed in order to obtain experience with the RD technique applied to measurements of large civil engineering structures. The ambient data have been analysed using four different techniques by different authors see Felber et al. [2] - Brincker et al. [5]. The four different approaches are.

- FFT - Spectral densities estimated using FFT, see Felber et al. [2].
- ARMAV - Auto Regressive Moving Average models, see Giorcelli et al. [3].
- TFD - Time-Frequency Domain models, see De Stefano et al. [4].
- RD - Random Decrement technique, see Asmussen et al. [6].

The results of the different approaches were discussed and compared at a single session at the 14th International Modal Analysis Conference. The first analysis of the data was presented in Ventura et al. [1]. The data analysis methodology, which constitutes the basis for the RD technique is described in the next section. The data analysis methodology used for the other approaches and their background can be seen in the corresponding papers.

The Queensborough bridge crosses the Fraser river near Vancouver B.C. Canada. The bridge has a length of 200 m and has 3 spans. A typical cross-section and an outline draft of the bridge are shown in figures 8.1 and 8.2. The illustrations are taken from Ventura et al. [1]. and Felber et al. [2].

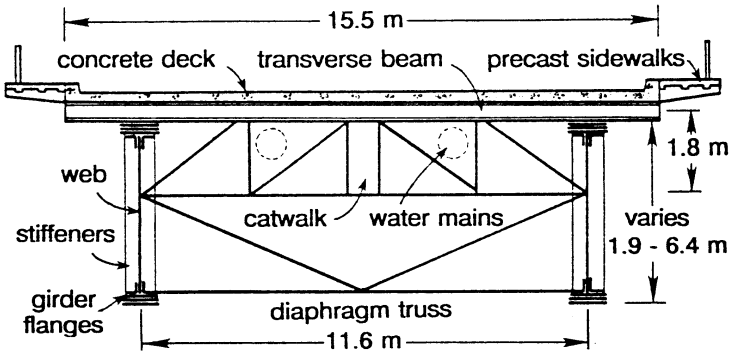

Figure 8.1: *Outline draft of the cross-section of the Queensborough bridge.*

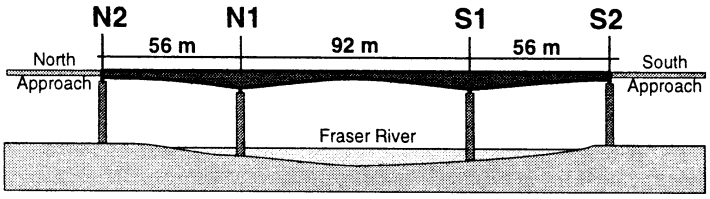

Figure 8.2: *Outline draft of the Queensborough bridge.*

During the measurement period the bridge was mainly loaded by the traffic on the bridge. The vibrations of the bridge were collected using 8 accelerometers at 46 locations on the bridge (including supports). The locations are chosen at equidistant distances on both sides of the bridge. The data are collected in 7 setups with 8 measurements in each setup and a single setup with 4 measurements. Each setup contains the response at two reference locations. This makes it possible to assemble the mode shapes from the different setups by normalizing the mode shapes with one of the reference location components. The data are filtered analogously before sampling at 40 Hz and 32000 points are collected at each locations. A description of the test equipment is given in Ventura et al. [1].

8.1.1 Data Analysis Methodology

An ambient vibration study of a large civil engineering structure usually starts with a pre-analysis of the data. The purpose is to have an idea about the number of modes represented in the data and the noise contents etc. One of the most frequently applied approaches is to average the spectral densities of all the measurements. This will give an idea about the frequencies of the modes and the average contribution from each mode to the measured response. Such an analysis is omitted, since a full analysis of the data has already been presented in Ventura et al. [1].

It is chosen to use the positive point triggering condition. This condition makes it possible to obtain sufficient triggering points for an accurate estimate of the RD functions. In order to investigate the influence of the triggering level 4 different conditions are formulated.

$$T^{P,1}_{X(t)} = \{1 \cdot \sigma_X < x(t) < 2 \cdot \sigma_X\} \qquad T^{P,2}_{X(t)} = \{2 \cdot \sigma_X < x(t) < 3 \cdot \sigma_X\} \tag{8.1}$$

$$T^{P,3}_{X(t)} = \{3 \cdot \sigma_X < x(t) < 4 \cdot \sigma_X\} \qquad T^{P,4}_{X(t)} = \{4 \cdot \sigma_X < x(t) < 5 \cdot \sigma_X\} \tag{8.2}$$

The auto RD functions are calculated from one of the reference measurements. The 4 different RD functions which have been normalized at the zero time lag are shown in figure 8.3. The number of triggering points for the four triggering levels was approximately 2000, 600, 300 and 50. There is no significant difference between the 4 RD functions, except for $T^{P,4}_{X(t)}$ which simply produces to few triggering points. The accuracy of the RD functions increases with the number of triggering points. If noise is present in the triggering measurement it will introduce false triggering points, especially at small triggering levels. To avoid these false triggering points and to have a reasonable estimation time the triggering bounds are chosen as $[a_1\ a_2] = [3\sigma_X\ 4\sigma_X]$.

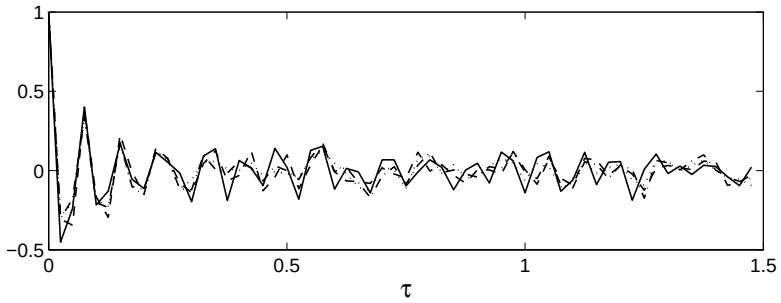

Figure 8.3: *4 different auto RD functions. [· · · ·]: [a_1 a_2]=[σ_X $2\sigma_X$]. [– · – · –]: [a_1 a_2]=[$2\sigma_X$ $3\sigma_X$]. [– – ––]: [a_1 a_2]=[$3\sigma_X$ $4\sigma_X$]. [———]: [a_1 a_2]=[$4\sigma_X$ $5\sigma_X$].*

All RD functions are estimated in each setup, which corresponds to estimating the full correlation matrix. The RD functions are only estimated for positive time lags. The modal parameters are extracted using ITD.

8.1.2 Results

In order to extract the modal parameters from the RD functions the ITD technique is used to extract modal parameters from each of the set of RD functions. The number of sets of RD functions is equal to the number of measurements collected. Figure 8.4 shows the estimated eigenfrequencies as a function of the identification number. It was assumed that 64 modes were sufficient to model both physical and computational modes. Only the modes with $\angle MCF < 10\,\text{deg}$ and $|MCF| > 90\%$ and damping ratios $< 10\ \%$ are selected.

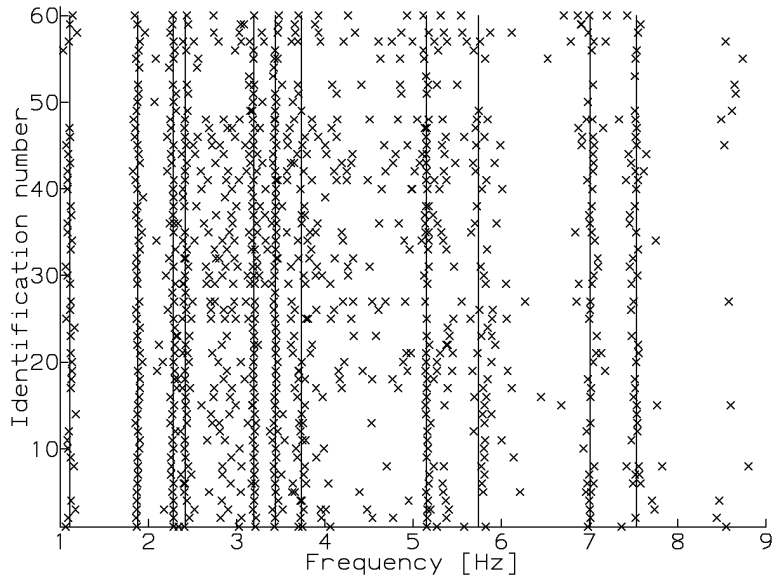

Figure 8.4: *Stabilization diagram with estimated natural frequencies from identification of different RD setups.*

The selected modes are indicated with a vertical line. The estimated eigenfrequencies and damping ratios, reported in Felber et al. [2] - Brincker et al. [5], are shown in table 8.1.

Mode	FFT	ARMAV	TFD	RD	TFD	RD
	F [Hz]	F [Hz]	F [Hz]	F [Hz]	ζ [%]	ζ [%]
1^t	1.11	1.12	1.10	1.10	1.94	7.36
2^t	1.87	1.87	1.87	1.88	0.87	1.45
3^r	2.28	2.29	2.28	2.28	0.49	1.86
4^t	2.42	2.42	2.42	2.42	0.84	2.15
5^r	3.20	3.20	3.20	3.20	0.78	1.51
6^r	3.43	3.43	3.45	3.44	0.58	1.08
7^t	3.71	3.70	3.74	3.73	1.40	1.68
8^r	5.16	5.15	5.16	5.15	0.25	0.64
9^t	5.33	-	-	-	-	-
10^t	5.80	5.78	5.84	5.74	0.96	1.15
11^t	7.01	7.04	7.12	7.01	0.65	0.77
12^t	7.52	7.52	7.52	7.53	0.82	0.69
13^t	8.59	8.56	8.64	-	0.32	-

Table 8.1: *Natural frequencies and damping ratios of the Queensborough bridge estimated using different approaches. Superscript t=translational mode and superscript r=rotational modes.*

Table 8.1 illustrates that there is good agreement between the eigenfrequencies and the damping ratios estimated using the different approaches. For the approaches based on FFT and ARMAV-models the estimated damping ratios have not been reported. It is interesting to note that only the FFT based approach identifies a strucutural mode at 5.33 Hz. The explanation could be that the measurements at opposite positions of the bridge have been subtracted and added in order to separate translational and rotational modes for the results of the FFT analysis. This data analysis strategy has not been applied in the analysis using the other approaches. The argument is that it is not correct to assume all modes to be either translational or rotational. Usually, the modes will contain contributions from both a translational and a rotational part.

The first rotational mode shape and the second translational mode shape are shown in figure 8.5. The mode shape components are almost in or out of phase.

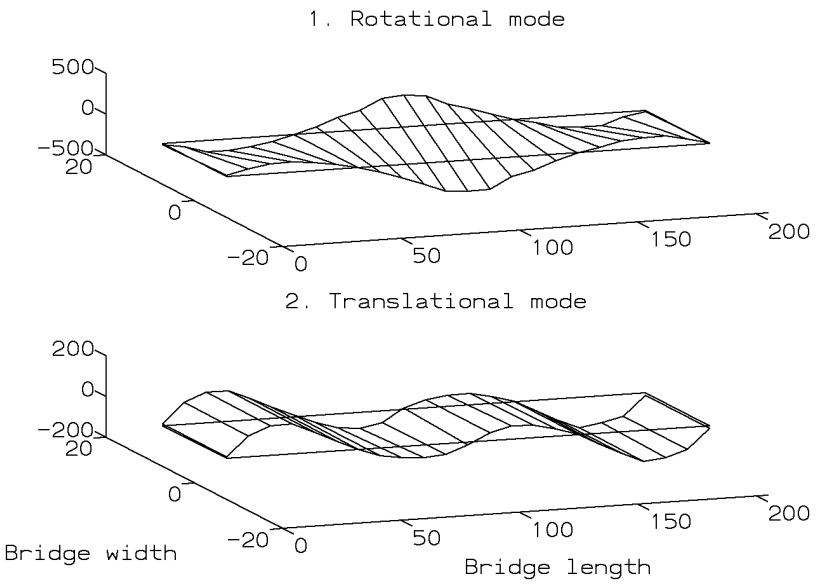

Figure 8.5: *First rotational mode (2.28 Hz) and second translational mode (1.88 Hz).*

The estimated mode shapes indicate that the identification of the modal parameters using the RD technique in combination with ITD seem to have been succesful.

8.1.3 Conclusion

The results of this introductory application of the RD technique for ambient testing of bridges encouraged continued investigations. It was possible to identify modal parameters with a satisfactory accuracy compared to the results of the other techniques. One of the reasons for this conclusion is that the accuracy of the RD technique can be improved. The following improvements are recommended.

- Estimate RD functions with both positive and negative time lags. This opens an opportunity for averaging and quality assessment of the RD functions.
- Shift the sign of the time series to obtain the maximum number of triggering points for the chosen triggering levels.
- Use broader triggering levels, e.g. $[a_1\ a_2] = [\sigma_X\ \infty]$ to obtain more triggering points.

8.2 Case Study 2: Laboratory Bridge Model

The purpose of this case study is to make the final development and documentation of the VRD technique. The case study is based on the response of a laboratory bridge model loaded by Gaussian white noise. The bridge model is a 3-span simply supported 0.01 m thick steel plate with a total length of 3 m and a width of 0.35 m. Figure 8.6 illustrates the laboratory bridge model (The bridge model is basically the same as the model analysed in chapter 3).

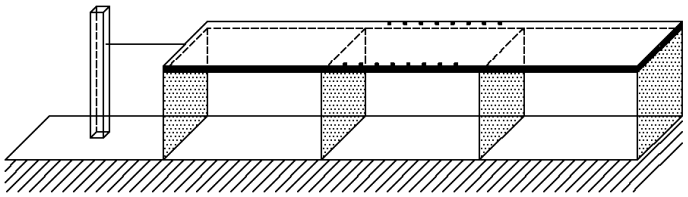

Figure 8.6: *Laboratory bridge model and sensor locations.*

The bridge is excited by a shaker attached at the right-hand span. Only identification of the mid span is considered. The 16 different locations of the accelerometers at the mid span are indicated in figure 8.6. The acceleration responses of the bridge are collected at a sampling rate of 150 Hz. The white noise load excites the structure in the frequency range 0-60 Hz. The acceleration response is filtered analogously and digitally after sampling. Each measurement consists of 32000 points corresponding to a sampling period of approximately 3.5 minutes. The measurements are collected using three setups with 7, 7 and 6 measurements in each setup, since two reference points are used.

8.2.1 Data Analysis Methodology

The data have been analysed using the traditional RD technique and the VRD technique. In the following the approaches for both method are discussed. Figure 8.7 shows a typical acceleration record of the bridge.

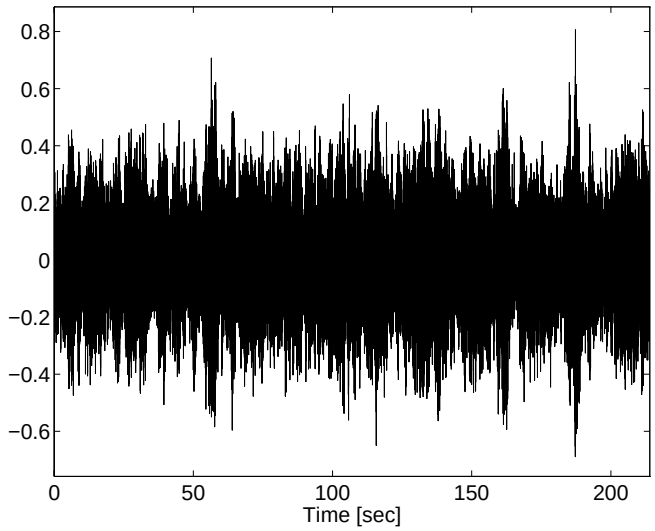

Figure 8.7: *Typical acceleration record from the laboratory bridge model.*

For the RD technique the positive point triggering condition has been chosen, since this condition ensures that sufficient triggering points can be obtained. The triggering levels are chosen as $[a_1\ a_2] = [0.5\sigma_X\ \infty]$. Any triggering point between 0 and $0.5\sigma_X$ is omitted to avoid false triggering points. This level is expected to be dominated by noise. Figure

8.8 shows a typical auto RD function, where the average function and the error function have been calculated using the symmetry relation as described in chapter 3.

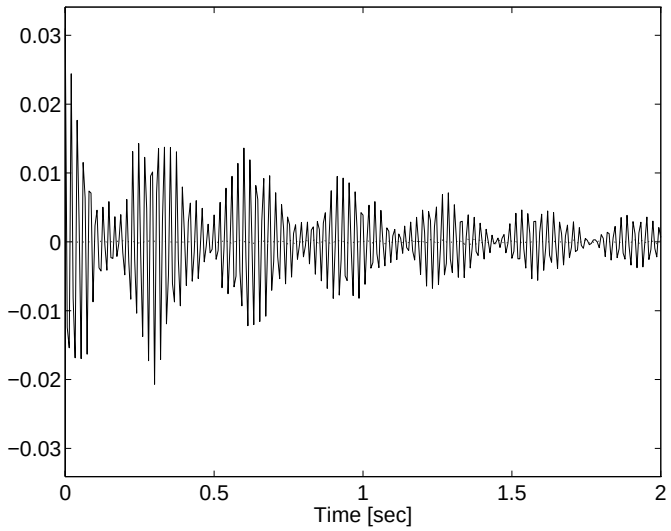

Figure 8.8: *Average and error RD function calculated by the symmetry relations. The error RD function is the curve fluctuating around zero.*

There are 301 points in the average RD and error RD functions in fig. 8.8. From fig. 8.8 it is concluded that for all 301 points it seems as if the error RD function is so small that all points can be used in the modal parameter extraction procedure if necessary. The number of triggering points was approximately 5000.

All RD functions are calculated for each setup corresponding to estimating the full correlation matrix. The average and the error RD functions are estimated using the symmetry relations. The problem is if all sets of RD functions (columns in the correlation matrix) should be used in the modal parameter extraction procedure. In order to investigate this problem the approach suggested in section 3.7. is used. For each RD function an error measure is calculated as the standard deviation of the error RD function divided by the standard deviation of the average RD function, see eq. (3.64). The result from this analysis from the setup containing six measurements is shown in fig. 8.9. The record number indicates the measurement number where the RD functions are calculated from and the reference number indicates the triggering measurement.

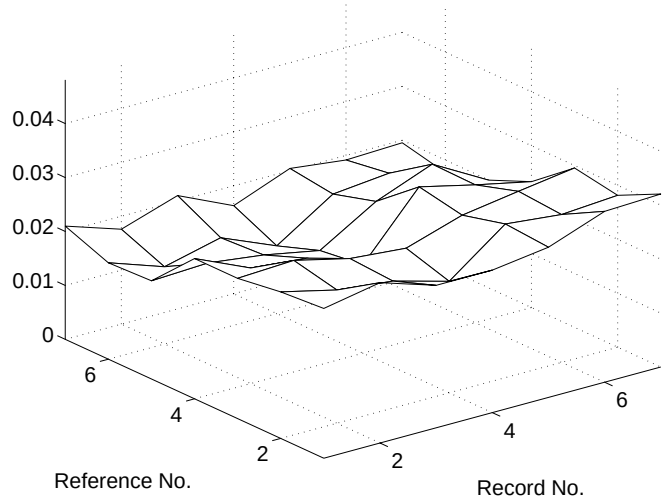

Figure 8.9: *Fraction between the standard deviation of the error and average RD function calculated by the symmetry relations and 301 points in each function.*

All fractions are small and there is no significant difference between the fractions so all sets of RD functions can be used in the modal parameter extraction procedure.

To illustrate the principle in a modal parameter extraction procedure the 3 full correlation matrices, estimated using the RD technique as described above, are considered. The PTD technique is used and for each setup the number of modes is varied from 26 to 28 and the number of points used from the RD functions is varied from 140 - 180. Figure 8.10 shows a stabilization diagram of the estimated frequencies without applying any restriction to the results except that the eigenvalues should have a complex conjugate.

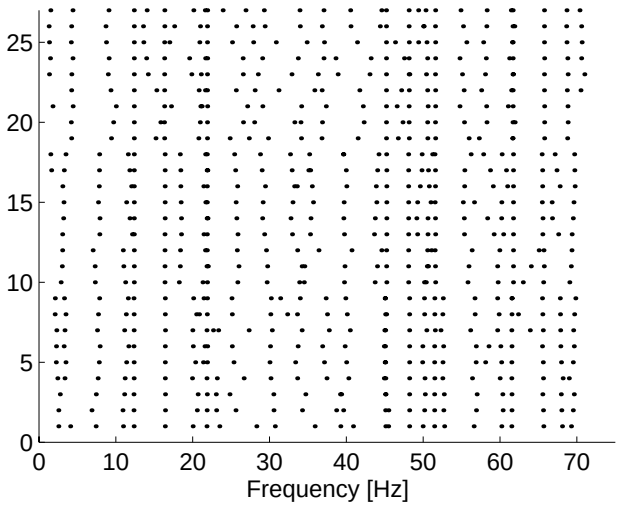

Figure 8.10: *Stabilization diagram.*

The following restrictions are applied to the different modes: $\zeta < 0.05$, $|MCF| > 0.9$ and $\angle MCF < 10°$. This results in the following stabilization diagram

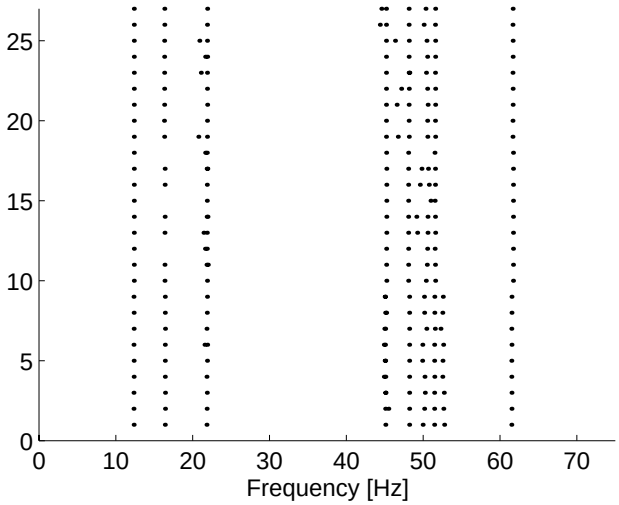

Figure 8.11: *Stabilization diagram.*

As seen it is much simpler to detect structural modes from fig. 8.11 compared to the stabilization diagram shown in fig. 8.10. This illustrates the advantage of applying different

mode selection criteria. The final resulting modal parameters are shown in section 8.2.2.

In order to apply the VRD technique, the time shifts between the elements of the vector triggering condition should be chosen. As an example, the setup with 6 measurements is considered. Figure 8.12 shows the initial estimate of the RD functions using level crossing triggering condition. The triggering level is $1.4\sigma_X$.

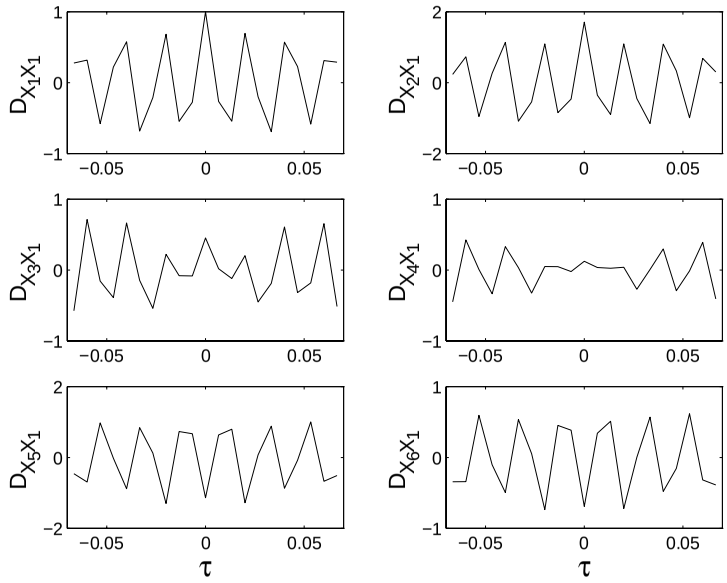

Figure 8.12: *Initial RD functions for selection of vector triggering time delays.*

The correlation is maximized by choosing the time vector as $t = [0\ 0\ 0.06\ 0.0533\ 0.0533]$ seconds, or if the number of time lags is considered $t = [0\ 0\ 9\ 9\ 8\ 8]$. A time shift vector chosen as $t = [0\ 0\ 9\ 9\ -3\ -3]$ would also have maximized the correlation.

The size of the vector triggering condition does not have to be equal to the number of measurements. Table 8.2 shows the actual number of triggering points as a function of the size of the vector triggering condition. The elements of the triggering levels are all chosen as $[a_1^i\ a_2^i] = [0.5\sigma_{X_i}\ \infty]$ in order to omit false triggering points introduced in the area $[0\ 0.5\sigma_{X_i}]$.

Size	1	2	3	4	5	6
N	9900	8200	4600	4200	2600	2400

Table 8.2: *Size of vector triggering condition and the corresponding number of triggering points.*

The number of triggering points decreases with the size of the vector triggering condition. About 2000 triggering points are sufficient for a reasonable convergence in the averaging process. So the vector triggering condition is chosen to be maximum size, which corresponds to the number of measurements in each setup. For each setup a single set of VRD functions is calculated. In order to calculate an error function for the VRD functions the sign of the triggering levels is shifted and the VRD functions are estimated again. A typical average and a typical error VRD function are shown in fig. 8.13.

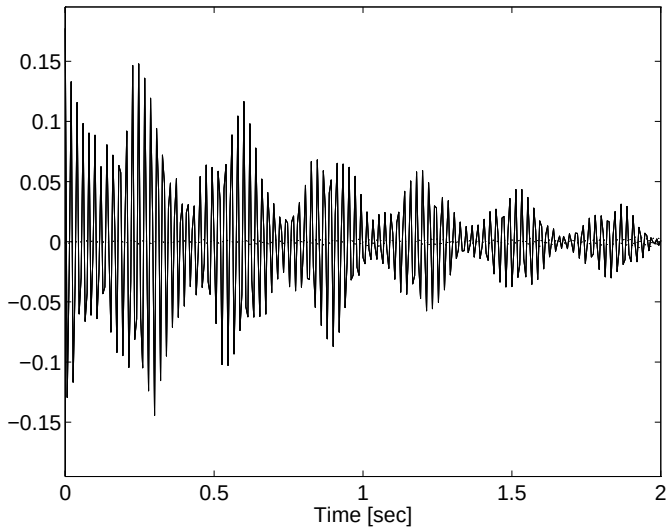

Figure 8.13: *Average and error VRD function calculated by the shifting sign of triggering levels (301 points).*

The error VRD functions are seen to be small compared to the average VRD function. But it is also clear that the significance of the error function increases with the number of time lags. It is not recommended to use all 300 points in the modal parameter extraction procedure. The number of points used should not exceed 150.

The modal parameters are extracted from the VRD functions using the same approach as described for the RD technique. The final results are presented in section 8.2.2.

8.2.2 Results

The modal parameters are extracted from the VRD and the RD functions using PTD. A stabilization diagram used with restrictions on the damping ratios ($\zeta < 10\%$) and the MCF (magnitude $> 90\%$, phase $< 10\,\text{deg}$) are used to select the structural modes from the computational modes. Table 8.3 shows the estimated modal parameters for the two approaches.

Approach	Parameter	1	2	3	4	5	6	7	8
RD_A^P	f [Hz]	12.31	16.31	21.72	45.14	48.11	49.91	51.53	61.60
VRD	f [Hz]	12.39	16.54	21.89	45.14	48.11	50.09	51.46	61.60
RD_A^P	ζ [%]	1.90	3.65	1.51	0.22	0.34	0.67	0.54	0.47
VRD	ζ [%]	1.82	4.80	1.54	0.22	0.36	0.47	0.47	0.24

Table 8.3: *Estimated natural eigenfrequencies and damping ratios for the laboratory bridge model.*

From table 8.3 it is seen that there is a high correlation between the estimated modal parameters, even for the damping ratios. The mode shapes are shown in figs. 8.14 - 8.17.

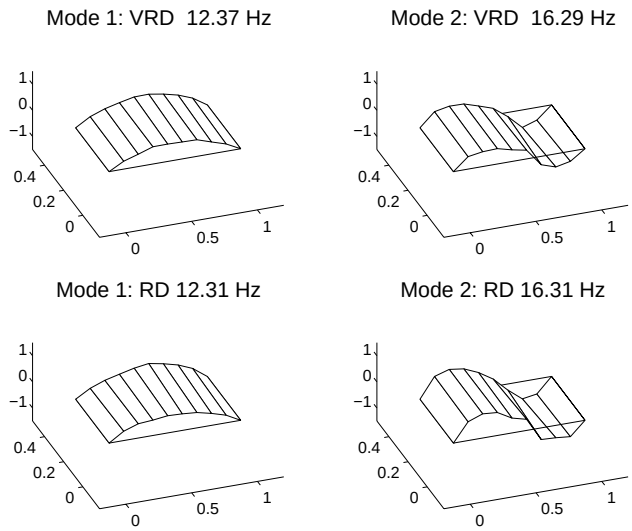

Figure 8.14: *First and second mode shape estimated using RD and VRD. MAC=0.99 and 0.54, respectively.*

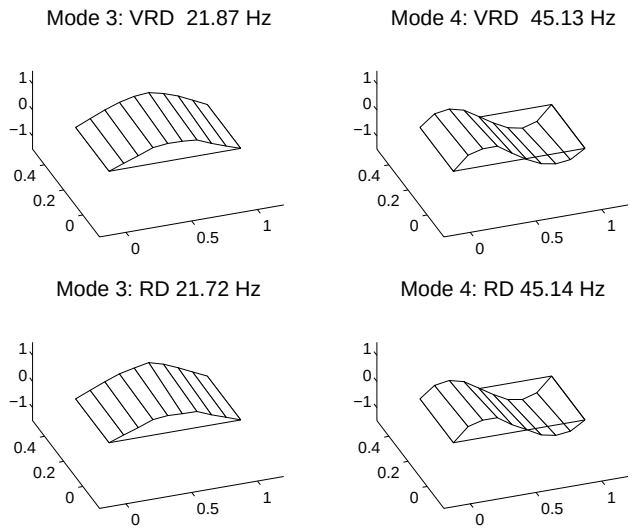

Figure 8.15: *Third and fourth mode shape estimated using RD and VRD. MAC=0.99 and 0.99, respectively.*

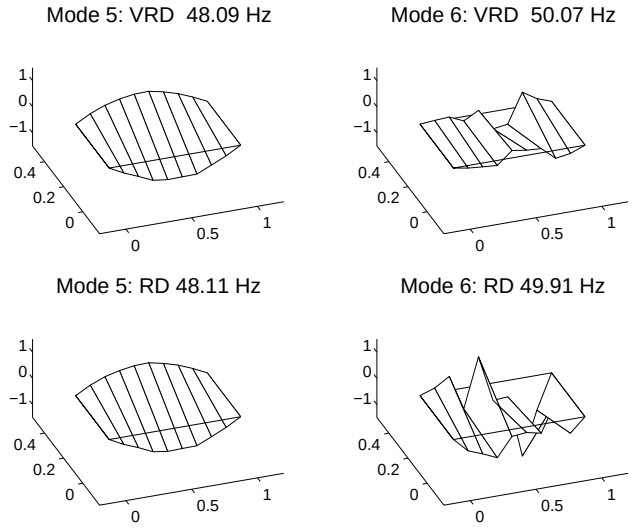

Figure 8.16: *Seventh and sixth mode shape estimated using RD and VRD. MAC=0.99 and 0.10, respectively.*

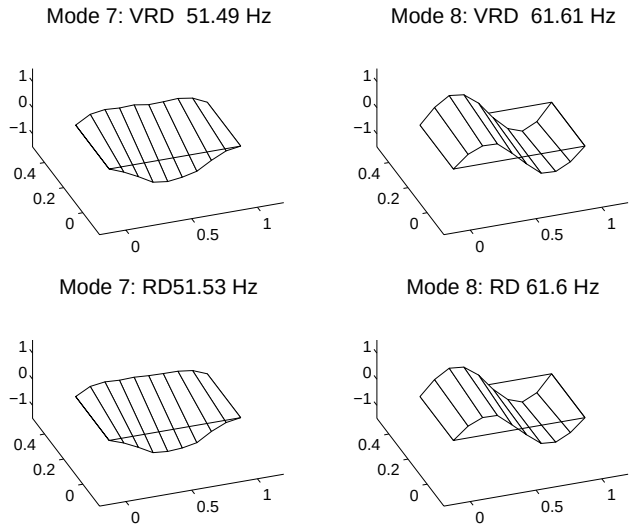

Figure 8.17: *Seventh and eigth mode shape estimated using RD and VRD. MAC=0.99 and 1.00, respectively.*

There is a high correlation between the mode shapes except for the mode at about 50 Hz. The explanation is that there is two closely spaced modes which only are excited weakly. It is not possible to obtain reasonable estimates of these modes with the RD or VRD technique from the available measurements of the response only.

8.2.3 Conclusions

The estimation time for the RD technique and the VRD technique including the estimation time for the initial RD functions is shown in table 8.4.

Method	RD	VRD	Initial
Time	565	120	5
N	8700	1700	1700

Table 8.4: *Estimation Time (CPU-time [sec]) and number of triggering points (average), N*

The initial estimation of the RD technique, used for selection of the time shift vector is seen to be extremely fast.

The application of the VRD technique is justified through an analysis of the acceleration response of a laboratory bridge model. The analysis resulted in a high correlation between the modal parameters estimated from RD and VRD functions. An approach to estimate the optimal time shifts for the formulation of the vector triggering condition is illustrated. The advantage of the VRD technique is illustrated through a 5 time reduction of the computational time.

8.3 Case Study 3: Vestvej Bridge

The ambient vibration study of the Vestvej bridge forms the initial part of a demonstration project concerning the application of vibration based inspection to bridges. The Vestvej bridge is shown in fig. 8.18.

Figure 8.18: *The Vestvej bridge.*

The aim of the project is to perform a continuous on-the-line surveyance of the bridge using the RD technique. The RD technique is capable of handling large data quantities, since it transforms the response into short data segments, correlation functions. In order to obtain information about the modal parameters of the bridge, ambient vibration tests

are carried out. The tests are described in this section. The ambient vibrations have been collected on 25/03 1997 and 04/06 1997. In this section the analysis of the data collected on 04/06 1997 is described in detail, whereas only some of the results of the data analysis of the data collected the 25/03 1997 are presented. The analysis are also reported in Asmussen et al. [9], [10] and summarized in [11].

8.4 Bridge Description

The Vestvej bridge is crossing the highway from Aalborg to Frederikshavn between Vodskov and Langholt just north of Aalborg, Denmark. The main geometry of the bridge is shown in fig. 8.19. The western 2/3 of the bridge was erected in 1986 and the remaining 1/3 in 1996. The bridge deck is made of post-tensioned concrete.

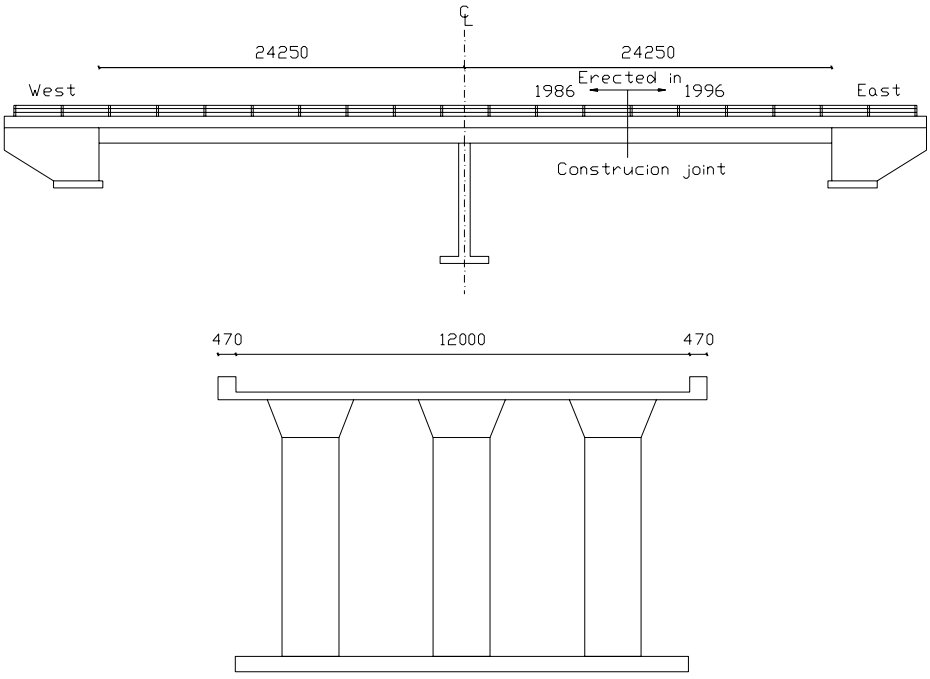

Figure 8.19: *The Vestvej bridge.*

The bridge is mainly loaded by the vehicles on the bridge. But also the vehicles passing under the bridge on the highway can contribute to the vibrations of the bridge. Furthermore, wind can generate vibrations of the bridge. Since all these forces are unmeasurable and ambient the vibration study is denoted ambient.

8.5 Measurement Setup

The acceleration response of the bridge is measured using STDI-BMS (Structural Time Domain Identification - Bridge Measurement System) currently developed as a part of this Ph.D.-project at Aalborg University. The measurement system is an 8 channel system, which means that the bridge response can be recorded, A/D-converted and saved to disk

from 8 channels or measurement location simultaneously. In order to measure the vibrations of the bridge at more than 8 locations and still preserve the possibility of estimating mode shapes, several setups with two reference locations, for the purpose of safety and flexibility, are collected. The chosen measurement locations and the reference locations are seen in fig. 8.20. Only 7 accelerometers are available at the moment so each setup contains 7 measurements. The accelerometers are Schaewitz type at 20V/g, full range of $\pm$ 0.25 g and secured in watertight steel boxes.

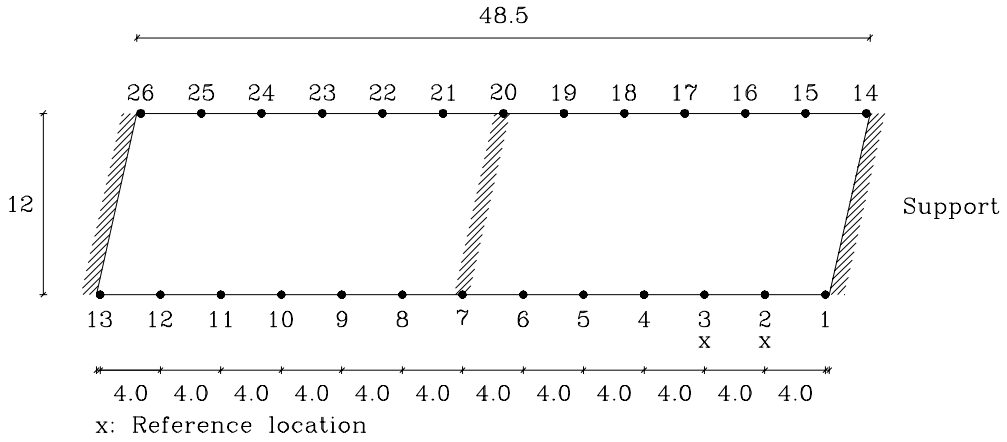

Figure 8.20: *Outline draft of the Vestvej bridge and the measurement locations.*

Since 26 measurement locations are chosen 5 different setups with data are collected. The number of the accelerometer (internal AU number) and the corresponding channel can be seen in table 8.5. Furthermore, the measurement locations defined in fig. 8.20 are linked to the different setups.

Acc.	Setup	1	2	3	4	5
No.	Channel	LB	LB	LB	LB	LB
7214	1	2	2	2	2	2
7706	2	3	3	3	3	3
9967	3	14	15	16	1	1
9969	4	25	23	21	19	17
10354	5	26	24	22	20	18
10355	6	12	10	8	6	4
14838	7	13	11	9	7	5

Table 8.5: *Setup and measurement location overview. LB=Location Bridge, see fig. 8.20.*

The measurements were sampled at 160 Hz for 900 seconds. The data were detrended and decimated twice (this includes lowpass digital filtering) before saved to disk. The resulting sampling frequency is thereby reduced to 80 Hz and the number of points in each measurement is 72000. Detrending removes any linear trend from the data and decimation reduces the sampling frequency and suppresses the noise in the records.

Figures 8.21 and 8.22 show the data collection equipment and data acquisition equipment

on site, respectively.

Figure 8.21: *Data collection equipment on site.*

Figure 8.22: *Data acquisition equipment on site.*

Figure 8.23 shows a typical acceleration record from the Vestvej bridge collected on 04/06 1997.

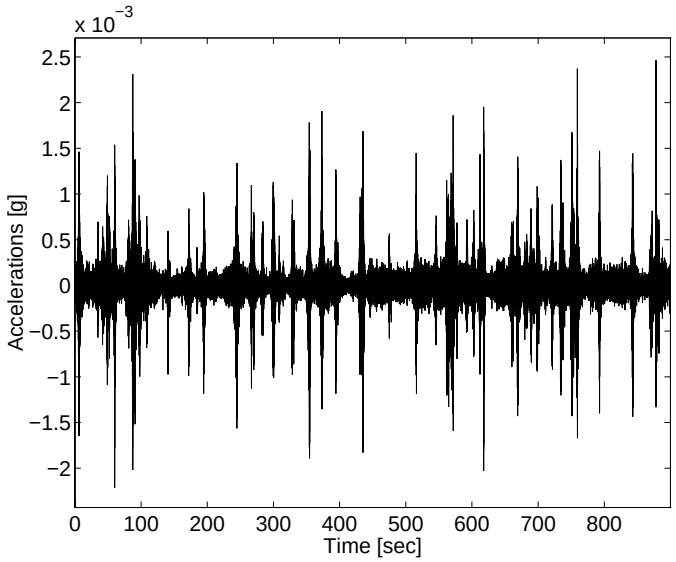

Figure 8.23: *Typical acceleration record from the Vestvej bridge.*

8.5.1 Data Analysis Methodology

The RD technique is applied for the analysis of the acceleration measurements. The data have a high noise content as seen in fig. 8.23. The reason is that only a few vehicles are crossing the bridge during the 900 second record period. This means that the accelerations are mainly due to the wind and the vechicles passing under the bridge. Furthermore, long cabling is used (20m-100m) and the sensitivity of the accelerometers is high compared to the small accelerations of the concrete bridge, see fig. 8.23. This makes the analysis of the data challenging.

Due to the high contents of noise it is chosen to use the positive point triggering condition, so that sufficient triggering points are available. On the other hand, using triggering bounds close to zero might introduce false triggering points, which will increase the uncertainty of the RD functions. The triggering levels should fulfil these three conditions:

- No false triggering points should be introduced.
- The number of triggering points should be sufficient to average out the contribution from the noise.
- The number of triggering points should be restricted so that the estimation time is reasonable.

Two different sets of triggering bounds are investigated: $[a_1\ a_2] = [0\ 1.5\sigma_X]$ and $[a_1\ a_2] = [1.5\sigma_X\ \infty]$. The auto RD function is calculated from one of the reference measurements. The number of triggering points was 33200 and 2780 and the estimation times in CPU were 2.69 and 0.44, respectively. As expected $[a_1\ a_2] = [1.5\sigma_X\ \infty]$ has the lowest number of triggering points and is thereby fastest. In order to evaluate the different estimates the symmetry relation is used to calculate the error and the average estimate of the auto

correlation function. The result for the triggering bounds $[a_1\ a_2] = [0\ 1.5\sigma_X]$ is shown in fig. (8.24) and the result for the triggering bounds $[a_1\ a_2] = [1.5\sigma_X\ \infty]$ is shown in fig. (8.25).

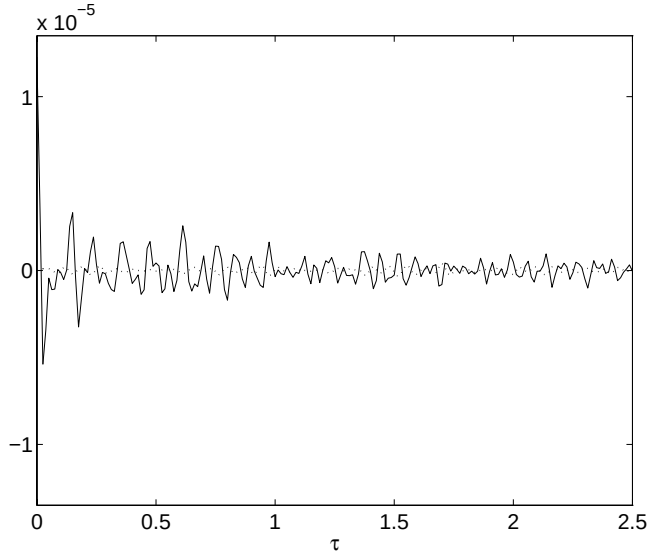

Figure 8.24: *The average and error estimate of an auto correlation function using* $[a_1\ a_2] = [0\ 1.5\sigma_X]$.

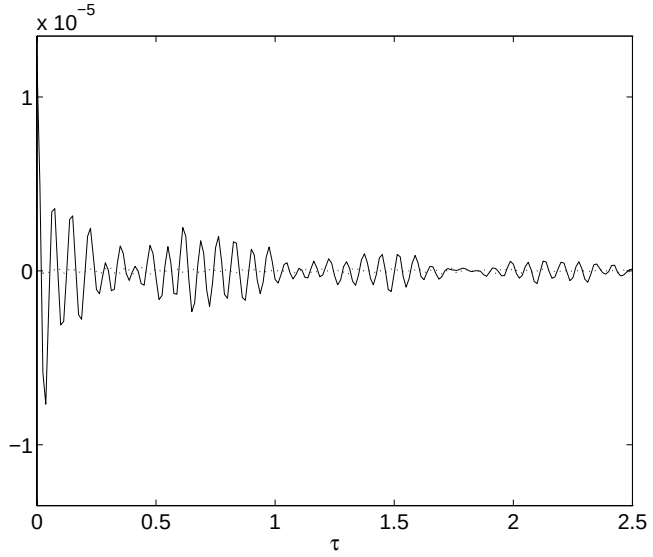

Figure 8.25: *The average and error estimate of an auto correlation function using* $[a_1\ a_2] = [1.5\sigma_X\ \infty]$.

The difference is significant and the error function shows that although there are only 0.1 times as many triggering points using $[a_1\ a_2] = [1.5\sigma_X\ \infty]$ the estimate is far more accurate. This is positive, since the most accurate approach is thereby also the fastest

approach. So the triggering levels are chosen as $[a_1\ a_2] = [1.5\sigma_X\ \infty]$.

For each of the five setups the full correlation matrix is estimated using the positive point triggering condition. After the estimation of the RD functions and before the modal parameters are extracted it is common in ambient testing of bridges to perform some kind of pre-analysis to have an idea about the number of structural modes present in the measurements. Such an analysis is developed for ambient testing based on FFT estimated spectral densities. The method is denoted Average Spectral Densities (ASD) and the idea is simply to average the spectral densities of all measurements. The ASD will strongly indicate the number of modes and the corresponding frequencies. Figure 8.26 shows the ASD calculated using FFT of the measurements.

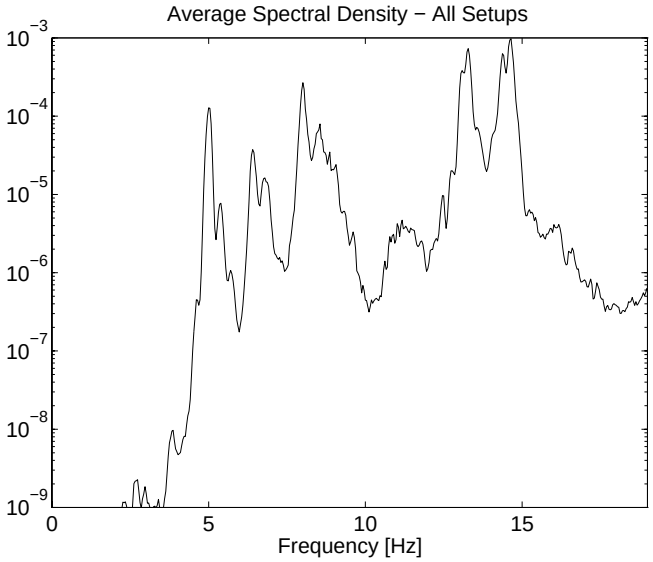

Figure 8.26: *The ASD calculated from the spectral densities of the measurements.*

The idea behind this approach is adapted to the RD technique. Instead of averaging the spectral densities of the measurements, the Fourier transform of the estimated RD functions are calculated and averaged. The estimates of the RD based ASD are shown in fig. 8.27.

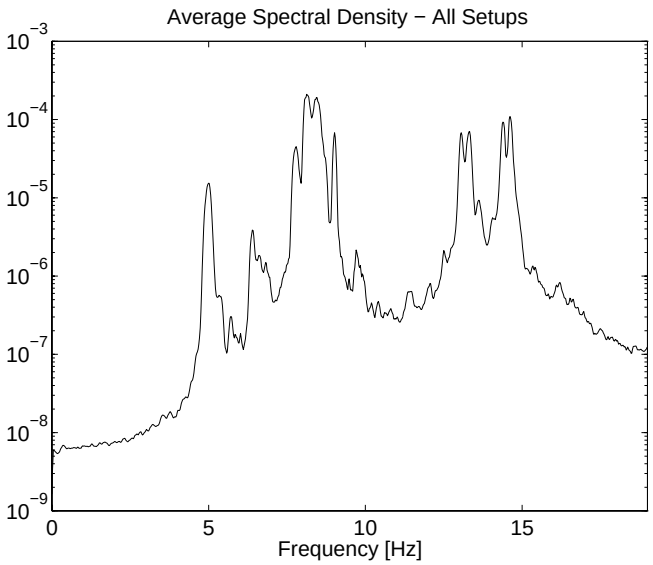

Figure 8.27: *The ASD calculated from the FFT of the RD functions of the measurements.*

From fig. 8.27 the structural modes with the following frequencies are detected.

5.00	6.40	6.62	6.81	7.80	8.13
8.44	9.02	13.06	13.37	14.39	14.61

Table 8.6: *Natural frequencies in Hz of the Vestvej Bridge.*

It seems as if the ASD based on the RD functions provides a better basis for detecting structural modes. The reason is that the ASD from RD functions is based on averaging in both time and frequency domain, whereas the ASD based on the spectral densities of the measurements is only based on averaging in the frequency domain. This is an important relation for the RD technique

8.5.2 Results

The modal parameters are extracted from the RD functions using the PTD algorithm. The aim is to estimate the mode shapes corresponding to the frequencies in table 8.6, but the noise content in the data is high so not all mode shapes might be estimated at a high confidence level. The influence of the number of points used from the RD functions and the model order are investigated by changing the number of modes from 25 to 30 and varying the number of points in the RD functions from 100 to 120. Corresponding to the analysis of the laboratory bridge model a the following restriction has been applied: $\zeta < 0.05$, $|\text{MCF}| > 0.9$ and $\angle\text{MCF} < 10\,\text{deg}$. Table 8.7 show the estimated eigenfrequencies and damping ratios.

Parameter	Date	1	2	3	4	5
f [Hz]	25/03	5.16	6.64	8.31	14.01	15.38
f [Hz]	04/06	5.02	6.58	8.04	13.23	14.56
ζ [%]	25/03	1.85	4.07	3.04	2.15	2.42
ζ [%]	04/06	1.21	3.52	2.45	1.20	1.17

Table 8.7: *Eigenfrequencies and damping ratios of the Vestvej Bridge.*

The corresponding mode shapes are shown in figs. 8.28 - 8.32.

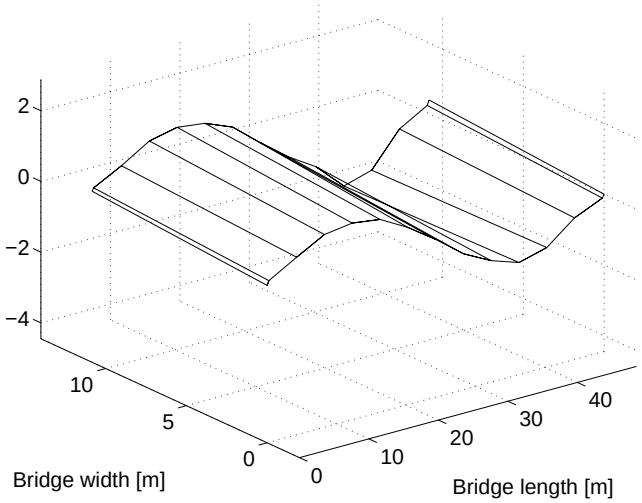

Figure 8.28: *First mode shape of the Vestvej bridge.*

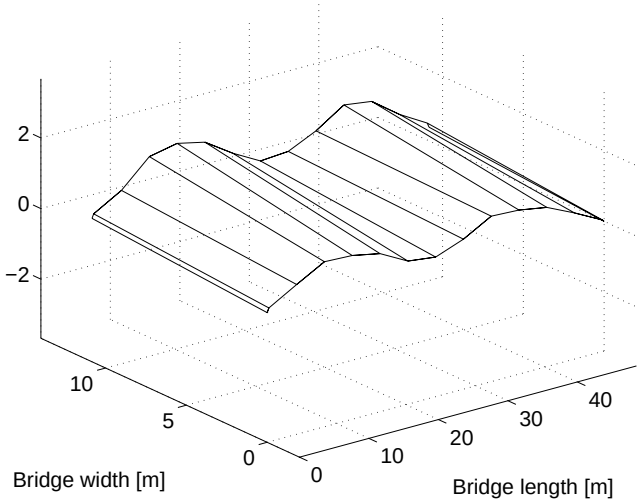

Figure 8.29: *Second mode shape of the Vestvej bridge.*

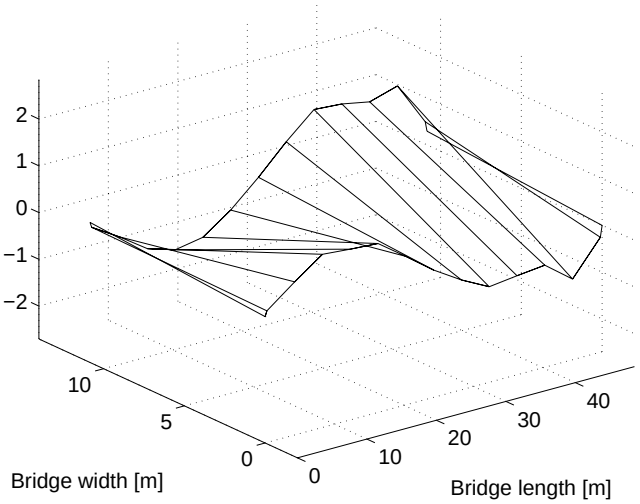

Figure 8.30: *Third mode shape of the Vestvej bridge.*

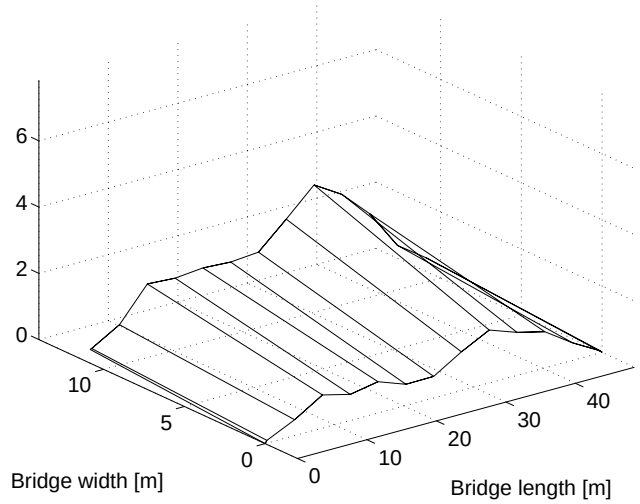

Figure 8.31: *Fourth mode shape of the Vestvej bridge.*

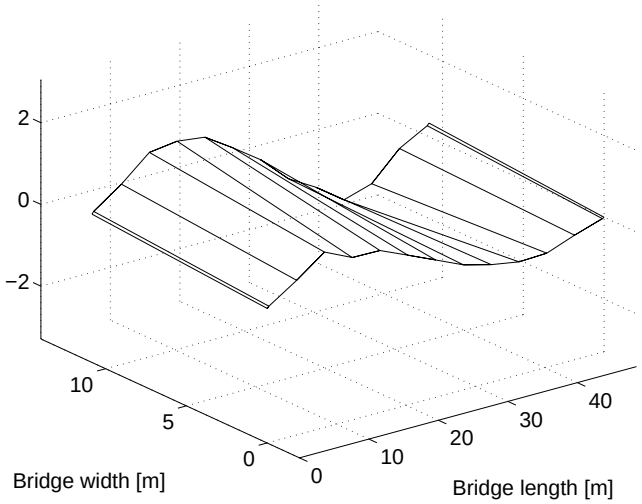

Figure 8.32: *Fifth mode shape of the Vestvej bridge.*

As seen it was not possible estimate the mode shapes of all the modes with sufficient accuracy. This is mainly due to the high noise contents in the meausurements. The result is that all modes are not sufficiently represented in all setups, so it becomes impossible to estimate the mode shapes.

8.5.3 Conclusions

An ambient testing of the Vestvej bridge has been performed. It was possible to detect the natural frequencies of the bridge using the RDD technique. But it was only possible to estimate some of the mode shapes of the bridge. Especially the modes at 5.02, 6.58 and 14.56 Hz were estimated with accurate mode shapes.

It is recommended to base a continuous on-the-line surveyance of the bridge on the RD functions or only the estimated natural eigenfrequencies. The RD functions should be calculated from longer time records than the 900 seconds used in the above analysis. This will increase the accuracy of the RD technique and due to the speed of the technique it is not impossible.

8.6 Summary

In this chapter the application of the RD technique has been demonstrated using different experimental tests. In general the technique have resulted in accurate modal parameters, but it has also been demonstrated that the technique has its limits, when closely spaced modes are present in the data. This corresponds to the experience with the FFT algorithm. But the lack of accuracy should always be compared with the speed of this technique.

The analysis of the Queensborough bridge with the RD technique was a pre-investigation of the performance of the RD technique compared to other techniques. For this purpose the data from the Queensborough bridge were an evident choice since the data have been

analysed using different techniques by different authors. The performance of the RD technique motivated the further work with this technique.

The VRD technique was tested in competition with the RD technique using data from a laboratory bridge model. This investigation was a natural continuation of the test of the performance of the VRD technique. The result of the VRD technique was high quality modal parameters, highly correlated with the result of the RD technique. At the same time the VRD technique were 4-5 times faster than the RD technique. This investigation concludes the introduction and justification of the VRD technique.

The chapter is concluded with an ambient vibration study of the Vestvej bridge. The purpose of this investigation is to obtain information of the modal parameters of the bridge and to investigate if the RD technique can be used as a basis for an on-line surveyance of the bridge. It is concluded that due to the low level accelerations of the bridge a surveyance should be based on long-term records of the accelerations.

Bibliography

[1] Ventura, C.E., Felber, J.A. & Prion, H.G.L. *Evaluation of a Long Span Bridge by Modal Testing.* Proc. 12th International Modal Analysis Conference, Honolulu, Hawaii, USA, 1994, Vol. II, pp. 1309-1315.

[2] Felber, A.J. & Ventura, C.E. *Frequency Domain Analysis of the Ambient Vibration Data of the Queensborough Bridge Main Span.* Proc. 14th International Modal Analysis Conference, Dearborn, Michigan, USA, February 1996, Vol. I, pp. 459-465.

[3] Giorcelli, E., Garibaldi, L., Riva, A. Fasana, A. *ARMAV Analysis of Queensborough Bridge Ambient Data.* Proc. 14th International Modal Analysis Conference, Dearborn, Michigan, USA, February 1996, Vol. I, pp. 466-469.

[4] De Stefano, A., Knaflitz, M., Bonato, P., Ceravolo, R. & Gagliati, G. *Analysis of Ambient Vibration Data From Queensborough Bridge Using Cohen Class Time-Frequency Distributions.* Proc. 14th International Modal Analysis Conference, Dearborn, Michigan, USA, February 1996, Vol. I, pp. 470-476.

[5] Brincker, R., De Stefano, A. & Piombo, B. *Ambient Data to Analyse the Dynamic Behaviour of Bridges: A First Comparison Between Different Techniques.* Proc. 14th International Modal Analysis Conference, Dearborn, Michigan, USA, February 1996, Vol. I, pp. 477-482.

[6] Asmussen J.C., Ibrahim, S.R. & Brincker, R. *Random Decrement and Regression Analysis of Traffic Responses of Bridges.* Proc. 14th International Modal Analysis Conference, Dearborn, Michigan, USA, February 1996, Vol. I, pp. 453-458.

[7] Asmussen J.C., Ibrahim, S.R. & Brincker, R. *Application of the Vector Triggering Random Decrement Technique.* Proc. 15th International Modal Analysis Conference, Orlando, Florida, USA, February 1997, Vol II, pp. 1165-1171.

[8] Ibrahim, S.R., Asmussen, J.C. & Brincker, R. *Theory of Vector Triggering Random Decrement.* Proc. 15th International Modal Analysis Conference, Orlando, Florida, USA, February 1997, Vol I, pp. 502-509.

[9] Asmussen, J.C., Brincker, R. Rytter, A., Hededal,P., Stoltzner, E. & Lauridsen, J. *Ambient Vibration Testing of the Vestvej Bridge - Full Virgin Measurement: 1st Study.* Internal note to RAMBOLL and The Danish Road Directorate, April 1997.

[10] Asmussen, J.C., Brincker, R. Rytter, A., Hededal,P., Stoltzner, E. & Lauridsen, J. *Ambient Vibration Testing of the Vestvej Bridge - Full Virgin Measurement: 2nd Study.* Internal note to RAMBOLL and The Danish Road Directorate, June 1997.

[11] Asmussen, J.C., Brincker, R. Rytter, A., Hededal,P., Stoltzner, E. & Lauridsen, J. *Application of the RD technique to Ambient Testing of The Vestvej Bridge.* To be Presented at the 16th International Modal Analysis Conference, Santa Barbara, California, USA, February 1998.

Chapter 9

Conclusions

This chapter concludes the thesis with the final comments to the investigations of the RD technique. First the contents and the results of each chapter are reviewed in section 9.1. The purpose is to give an overview before the general conclusions are given in section 9.2. The general conclusions contain a step-by-step *recipe* for the application of the RD technique to identify the dynamic characteristica of structures from ambient data. The chapter is concluded with a perspectivation in section 9.3. This will include topics and areas on which future work can be based.

9.1 Summary

9.1.1 Chapter 1

This chapter introduces and delimits the work concerning vibrations of civil engineering structures presented in this thesis. This work is delimited to deal with the RD technique for estimation of modal parameters of structures, where the vibrations can be modelled by a time invariant linear lumped mass parameter system. Furthermore, it is assumed that the loads can be described using filtered stationary Gaussian white noise. The loads can be created artificially or be ambient. A review of the RD technique is performed as a natural starting point. The major result is that it is chosen to interpret RD functions in terms of correlation functions. The scope of the work is formulated as:

The objective of the present Ph.D.-thesis is a description, implementation, and futher development of the theory behind the RD technique as well as a comparison of the performance of the RD technique with the FFT algorithm.

The introduction is concluded with a description of the contents of each chapter.

9.1.2 Chapter 2

This chapter contains a review of linear and linear stochastic vibration theory. The purpose is to describe how modal parameters can be extracted from correlation functions under the previously mentioned assumptions. It is shown in chapter 3 and appendix A that the RD functions are proportional to the correlation functions of the response. The lumped mass parameter system is introduced and the modal parameters are defined. The practical application and implementation of two algorithms, the Ibrahim Time Domain (ITD) and

the Polyreference Time Domain (PTD), for extraction of modal parameters from the free decays of a structure are described. The load modelling is defined and it is shown that the correlation functions of the response of the linear lumped mass parameter system subjected to the load have exactly the same relation as the free decays of the structure. This means that the ITD and PTD algorithms can be used to extract modal parameters from RD functions.

9.1.3 Chapter 3

The RD functions are defined as conditional mean values of a stationary stochastic process and the unbiased estimation of RD functions is shown. The condition is denoted the triggering condition. The applied general triggering condition is introduced. Using this condition it is shown that the RD functions are a weighted sum of the correlation functions and the time derivative of the correlation functions dependent on the formulation of the condition. From this condition the link between the correlation functions and four particular triggering conditions can be derived. These triggering conditions are: Level crossing, local extremum, positive point and zero crossing. The main difference between these triggering conditions is the resulting number of triggering points in the estimation process of the RD functions. The main assumption of these results is that the stochastic processes are stationary and Gaussian distributed with zero mean. The results are derived in detail in appendix A. The response af the structures subjected to the filtered Gaussian distributed white noise load, described in chapter 2, will fulfil these assumptions.

Quality assessment of an estimated RD function is an important problem in any application. Two different approaches to quality assessment of RD functions are suggested. The first approach is based on the shape invariance relation of the RD functions and the second approach is based on the symmetry relation for correlation functions of stationary processes. The strength of the suggested methods is that the experience can be used from one structure to another. Another problem is to choose triggering levels for the different triggering conditions. Some guidelines are given, but it is extremely difficult to obtain some general and consistent rules. Chapter 3 is concluded with a comparison of the speed and accuracy of the RD technique for estimation of correlation functions with an FFT based approach. The result is that the RD technique can be faster and still estimate as accurate correlation functions as the FFT based approach. The absolute main advantage of the RD technique, speed, is underlined.

9.1.4 Chapter 4

This chapter introduces a new technique: Vector triggering Random Decrement (VRD). The motivation for developing this technique is that if the RD technique is applied to a large number of measurements, it becomes time consuming to estimate the full correlation matrix. Instead a vector triggering condition is formulated. It is shown that the VRD functions are a sum of correlation functions corresponding to the size of the vector condition. The assumption is the same: The stochastic processes are stationary and Gaussian distributed with zero mean. The advantage of the VRD technique and its application are illustrated by different simulation studies. This includes the solution to the problem of formulating the vector triggering condition. It is concluded that the VRD technique is an attractive alternative to the RD technique in the analysis of data setups with many

measurements.

9.1.5 Chapter 5

The chapter contains a proposal for a new method to predict the variance of the RD functions. A simple method exists to predict the variance of RD functions, which only uses the RD functions and the number of triggering points, see Appendix A. The main assumption of this method is that the time segments used in the averaging process are uncorrelated. The validity of this assumption has never been investigated. The new method takes the correlation between the time segments into account. The method seems to perform well on simple systems and it illustrates how difficult it is to estimate the variance, since usually only a single realization (measurement) of the processes is available. In the vicinity of zero and far away from zero the method predicts the variance well. It is much more accurate compared to the existing simple method, but it also uses more computational time. Whether or not this increase in accuracy can pay off the increase in computational time is an open question.

9.1.6 Chapter 6

This chapter considers the problems, which arise in practical applications of the RD technique. Several bias problems are described. It is shown how these bias problems can be avoided and how they influence the estimate of the correlation functions and the estimate of the modal parameters. The different implementations of the RD and VRD technique performed as a part of this Ph.D.-project are discussed. It is described how the RD technique and the VRD technique should be implemented in MATLAB. The chapter is concluded with an example of the use of the implemented functions.

9.1.7 Chapter 7

A new method for estimating the frequency response matrix (FRM) of the linear lumped mass parameter system is investigated. The method is based on the RD technique and assumes that both the response and the loads are measured. If the RD functions of the response and the load are calculated and Fourier transformed the FRM can be estimated by simple division. The advantage is that the RD functions dissipate towards zero with increasing and decreasing time lags from zero if the load is white noise. This means that leakage free estimates of the FRM are obtained, since it is not necessary to apply any other window in the time domain than the exponential window. The influence of this window is well-known from investigations in impact testing. It increases the damping ratio corresponding to the exponential decay of the window. The performance of the method is investigated by a simulation study and analysis of a laboratory bridge model loaded by white noise through a shaker. The method can remove the leakage error, but at the expense of higher random uncertainty. It is very difficult to use the method on lightly damped systems, since the results are very sensitive to the number of points in the RD functions and the choice of window function.

9.1.8 Chapter 8

This chapter describes the different analyses of structures, which have been performed. The ambient measurements of the Queensborough bridge have been analysed using a

combination of the RD technique and the ITD algorithm. The results were promising, since the RD technique produced results, which were comparable with the results obtained by different authors using several other well-known algorithms such as FFT, ARMAV and time-frequency domain algorithms. These results encouraged to continue the work with the RD technique. As a final documentation of the VRD technique the response of laboratory bridge model subjected to Gaussian white noise has been analysed using both the VRD and the RD technique. The VRD technique was faster and the modal parameters were identical to those obtained using the RD technique. This underlines that the VRD technique is an attractive alternative to the RD technique, for systems with a high number of measurements.

The work in this thesis is concluded with the ambient vibration study of the Vestvej bridge. The ambient vibrations have been collected using a bridge measurement system developed as a part of this Ph.D.-project. The study is the initial investigations for a demonstration project of vibration based inspection. The data are analyzed using the RD technique. The future perspective of the projcet is to perform continuous on-the-line surveyance using the RD technique in order to utilize the advantages of the RD technique.

9.2 General Conclusions

During this work the RD technique has been investigated intensively through analysis of a broad band of different structures: From simulations of a simple SDOF system loaded by white noise over a laboratory bridge model to the analysis of ambient measurements from existing bridges.

The theory of the RD technique has been summarized and further developed, especially with the results of the applied general triggering condition, the new VRD technique and the new approach for predicting the variance of RD functions. An analytical relation between the RD functions and the modal parameters of a linear lumped mass parameter system loaded by filtered white noise has been established.

Because of the presentation of the theoretical background combined with the experimental experience, is it decided to give a *recipe* for the application of the RD technique for identification of modal parameters from response measurements. The purpose is to give a guideline for potential users with no or little experience with the technique. In the following the recipe is given step by step.

1. **Validation of the measurements:** The first step is to validate the measurements. The purpose is to check that the measurements are stationary and Gaussian distributed. The user should determine if the assumptions of a time-invariant linear structure and stationary Gaussian distributed loads are fulfilled. It can be checked by e.g. a normal probability plot or various tests if the measured response is Gaussian distributed.

   It is standard procedure to apply the above assumptions if the loads are ambient such as wind, waves or traffic. If the loads are deterministic the RD technique should

be used carefully. An example could be a structure loaded by a few impulses. The response should be analysed carefully using the RD technique and therefore the guidelines given below are not valid.

2. **Choice of triggering condition and levels:** The first problem is to choose a triggering condition. It is recommended to use the positive point triggering condition. Only if the records consist of many data points the level crossing or the local extremum triggering condition should be used. It is not recommended to use the zero crossing triggering condition. The reason is that noise has a high influence of the response around zero, so false triggering points will be detected resulting in RD functions with slow convergence. During this thesis it has been emphasized repeatedly by experimental results that low level triggering points should not be used. This illustrates the disadvantages of the zero crossing triggering condition.

   The second problem is the choice of triggering levels. From all the measurements pick out a single reference measurement or a measurement with a relatively high standard deviation. Choose different triggering levels and calculate the RD functions and the estimation time. An appropriate division would be $[a_1\ a_2] = [0.5\ 1]\sigma_X$, $[a_1\ a_2] = [1\ 1.5]\sigma_X$ and $[a_1\ a_2] = [1.5\ \infty]\sigma_X$ or $[a_1\ a_2] = [1\ \infty]\sigma_X$ and $[a_1\ a_2] = [1.5\ \infty]\sigma_X$, etc. The SIC can be used to check the shape invariance of the RD functions. Any levels without the value SIC ≈ 1 should be omitted. If all RD functions have high a SIC and the computational time is not important the minumum and maximum levels, which have been investigated should be used. If the computational time is important the levels which have the lowest number of triggering points and a high SIC value should be chosen. The number of points used in the RD functions can also be determined from this initial investigation by taking a number of points, which ensures that the RD functions just have dissipated sufficiently. Remember to use positive and negative time lags.

3. **Validation of the RD functions:**

   After choosing of triggering condition and determining the triggering levels and the number of points, the RD functions can be calculated. Calculate all RD functions corresponding to estimating the full correlation matrix. In order to extract maximum information from the measurements the sign of the triggering levels should be shifted and the RD functions calculated again. The averages of the RD functions normalized to be the correlation functions are the final estimate of the correlation functions with positive and negative time lags.

   The validation of the quality of the RD functions is very important. Use the symmetry relation to calculate an estimate of the correlation functions for positive time lags and the error function for the correlation functions for positive time lags, see section 3.7.2. By plotting the average correlation functions and the error function the quality can be assessed and the number of points used in the modal parameter extraction procedure can be determined. To check if all RD functions should be used in the modal parameter extraction procedure the fraction between the standard deviation of the estimated correlation function and the error function can be calculated using eq. (3.64). This approach makes it possible to omit the RD functions with a high noise contents.

The last procedure in the validation of the RD functions is to calculate the absolute values of the FFT of all RD functions and average them. The final spectral density contains information about the number of modes present in the RD functions and the corresponding natural frequencies. This gives an opportunity to select a proper model order in the modal parameter extraction procedure.

4. **Extraction of Modal parameters:**

   From the validation process the approximate number of physical modes and the appropriate number of points from the RD functions are known. Using this information the model order and the number of points should be varied in order to investigate the sensitivity of the modal parameters to these choices. By using stabilization diagrams in combination with the MCF and a restriction of small damping ratios a proper model order can be selected and the eigenfrequencies, damping ratios and the mode shapes can be extracted. Usually the mode shapes indicate how accurately the modal parameters are estimated.

This recipe can of course only be a guideline for the application of the VRD technique. Experience with the technique will make it easier to select proper triggering levels, in order to have accurate RD functions and low estimation time.

9.3 Perspectivation and Future Work

There are several different aspects of the RD technique which can be further developed and investigated. The following sections describe these aspects and how they can be investigated.

9.3.1 Non-Gaussian Processes

The main assumption for the theory of the link between the RD functions and the correlation functions of a stochastic vector process is that the process should be Gaussian distributed. It would be interesting to investigate how sensitive the estimate of the RD functions is to this assumption. Will the RD functions differ significantly from the correlation functions if the vector process is non-Gaussian distributed and how sensitive are will the modal parameters be?

A natural starting point for an investigation would be to consider an ideal linear system loaded by Gaussian white noise, where the response will be Gaussian distributed. By adding non-Gaussian measurement noise to the realizations of the response the final process becomes non-Gaussian distributed. By changing the distribution of the meausurement noise and the contribution (signal-to-noise ratio) of the noise, the sensitivity of the accuracy of the estimated RD functions, and the correlation functions of the noise-free system, the estimated modal parameters and the theoretical modal parameters can be investigated by a comparison.

9.3.2 Non-Linear Structures

Further to the above suggestion for future work, non-linear structures can be considered. Non-linear structures subjected to Gaussian load will be non-Gaussian distributed so this

can be considered as an extension to the previous situation where only the measurement noise is non-Gaussian. There is a possibility that it will be possible to use amplitude dependent RD functions for identification of non-linear structures.

9.3.3 Improvement of the Variance Model

The variance model suggested in chapter 5 can probably be improved. The applicability of this model should be tested using real data and used as information for improvement of the accuracy of the modal parameters. The information in the form of variance should be used in the modal parameter extraction process.

9.3.4 Extraction of Modal Parameters

Estimating modal parameters from RD functions is as difficult a task as estimating accurate RD functions. The main problem is that methods used to extract modal parameters from free decays have been used. The noise present in the RD functions is thereby modelled by adding noise or computational modes. This means that a high number of modes have to be used. This rises two main problems, namely the book-keeping of all the modes and the separation of physical or structural modes from the noise modes.

The solution could be to use methods where the noise is modelled as a stochastic process. This might result in more accurate modal parameters and also remove the book-keeping problem. The number of different models (model order, number of points), which have to be tested, is also reduced.

9.3.5 Damage Detection by on-the-line Continuous Surveyance

Using the RD technique for continuous on-the-line surveyance of civil engineering structures is considered to be the most promising application of the technique. The reason is that the RD technique can transform long-term observations into a small amount of data, the RD functions. From these RD functions the modal parameters can be extracted and used as input to a vibration based inspection scheme - or even the RD functions themselves can be used as input. Although the RD technique is not the most accurate technique for estimation of modal parameters, the technique can compensate for the lack of accuracy by extracting the RD functions from the response continuously. The RD functions can be estimated from a huge amount of information.

Chapter 10

Summary in Danish

Dette kapitel giver et kort referat på dansk af indholdet og delkonklusionerne i de enkelte kapitler i afhandlingen.

Kapitel 1: Kapitlet introducerer og afgrænser arbejdet med vibrationer af bygningskonstruktioner, der rapporteres i denne thesis. Det forudsættes, at vibrationsmålingerne er foretaget så omhyggeligt som muligt. Arbejdet afgrænses til at omhandle random dekrement (RD) teknikken til estimering af modal parametre fra konstruktioner, hvor vibrationerne kan modelleres ved hjælp af et system af diskrete masser med tidsinvariante og lineære egenskaber. En eventuel anvendelse af de estimerede modal parametre betragtes ikke. Det forudsættes, at belastningen kan modelleres ved hjælp af hvid støj eller hvid støj formet ved hjælp af et lineært filter. I alle tilfælde er belastningen Gaussisk fordelt og stationær. Belastningen på konstruktionerne kan være naturlig (vind, bølger, køretøjer) eller kunstig (shaker). Kapitlet indeholder også en gennemgang af den allerede eksisterende litteratur omhandlende RD teknikken. Hovedresultatet fra gennemgangen er, at RD teknikken vælges tolket ved hjælp af korrelationsfunktioner. Formålet med arbejdet i denne thesis kan kort beskrives ved:

Formålet med denne Ph.D.-thesis er at beskrive, implementere, videre udvikle teorien bag og sammenligne præstationerne for RD algoritmen med den velkendte FFT algoritme.

Introduktionen afsluttes med en præsentation of indholdet af de enkelte kapitler.

Kapitel 2: I dette kapitel gennemgåes lineær svingningsteori og lineær stokastisk svingningsteori. Hensigten med kapitlet er at beskrive, hvorledes modal parametrene kan estimeres udfra korrelationsfunktionerne for responset under de førnævnte forudsætninger. Det vises senere i kapitel 3 og appendix A, at under disse forudsætninger bliver RD funktionerne proportionale med korrelationsfunktionerne. Den lineære diskrete masse model beskrives og udfra denne defineres modal parametrene. Den praktiske anvendelse af to forskellige algoritmer Ibrahim Time Domain (ITD) og Polyreference Time Domain (PTD) er beskrevet. Disse algoritmer anvendes til at estimere modal parametre udfra målinger af frie henfald af konstruktioner. Den valgte modellering og beskrivelse af kræfterne på konstruktionerne er gennemgået, og det vises, at korrelationsfunktioner for responset af den diskrete masse model, belastet med disse kræfter har samme egenskaber som frie henfald af den diskrete masse model. Derfor kan algoritmer som ITD og PTD anvendes til at

estimere modal parametre fra korrelationsfunktioner. Responset bliver Gaussisk fordelt, idet det er forudsat, at konstruktionerne har lineære egenskaber, og at belastningen er Gaussisk fordelt.

Kapitel 3: RD funktioner defineres som betingede middelværdier ved hjælp af en trig betingelse, og det vises, hvorledes RD funktioner estimeres udfra tidsserier, f.eks. det målte respons af en bygningskonstruktion. Estimeringen af RD funktioner foretages uden systematiske fejl. En generel trig betingelse defineres. Udfra denne betingelse vises det, at RD funktionerne bliver en vægtet sum af korrelationsfunktionerne og de tidsafledede korrelationsfunktioner under forudsætningen af, at tidsserierne er Gaussisk fordelte. Derved er der skabt en sammenhæng mellem modal parametrene for den lineære diskrete masse model og RD funktionerne fra responset af den lineære diskrete masse model belastet med hvid støj.

I kapitlet beskrives også to forskellige metoder, der foreslås anvendt til kvalitetsvurdering af RD funktionerne. Metoderne er generelle, således at erfaring med metoderne kan medbringes fra *én* konstruktion til en anden. Desuden er det angivet, hvorledes trig niveauer kan vælges, således at RD funktionerne estimeres så præcist som muligt. Kapitlet afsluttes med en sammenligning af forskellige metoder til estimering af korrelationsfunktioner. Det vises, ved hjælp af simulering, at RD teknikken kan være lige så præcis som en metode baseret på FFT algoritmen og samtidig have en væsentlig hurtigere beregningstid.

Kapitel 4: Dette kapitel introducerer en ny teknik: Vektor trig random dekrement (VRD). Motiveringen for at udvikle denne teknik er, at ved analyse af et stort antal tidsserier ved hjælp af RD teknikken, kan estimeringstiden blive forholdsvis stor, hvis hele korrelationsmatricen estimeres. I stedet udvides RD teknikken, fra at være defineret ved en skalær trig betingelse, til at være defineret ved en vektor trig betingelse (VRD). Derved bliver det maksimale antal af funktioner minimeret svarende til størrelsen af vektor betingelsen. Det vises, at VRD funktionerne er en sum af korrelationsfunktioner svarende til størrelsen af vektor betingelsen. Forudsætningerne er, at tidsserierne er stationære og Gaussisk fordelte. Fordelene ved, og den praktiske anvendelse af VRD teknikken er illustreret ved hjælp af forskellige simuleringsstudier. Dette inkluderer løsning af de problemer, der opstår ved formulering af vektor betingelsen. VRD teknikken fremstår som et attraktivt og pålideligt alternativ til RD teknikken ved tilfælde, hvor et stort antal målinger er opsamlet simultant.

Kapitel 5: I kapitlet foreslåes en ny metode til prediktion af variansen på RD funktioner. Der findes en simpel metode til prediktion af variansen udfra RD funktionerne alene, som beskrevet i kapitel 3 og appendix A. Forudsætningen for denne metode er, at tidssegmenterne, der anvendes i midlingsprocessen, er ukorrelerede. Denne forudsætning er ikke opfyldt, og betydningen har ikke været testet. Den ny metode der foreslåes tager hensyn til korrelationen mellem de enkelte tidssegmenter. Metoderne undersøges ved hjælp af forskellige simuleringsstudier. Den ny metode er beregningsmæssigt mere tidskrævende end den gamle metode. Til gengæld er præcisionen kraftigt forbedret. Metoden er i stand til at forudsige variansen på RD funktionerne præcist omkring centrum og langt væk fra centrum af dobbeltsidede kryds og auto RD funktioner. Det er et åbent spørgsmål, om denne gevinst i præcision kan betale for den ekstra beregningstid. Yderligere udvikling og

afprøvning af metoden foreslås.

Kapitel 6: Kapitlet omhandler den praktiske anvendelse af RD teknikken. Selvom teknikken teoretisk set er uden systematisk fejl, opstår disse alligevel på grund af, at teknikken anvendes på diskrete tidsserier (målinger). De systematiske fejl illustreres ved hjælp af simuleringsstudier af forskellige systemer. Der gøres opmærksom på, hvornår man skal være opmærksom på problemerne, og hvilken indflydelse de har på estimaterne af både korrelationsfunktionerne og modal parametrene. En systematisk fejl på korrelationsfunktionerne øver ikke nødvendigvis nogen indflydelse på eventuelle estimater af modal parametrene. Generelt kan det siges, at de systematiske fejl aftager med stigende samplingsfrekvens i forhold til den maksimale egenfrekvens af konstruktionen. Foruden beskrivelsen af systematiske fejl beskrives det, hvorledes RD og VRD funktionerne er implementeret. De forskellige funktioner er programmeret i HIGH-C og koblet til MATLAB ved hjælp af MATLABs eksterne interface muligheder.

Kapitel 7: Her undersøges en ny metode til estimering af frekvensresponsfunktioner. Fra det målte respons og belastning af en konstruktion beregnes auto og kryds RD funktionerne. Ved at Fourier transformere disse, opnåes en simpel metode til estimering af frekvensresponsfunktionerne. Fordelen ved denne metode, sammenlignet med den traditionelle metode baseret på Fourier transformationer alene, er mindre beregningstid og frekvensresponsfunktioner estimeret uden systematiske fejl. Begrundelsen er, at RD funktionerne dissiperer mod nul langt væk fra centrum. Dette medfører, at kravet om uendelig lange tidssserier til Fourier transformationen kan udelades. Metoden undersøges ved hjælp af et simuleringsstudie af et *é*tfrihedsgradsystem og analyse af et vibrationstest på en laboratorie bro-model. Undersøgelsen understreger fordelene ved metoden, men specielt for lavt dæmpede systemer vil metoden ikke være mere velegnet end metoder baseret på FFT-algoritmen, hvis ikke der anvendes vinduesfunktioner.

Kapitel 8: I kapitlet beskrives de forskellige analyser af vibrationsmålinger fra eksisterende konstruktioner. Den første konstruktion er Queensborough broen i Canada. Målinger af denne bro, der hovedsageligt er belastet med trafiklast, er analyseret ved hjælp af forskellige metoder: FFT, ARMAV og simultan tids-frekvensdomæne metoder af forskellige forfattere. Resultaterne opnået ved hjælp af RD teknikken rapporteres og sammenlignes med resultaterne opnået ved hjælp af de andre metoder. Det viser sig, at anvendelsen af RD teknikken resulterer i modal parametre, der er sammenlignelige med resultater opnået ved hjælp af andre metoder. Bl.a. dette resultat motiverede det videre arbejde med RD teknikken.

Foruden målingerne af Queensborough broen er der analyseret en laboratorie bro-model og Vestvej broen beliggende nord for Aalborg. Formålet med undersøgelsen af laboratorie bro-modellen er at afslutte sammenligningen mellem RD og VRD teknikken. Det viser sig, at VRD-teknikken kan anvendes i forbindelse med et stort antal målinger. Resultatet er en reduktion i estimeringstiden uden at præcisionen falder betydeligt. Specielt ved analyse af tidsserier med et stort antal punkter vil VRD teknikken være fordelagtig. Analysen af Vestvej broen er baseret på målinger foretaget med et bromålesystem udviklet som en del af dette Ph.D.-projekt. Modal parametrene for broen estimeres ved hjælp af RD teknikken. Undersøgelserne skal danne grundlag for et demonstrationsprojekt for vibrationsbaseret

inspektion af broen.

Kapitel 9: Konklusionen afrunder denne thesis. Indhold og resultater fra de enkelte kapitler resumeres her for at give et afsluttende overblik. Derefter opsummeres den endelige konklusion, der udgøres af en punkt for punkt *opskrift* for, hvorledes RD teknikken kan anvendes til analyse af vibrationsmålinger af bygningskonstruktioner. Konklusionen afsluttes med en perspektivering, hvor bl.a. eventuelle fremtidige emner for RD teknikken beskrives.

Appendix A

Random Decrement and Correlation Functions

The purpose of this appendix is to derive the relations between RD functions and correlation functions of stationary zero mean Gaussian distributed stochastic processes. These relations are considered to be the fundamental mathematical description and basis of this technique. So the main assumption of the results presented in this apendix is that the stochastic processes have a zero mean Gaussian distribution and are stationary. Only a few authors have interpreted RD functions in terms of correlation functions. Vandiver et al. [1] derived the proportional relation between the auto RD functions defined by the level triggering condition and the auto correlation functions using the above-mentioned assumptions. This result was extended by deriving a proportional relation between cross RD functions defined using the theoretical general triggering condition and cross correlation functions, see Brincker et al. [2], [3]. This proof is important since the mathematical description in terms of correlation functions was extended not only to cover the analysis of single measurements but also to cover multivariate measurements. Bedewi et al. [4] and Yang et al. [5] also have some theoretical considerations concerning RD functions and correlation functions. This appendix describes the state of the art of interpreting RD functions in terms of correlation functions and derives the necessary relation to fill out some remaining parts. This is done by introducing the applied general triggering condition, which is a generalization of the theoretical general triggering condition.

Sections A.1 and A.2 describe the mathematical tools, which are applied in the derivations in later sections. The density function of a conditional multivariate Gaussian distributed stochastic variable is described in section A.1. In section A.2 a relation between the density functions of two stochastic variables on different conditions is derived.

In section A.3 the definition of RD functions is given. Furthermore, the estimate of the RD functions is introduced. Based on these definitions the theoretical general triggering condition introduced by Brincker et al. [2], [3] is described in section A.4. In section A.5 the condition is generalized to the applied general triggering condition. This triggering condition is important, since the relation between the RD functions of any particular triggering condition and the correlation functions can be extracted directly from the results of the applied general triggering condition.

Sections A.6 - A.9 describes four commonly used triggering conditions. The relation between the RD functions using these triggering conditions and the correlation functions is derived directly from the results of section A.5. Furthermore, an approximate expression for the variance of the estimated RD functions is derived. The expected number of triggering points, which can be obtained by applying the different triggering conditions is also given.

A.1 Multivariate Gaussian Variables

A multivariate ($n \times 1$-dimensional) Gaussian distributed stochastic variable, $\mathbf{X}$, is described by the general n-dimensional Gaussian density function, $p_{\mathbf{X}}(\mathbf{x})$.

$$p_{\mathbf{X}}(\mathbf{x}) = \frac{1}{(2\pi)^{n/2}(\det(\mathbf{V_{XX}}))^{\frac{1}{2}}} \cdot \exp\left[-\frac{1}{2}(\mathbf{x}-\mu_{\mathbf{X}})^T \mathbf{V_{XX}^{-1}}(\mathbf{x}-\mu_{\mathbf{X}})\right] \tag{A.1}$$

where $\mathbf{V_{XX}}$ is the $n \times n$-dimensional covariance matrix and $\mu_{\mathbf{X}}$ is the $n \times 1$-dimensional mean value vector. Consider an $(n+m) \times 1$ dimensional Gaussian variable, $\mathbf{X}$, which is partitioned into the $n \times 1$ dimensional variable $\mathbf{X}_1$ and the $m \times 1$-dimensional variable $\mathbf{X}_2$, $\mathbf{X} = [\mathbf{X}_1^T \ \mathbf{X}_2^T]^T$. Correspondingly the mean value vector and covariance matrix are partitioned.

$$\mu_{\mathbf{X}} = \begin{bmatrix} \mathbf{X}_1 \\ \mathbf{X}_2 \end{bmatrix}, \quad \mathbf{V_{XX}} = \begin{bmatrix} \mathbf{V_{X_1X_1}} & \mathbf{V_{X_1X_2}} \\ \mathbf{V_{X_2X_1}} & \mathbf{V_{X_2X_2}} \end{bmatrix} \tag{A.2}$$

An important property of a multivariate Gaussian distributed stochastic variable is that the density function of $\mathbf{X}_1$ on condition of $\mathbf{X}_2$ is also Gaussian distributed, Melsa & Sage [6]. The mean value vector and the covariance matrix of $\mathbf{X}_1$, on condition of $\mathbf{X}_2$, are given by, Melsa & Sage [6], Söderström [7].

$$\mathrm{E}[\mathbf{X}_1|\mathbf{X}_2] = \mu_{\mathbf{X}_1} + \mathbf{V_{X_1X_2}}\mathbf{V_{X_2X_2}^{-1}}(\mathbf{x}_2 - \mu_{\mathbf{X}_2}) \tag{A.3}$$

$$\mathrm{Cov}[\mathbf{X}_1|\mathbf{X}_2] = \mathbf{V_{X_1X_1}} - \mathbf{V_{X_1X_2}}\mathbf{V_{X_2X_2}^{-1}}\mathbf{V_{X_2X_1}} \tag{A.4}$$

If $\mu_{\mathbf{X}} = \mathbf{0}$ then eq. (A.3) is reduced to.

$$\begin{aligned} \mathrm{E}[\mathbf{X}_1|\mathbf{X}_2] &= \mathbf{V_{X_1X_2}}\mathbf{V_{X_2X_2}^{-1}}\mathbf{x}_2 \\ &= \mathbf{R_{X_1X_2}}\mathbf{R_{X_2X_2}^{-1}}\mathbf{x}_2 \end{aligned} \tag{A.5}$$

where $\mathbf{R}$ denotes a correlation matrix. The zero mean value vector implies that the covariance matrix and the correlation matrix are identical. Eqs. (A.3) - (A.5) are the basic equations when the relationship between the RD functions and the correlation functions and an approximate expression for the variance of the RD functions is derived in sections A.4 and A.5.

A.2 Conditional Densities

A conditional variable is written as $\mathbf{X_1}|\mathbf{T}$. The condition $\mathbf{T}$ could e.g. be of different complexity.

$$\mathbf{T}_1 = \{\mathbf{X}_2 = \mathbf{a}, \mathbf{X}_3 = \mathbf{b},\} \tag{A.6}$$

$$\mathbf{T}_2 = \{\mathbf{a}_1 \leq \mathbf{X}_2 < \mathbf{a}_2, \mathbf{b}_1 \leq \mathbf{X}_3 \leq \mathbf{b}_2\} \tag{A.7}$$

In the following sections it will be necessary to have a relation between the density function of a variable on the condition in eq. (A.6) and the density function of a variable on the condition in eq. (A.7). This relation is derived from general relations between the density and the distribution functions and the relation between conditional distribution functions and probabilities.

$$\begin{aligned} p_{\mathbf{X}_1|\mathbf{T}_2}(\mathbf{x}_1|\mathbf{T}_2) &= \frac{\partial \mathcal{P}(\mathbf{X}_1 \leq \mathbf{x}_1)|\mathbf{a}_1 \leq \mathbf{X}_2 < \mathbf{a}_2, \mathbf{b}_1 \leq \mathbf{X}_3 < \mathbf{b}_2)}{\partial \mathbf{x}_1} \\ &= \frac{1}{k} \cdot \frac{\partial (P_{\mathbf{X}_1\mathbf{X}_2\mathbf{X}_3}(\mathbf{x}_1, \mathbf{a}_2, \mathbf{b}_2) - P_{\mathbf{X}_1\mathbf{X}_2\mathbf{X}_3}(\mathbf{x}_1, \mathbf{a}_1, \mathbf{b}_1))}{\partial \mathbf{x}_1} \\ &= \frac{1}{k} \cdot \int_{\mathbf{a}_1}^{\mathbf{a}_2} \int_{\mathbf{b}_1}^{\mathbf{b}_2} p_{\mathbf{X}_1\mathbf{X}_2\mathbf{X}_3}(\mathbf{x}_1, \mathbf{x}_2, \mathbf{x}_3) d\mathbf{x}_2 d\mathbf{x}_3 \\ &= \frac{1}{k} \cdot \int_{\mathbf{a}_1}^{\mathbf{a}_2} \int_{\mathbf{b}_1}^{\mathbf{b}_2} p_{\mathbf{X}_1|\mathbf{A}_1}(\mathbf{x}_1|\mathbf{A}_1) p_{\mathbf{X}_2\mathbf{X}_3}(\mathbf{x}_2) d\mathbf{x}_2 d\mathbf{x}_3 \end{aligned} \tag{A.8}$$

where

$$k = \mathcal{P}(\mathbf{a}_1 \leq \mathbf{X_2} < \mathbf{a_2}, \mathbf{b_1} \leq \mathbf{X_3} < \mathbf{b_1}) = \int_{\mathbf{a}_1}^{\mathbf{a}_2} \int_{\mathbf{b}_1}^{\mathbf{b}_2} p_{\mathbf{X}_2\mathbf{X}_3}(\mathbf{x}_2, \mathbf{x}_3) d\mathbf{x}_2 d\mathbf{x}_3 \tag{A.9}$$

Consider a special case of the condition in eq. (A.7).

$$\mathbf{T}_3 = \{\mathbf{a}_1 \leq \mathbf{X}_2 < \mathbf{a}_2, \mathbf{X}_3 = \mathbf{b}\} \tag{A.10}$$

A relation between the density functions $p_{\mathbf{X}_1|\mathbf{T}_2}(\mathbf{x}_1|\mathbf{T}_2)$ and $p_{\mathbf{X}_1|\mathbf{T}_3}(\mathbf{x}_1|\mathbf{T}_3)$ can be established directly from the last statement in eq. (A.8) by setting $\mathbf{b}_1 = \mathbf{b}$, $\mathbf{b}_2 = \mathbf{b} + \Delta\mathbf{b}$ and then let $\Delta\mathbf{b} \to 0$. This procedure is used in section A.6 - A.9. The above equations follow Papoulis [8].

A.3 Definition of Random Decrement Functions

Consider two stochastic processes $Y(t)$ and $X(t)$. The index t will be interpreted as time. The auto RD functions are defined as the mean value af a process on condition of the process itself.

$$D_{XX}(\tau) = \mathrm{E}[X(t+\tau)|T_{X(t)}] \tag{A.11}$$

$$D_{YY}(\tau) = \mathrm{E}[Y(t+\tau)|T_{Y(t)}] \tag{A.12}$$

The conditions $T_{Y(t)}$ and $T_{X(t)}$ are denoted triggering conditions. The cross RD functions are defined as the mean value of a process on condition of another process.

$$D_{XY}(\tau) = \mathrm{E}[X(t+\tau)|T_{Y(t)}] \tag{A.13}$$

$$D_{YX}(\tau) = \mathrm{E}[Y(t+\tau)|T_{X(t)}] \tag{A.14}$$

The first subscript in e.g. D_{XY} refers to the process where the mean value is calculated, $X(t)$ and the second subscript refers to the process where the condition is applied, $Y(t)$. The definitions of eqs. (A.11) and (A.12) can be derived from eqs. (A.13) and (A.14) by replacing $X(t)$ by $Y(t)$ or the opposite, respectively. This property is used throughout the rest of this appendix, so only results for the cross RD functions are stated.

The estimate of the RD functions are calculated as the emperical mean. This implies that the processes $X(t)$ and $Y(t)$ are assumed to be ergodic.

$$\hat{D}_{XY}(\tau) = \frac{1}{N}\sum_{i=1}^{N} x(t_i+\tau)|T_{y(t_i)} \tag{A.15}$$

$$\hat{D}_{YX}(\tau) = \frac{1}{N}\sum_{i=1}^{N} y(t_i+\tau)|T_{x(t_i)} \tag{A.16}$$

where $x(t)$ and $y(t)$ are realizations of the stochastic processes $X(t)$ and $Y(t)$. The important parameter in these estimates is the number of triggering points, N. The conditions $T_{Y(t)}$ and $T_{X(t)}$ should always be chosen so that the number of triggering points is high enough to secure a satisfactory convergence of the estimates.

It is important that the estimates of the RD functions in eqs. (A.15) and (A.16) are unbiased, which is shown below.

$$\mathrm{E}[\hat{D}_{XY}(\tau)] = \frac{1}{N}\sum_{i=1}^{N}\mathrm{E}[x(t_i+\tau)|T_{y(t_i)}] = D_{XY}(\tau) \tag{A.17}$$

Systematic errors of the correlation functions are avoided by applying the RD technique to Gaussian distributed processes.

The following sections introduce different formulations of the triggering conditions and link the RD functions to the correlation functions of the processes.

A.4 General Theoretical Triggering Condition

Consider two univariate Gaussian distributed stochastic processes, $X(t)$ and $Y(t)$. It is assumed that $X(t)$ and $Y(t)$ have zero mean and are stationary processes. The theoretical general triggering condition is denoted $T_{X(t)}^{G_T}$ and is given by the following conditions on $X(t)$ and its time derivative $\dot{X}(t)$.

$$T_{X(t)}^{G_T} = \{X(t) = a, \dot{X}(t) = b\} \tag{A.18}$$

This triggering condition is denoted theoretical, since it is too strict to be used in any practical application of the RD technique. The probability of the event $T_{X(t)}^{G_T}$ is very small, so the realizations of $X(t)$ and $Y(t)$ have to be extremely long in order to estimate the conditional mean value using eqs. (A.15) or (A.16) with a satisfactory number of triggering points. The reason for introducing this triggering condition is that the results are used in the next section, where the applied general triggering condition is introduced. Using $T_{X(t)}^{G_T}$ a relationship between the RD functions and the correlation functions of stationary multivariate Gaussian processes is obtained. The vector processes $\mathbf{X}_1$ and $\mathbf{X}_2$ are created.

$$\mathbf{X}_1 = [X(t+\tau)\ Y(t+\tau)]^T \qquad \mathbf{X}_2 = [X(t)\ \dot{X}(t)]^T \tag{A.19}$$

$X(t)$ is assumed to be stationary so $X(t)$ and $\dot{X}(t)$ are uncorrelated and thereby independent, since $X(t)$ is Gaussian. The auto and cross correlation matrices of $\mathbf{X}_1$ and $\mathbf{X}_2$ becomes.

$$\mathbf{R}_{\mathbf{X}_1\mathbf{X}_1} = \begin{bmatrix} \sigma_X^2 & R_{XY}(0) \\ R_{YX}(0) & \sigma_Y^2 \end{bmatrix} \tag{A.20}$$

$$\mathbf{R}_{\mathbf{X}_2\mathbf{X}_2} = \begin{bmatrix} \sigma_X^2 & 0 \\ 0 & \sigma_{\dot{X}}^2 \end{bmatrix} \qquad \mathbf{R}_{\mathbf{X}_2\mathbf{X}_2}^{-1} = \begin{bmatrix} \sigma_X^{-2} & 0 \\ 0 & \sigma_{\dot{X}}^{-2} \end{bmatrix} \tag{A.21}$$

$$\mathbf{R}_{\mathbf{X}_1\mathbf{X}_2}(\tau) = \begin{bmatrix} R_{XX}(\tau) & R_{X\dot{X}}(\tau) \\ R_{YX}(\tau) & R_{Y\dot{X}}(\tau) \end{bmatrix} = \begin{bmatrix} R_{XX}(\tau) & -R'_{XX}(\tau) \\ R_{YX}(\tau) & -R'_{YX}(\tau) \end{bmatrix} \tag{A.22}$$

R' is the time derivative of R and σ_X^2 is the variance of $X(t)$ and equal to $R_{XX}(0)$. The mean value of $\mathbf{X}_1$ on condition that $\mathbf{X}_2 = [a\ b]^T$ is calculated from standard results for the conditional mean value of multivariate Gaussian variables, see eq. (A.5).

$$\mathrm{E}[\mathbf{X}_1|\mathbf{X}_2] = \begin{bmatrix} R_{XX}(\tau) & -R'_{XX}(-\tau) \\ R_{YX}(\tau) & -R'_{YX}(-\tau) \end{bmatrix} \begin{bmatrix} \sigma_X^{-2} & 0 \\ 0 & \sigma_{\dot{X}}^{-2} \end{bmatrix} \begin{bmatrix} a \\ b \end{bmatrix} \tag{A.23}$$

Since the condition $\mathbf{X}_2 = [a\ b]$ is equal to $T_{X(t)}^{G_T}$ defined in eq. (A.18) the results of eq. (A.23) is equal to the RD functions, see eqs. (A.11) and (A.14). The relation between RD functions defined using $T_{X(t)}^{G_T}$ and correlation functions follows

$$D_{XX}(\tau) = \frac{R_{XX}(\tau)}{\sigma_X^2} \cdot a - \frac{R'_{XX}(\tau)}{\sigma_{\dot{X}}^2} \cdot b \tag{A.24}$$

$$D_{YX}(\tau) = \frac{R_{YX}(\tau)}{\sigma_X^2} \cdot a - \frac{R'_{YX}(\tau)}{\sigma_{\dot{X}}^2} \cdot b \tag{A.25}$$

These fundamental solutions relate the auto and cross RD functions of two Gaussian distributed stochastic processes to their correlation functions. Corresponding to the conditional mean value in eq. (A.23) the covariance of $\mathbf{X}_1$ on condition that $\mathbf{X}_2 = [a\ b]^T$ can be calculated from standard results for multivariate Gaussian variables, see eq. (A.4).

$$\mathrm{Cov}[\mathbf{X}_1|\mathbf{X}_2] = \begin{bmatrix} \sigma_X^2 & R_{XY}(0) \\ R_{YX}(0) & \sigma_Y^2 \end{bmatrix} - \begin{bmatrix} R_{XX}(\tau) & -R'_{XX}(\tau) \\ R_{YX}(\tau) & -R'_{YX}(\tau) \end{bmatrix} \begin{bmatrix} \sigma_X^{-2} & 0 \\ 0 & \sigma_{\dot{X}}^{-2} \end{bmatrix} \begin{bmatrix} R_{XX}(\tau) & R_{YX}(\tau) \\ -R'_{XX}(\tau) & -R'_{YX}(\tau) \end{bmatrix} \tag{A.26}$$

The variance of the conditional process can be extracted from the diagonals of the final results of eq. (A.26).

$$\mathrm{Var}[X(t+\tau)|T_{X(t)}^{G_T}] = \sigma_X^2 \left(1 - \left(\frac{R_{XX}(\tau)}{\sigma_X^2}\right)^2 - \left(\frac{R'_{XX}(\tau)}{\sigma_X \sigma_{\dot{X}}}\right)^2\right) \tag{A.27}$$

$$\mathrm{Var}[Y(t+\tau)|T_{X(t)}^{G_T}] = \sigma_Y^2 \left(1 - \left(\frac{R_{YX}(\tau)}{\sigma_Y \sigma_X}\right)^2 - \left(\frac{R'_{YX}(\tau)}{\sigma_Y \sigma_{\dot{X}}}\right)^2\right) \tag{A.28}$$

These general relationships were first established in Brincker et al. [2], [3]. From the results of this section it is possible to derive the relation between the RD functions and the correlation functions of some of the triggering conditions with practical interest, see e.g. section A.6. But in general the process becomes very complex. This is the motivation for introducing the applied general triggering condition.

A.5 Applied General Triggering Condition

The zero mean Gaussian stationary processes $X(t)$ and $Y(t)$ are considered. In application of the RD technique less strict triggering conditions, compared with the theoretical general triggering condition, are used. The reason is that the theoretical general triggering condition produces too few triggering points in order to secure a satisfactory averaging process. This leads to the formulation of the applied general triggering condition, $T_{X(t)}^{G_A}$. From the results of this triggering condition the relation between the RD functions of all known triggering conditions and the correlation functions can be established directly. The applied general triggering condition, $T_{X(t)}^{G_A}$, is defined by.

$$T_{X(t)}^{G_A} = \{a_1 \leq X < a_2, b_1 \leq \dot{X} < b_2\} \tag{A.29}$$

Notice that no restriction is made on the triggering bounds, $[a_1\ a_2]$, $[b_1\ b_2]$. This means e.g. that the bounds on $\dot{X}(t)$ could be chosen as $[b_1\ b_2] = [-\infty\ \infty]$, which is a way of omitting a condition on $\dot{X}(t)$. The RD function is defined as the mean value of $Y(t+\tau)$ on condition of $T_{X(t)}^{G_A}$. In the following only the cross RD functions are considered.

$$\begin{aligned} D_{YX}(\tau) &= \mathrm{E}[Y(t+\tau)|T_{X(t)}^{G_A}] \\ &= \int_{-\infty}^{\infty} y \cdot p_{Y|T_{X(t)}^{G_A}}(y|T_{X(t)}^{G_A})dy \\ &= \frac{1}{k_1} \cdot \int_{a_1}^{a_2}\int_{b_1}^{b_2}\int_{-\infty}^{\infty} y \cdot p_{YX\dot{X}}(y,x,\dot{x})dy d\dot{x} dx \\ &= \frac{1}{k_1} \cdot \int_{a_1}^{a_2}\int_{b_1}^{b_2} E[Y(t+\tau)|T_{X(t)}^{G_T}] \cdot p_{X\dot{X}}(x,\dot{x})d\dot{x}dx \end{aligned} \tag{A.30}$$

where the results of eq. (A.8) and eq. (A.9) and the following have been used.

$$k_1 = \int_{a_1}^{a_2}\int_{b_1}^{b_2} p_{X\dot{X}}(x,\dot{x})d\dot{x}dx \tag{A.31}$$

$$T_{X(T)}^{G_T} = \{X(t) = x, \dot{X}(t) = \dot{x}\} \tag{A.32}$$

The results from the theoretical general triggering condition, see eq. (A.25), are inserted in eq. (A.30).

$$\begin{aligned} D_{YX}(\tau) &= \mathrm{E}[Y(t+\tau)|T_{X(t)}^{G_A}] \\ &= \frac{1}{k_1} \cdot \int_{a_1}^{a_2} \int_{b_1}^{b_2} \left(\frac{R_{YX}(\tau)}{\sigma_X^2} x - \frac{R'_{YX}(\tau)}{\sigma_{\dot{X}}^2} \dot{x} \right) p_{X\dot{X}}(x, \dot{x}) d\dot{x} dx \\ &= \frac{R_{YX}(\tau)}{\sigma_X^2} \cdot \tilde{a} \; - \; \frac{R'_{YX}(\tau)}{\sigma_{\dot{X}}^2} \cdot \tilde{b} \end{aligned} \tag{A.33}$$

where $\tilde{a}$ and $\tilde{b}$ are given by.

$$\tilde{a} = \frac{\int_{a_1}^{a_2} \int_{b_1}^{b_2} x p_{X\dot{X}}(x, \dot{x}) d\dot{x} dx}{\int_{a_1}^{a_2} \int_{b_1}^{b_2} p_{X\dot{X}}(x, \dot{x}) d\dot{x} dx} = \frac{\int_{a_1}^{a_2} x p_X(x) dx}{\int_{a_1}^{a_2} p_X(x) dx} \tag{A.34}$$

$$\tilde{b} = \frac{\int_{a_1}^{a_2} \int_{b_1}^{b_2} \dot{x} p_{X\dot{X}}(x, \dot{x}) d\dot{x} dx}{\int_{a_1}^{a_2} \int_{b_1}^{b_2} p_{X\dot{X}}(x, \dot{x}) d\dot{x} dx} = \frac{\int_{b_1}^{b_2} \dot{x} p_{\dot{X}}(\dot{x}) d\dot{x}}{\int_{b_1}^{b_2} p_{\dot{X}}(\dot{x}) d\dot{x}} \tag{A.35}$$

In the statement of eqs. (A.33), (A.34) and (A.35) it has been used that $X(t)$ and $\dot{X}(t)$ are independent, which is true, since $X(t)$ is assumed to be Gaussian distributed and stationary.

Equation (A.33) describes the relationship between the RD functions from the applied general triggering condition and the correlation functions and the time derivative of the correlation functions. From the result the weights or triggering bounds of $R_{YX}(\tau)$ and $R'_{YX}(\tau)$ can be extracted directly by inserting the triggering bounds $[a_1 \; a_2]$, $[b_1 \; b_2]$ in eqs. (A.34) and (A.35). In principle there is no significant difference between the results of $T_{X(t)}^{G_T}$ and $T_{X(t)}^{G_A}$. The only difference is the scaling or weight of the correlation functions.

The variance of the conditional stochastic process $Y(t+\tau)|T_{X(t)}^{G_A}$ is defined as

$$\begin{aligned} \mathrm{Var}[Y(t+\tau)|T_{X(t)}^{G_A}] &= \int_{-\infty}^{\infty} (y - \mu_{Y|T_{X(t)}^{G_A}})^2 p_{Y|T_{X(t)}^{G_A}}(y|T_{X(t)}^{G_A}) dy \\ &= \int_{-\infty}^{\infty} y^2 p_{Y|T_{X(t)}^{G_A}}(y|T_{X(t)}^{G_A}) dy \; - \; \mu_{Y|T_{X(t)}^{G_A}}^2 \end{aligned} \tag{A.36}$$

where the conditional mean value is equal to the RD functions (the term $\mu_{Y|T_{X(t)}^{G_A}}$ is used for simplicity)

$$\mu_{Y|T_{X(t)}^{G_A}}^2 = \mathrm{E}[Y(t+\tau)|T_{X(t)}^{G_A}]^2 = D_{YX}^2(\tau) \tag{A.37}$$

and straightforward can be calculated from eqs. (A.33) - (A.35). The first term in eq. (A.36) is calculated using eq. (A.8).

$$\begin{aligned}\int_{-\infty}^{\infty} y^2 p_{Y|T^{G_A}_{X(t)}}(y|T^{G_A}_{X(t)})dy &= \frac{1}{k_1}\int_{-\infty}^{\infty}\int_{a_1}^{a_2}\int_{b_1}^{b_2} y^2 p_{YX\dot{X}}(y,x,\dot{x})d\dot{x}dxdy \\ &= \frac{1}{k_1}\int_{a_1}^{a_2}\int_{b_1}^{b_2}\int_{-\infty}^{\infty} y^2 p_{Y|T^{G_T}_{X(t)}}(y|T^{G_T}_{X(t)})dy p_{X\dot{X}}(x,\dot{x})d\dot{x}dx \\ &= \frac{1}{k_1}\int_{a_1}^{a_2}\int_{b_1}^{b_2} \mathrm{Var}[Y|T^{G_T}_{X(t)}]p_{X\dot{X}}(x,\dot{x})d\dot{x}dx \; + \\ &\quad \frac{1}{k_1}\int_{a_1}^{a_2}\int_{b_1}^{b_2} \mathrm{E}[Y|T^{G_T}_{X(t)}]^2 p_{X\dot{X}}(x,\dot{x})d\dot{x}dx \end{aligned} \tag{A.38}$$

where k_1 is given by eq. (A.31). The conditional variance is calculated using the results of eqs. (A.37) and (A.38) and the results of eqs. (A.25) and (A.28).

$$\begin{aligned}&\mathrm{Var}[Y(t+\tau)|T^{G_A}_{X(t)}] \; = \\ &\mathrm{Var}[Y|T^{G_T}_{X(t)}] \; + \; \frac{1}{k_1}\int_{a_1}^{a_2}\int_{b_1}^{b_2}\left(\frac{R_{YX}(\tau)}{\sigma^2_X}x - \frac{R'_{YX}(\tau)}{\sigma^2_{\dot{X}}}\dot{x}\right)^2 p_{X\dot{X}}(x,\dot{x})d\dot{x}dx \; - \\ &\left(\frac{1}{k_1}\left(\frac{R_{YX}(\tau)}{\sigma^2_X}\right)k_2 - \frac{1}{k_1}\left(\frac{R'_{YX}(\tau)}{\sigma^2_{\dot{X}}}\right)k_3\right)^2 \end{aligned} \tag{A.39}$$

where the following abbreviations are used.

$$k_1 \; = \; \int_{a_1}^{a_2}\int_{b_1}^{b_2} p_{X\dot{X}}(x,\dot{x})d\dot{x}dx \tag{A.40}$$

$$k_2 \; = \; \int_{a_1}^{a_2}\int_{b_1}^{b_2} x p_{X\dot{X}}(x,\dot{x})d\dot{x}dx \tag{A.41}$$

$$k_3 \; = \; \int_{a_1}^{a_2}\int_{b_1}^{b_2} \dot{x} p_{X\dot{X}}(x,\dot{x})d\dot{x}dx \tag{A.42}$$

$$k_4 \; = \; \int_{a_1}^{a_2}\int_{b_1}^{b_2} x^2 p_{X\dot{X}}(x,\dot{x})d\dot{x}dx \tag{A.43}$$

$$k_5 \; = \; \int_{a_1}^{a_2}\int_{b_1}^{b_2} \dot{x}^2 p_{X\dot{X}}(x,\dot{x})d\dot{x}dx \tag{A.44}$$

The conditional variance in eq. (A.39) is reduced to

$$\begin{aligned}\mathrm{Var}[Y(t+\tau)|T^{G_A}_{X(t)}] \; &= \sigma^2_Y\left(1 - \left(\frac{R_{YX}(\tau)}{\sigma_Y\sigma_X}\right)^2 - \left(\frac{R'_{YX}(\tau)}{\sigma_Y\sigma_{\dot{X}}}\right)^2\right) \; + \\ &\left(\frac{R_{YX}(\tau)}{\sigma^2_X}\right)^2\left(\frac{k_4}{k_1} - \left(\frac{k_2}{k_1}\right)^2\right) \; + \; \left(\frac{R'_{YX}(\tau)}{\sigma^2_{\dot{X}}}\right)^2\left(\frac{k_5}{k_1} - \left(\frac{k_3}{k_1}\right)^2\right) \end{aligned} \tag{A.45}$$

The variance of the conditional stochastic process $Y(t+\tau)|T^{G_A}_{X(t)}$ is basically only a function of the correlation functions and the time derivative of the correlation functions.

Equations (A.33) and (A.45) are the mathematical basis for the RD technique applied to stationary Gaussian stochastic processes. The result has been derived for the case of cross RD functions. The results for auto RD functions are obtained by substituting $Y(t+\tau)$ with $X(t+\tau)$ or the opposite. The relation between the RD function of any triggering condition can immediately be derived from the results of eqs. (A.33) and (A.45). The derivation is shown in the sections A.6 - A.9 for commonly used triggering conditions.

A.6 Level Crossing Triggering Condition

The level crossing triggering condition is the *original* triggering condition and has been by far the most popular triggering condition. A triggering point is detected if the process $X(t)$ is equal to the chosen triggering level a. Superscript L is an abbreviation for the *L*evel crossing triggering condition.

$$T^L_{X(t)} \;=\; \{X(t) \;=\; a\} \tag{A.46}$$

Equation (A.46) is reformulated to be of the same form as the applied general triggering condition

$$T^L_{X(t)} \;=\; \{a \le X(t) < a+\Delta a, -\infty \le \dot{X}(t) < \infty\}\;, \quad \Delta a \to 0 \tag{A.47}$$

From the above reformulation of the level crossing triggering condition the weights $\tilde{a}$ and $\tilde{b}$ in eqs. (A.34) and (A.35) are calculated by letting $\Delta a \to 0$.

$$\tilde{a} \;=\; \frac{\int_a^{a+\Delta a} x p_X(x) dx}{\int_a^{a+\Delta a} p_X(x) dx} \;=\; a \tag{A.48}$$

$$\tilde{b} \;=\; \frac{\int_{-\infty}^{\infty} \dot{x} p_{\dot{X}}(\dot{x}) d\dot{x}}{\int_{-\infty}^{\infty} p_{\dot{X}}(\dot{x}) d\dot{x}} \;=\; 0 \tag{A.49}$$

The final result for the level crossing triggering condition states that the RD functions are proportional to the correlation functions.

$$D_{YX}(\tau) \;=\; \mathrm{E}[Y(t+\tau)|T^L_{X(t)}] \;=\; \frac{R_{YX}(\tau)}{\sigma^2_X} \cdot a \tag{A.50}$$

The variance of the conditional process $Y(t+\tau)|T^L_{X(t)}$ is obtained by calculating k_1, k_2, k_3, k_4 and k_5 from eqs. (A.40) - (A.44). The fractions used in eq. (A.45) become

$$\frac{k_4}{k_1} = a^2,\; \left(\frac{k_2}{k_1}\right)^2 = a^2,\; \frac{k_5}{k_1} = \sigma^2_{\dot{X}},\; \left(\frac{k_3}{k_1}\right)^2 = 0 \tag{A.51}$$

The variance follows by inserting the results of eq. (A.51) into eq. (A.45)

$$\mathrm{Var}[Y(t+\tau)|T^L_{X(t)}] \;=\; \sigma^2_Y \left(1 \;-\; \left(\frac{R_{YX}(\tau)}{\sigma_Y \sigma_X}\right)^2\right) \tag{A.52}$$

It is important that if an auto conditional process is considered, $X(t+\tau)|T^L_{X(t)}$, the variance of this process will always be zero, since $R_{XX}(0) = \sigma^2_X$ for stationary processes. Furthermore, the variance is independent of the triggering level, a. The RD functions using level triggering are estimated as the emperical mean value. The processes are assumed to be ergodic

$$\hat{D}_{YX}(\tau) \;=\; \frac{1}{N}\sum_{i=1}^{N} y(t_i+\tau)|x(t_i) \;=\; a \tag{A.53}$$

where $x(t)$ and $y(t)$ are realizations of the processes $X(t)$ and $Y(t)$. If the different time segments in the averaging process of eq. (A.53) are assumed to be independent the variance of $\hat{D}_{YX}$ can be derived from eq. (A.52)

$$\mathrm{Var}(\hat{D}_{YX}(\tau)) \;\approx\; \frac{\sigma^2_Y}{N}\left(1 \;-\; \left(\frac{R_{YX}(\tau)}{\sigma_Y\sigma_X}\right)^2\right) \tag{A.54}$$

Eqs. (A.50), (A.52) and (A.54) were first derived by Vandiver et al. [1] for the auto RD functions. Their work was based on a more complicated and less general approach, since they operated directly on the density functions instead of using eqs. (A.3) and (A.4). Brincker et al. [2], [3] derived eqs. (A.50), (A.52) and (A.54) using the results from section A.4 and the total representation theorem, see Ditlevsen [9]. Their proof included cross RD functions.

A.6.1 Expected Number of Triggering Points

The expected number of level crossings per unit time of a Gaussian process is given by Rices formula, see Rice [10]

$$\mathrm{E}[\frac{dN(a)}{dt}] \;=\; \frac{1}{\pi}\frac{\sigma_{\dot{X}}}{\sigma_X}\cdot exp\left(-\frac{a^2}{2\cdot\sigma^2_X}\right) \tag{A.55}$$

The expected number of triggering points of a Gaussian time series is given by

$$\mathrm{E}[N(a)] \;=\; \Delta T\cdot(N_X - N_\tau)\cdot\frac{1}{\pi}\frac{\sigma_{\dot{X}}}{\sigma_X}exp\left(-\frac{a^2}{2\cdot\sigma^2_X}\right) \tag{A.56}$$

where ΔT is the sampling interval, N_X is the number of points in the time series, X, and N_τ is the number of points in the RD functions. The number of level crossings, $N(a)$, or triggering points is of course dependent on the triggering level, a.

One of the problems with the level crossing triggering condition is how to choose the triggering level a. It can be shown that the optimal triggering level, in the sense of minimizing the variance of the RD functions (see eq. (A.52)) is $a = \sqrt{2}\sigma_X$, see Hummelshøj et al. [11]. This has been supported by a simulation study by Brincker et al. [12], where the results indicate that a triggering level between 1 and 2 times σ_X should be chosen. These results are based on the assumption of an ergodic Gaussian stochastic process and that the averaged time segments are independent.

A.7 Local Extremum Triggering Condition

The local extremum triggering condition, $T^E_{X(t)}$, has not been widely used. Nevertheless the triggering condition is attractive since the contribution from the time derivative of the process is not averaged out, but demanded to be zero. A triggering point is detected if the time derivative of the process is zero and the process itself is bounded by a_1 and a_2

$$T^E_{X(t)} \;=\; \{a_1 \le X(t) < a_2, \dot{X}(t) = 0\} \;, \quad 0 \le a_1 < a_2 < \infty \tag{A.57}$$

In general a_1 and a_2 should have equal sign. Otherwise information is lost since the contribution from $\{a_1 \le X(t) < 0, \dot{X}(t) = 0\}$ will average out the contribution from $\{0 \le X(t) < |a_1|, \dot{X}(t) = 0\}$. The only part left will be the contribution from $\{|a_1| \le X(t) < a_2, \dot{X}(t) = 0\}$. Equation (A.57) is reformulated to be of the same form as the applied general triggering condition.

$$T^E_{X(t)} \;=\; \{a_1 \le X(t) < a_2, 0 \le \dot{X}(t) < 0 + \Delta b\} \;, \quad \Delta b \to 0 \tag{A.58}$$

From the above reformulation of the local extremum triggering condition the weights $\tilde{a}$ and $\tilde{b}$ in eqs. (A.34) and (A.35) are calculated by letting $\Delta b \to 0$

$$\tilde{a} \;=\; \frac{\int_{a_1}^{a_2} x p_X(x) dx}{\int_{a_1}^{a_2} p_X(x) dx} \tag{A.59}$$

$$\tilde{b} \;=\; \frac{\int_0^{0+\Delta v} \dot{x} p_{\dot{X}}(\dot{x}) d\dot{x}}{\int_0^{0+\Delta v} p_{\dot{X}}(\dot{x}) d\dot{x}} \;=\; 0 \tag{A.60}$$

The RD functions for the local extremum triggering conditions are proportional to the correlation functions

$$D_{YX}(\tau) \;=\; \mathrm{E}[Y(t+\tau)|T^E_{X(t)}] \;=\; \frac{R_{YX}(\tau)}{\sigma_X^2} \cdot \tilde{a} \tag{A.61}$$

If the triggering levels are chosen as $[a_1\ a_2] = [0\ \infty]$ (or alternatively $[-\infty\ 0]$) the maximum number of triggering points are always obtained. The resulting triggering level in this case is

$$\tilde{a} \;=\; \frac{\int_{a_1}^{a_2} x p_X(x) dx}{\int_{a_1}^{a_2} p_X(x) dx} \;, \qquad [a_1\ a_2] = [0\ \infty] \;\Rightarrow\; a \;= \sqrt{\frac{2}{\pi}} \sigma_X \tag{A.62}$$

The variance of $Y(t+\tau)|T^E_{X(t)}$ is obtained by calculating k_1, k_2, k_3, k_4 and k_5 from eqs. (A.40) - (A.44). The fractions used in eq. (A.45) become

$$\left(\frac{k_2}{k_1}\right)^2 = \left(\frac{\int_{a_1}^{a_2} x p_X(x) dx}{\int_{a_1}^{a_2} p_X(x) dx}\right)^2 \;, \quad \frac{k_4}{k_1} = \frac{\int_{a_1}^{a_2} x^2 p_X(x) dx}{\int_{a_1}^{a_2} p_X(x) dx} \;, \quad \frac{k_3}{k_1} = \frac{k_5}{k_1} = 0 \tag{A.63}$$

The variance of the conditional process follows by inserting the results of eq. (A.63) into eq. (A.45)

$$\mathrm{Var}[Y(t+\tau)|T^E_{X(t)}] = \sigma_Y^2 \left(1 - \left(\frac{R_{YX}(\tau)}{\sigma_Y \sigma_X}\right)^2 - \left(\frac{R'_{YX}(\tau)}{\sigma_Y \sigma_{\dot{X}}}\right)^2\right) + k^E \left(\frac{R_{YX}(\tau)}{\sigma_X^2}\right)^2 \tag{A.64}$$

where k^E is

$$k^E = \frac{\int_{a_1}^{a_2} x^2 p_X(x)dx}{\int_{a_1}^{a_2} p_X(x)dx} - \left(\frac{\int_{a_1}^{a_2} x\, p_X(x)dx}{\int_{a_1}^{a_2} p_X(x)dx}\right)^2 \tag{A.65}$$

If especially the triggering levels are chosen to $[a_1\ a_2] = [0\ \infty]$ then the variance become

$$\mathrm{Var}[Y(t+\tau)|T^E_{X(t)}] = \sigma_Y^2 \left(1 - \frac{2}{\pi}\left(\frac{R_{YX}(\tau)}{\sigma_X \sigma_Y}\right)^2 - \left(\frac{R'_{YX}(\tau)}{\sigma_{\dot{X}} \sigma_Y}\right)^2\right) \tag{A.66}$$

The variance of the conditional variable becomes dependent on the chosen triggering levels. Furthermore, the variance of $X(t+\tau)|T^E_{X(t)}$ at time lag zero is

$$\mathrm{Var}[X(t+\tau)|T^E_{X(t)}] = \sigma_X^2(1 - \frac{2}{\pi}) \tag{A.67}$$

This result differs from the level crossing triggering condition, since the variance at time lag zero is not zero. The reason is that the triggering levels, a_1, a_2, define two bounds instead of only a single value.

The RD functions using local extremum triggering are estimated as the empirical mean. The processes are assumed to be ergodic

$$\hat{D}_{YX}(\tau) = \frac{1}{N}\sum_{i=1}^{N} y(t_i+\tau)|a_1 \le x(t_i) < a_2, \dot{x}(t_i) = 0 \tag{A.68}$$

where $x(t)$ and $y(t)$ are realizations of $X(t)$ and $Y(t)$. If the different time segments in the averaging process are assumed to be independent the variance of the RD functions can be derived from eq. (A.66)

$$\mathrm{Var}[\hat{D}_{YX}(\tau)] \approx \frac{\sigma_Y^2}{N}\left(1 - \left(\frac{R_{YX}(\tau)}{\sigma_Y \sigma_X}\right)^2 - \left(\frac{R'_{YX}(\tau)}{\sigma_Y \sigma_{\dot{X}}}\right)^2\right) + \frac{k^E}{N}\left(\frac{R_{YX}(\tau)}{\sigma_X^2}\right)^2 \tag{A.69}$$

A.7.1 Expected Number of Triggering Points

In general the expected number of local extremes can only be calculated using tedius integrations, see e.g. Lin [13]. In the case of a narrow banded process a simpler approach can be used. For narrow banded processes the expected number of local extremes (maxima) above a certain level is equal to the expected number of up or down crossings of this level. This implies that the local extremes are all local maxima. The expected number of triggering points in a narrow banded Gaussian process can be calculated from the result of eq. (A.56)

$$\mathrm{E}[N(a_1, a_2)] = \Delta T(N_X - N_\tau) \cdot \frac{1}{2\pi}\frac{\sigma_{\dot{X}}}{\sigma_X}\left(\exp(\frac{-a_1^2}{2\cdot\sigma_X^2}) - \exp(\frac{-a_2^2}{2\cdot\sigma_X^2})\right) \tag{A.70}$$

A.8 Positive Point Triggering Condition

The positive point triggering condition can be interpreted as a generalization of the level crossing triggering condition. It is the most versatile of the different triggering conditions presented. A triggering point is detected if the process is bounded by a_1 and a_2. The bounds should have equal sign. Usually positive signs are used.

$$T^P_{X(t)} = \{a_1 < X(t) \leq a_2\} \tag{A.71}$$

Equation (A.71) is reformulated to be of the same form as the applied general triggering condition.

$$T^P_{X(t)} = \{a_1 < X(t) \leq a_2, -\infty < \dot{X}(t) < \infty\} \qquad a_2 > a_1 \geq 0 \tag{A.72}$$

Notice that if $a_1 \to a_2$ the positive point triggering condition is equal to the level triggering condition. The RD functions calculated using $T^P_{X(t)}$ are derived from eq. (A.33). The triggering levels or weights become, see eqs. (A.34) and (A.35)

$$\tilde{a} = \frac{\int_{a_1}^{a_2} x p_X(x) dx}{\int_{a_1}^{a_2} p_X(x) dx} \tag{A.73}$$

$$\tilde{b} = \frac{\int_{-\infty}^{\infty} \dot{x} p_{\dot{X}}(\dot{x}) d\dot{x}}{\int_{-\infty}^{\infty} p_{\dot{X}}(\dot{x}) d\dot{x}} = 0 \tag{A.74}$$

The RD functions for the positive point triggering condition are proportional to the correlation functions

$$D_{YX}(\tau) = \mathrm{E}[Y(t+\tau)|T^P_{X(t)}] = \frac{R_{YX}(\tau)}{\sigma^2_X} \cdot \tilde{a} \tag{A.75}$$

If the triggering bounds are chosen as $[a_1\ a_2] = [0\ \infty]$ the maximum number of triggering points is obtained

$$[a_1\ a_2] = [0\ \infty] \ \Rightarrow\ \tilde{a} = \sqrt{\frac{2}{\pi}}\sigma_X \tag{A.76}$$

The variance of the conditional process $Y(t+\tau)|T^P_{X(t)}$ is obtained by calculating k_1, k_2, k_3, k_4 and k_5 from eqs. (A.40) - (A.44). The fractions used in eq. (A.45) become

$$\frac{k_4}{k_1} = \frac{\int_{a_1}^{a_2} x^2 p_x(x) dx}{\int_{a_1}^{a_2} p_x(x) dx},\ \frac{k_2}{k_1} = \frac{\int_{a_1}^{a_2} x p_x(x) dx}{\int_{a_1}^{a_2} p_x(x) dx},\ \frac{k_5}{k_1} = \sigma^2_{\dot{X}},\ \frac{k_3}{k_1} = 0 \tag{A.77}$$

The variance of the conditional process $Y(t+\tau)|T^P_{X(t)}$ reduces to

$$\mathrm{Var}[Y(t+\tau)|T^Z_{X(t)}] = \sigma^2_Y \left(1 - \left(\frac{R_{YX}(\tau)}{\sigma_X \sigma_Y}\right)^2\right) + k^P \left(\frac{R_{YX}(\tau)}{\sigma^2_X}\right)^2 \tag{A.78}$$

where k^P is

$$k^P = \frac{\int_{a_1}^{a_2} x^2 p_X(x) dx}{\int_{a_1}^{a_2} f_X(x) dx} - \left(\frac{\int_{a_1}^{a_2} x f_X(x) dx}{\int_{a_1}^{a_2} p_X(x) dx}\right)^2 \tag{A.79}$$

If especially $[a_1\ a_2] = [0\ \infty]$ the variance reduces to

$$\mathrm{Var}[Y(t+\tau)|T^P_{X(t)}] \ = \ \sigma^2_Y \left(1 - \frac{2}{\pi}\left(\frac{R_{YX}(\tau)}{\sigma_X \sigma_Y}\right)^2\right) \tag{A.80}$$

The variance of the conditional auto process at time lag zero is

$$\mathrm{Var}[X(t+\tau)|T^P_{X(t)}] \ = \ \sigma^2_X \left(1 - \frac{2}{\pi}\right) \tag{A.81}$$

which is different from the variance of the conditional auto process using level triggering, since the above is not zero.

The RD functions using positive point triggering are estimated as the empirical mean. The processes are assumed to be ergodic

$$\hat{D}_{YX}(\tau) \ = \ \frac{1}{N}\sum_{i=1}^{N} y(t_i+\tau)|a_1 < x(t_i) \leq a_2 \tag{A.82}$$

where $x(t)$ and $y(t)$ are realizations of $X(t)$ and $Y(t)$. If the different time segments in the averaging process are assumed to be independent the variance of the RD functions can be derived from eq. (A.80)

$$\mathrm{Var}[\hat{D}_{YX}(\tau)] \ \approx \ \frac{\sigma^2_Y}{N}\left(1 - \left(\frac{R_{YX}(\tau)}{\sigma_Y \sigma_X}\right)^2\right) \ + \ \frac{k^P}{N}\left(\frac{R_{YX}(\tau)}{\sigma^2_X}\right)^2 \tag{A.83}$$

The above relation for the variance should be used with care, since it is very unlikely that the time segments are independent.

A.8.1 Expected Number of Triggering Points

The expected number of triggering points per unit time, $\frac{dN(a_1,a_2)}{dt}$ is simply the probability that $a_1 \leq X(t) \leq a_2$.

$$\mathrm{E}[\frac{dN(a_1,a_2)}{dt}] \ = \ \int_{a_1}^{a_2} p_X(x)dx \tag{A.84}$$

The expected number of triggering points in a time series is given by.

$$\mathrm{E}[N(a_1,a_2)] \ = \ \Delta T(N_X - N_\tau) \cdot \int_{a_1}^{a_2} p_X(x)dx \tag{A.85}$$

If for instance the bounds are chosen as $[a_1\ a_2] = [0\ \infty]$ then the expected number of triggering points will be:

$$\mathrm{E}[N_T] \ = \ \Delta T(N_X - N_\tau) \cdot 0.5 \tag{A.86}$$

Half of the points in the time series will be triggering points. This is the major difference between RD functions estimated using positive point triggering and local extremum triggering. The number of triggering points is much higher for the positive point triggering condition.

A.9 Zero Crossing Triggering Condition

The zero crossing with positive slope triggering condition was the second triggering condition introduced in RD estimation. This condition was used, since the resulting RD functions were interpreted as impulse response functions. A triggering point is detected if the process crosses the zero line with positive slope

$$T^Z_{X(t)} = \{X(t) = 0, \dot{X}(t) \geq 0\} \tag{A.87}$$

This triggering condition could also have been formulated with more general bounds instead of $[b_1\ b_2] = [0\ \infty]$. In practice only a realization of $X(t)$ is known. So if more general bounds are used a numerical differentiation of $X(t)$ is neccessary, which will introduce uncertainty and thereby false triggering points. The bounds in eq. (A.87) also ensure a maximum number of triggering points.

Equation (A.87) is reformulated to be of the same form as the applied general triggering condition

$$T^Z_{X(t)} = \{0 \leq X(t) < 0 + \Delta a, 0 \leq \dot{X}(t) < \infty\} \tag{A.88}$$

The RD functions calculated using $T^Z_{X(t)}$ are derived from eq. (A.33). The triggering levels or weights become, see eqs. (A.34) and (A.35)

$$\tilde{a} = \frac{\int_0^{0+\Delta a} x p_X(x) dx}{\int_0^{0+\Delta a} p_X(x) dx} = 0 \tag{A.89}$$

$$\tilde{b} = \frac{\int_0^{\infty} \dot{x} f_{\dot{X}}(\dot{x}) d\dot{x}}{\int_0^{\infty} f_{\dot{X}}(\dot{x}) d\dot{x}} = \sqrt{\frac{2}{\pi}} \sigma_{\dot{X}} \tag{A.90}$$

From the weights it follows that the RD functions are proportional to the time derivative of the correlation functions

$$D_{YX}(\tau) = \mathrm{E}[Y(t+\tau)|T^Z_{X(t)}] = -\frac{R'_{YX}(\tau)}{\sigma^2_{\dot{X}}} \sqrt{\frac{2}{\pi}} \sigma_{\dot{X}} \tag{A.91}$$

The variance of the conditional process $Y(t+\tau)|T^E_{X(t)}$ is obtained by calculating k_1, k_2, k_3, k_4 and k_5 from eq. (A.40) - eq. (A.41). The fractions used in eq. (A.45) become

$$\frac{k_3}{k_1} = \sqrt{\frac{2}{\pi}} \sigma_{\dot{X}},\ \frac{k_5}{k_1} = \sigma^2_{\dot{X}},\ \frac{k_2}{k_1} = \frac{k_4}{k_1} = 0 \tag{A.92}$$

The variance of the conditional process $Y(t+\tau)|T^Z_{X(t)}$ reduces to

$$\mathrm{Var}[Y(t+\tau)|T^Z_{X(t)}] = \sigma^2_Y \left(1 - \left(\frac{R_{YX}(\tau)}{\sigma_X \sigma_Y}\right)^2 - \frac{2}{\pi} \left(\frac{R'_{YX}(\tau)}{\sigma_{\dot{X}} \sigma_Y}\right)^2\right) \tag{A.93}$$

This relation is equivalent to the result for the local extremum triggering condition, see eq. (A.66). The RD functions using zero crossing triggering condition are estimated as the empirical mean. The processes are assumed to be ergodic

$$\hat{D}_{YX}(\tau) = \frac{1}{N} \sum_{i=1}^{N} y(t_i + \tau) | x(t_i) = 0, \dot{x}(t_i) \geq 0 \tag{A.94}$$

If the different time segments in the averaging process are assumed to be independent the variance of the RD functions can be derived from eq. (A.93).

$$\mathrm{Var}[\hat{D}_{YX}(\tau)] \approx \frac{\sigma_Y^2}{N}\left(1-\left(\frac{R_{YX}(\tau)}{\sigma_X\sigma_Y}\right)^2-\frac{2}{\pi}\left(\frac{R'_{YX}(\tau)}{\sigma_Y\sigma_{\dot{X}}}\right)^2\right) \tag{A.95}$$

A.9.1 Expected Number of Triggering Points

The expected number of triggering points is derived from Rices formula, see eq. (A.55). The argument is that half of the zero crossings has positive slope

$$\mathrm{E}[\frac{dN(0)}{dt}] = \frac{1}{2\pi}\frac{\sigma_{\dot{X}}}{\sigma_X} \tag{A.96}$$

The expected number of triggering points in a time series with N_X points and a sampling period ΔT is

$$\mathrm{E}[N(0)] = \Delta T(N_X - N_\tau)\cdot\frac{1}{2\pi}\frac{\sigma_{\dot{X}}}{\sigma_X} \tag{A.97}$$

where N_τ is the number of points in the RD functions.

A.10 Summary

This appendix establishes the mathematical basis for the RD technique applied to stationary zero mean Gaussian distributed processes. A definition of the RD functions is given in section A.3. Furthermore, the estimation process is discussed and it is shown that the estimates of the RD functions are unbiased. Section A.4 introduces the general theoretical triggering condition. The relations between the RD functions of this condition and the correlation functions are derived. Since this triggering condition only has theoretical interest, a generalization of this condition, the generally applied triggering condition is introduced in section A.5. The relation between the RD functions and the correlation functions is derived. This triggering condition is important, since the relations between the RD functions of the triggering conditions used in practice and the correlation functions can be derived directly from the results of section A.5. The four different triggering conditions which are used in practice, level crossing, local extrumum, positive point and zero crossing with positive slope triggering, are described in sections A.6 - A.9. The relations between the RD functions and the correlation functions are derived, an approximate equation for the variance of the estimated RD functions are given and finally the expected number of triggering points are given. Sections A.6 - A.9 give the fundamental mathematical description of the RD functions. The results of this appendix are used throughout the thesis.

Bibliography

[1] Vandiver, J.K., Dunwoody, A.B., Campbell, R.B. & Cook, M.F. *A Mathematical Basis for the Random Decrement Vibration Signature Analysis Technique.* Journal of Mechanical Design, Vol. 104, April 1982, pp. 307-313.

[2] Brincker, R., Krenk, S., Kirkegaard, P.H. & A. Rytter. *Identification of Dynamical Properties from Correlation Function Estimates.* Bygningsstatiske Meddelelser, Vol. 63, No. 1, 1992, pp. 1-38.

[3] Brincker, R., Krenk, S. & J.L. Jensen *Estimation of Correlation Functions by the Random Dec Technique.* Proc. Skandinavisk Forum for Stokastisk Mekanik, Lund, Sweden, Aug. 30-31, 1990.

[4] Bedewi, N.A. & Yang, J.C.S. *The Random Decrement Technique: A More Efficient Estimator of the Correlation Function.* Proc. 1990 ASME International Conference and Exposition, Boston, MA, USA, August 5-9, pp. 195-201.

[5] Yang, J.C.S., Qi, G.Z. & Kan, C.D. *Mathematical Base of the Random Decrement Technique.* Proc. 8th International Modal Analysis Conference, Kissimee, Florida, USA, 1990, pp. 28-34.

[6] Melsa, J.L. & Sage, A.P. *An Introduction to Probability and Stochastic Processes.* Prentice-Hall, Inc. Englewood Cliffs, N.J., 1973. ISBN: 0-13-034850-3.

[7] Söderström, T. & Stoica, P. *System Identification.* Prentice Hall International (UK) Ltd, 1989. ISBN: 0-13-881236.

[8] Papoulis, A. *Probability, Random Variables and Stochastic Processes.* McGraw-Hill, Inc. 1991. ISBN 0-7-100870-5.

[9] Ditlevsen, O. *Uncertainty Modelling.* McGraw-Hill Inc. 1981. ISBN: 0-07-010746-0.

[10] Rice, S.O. *Mathematical Analysis of Random Noise.* Bell Syst. Tech. J., Vol. 23, pp. 282-332; Vol 24, pp. 46-156. Reprinted in N. Wax, Selected Papers on Noise and stochastic processes. Dover Publications, Inc., New York.

[11] Hummelshøj, L.G., Møller, H. & Pedersen, L. *Skadesdetektering ved Responsmåling.* M.sc. Thesis (In Danish), Aalborg University, 1991.

[12] Brincker, R., Jensen, J.L. & Krenk, S. *Spectral Estimation by the Random Dec Technique* Proc. 9th International Conference on Experimental Mechanics, Lyngby, Copenhagen, August 20-24, 1990.

[13] Lin, Y.K. *Probabilistic Theory of Structural Dynamics.* 3rd Edition, McGraw-Hill, Inc., 1986. ISBN: 0-88275-377-0.